Post-Translational Regulation of Bacterial Physiology by Ser/Thr Kinases HipA and HipH - A Mass Spectrometry Study

Dissertation

der Mathematisch-Naturwissenschaftlichen Fakultät
der Eberhard Karls Universität Tübingen
zur Erlangung des Grades eines Doktors der Naturwissenschaften
(Dr. rer. nat.)

vorgelegt von

Payal Nashier
aus Sonipat/Indien

Tübingen
2024

Gedruckt mit Genehmigung der Mathematisch-Naturwissenschaftlichen Fakultät der Eberhard Karls Universität Tübingen.

Tag der mündlichen Qualifikation:	19.12.2024
Dekan:	Prof. Dr. Thilo Stehle
1. Berichterstatter:	Prof. Dr. Boris Macek
2. Berichterstatter:	Prof. Dr. Heike Brötz-Oesterhelt

Erklärung

Ich erkläre hiermit, dass ich die zur Promotion eingereichte Arbeit:

“Post-translational regulation of bacterial physiology by Ser/Thr kinases HipA and HipH - a mass spectrometry study”,

selbständig verfasst, nur die angegebenen Quellen und Hilfsmittel benutzt un wörtlich oder inhaltlich übereinstimmende Stellen als solche gekennzeichnet habe. Ich erkläre, dass die Richtlinien zur Sicherung guter wissenschaftlicher Praxis der Universität Tübingen beachtet wurden. Eine detaillierte Abgrenzung meiner eigenen Leistung habe ich im Kapitel „Declaration of author contributions“ vorgenommen. Ich bin mir bewusst, dass die falsche Abgabe einer Versucherung an Eides statt mit Freiheitsstafe bis zu drei Jahren oder mit Geldstrafe bestraft wird.

Declaration

I hereby declare that I have produced the work:

“Post-translational regulation of bacterial physiology by Ser/Thr kinases HipA and HipH - a mass spectrometry study”,

Submitted for the award of a doctorate, on my own (without external help), have used only the sources and aids indicated, and have marked passages included from other works, whether verbatim or in content, as such. I swear upon oath that these statements are true and that I have not concealed anything. I have made a detailed definition of my own achievements in the chapter “Declaration of author contributions”. I am aware that making a false declaration under oath is punishable by a term of imprisonment of up to three years or by a fine.

Tübingen, den 02.10.2024

Table of Contents

Abbreviations

Abi	Abortive Infection
AMR	Antimicrobial Resistance
AQUA	Absolute Quantification
Astral	Asymmetric Track Lossless analyzer
ATP	Adenosine Triphosphate
BY	Bacterial Tyrosine
CDC	Centers for Disease Control and Prevention
Ccm	Carbon-Dioxide Concentrating Mechanism
CID	Collision-Induced Dissociation
CPS	Capsule Polysaccharide
DDA	Data-Dependent Acquisition
DIA	Data-Independent Acquisition
DML	Dimethyl Labeling
ESBLs	Extended-Spectrum β-Lactamases
ESI	Electrospray Ionization
ETD	Electron Transfer Dissociation
FT-ICR	Fourier Transform-Ion Cyclotron Resonance
GTP	Guanosine Triphosphate
HCD	Higher-energy Collisional Dissociation
HILIC	Hydrophilic Interaction Liquid Chromatography
HipA	High persistence A
HK	Histidine Kinase
HPLC	High-Pressure Liquid Chromatography
ICAT	Isotope Coded Affinity Tag
IL	Interleukin
IMAC	Immobilized Metal Affinity Chromatography
iBAQ	Intensity-Based Absolute Quantification

iTRAQ	Isobaric Tags for Relative and Absolute Quantification
LC-MS/MS	Liquid Chromatography-Tandem Mass Spectrometry
LFQ	Label-Free Quantification
LMP	Lysosomal Membrane Permeabilization
LPS	Lipopolysaccharide
LUCA	Last Universal Common Ancestor
MALDI	Matrix-Assisted Laser Desorption/Ionization
MBP	Myelin Basic Protein
MDR	Multidrug-Resistant
MIC	Minimum Inhibitory Concentration
MOAC	Metal Oxide Affinity Chromatography
MS	Mass Spectrometry
m/z	Mass-to-Charge ratio
OD	Optical Density
OMP	Outer Membrane Proteins
PASTA	Penicillin-binding and Serine/Threonine Kinase Associated Domain
PEP	Phosphoenolpyruvate
PI	Pathogenicity Islands
PTM	Post-Translational Modification
ROS	Reactive Oxygen Species
RR	Response Regulator
SCV	Salmonella-Containing Vesicles
SCX	Strong Cation Exchange
SCoPE	Single Cell Proteomics
SDS-PAGE	Sodium Dodecyl Sulphate Polyacrylamide Gel Electrophoresis
SILAC	Stable Isotope Labeling by Amino acids in Cell culture
STK	Serine/Threonine Kinase
STY	Serine/Threonine/Tyrosine

TA	Toxin-Antitoxin
TCS	Two-Component System
TMT	Tandem Mass Tag
TNF-α	Tumor Necrosis Factor Alpha
UTI	Urinary Tract Infection
WHO	World Health Organization
2-DE	Two-Dimensional Gel

Summary

Post-translational modifications (PTMs) play an indispensable role in the rapid execution of responses that regulate a number of biological functions. Protein Ser/Thr kinases (STKs) are key regulators of vital cellular processes, including antibiotic tolerance, metabolism, virulence, and stress response. Despite their importance, the molecular mechanisms and targets of STKs are underinvestigated, especially in the context of post-translational regulation in pathogenic bacteria. Antibiotic tolerance and persistence are a major contributor to the relapse of many chronic infections and frequently result in antibiotic overuse and the development of antibiotic resistance. One of the best-studied drivers of persistence is a Ser/Thr kinase HipA, first characterized in *Escherichia coli*. Multiple HipA-like kinases have been recently reported to be present in bacteria, including pathogens such as *Klebsiella pneumoniae*, but their functions remain poorly understood. In my thesis, I focused on elucidating the function of two such STKs, HipH (YjjJ) in *E. coli* and HipA in *K. pneumoniae* to understand their potential role in regulating cellular processes.

To explore this, I applied state-of-the-art mass spectrometry-based quantitative phosphoproteomics to gain new insights into the functions and substrates of these kinases and fill crucial gaps in knowledge of bacterial physiology and pathogenesis. I first reviewed recent advances in quantitative phosphoproteomics to highlight the utility of LC-MS/MS technologies combined with quantitative proteomics strategies to investigate dynamic phosphorylation changes during various biological processes. I then applied this technology to study HipA-family Ser/Thr kinase HipH (YjjJ) in *E. coli*. Using quantitative phosphoproteomics based on stable isotope labeling by amino acids in cell culture (SILAC) and *in vitro* kinase assay, I demonstrated that HipH phosphorylates specific targets such as the ribosomal protein RpmE and the carbon storage regulator CsrA. Therefore, HipH plays an important role in regulating ribosome assembly, cell division, and central carbon metabolism, but it does not confer antibiotic tolerance like its homolog HipA. I have also shown that HipH cross-talks with other bacterial kinases, revealing a complex network of regulatory interactions. The final part of my work focused on *Klebsiella pneumoniae*, a major cause of antibiotic-resistant

nosocomial infections worldwide. I demonstrated that overproduced *K. pneumoniae* HipA ($HipA_{kp}$) is toxic to both *E. coli* and *K. pneumoniae*, and this toxicity can be rescued by overproduction of the antitoxin $HipB_{kp}$. Importantly, I showed that $HipA_{kp}$ overproduction leads to increased tolerance against ciprofloxacin, linking HipA activity to antibiotic persistence in this organism. Through proteome and phosphoproteome analyses, I confirmed that $HipA_{kp}$ has Ser/Thr kinase activity, auto-phosphorylates at S150, and shares multiple substrates with its *E. coli* counterpart. I performed a comprehensive analysis of the *K. pneumoniae* phosphoproteome with $HipA_{kp}$ overproduction to generate the largest dataset of phosphorylated proteins for this bacterium.

Overall, my work provides an in-depth analysis of the roles of the two HipA-like kinases in antibiotic tolerance and metabolism, offering new insights into their functions and regulatory networks. These findings also provide a foundation for future research on post-translational regulation of bacterial physiology.

Zusammenfassung

Posttranslationale Modifikationen (PTM) spielen eine wesentliche Rolle bei der schnellen Ausführung von Antworten, die eine Vielzahl biologischer Funktionen regulieren. Protein-Ser/Thr-Kinasen (STKs) sind Schlüsselregulatoren für wichtige zelluläre Prozesse, einschließlich Antibiotikatoleranz, Stoffwechsel, Virulenz und Stressreaktionen. Trotz ihrer Bedeutung sind die molekularen Mechanismen und Ziele der STKs noch nicht vollständig geklärt, insbesondere im Zusammenhang mit der posttranslationalen Regulation in pathogenen Bakterien. Antibiotikatoleranz und Persistenz tragen bei vielen chronischen Infektionen wesentlich zu einem Rückfall bei und führen häufig zu einem übermäßigen Einsatz von Antibiotika und zur Entwicklung von Antibiotikaresistenzen. Eine der am besten untersuchte Auslöser für Persistenz ist die Ser/Thr-Kinase HipA, die zuerst in *Escherichia coli* charakterisiert wurde. Kürzlich wurde gezeigt, dass mehrere HipA-ähnliche Kinasen in Bakterien vorkommen, darunter auch in Krankheitserregern wie *Klebsiella pneumoniae*, aber ihre Funktionen sind nach wie vor schlecht verstanden. In meiner Dissertation konzentrierte ich mich auf die Aufklärung der Funktion von zwei dieser STKs, HipH (YjjJ) in *E. coli* und HipA in *K. pneumoniae*, um ihre mögliche Rolle bei der Regulierung zellulärer Prozesse zu verstehen.

Um dies zu untersuchen, habe ich modernste, auf Massenspektrometrie basierende quantitative Phosphoproteomik angewandt, um neue Einblicke in die Funktionen und Substrate dieser Kinasen zu gewinnen und so entscheidende Wissenslücken in der bakteriellen Physiologie und Pathogenese zu schließen. Zunächst habe ich einen Überblick über die jüngsten Fortschritte in der quantitativen Phosphoproteomik gegeben, um den Nutzen von LC-MS/MS-Technologien in Kombination mit quantitativen Proteomik-Strategien zur Untersuchung dynamischer Phosphorylierungsänderungen während verschiedener biologischer Prozesse hervorzuheben. Anschließend habe ich diese Technologie zur Untersuchung der Ser/Thr-Kinase der HipA-Familie HipH (YjjJ) in *E. coli* eingesetzt. Verwendung quantitativer Phosphoproteomik basierend auf der Markierung stabiler Isotope durch Aminosäuren in Zellkulturen (SILAC) und In-vitro-Kinasetests konnte ich zeigen, dass

HipH spezifische Ziele wie das ribosomale Protein RpmE und den Kohlenstoffspeicherregulator CsrA phosphoryliert.

HipH spielt also eine wichtige Rolle bei der Regulierung des Ribosomenaufbaus, der Zellteilung und des zentralen Kohlenstoffstoffwechsels, verleiht aber keine Antibiotikatoleranz wie sein Homolog HipA. Ich habe auch gezeigt, dass HipH mit anderen bakteriellen Kinasen in Wechselwirkung steht, was ein komplexes Netzwerk von regulatorischen Interaktionen offenbart. Der letzte Teil meiner Arbeit konzentrierte sich auf *Klebsiella pneumoniae*, einer der Hauptverursacher antibiotikaresistenter nosokomiale Infektionen weltweit. Ich konnte zeigen, dass überproduziertes K. pneumoniae HipA ($HipA_{kp}$) sowohl für *E. coli* als auch für *K. pneumoniae* toxisch ist, und dass diese Toxizität durch Überproduktion des Antitoxins $HipB_{kp}$ aufgehoben werden kann. Außerdem konnte ich zeigen, dass die Überproduktion von $HipA_{kp}$ zu einer erhöhten Toleranz gegenüber Ciprofloxacin führt, was einen Zusammenhang zwischen der HipA-Aktivität und der Antibiotika-Persistenz in diesem Organismus herstellt. Durch Proteom- und Phosphoproteomanalysen konnte ich bestätigen, dass $HipA_{kp}$ eine Ser/Thr-Kinaseaktivität besitzt, an S150 autophosphoryliert und mehrere Substrate mit seinem Gegenstück in *E. coli* teilt. Ich habe eine umfassende Analyse des Phosphoproteoms von K. pneumoniae mit $HipA_{kp}$-Überproduktion durchgeführt, um den größten Datensatz an phosphorylierten Proteinen für dieses Bakterium zu erstellen.

Insgesamt bietet meine Arbeit eine eingehende Analyse der Rolle der beiden HipA-ähnlichen Kinasen bei der Antibiotikatoleranz und dem Metabolismus und bietet neue Einblicke in ihre Funktionen und regulatorischen Netzwerke. Diese Ergebnisse bilden auch eine Grundlage für künftige Forschungen zur posttranslationalen Regulation der bakteriellen Physiologie.

List of Publications

Published:

Zittlau, K., **Nashier, P.**, Cavarischia-Rega, C., Macek, B., Spät, P. and Nalpas, N., 2023. Recent progress in quantitative phosphoproteomics. Expert Review of Proteomics, 20(12), pp.469-482.

Gratani, F.L., Englert, T., **Nashier, P.**, Sass, P., Czech, L., Neumann, N., Doello, S., Mann, P., Blobelt, R., Alberti, S. and Forchhammer, K., Bange, G., Höfer, K., Macek, B. 2023. *E. coli* toxin YjjJ (HipH) is a Ser/Thr protein kinase that impacts cell division, carbon metabolism, and ribosome assembly. mSystems, 8(1), pp. e01043-22.

Under Revision:

Nashier, P., Samp, I., Adler, M., Jers, C., Mijakovic, I., Schwarz, S., Macek, B. 2024. Deep phosphoproteomics of *Klebsiella pneumoniae* reveals HipA-mediated tolerance to ciprofloxacin. Under revision in PLOS Pathogens.

Not included in this Thesis:

Dhasmana, N., Kumar, N., Gangwal, A., Keshavam, C.C., Singh, L.K., Sangwan, N., **Nashier, P.**, Biswas, S., Pomerantsev, A.P., Leppla, S.H. and Singh, Y., 2021. PrkC, a Transmembrane Serine/Threonine Protein Kinase, Regulates Bacterial Chain Length in Bacillus anthracis. Journal of Bacteriology, 203(11), pp.10-1128.

Semanjski, M., Gratani, F.L., Englert, T., **Nashier, P.**, Beke, V., Nalpas, N., Germain, E., George, S., Wolz, C., Gerdes, K. and Macek, B., 2021. Proteome dynamics during antibiotic persistence and resuscitation. mSystems, 6(4), pp.10-1128.

Declaration of Author Contributions

In the review article Zittlau, K. *et al.* (2023) “Recent progress in quantitative phosphoproteomics”, I contributed to the chapter on Streamlining the (quantitative) phosphoproteomic workflow and table 1 about Overview on features of improved LC-MS sample preparation methods and their advantages.

The peer-reviewed research article by Gratani, F.L. *et al.* (2023) “*E. coli* toxin YjjJ (HipH) is a Ser/Thr protein kinase that impacts cell division, carbon metabolism, and ribosome assembly”, I contributed to the Figure 3D and 4A as well as supplementary figures S4D-F, S5C, and S8. This study was designed by Fabio Lino Gratani and Boris Macek. I performed the validation experiments for substrates of YjjJ. This included performing growth assay, proteome, and phosphoproteome analysis in Δ*hipBA E. coli* to validate the findings from WT background. I also performed the cloning and growth assays for CsrA and CsrA mutant overexpression, the *in vitro* kinase assay, and the growth assay and proteome analysis for Δ*yjjJ*. For these experiments, I also prepared the samples for mass spectrometry measurements and analyzed the MS data under the supervision of Boris Macek.

The research article by Nashier, P. *et al.* (2024) “Deep phosphoproteomics of *Klebsiella pneumoniae* reveals HipA-mediated tolerance to ciprofloxacin”, underwent peer-review and is currently under revision in PLOS Pathogens. It has received mostly positive comments from the reviewers but requires a few additional experiments before re-submission. This study was designed by Boris Macek, Sandra Schwarz, and me. I performed cloning and transformation of HipA and HipB genes to perform growth assays in *E. coli*. Due to the lack of Bio Safety Level 2 availability in our lab, most of the *K. pneumoniae* work was performed in collaboration with Dr. Schwarz where I participated in cloning and initial overexpression experiments in *K. pneumoniae*. All proteomics and phosphoproteomics experiments in both *E. coli* and *K. pneumoniae* were designed and performed by me including MS sample preparation, measurement, processing, statistical analysis, and its interpretation under the supervision of Boris Macek. I also prepared all the figures, tables, datasets, and manuscript contents with inputs from Boris Macek, Sandra Schwarz, and other authors.

1. Introduction

Signal transduction is the mechanism by which an external stimulus or signal is transmitted to the cell. These signals can be transmitted through the signaling molecules present inside or on the surface of cells. These molecules bind to a specific protein receptor on the cell and pass the signal inside. This binding gives rise to a chain of biochemical events, which form a signaling pathway, where the signal is transferred via molecules within the cell to trigger specific responses inside the cell such as cell death or proliferation. Signal transduction plays an essential role in normal cellular function and growth as well as in a rapid response to changing environments. The cascade of events in signal transduction can eventually modulate the expression of certain genes and proteins by up- or down-regulating the transcription and translation levels required for the response.

1.1 Protein phosphorylation in bacteria

One of the fastest mechanisms to transmit signals is the modification of pre-existing proteins in the cell via post-translational modifications (PTM). PTMs include the addition or modification of small proteins, such as ubiquitin, or functional groups to the side chains or C- or N-termini of an amino acid in a protein. It also includes the formation or breakdown of certain bonds in a protein such as peptide bond cleavage or disulfide bond formation in cysteines. For instance, the discovery of proinsulin by Donald F. Steiner in 1967 was the first demonstration of proteins undergoing post-translational processing to form a functionally active protein (*1, 2*). PTMs can play several important roles in governing different cellular functions such as cell cycle regulation (*3, 4*), cellular pluripotency (*5*), cell metabolism (*6*), dormancy, and sporulation (*7*).

More than 300 PTMs have been identified, however, the most common covalent modifications include phosphorylation, glycosylation, lipidation, succinylation, ubiquitylation, and acetylation. PTMs are often dynamic and reversible, allowing a faster adaptation to stimuli by modulating the protein levels without the need for synthesis or degradation of the protein. They are also sub-stoichiometric, meaning that all copies of a protein in the cell at a given time might not have the modification (*8*). The fact that

these modifications can also occur in various combinations vastly increases the overall diversity of proteins in a cell (**Figure 1**).

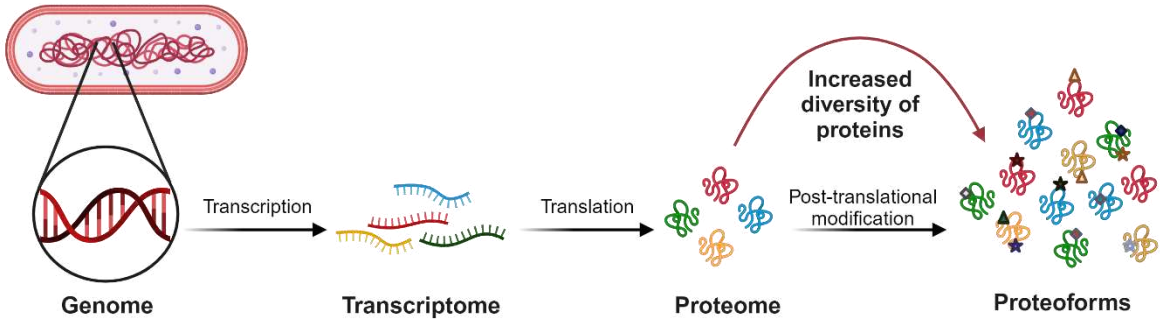

Figure 1. **Increase in protein diversity through post-translational modifications in bacteria.** This figure depicts the flow of genetic information in bacteria, showcasing how PTMs play an important role in increasing protein diversity by generating multiple proteoforms from a single protein. This figure was created with BioRender.com.

Protein phosphorylation is the most widespread and extensively studied regulatory mechanism for signaling via post-translational modifications across all domains of life. Protein phosphorylation is catalyzed by protein kinases through an addition of a phosphate group ($-PO_4^{3-}$) on the side chain of certain amino acids in a protein. Protein phosphorylation majorly uses ATP (adenosine triphosphate) as a phosphoryl donor but can also utilize guanosine triphosphate (GTP) and phosphoenol pyruvate (PEP) in the cell (*9*). The phosphorylation can be on a single amino acid or at multiple positions within the same protein. Protein phosphorylation can be reversed by the removal of the phosphate group by proteins called phosphatases. Kinases and phosphatases are tightly regulated to control the protein function by resulting in conformational changes, altering their interaction, activity, stability, folding, and localization to quickly adapt to extracellular signals by addition or removal of a phosphate group (*10*). Due to the distinct size of the ionic shell and the charge associated with the covalently bound phosphate, specific and inducible interactions are facilitated, such as the modification of the biological activity of a protein, its localization, stability, and interactions with other proteins or DNA or RNA (*9, 11*). Serine, threonine, and tyrosine are the most frequently phosphorylated amino acids. These amino acids undergo O- phosphorylation as they make a stable phosphomonoester bond between the -OH group and phosphate (**Figure**

2) (*11*). Besides the canonical phosphorylation of S, T, and Y, recent studies have revealed that phosphorylation can occur on the side chains of several other amino acids such as arginine, lysine, histidine, cysteine, glutamic and aspartic acid (*12-15*). These non-canonical phosphorylation events expand our understanding of protein regulation and signaling mechanisms. These include the A- phosphorylation via -COOH group of aspartic acid and glutamic acid, the S- phosphorylation via -SH group of cysteine and the N- phosphorylation via ε-NH_2 group of lysine, any of the nitrogen from guanidine group of arginine (primarily occurring on terminal -NH_2) (*16*) and either of the two nitrogen on -$C_3H_4N_2$ (Imidazole) group of histidine (*17*). These non-canonical phosphorylations are highly prone to hydrolysis at high temperatures and low pH and require enrichment techniques with neutral pH (*13*).

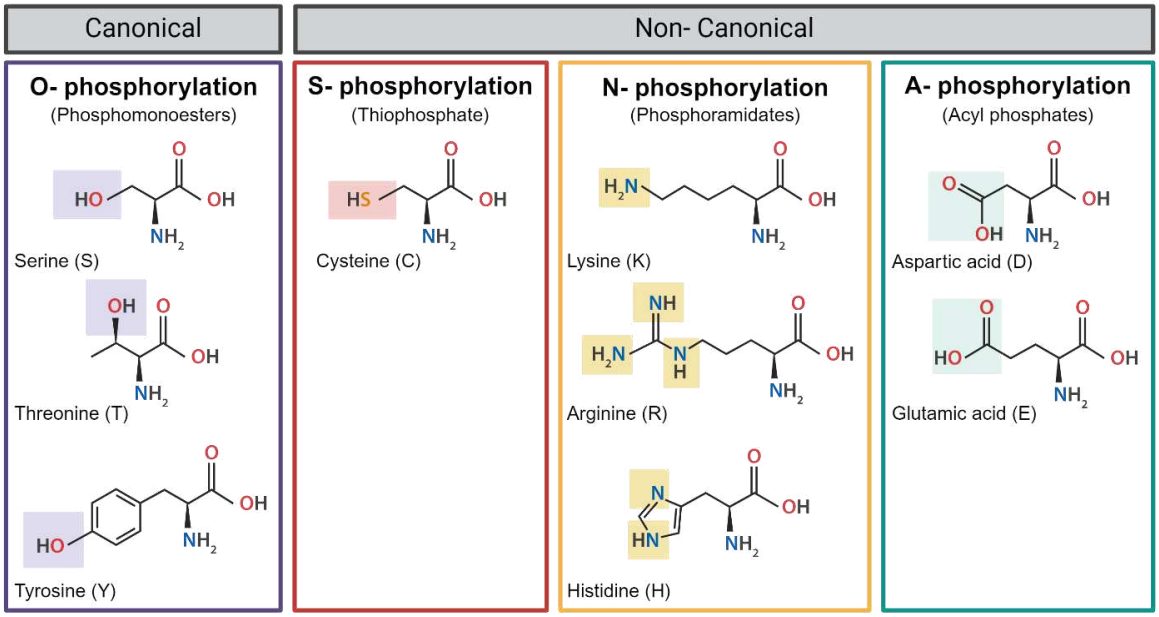

Figure 2. **Phosphorylation of amino acids in proteins**. This figure illustrates the various amino acids that can be phosphorylated in proteins. Canonical phosphorylation primarily occurs on serine (S), threonine (T), and tyrosine (Y) residues. In contrast, non-canonical phosphorylation can take place on cysteine (C), lysine (K), arginine (R), histidine (H), aspartic acid (D), and glutamic acid (E) residues. This figure was adapted from Low *et al.* 2020 (*18*) and created with BioRender.com.

In bacteria, the proteins are phosphorylated by the two-component system (TCS). TCS comprises a histidine kinase (HK), that acts as a sensor and a response regulator (RR). An external stimulus causes the N-terminal sensor domain of HK to undergo conformational changes, which are then transmitted to the C-terminal transmitter

domain (*19*). Then, the kinase becomes active and autophosphorylates itself at a histidine residue in the C-terminal domain. Next, this phosphorylation is transferred to the response regulator on a conserved aspartate residue in its regulatory domain. Aspartate phosphorylation activates the variable effector domain and undergoes conformational changes to control the expression of target genes triggering the necessary response (*20*). The effector domains are mainly DNA-binding acting as transcriptional regulators but also include RNA binding or participate in protein-protein interactions (*21, 22*). Many HK also have phosphatase activity to dephosphorylate their corresponding RR (*23*). His-Asp systems have also been found in archaea and a few eukaryotes like plants (*24*).

While the TCSs were predominantly thought to regulate multi-step signal transduction by phosphorylation in bacteria, Serine/Threonine kinases (STKs) were considered mainly phosphorylating proteins in eukaryotes. This changed in 1969 when a cAMP-dependent Ser/Thr kinase was identified in *Escherichia coli (25)*, although the substrate of this kinase was not identified. A decade later, isocitrate dehydrogenase in *E. coli,* was the first protein substrate identified to be phosphorylated in bacteria *(26)*. However, the kinase responsible for this phosphorylation did not exhibit sequence homology to eukaryotic kinases, as it was a bifunctional protein with both kinase and phosphatase activities (*27*). Subsequently, the first eukaryotic-type STK was identified in *Myxococcus xanthus*. Initially, only a few bacteria were shown to have eukaryotic-type STKs. However as whole genome sequencing became available, more STKs were predicted and discovered in various bacteria (*28*). In the last few decades, additional research has confirmed that STKs are quite prevalent in bacteria and regulate various cellular processes.

1.1.1 Types of protein kinases in bacteria

Bacterial protein kinases can be categorized into four major groups: Ser/Thr kinases, Bacterial tyrosine kinases (BY), Histidine kinases, and Arginine kinases (**Figure 3**). All of these kinases play an essential role in various cellular pathways such as metabolism, cell division, sporulation, and stress response (*29*).

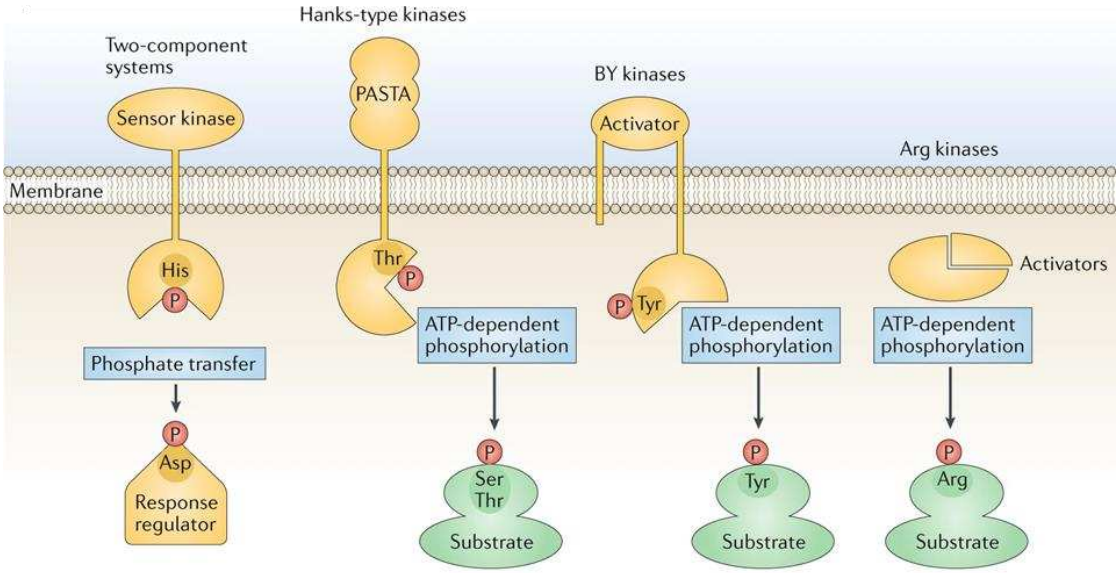

Figure 3. **Types of kinases involved in phosphorylation in bacteria**. This figure shows different types of kinases that facilitate phosphorylation in bacteria. They are categorized into different groups based on the specific amino acid modified. This figure was taken from Macek *et al.* 2019 (*8*).

1. STK phosphorylate serine or threonine residues on their substrates. These are the most abundant kinases and are known to have diverse roles in bacterial physiology including metabolism, virulence, and stress response. Ser/Thr protein kinases can be further categorized as classical eukaryotic-type (Hanks-type) and atypical kinases. Hanks-type kinases, as defined by Hanks and Hunter in 1995, possess a well-conserved catalytic domain of 250-300 amino acids, which fold into a common catalytic core structure (*30*). In contrast, atypical protein kinases share low sequence similarity with Hanks-type kinases, yet they still adopt the canonical eukaryotic protein kinase fold. Both kinase type features two main structural lobes, the N-lobe, composed of beta-sheets, and the C-lobe, made up of alpha-helices. These two lobes are connected by a short linker of three to five residues, and ATP binds in the cleft formed between them (*31*). Atypical kinases lack some of the highly conserved motifs found in typical kinases, such as the glycine-rich motif, and instead contain an inverted HRD (His-Arg-Asp) motif. They also display modifications in their regulatory and catalytic hydrophobic spines, distinguishing them from classical kinases (*31*). For example, YihE is an atypical Ser/Thr kinase in *E. coli* that shows high structural similarity to classical Ser/Thr kinases despite low sequence homology (*32*). Similarly,

CotH, a spore coat protein H, is an atypical protein kinase in *Bacillus subtilis,* which possesses a unique ATP binding mechanism along with a protein-kinase fold (*33*).

2. Bacterial tyrosine kinases specifically phosphorylate tyrosine residues. They typically consist of two different polypeptides that interact to activate the kinase or a single membrane protein. When a ligand binds to the extracellular domain, it activates the transmembrane part leading to its conformational change that facilitates phosphorylation via the C-terminal catalytic domain. This domain consists of four conserved structural motifs including Walker A, A' and B motifs, and a tyrosine cluster, which can undergo autophosphorylation to regulate the kinase activity (*34, 35*).
3. Histidine kinases are a part of two-component systems that are involved in bacterial sensing and responding to environmental changes (*19*). These kinases autophosphorylate on a histidine residue followed by its subsequent transfer to the response regulator, which results in the activation of various downstream signaling pathways.
4. Arginine kinases phosphorylate their substrates on arginine residues, forming a phosphoramidate bond (P-N bond). In *B. subtilis*, the McsB protein arginine kinase regulates the levels of ClpC-ClpP proteases by phosphorylating their repressor, CtsR (*36*). In addition, McsB also phosphorylates several other proteins, including misfolded or aggregated proteins, at arginine residues. This pArg acts as a degradation tag, which is later recognized by ClpCP proteases for targeted degradation (*37*).

However, some proteins can also exhibit dual-specificity, possessing both kinase and phosphatase activity. HPrK/P (kinase/phosphorylase), found in Gram-positive bacteria, is a bifunctional protein that can phosphorylate and dephosphorylate HPr on serine residue using the same active site. This protein is important for catabolite repression and allows the enzyme to regulate the activity of HPr protein and control metabolic processes based on nutrient availability (*33*).

1.1.2 Cross-talk between different types of kinases

Numerous bacteria have been shown to exhibit functional cross-talk between TCSs and STKs, including *M. xanthus*, *E. coli*, *Streptococcus pneumoniae*, *Bacillus subtilis*, and *Mycobacterium tuberculosis (32, 38-41)*. In these systems, activation of TCSs upregulates the transcription or activation of Ser/Thr kinases or vice-versa. Response regulators may be phosphorylated by STKs, irrespective of their cognate histidine kinase. This dual regulation by both HKs and STKs adds complexity to the regulation of RR activity (*42*).

The first example of a kinase cascade interacting with two-component signaling was found in *M. xanthus* where a transcription activator, MrpC, essential for fruit body formation and sporulation is regulated by the TCS MrpAB. However, the regulation of MrpC involves an additional layer, where the STK Pkn8 phosphorylates another STK Pkn14, which in turn phosphorylates and inhibits MrpC (*41*). In *E. coli,* YihE participates in a phospho-relay mechanism involving a modified TCS, with CpxA as the sensor HK, CpxR as RR, and a periplasmic protein CpxP, which inactivates the Cpx pathway (*43*). TCS phosphorylation is crucial for sensing stress and transcriptionally upregulating Ser/Thr kinase to maintain the cell envelope integrity, ensuring stress response (*32*). Similarly, PrkC, a Ser/Thr kinase in *B. subtilis,* regulates the TCS WalRK by phosphorylating WalR, impacting gene regulation in cell wall metabolism (*38*). StkP in *S. pneumoniae* phosphorylates ComE, a response regulator of the histidine kinase ComD, enhancing its DNA-binding affinity and regulating the genes associated with stress response (*39*). In *M. tuberculosis,* phosphorylation of the NarS, a histidine kinase by Ser/Thr kinases activates it, leading to auto-phosphorylation and stimulation of downstream signaling (*40*).

As serine/threonine kinases can phosphorylate a wide range of substrates and interact with other kinases via cross-talk, they play a crucial role in bacterial signaling networks. In *B. subtilis,* various kinases such as tyrosine kinase, Hanks-type Ser/Thr kinase, two-component-like Ser/Thr kinase, and dual-function kinase/phosphatase, have been shown to interact and phosphorylate each other. (*44*). In *M. tuberculosis*, Hanks-type Ser/Thr kinases can be phosphorylated by tyrosine kinases, which regulate their activity

(*45*). This functional cross-talk highlights the intricate relationships between different kinases and their dynamic role in regulating bacterial signaling.

1.1.3 Ser/Thr kinases in bacteria and their role

Serine/threonine phosphorylation affects both fundamental physiology and pathogen-specific processes in bacteria. Many Ser/Thr kinases have been associated with multiple functions related to infectious diseases, including their role in cell adherence to the host, as well as pathogen virulence, replication, and persistence. In the late 1980s, Ser/Thr and Tyr (STY) phosphorylation was found in many bacteria such as *E. coli*, *Salmonella typhimurium*, *B. subtilis,* among others, using biochemical analysis (*46*). The first well-characterized eukaryotic-type Ser/Thr kinase was identified in *M. xanthus,* a Gram-negative bacterium typically found in soil, which demonstrated how kinase contributes to the onset of cell differentiation for spore formation (*47*). This highlighted the significance of STK in the regulation of bacterial cellular processes.

The presence of eukaryotic-type Ser/Thr kinases in prokaryotes raised the question if they originated from eukaryotes. The average GC content and codon usage of these Ser/Thr kinase genes in cyanobacteria were analyzed, as cyanobacteria had the highest number of STK in sequenced bacteria. They were found to have a similar average GC content and codon usage to other cyanobacterial genes, pointing towards their origin to be authentic prokaryotic ones (*48*). A more recent phylostratigraphy analysis showed the origin of eukaryotic-type protein kinases to LUCA (Last Universal Common Ancestor). These kinases belong to an ancient and universal protein family that has a monophyletic origin and are not solely connected to eukaryotes. Therefore, Hanks-type kinases are a more appropriate name rather than eukaryotic-type protein kinases as it incorrectly points to their origin from eukaryotes via horizontal gene transfer or convergent evolution, which is not the case (*49*).

STKs play an essential role in bacterial physiology and can perform many diverse functions in different bacteria. These include regulation of metabolism, virulence, sporulation, antibiotic tolerance, stress adaptation, and phage defense (**Figure 4**). These functions are further explained in the sections below. Special attention will be put

to the role of STKs in the regulation of metabolism and antibiotic tolerance in *E. coli* and *K. pneumoniae*, in manuscripts II and III, respectively.

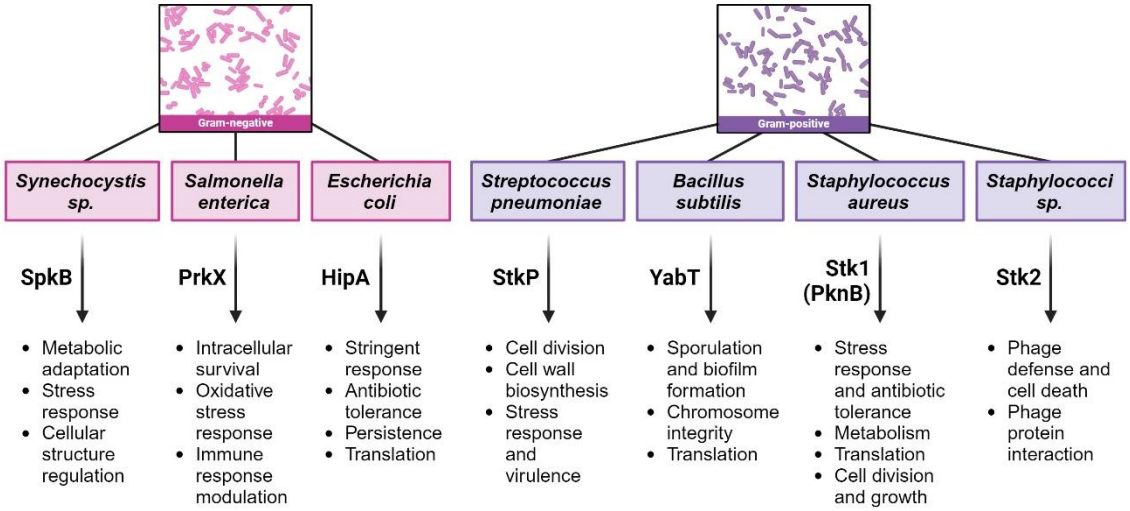

Figure 4. **Role of different Ser/Thr kinases in regulating various bacterial processes**. Different cellular pathways/ processes are regulated by STKs in bacteria. Gram-negative bacteria are shown in pink and Gram-positive in purple. STK found in each bacterium are written alongside arrows and points to the functions affected by them. This figure was created with BioRender.com.

1.1.3.1 Role in response to environmental stimuli in *Synechocystis sp.*

Protein phosphorylation is a dynamic process that can occur in response to various environmental stimuli, such as changes in light, nutrient supply, or osmolarity. Under nitrogen starvation conditions, in cyanobacteria, *Synechocystis sp.*, many proteins involved in different metabolic pathways are shown to be phosphorylated (*50*). This includes upregulation of phosphorylation on sensory nitrogen signaling protein, P_{II} protein on its Ser49. This protein is a marker for nitrogen-limited conditions. Proteins involved in the uptake of inorganic carbon, such as carbon-dioxide concentrating mechanism (Ccm) proteins M and N, also exhibited multiple phosphorylation sites. Protein phosphoribulokinase has also shown increased phosphorylation upon nitrogen starvation. In addition, proteins involved in photosynthesis, the pentose phosphate pathway, and glycolysis also depicted increased phosphorylated under nitrogen depletion conditions. Two Ser/Thr protein kinase F (Slr1225) and kinase C (Slr0599) also show varying phosphorylation levels (*50*). These kinases were previously shown to autophosphorylate in an *in vitro* radiolabeling experiment. This demonstrates that

protein phosphorylation plays an important role in regulating metabolic adaptation in cyanobacterium *Synechocystis*.

SpkB (Slr1697) is a Ser/Thr kinase in cyanobacteria *Synechocystis sp.* PCC6803 with significant roles in various cellular processes including response to environmental stress, carbon metabolism, and cellular signaling. Δ*spkB* mutant (gene knockout) demonstrates slower growth, particularly under glucose supplementation and low carbon conditions. Low carbon condition also shows a bleaching phenotype due to decreased amounts of phycobilipigments and chlorophyll *a* (*51*). Proteome analysis of mutant reveals significant changes in cell surface and pilin proteins, leading to a loss of motility, which was also previously shown in Kamei *et al.* 2003 (*52*). SpkB exhibits autophosphorylation activity that is sensitive to redox conditions. This regulation allows phosphorylation of proteins like Glycyl-tRNA synthetase β-subunit (GlyS) (*53*). Further confirmation of the role of SpkB in the cellular response to oxidative stress is shown by the phosphorylation of essential proteins for redox regulation such as glutathione S-transferase. Growth of Δ*spkB* mutant is also affected under conditions such as high light or iron starvation, which also causes redox imbalance in bacteria (*53*). This indicates the role of Ser/Thr kinase in adapting to different redox conditions.

1.1.3.2 Role in pathogenesis in *Salmonella enterica*

Salmonella species are important global pathogen that infects a range of hosts, causing several diseases such as typhoid fever and gastroenteritis. These bacteria are one of the leading causes of disease and mortality in underdeveloped nations among humans. (*54*). After ingestion of bacteria orally, long-term survival of *Salmonella* is possible in the acidic environment of the stomach. It then moves to the intestine and invades intestinal epithelial cells through bacterial-mediated endocytosis. This invasion stimulates inflammation and fluid secretion, leading to gastroenteritis, or allows bacteria to enter intestinal macrophages and spread throughout the reticuloendothelial system, causing typhoid fever (*55*). Among *Salmonella* species, *S. enterica* is considered the most pathogenic species, with multiple serotypes contributing to its virulence.

Genomic analysis has shown that genes necessary for specific virulence phenotypes are clustered in localized regions of chromosomes called pathogenicity islands (PIs).

These PIs are often acquired by horizontal gene transfer and usually have a distinct GC content in comparison to the rest of the chromosome. They are flanked by genes that are contiguous in related bacteria and often contain remnants of bacteriophage or transposon insertion sequences near their borders. In *Salmonella,* two pathogenicity islands have been identified, namely SPI-1, which contains genes necessary for the invasion of the intestinal epithelium, and SPI-2, which mediates the survival of bacteria within macrophages (*56*).

Three ORFs in the genome of *S. enterica* serovar Typhi (S. Typhi) were found in PIs, encoding proteins homologous to STKs (*prkX* and *prkY*) and STPs (*prpZ*). The transcription of *prpZ, prkX,* and *prkY* genes is down-regulated by oxidative stress induced by HOCl, whereas H_2O_2 leads to the downregulation of *prpZ* and *prkY*. There is marginal up-regulation of transcription of *prkX* by oxidative stress induced by H_2O_2. While not necessary for bacterial survival in oxidative stress, this gene cluster influences bacterial uptake and long-term survival in macrophages. The knockout of the *prpZ* gene cluster shows an increased level of phagocytosis and lower survival of bacteria 48 hours post-infection compared to normal bacteria containing the *prpZ* gene cluster (*57*).

Additional studies showed that PrkX (T4519) is a Hanks-type Ser/Thr kinase that exhibits autophosphorylation activity when stimulated in a reactive oxygen species (ROS)-dependent manner within macrophages. PrkX is translocated from *Salmonella*-containing vesicles (SCV) to the host cytoplasm, modulating the immune response of macrophage. It acts on host cellular proteins, such as phosphorylation of myelin basic proteins (MBPs) significantly increases the levels of proinflammatory cytokines. Decreased amounts of cytokines, tumor necrosis factor-alpha (TNF-α), and interleukin-6 (IL-6), are observed in mouse serum and supernatant of macrophage cultures infected with the *prkX* mutant in comparison to wild-type bacterial infections. In wild-type bacterial infections, increased levels of cytokines such as TNF-α can enhance intracellular pathogen survival by inducing Lysosomal membrane permeabilization (LMP) or by inhibiting antimicrobial peptide expression (*58*). This kinase plays an important role in the pathogenesis of *S. Typhi*, as shown in an *in vivo* study where infection of mice with wild-type and *prkX* mutant bacterial strains displayed an increased survival of mice

infected with mutant compared to 100% lethality in wildtype bacterial infections. Therefore, PrkX enhances the intracellular survival of the bacteria, making it a key factor in *S. enterica* virulence increased (*58*).

1.1.3.3 Role in cell division in *Streptococcus pneumoniae*

S. pneumoniae is an opportunistic bacteria whose virulent and encapsulated strains are a major cause of sepsis, pneumonia, and meningitis in children (*59*). These bacteria have several TCSs and only one Hanks-type STK, StkP. These eukaryotic-type kinases have been associated with several functions in pneumococcal physiology including regulation of virulence, competence, stress resistance, and gene expression. StkP is a transmembrane protein containing a kinase domain on the cytosolic side and an extracellular signaling domain at C-terminus. This extracellular domain contains repeats of penicillin-binding protein and Serine/Threonine kinase-associated domain (PASTA), which are required for activation of the kinase and its substrate recognition at the C-terminus and also shown to bind to the beta-lactam rings of antibiotics (*60*), which resemble D-Alanine-D-Alanine motif of peptidoglycan stem peptide. Therefore, STKs with the PASTA domain can regulate cell wall synthesis by sensing unlinked peptidoglycan subunits. This signaling leads StkP to localize at the cell-division site and promotes its activation and autophosphorylation (*61*). StkP has its cognate protein phosphatase, PhpP, which specifically dephosphorylates the autophosphorylation on StkP in the presence of manganese ions (*62*). Sublethal quantities of penicillin and cefotaxime are shown to act as environmental inducers increasing the expression of genes *stkP* and *phpP* and phosphorylation of StkP. Deletion of PhpP leads to a phenotype exhibiting higher levels of StkP phosphorylation and penicillin-binding protein-independent antibiotic resistance in *S. pneumoniae (63)*.

Phosphoglucosamine mutase GlmM is a substrate of StkP. GlmM facilitates the first step in the biosynthesis of a precursor, peptidoglycan, which is an important component of the cell envelope (*62*). Immunofluorescence microscopy has shown the localization of StkP along with FtsZ to the cell-division site, where it also phosphorylates FtsZ (*64*). Further analysis confirmed that StkP localizes in the midcell and comes to the cell-division site soon after the assembly of FtsA, an early cell division protein, but before

DivIVA, and it remains there until the division is complete. Inactivation of the kinase (Δ*stkP*) led to an elongated phenotype with multiple unconstricted FtsA and DivIVA rings, indicating the role of this kinase in regulating cell growth and division (*65*). Several substrates of StkP have been identified highlighting its role in bacterial physiology. These include the phosphorylation of proteins, such as DivIVA, FtsZ, GpsB, Jag, and LocZ/MapZ, which are associated with cell division. Other cell division proteins, FtsA and MurC are also shown as indirect substrates of StkP for controlling correct septum progression and closure. GlmM, GlmS, UppS, MltG, MurM, and MacP are the phosphorylated proteins involved in cell wall precursor synthesis. StkP cross-talks with WalRK TCS and also targets three response regulators: RR06 and ComE, and the orphan response regulator RitR. These proteins are identified as targets of both StkP for phosphorylation and PhpP for dephosphorylation based on the hyperphosphorylation of StkP targets observed in the Δ*phpP* mutant strain. In addition, numerous proteins associated with replication, transcription, translation, and metabolism are also phosphorylated (*66*).

These diverse roles of StkP in *S. pneumoniae* are important for understanding its pathogenicity and survival mechanism. These findings can play a significant role in uncovering new therapeutic targets and strategies for the eradication of bacterial infections. With the information about the potential involvement of this kinase in various biological processes, this kinase and its affected pathways can be targeted for developing novel antibiotics that inhibit these pathways to overcome antibiotic resistance and improve the treatment of pneumococcal diseases.

1.1.3.4 Role in sporulation in *Bacillus subtilis*

In *B. subtilis*, four Ser/Thr kinases have been characterized, with three of them, PrkA, PrkC, and YabT, playing important roles in different stages of the sporulation process (*67*). YabT is a transmembrane protein kinase that lacks the characteristic extracellular sensing domain of STKs. Instead, it is attached to the membrane via a transmembrane helix at the C-terminal. It possesses a DNA-binding motif, which is required for its activation.

YabT is expressed at the beginning of sporulation under the control of a sigma factor σ^F, which is active only in the forespore and not in the mother cell. It has been experimentally shown to be expressed only in the forespore (*68*). YabT gets activated by the binding of DNA that enters the forespore. This DNA-binding supports the formation of dimers and activation of the kinase by trans-autophosphorylation (*69*). YabT localizes to the asymmetric septum and phosphorylates DNA-recombinase RecA, ensuring chromosome integrity during spore development. Phosphorylation of RecA results in the formation of RecA foci that move with the nucleoid in the mother cell. The mutant of Δ*yabT* has similar phenotypes to those of the phospho-ablative RecA mutant, which sporulates more slowly and shows reduced resistance to DNA damage during sporulation. This indicates that YabT acts via phosphorylation of RecA (*7*). In addition, the single-stranded DNA-binding protein SsbA is a target of YabT, which enhances its cooperative binding to DNA (*70*). YabT also targets the replication controller YabA, which plays a dual role in the regulation of replication initiation and switching the life cycle to sporulation or biofilm formation. Biofilms are collections of bacteria encased in an extracellular polymeric matrix that the bacteria generate on their own using materials such as polysaccharides, DNA, and proteins to aid in adhesion to surfaces or one another. Increased phosphorylation of YabA has been shown to increase the efficiency of sporulation and strongly inhibit the formation of biofilms. This also connects with increased cellular levels of Spo0A-P, a key regulator that stimulates sporulation (*71*).

During dormancy, the mature spore is released by the mother cell. The overall metabolism, including protein synthesis, is downregulated. YabT phosphorylates elongation factor Tu (EF-Tu), and this phosphorylation mediates the downregulation of protein synthesis. The phosphorylated EF-Tu does not have GTPase activity and remains attached to the ribosomes, stalling the process of translation elongation and thereby inhibiting overall protein synthesis. This phosphorylation was shown to be not present in spores of the *yabT* mutant, confirming that YabT is responsible for the phosphorylation of EF-Tu (*68*). These findings highlight the role of YabT in maintaining genetic stability and regulating protein synthesis during sporulation in *B. subtilis*. Understanding the role of this Ser/Thr kinase, in addition to others like PrkA,

PrkC, and PrkD, can provide additional insights into the regulation of bacterial adaptation and survival mechanisms, which can lead to novel targets for antimicrobial strategies.

1.1.3.5 Role in quiescence and tolerance in *Staphylococcus aureus*

S. aureus is an opportunistic pathogen, generally prevalent in the human microbiota, but it also causes a wide range of infections that can be acquired in hospitals or the community. In addition to causing skin and soft-tissue infections, it can result in serious, perhaps fatal illnesses such as bacteremia, endocarditis, sepsis, meningitis, and toxic shock syndrome (*72*). The rise in antimicrobial resistance has made the treatment of these infections even more challenging. This resistance requires prolonged treatments and extended hospitalization, thereby increasing the burden on the healthcare systems.

Beyond antibiotic resistance, *S. aureus* can also develop antibiotic tolerance or persistence, which leads to chronic and reoccurring infections, even when the bacteria remain susceptible to antibiotics. One of the mechanisms underlying antibiotic tolerance is bacterial quiescence, where bacteria enter an inactive dormant-like state to survive unfavorable environmental conditions. Since most antibiotics target actively growing cells, these slow-growing or growth-arrested bacteria can survive prolonged antibiotic treatments. This quiescent persister state, therefore, serves as a survival strategy during infections (*73*).

In *S. aureus*, the Hanks-type Serine/Threonine kinase Stk1/PknB has been associated with the regulation of bacterial signaling, central metabolism, stress response, antibiotic resistance, and virulence. PknB is associated with its cognate phosphatase Stp, forming a kinase-phosphatase pair that has been broadly studied for its role in regulating bacterial growth and antibiotic tolerance in *S. aureus*. PknB exhibits autokinase activity and is localized to the bacterial membrane. It is shown to be dephosphorylated by Stp in the presence of manganese (*74*). PknB has several phosphorylation sites in the activation loop that regulate the catalytic activity of this protein kinase. Out of these, phosphorylation of Thr172 is the first step, which causes conformational changes and is essential for functionally active kinase. Following Thr172, further interactions with other molecules of PknB phosphorylate other residues by trans-autophosphorylation to

support kinase activity (*75*). Additionally, a study on a methicillin-resistant strain has shown that the mutant of *pknB* showed increased susceptibility to β-lactam antibiotics, potentially regulating sigma factor SigB, which is involved in the stress response. Activation of SigB is linked to reduced virulence in *S. aureus* and the mutant also showed compromised response to heat and oxidative stresses (*76*).

Further research demonstrated that acidic environments, akin to those present in host tissues, caused *S. aureus* to develop more slowly and enhanced its resistance to antibiotics. Under acidic conditions, PknB becomes activated and phosphorylates several proteins associated with processes such as cell growth, translation, and metabolism. Phosphoproteome analysis showed increased phosphorylation in bacteria exposed to acidic stress compared to those grown at neutral pH. These phosphorylated proteins include those involved in cell division, glycolysis, signaling, and translation, such as ribosomal proteins and elongation factors, along with increased threonine phosphorylation in the activation loop of PknB. It was shown that deletion mutant of *stp* extended the lag phase, reduced intracellular ATP levels and protein synthesis, and ultimately enhanced persistence and antibiotic tolerance in bacteria grown in the presence of acidic stress, cultured with human cells, or harvested from abscesses in mice (*73*). This highlights the involvement of Stp in modulating the function of PknB. Both the active, phosphorylated PknB and the *stp* mutant exhibited similar phenotypes, characterized by an extended lag phase and increased antibiotic tolerance. Thus, strategies aimed at inhibiting PknB or overexpressing Stp during infection can make *S. aureus* more susceptible to specific medications and prevent the formation of persister cells. While different classes of PknB inhibitors have been proposed and tested as novel antibacterial compounds, their efficacy has been limited. Therefore, the development of novel inhibitors and optimization of existing ones are essential for fighting *S. aureus* infections (*77*).

1.1.3.6 Role in defense against phage infection in *Staphylococci sp.*

Bacteria have developed several strategies to fight bacteriophage (bacterial viruses) infections, targeting different stages of the phage life cycle. These strategies include blocking phage adsorption, preventing entry of DNA via superinfection exclusion

systems, cleavage of phage DNA through restriction-modification systems, interfering with DNA replication using CRISPR-Cas systems, and inhibiting phage protein synthesis, maturation, and host lysis through abortive infection (Abi) systems, which often result in death of infected bacterial cells (*78*). These mechanisms are highly diverse across bacterial species and even between strains of the same species.

In *Staphylococci*, the Hanks-type Ser/Thr kinase Stk2 has been recognized as a key player in phage defense. Research on different strains of *S. epidermidis* with deletions in the CRISPR locus revealed that sensitivity to a temperate bacteriophage correlated with the presence of a gene identical to *S. aureus* gene *stk2*. When *stk2* was expressed in other *S. aureus* strains lacking this gene, those strains gained resistance to multiple phages. The kinase activity of Stk2 was found to be essential for its role in phage defense. Notably, it has been demonstrated that Stk2 is only activated when a phage protein is present (*79*). Stk2 activation leads to abortive infection where phage-infected bacteria undergo self-destruction to prevent phage amplification and spread (*80*). Among the identified phage proteins, PacK, which is involved in phage DNA packaging, directly interacts with Stk2 triggering its activation. Upon activation, Stk2 phosphorylates a large number of bacterial proteins, leading to cell death and thus halting phage propagation. Another kinase in *Staphylococci,* Stk1/PknB, also contributes to the phage defense pathway, particularly by preventing the release of phage particles before Stk2-mediated cell death occurs. While *stk1* mutants showed a decline in the ability of Stk2 to protect against phages, Stk2 activation alone led to cell death. This indicates that while Stk1 contributes to effective antiviral immunity, Stk2-mediated antiviral immunity does not require Stk1 to function. (*79*).

Phages are increasingly used as potential antimicrobial agents in phage therapy, particularly against antibiotic-resistant bacteria. Phage therapy could offer an effective treatment for difficult-to-treat infections such as those involving biofilms or persistent cells, which are otherwise difficult to treat with conventional antibiotics. However, not all classes of phages are suitable for phage therapy. For instance, Siphoviridae phages, often temperate, go through a lysogenic cycle in which they incorporate their genetic material into the bacterial genome, possibly transferring antibiotic-resistance genes or

enhancing bacterial virulence. In contrast, Podoviridae phages, which have a compulsory lytic cycle and a compact genome, are ideal candidates for therapeutic applications. Recent studies have isolated and characterized *S. epidermidis*- infecting phages from the human skin microbiome to test their effectiveness against a range of staphylococcal strains, including those making biofilms (*81*). Therefore, continued exploration of phage diversity and their interactions with bacterial hosts could significantly advance phage therapy approaches.

1.1.3.7 Role in antibiotic tolerance and persistence in *Escherichia coli*

In *E. coli*, the Ser/Thr kinase HipA (high persistence A) is a well-characterized protein associated with the induction of bacterial persistence. During persistence, a subpopulation of bacteria enters a dormant-like state, which allows them to survive during antibiotic treatments, despite being genetically identical to the sensitive population. These bacteria are capable of giving rise to a normal population upon removal of antibiotics, leading to the development of multidrug-tolerant persister cells (*82*). A mutant of this kinase, *hipA7* was the first gene identified to increase antibiotic persistence by increasing the frequency of persister cell formation in *E. coli (83)*.

HipA is a part of a type II toxin-antitoxin (TA) system. In this type of TA system, both the toxin and antitoxin are proteins, and under normal conditions, they are bound to each other. This inhibits the activity of the toxin. The transcription of TA is repressed by binding to both the antitoxin and the TA complex. However, stress conditions activate cellular proteases such as Lon and ClpXP, which cleave the antitoxins. This leads to growth arrest by inhibiting translation or replication via free toxins (*84*). In the case of HipBA, HipA functions as the toxin and binds to the antitoxin HipB to form an inactive complex, neutralizing the toxic effect of HipA (*85*). HipB also contains a DNA-binding region (helix-turn-helix, HTH domain) and represses the *hipBA* operon by cooperative binding to four operator sites in the promoter region (**Figure 5**) (*85, 86*). This interaction between HipA and HipB leads to the formation of the HipA-HipB complex, causing the dimerization of HipA, which blocks its active site and causes conformational inactivation (*87, 88*).

The regulation of HipB involves its degradation by proteolysis. When HipA binds to HipB, it blocks its access to Lon proteases by shielding the C-terminus of HipB. During environmental stresses, such as nutrient starvation or antibiotic exposure, Lon proteases are upregulated, degrading HipB and releasing active HipA (*89*). This release induces a dormant-like state in the bacteria, which helps in their survival under adverse conditions. The levels of *hipBA* regulate the onset and duration of a transient growth arrest such that only above a certain threshold level of *hipA,* does this transient dormant state take place. This variability in gene expression resulted in the co-existence of normally growing and dormant cells in the genetically identical population (*90*).

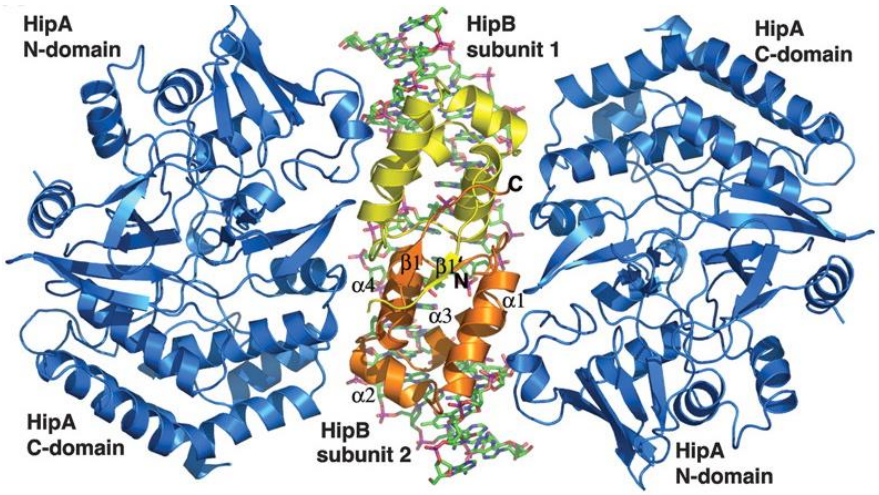

Figure 5. **The complex of HipA-HipB-DNA operator in *E. coli*.** Two HipA monomers (in blue) interact with the HipB dimer (in orange and yellow). The HTH domain of HipB interacts with DNA in the operator region of the promoter of the *hipBA* operon (shown in sticks). HipB binds to the region of HipA away from the active site. This figure was taken from Schumacher *et al.* 2009 (*87*).

The HipA7 mutant, a gain-of-function variant, contains two amino acid substitutions at G22S and D291A that weaken its interaction with HipB, resulting in higher kinase activity and increased persistence (*87, 91*). Clinically, *hipA7*-like mutations such as P86L have been linked to recurrent urinary tract infections (UTIs) caused by *E. coli*, highlighting the importance of HipA-mediated persistence in antibiotic resistance (*88*). Overexpression of HipA in the absence of HipB causes growth arrest by shutting down macromolecular synthesis, without causing cell death, also supporting that HipB forms a complex with HipA to keep it inactive (*91*). This enables persister cells to escape antibiotics, particularly β-lactams, and survive until conditions become favorable to resume growth.

The kinase activity of HipA is essential to prevent bacterial growth and to confer multidrug tolerance against antibiotics such as cefotaxime, ofloxacin and mitomycin C. Mutants of HipA showed that conserved Asp309 in the kinase active site and Asp332 in the Mg^{2+}-binding site are essential for the activity of HipA. Replacing these residues with glutamine, resulted in an inactive HipA protein, leading to a loss of both growth arrest and antibiotic tolerance phenotypes (*92*). The mechanism of action of HipA has been extensively studied. HipA autophosphorylates itself on Ser150, a modification essential for its toxicity and the antibiotic resistance it confers. This phosphorylation is unusual because Ser150 is located in the catalytic core ATP-binding P-loop motif of the protein and not in a solvent-accessible loop, as seen in other kinases. Phosphorylation of Ser150 triggers a transition from an “in-state” to an “out-state”, where the p-Ser residue becomes solvent-exposed, thereby inactivating the kinase by disrupting its ATP-binding pocket (*93*). A phospho-ablative mutant of autophosphorylation site Ser150, with the replacement of serine to alanine, also resulted in the loss of toxic phenotype and antibiotic tolerance by HipA (*92*). Structural analysis of the S150A mutant revealed that this mutation also results in an “out-state” conformation of HipA. This is probably due to the lack of interaction between Ser150 and Leu64, which forms a hydrogen bond that stabilizes the “in-bound” active kinase state (*93*).

One of the most important phosphorylation targets of HipA is GltX (GluSR, glutamyl-tRNA synthetase), particularly at the conserved Ser239 residue in its ATP-binding site (*94, 95*). This phosphorylation inhibits the aminoacylation of tRNAGlu, leading to an increase in the concentrations of uncharged tRNAGlu, which goes and binds to the ribosomal A-site. This results in stalling of the ribosome, where RelA gets recruited. RelA interacts with the uncharged tRNA and ribosome to become active and synthesize (p)ppGpp, which subsequently leads to the activation of stringent response and persistence (**Figure 6**) (*96*). HipA expression also directly activates (p)ppGpp synthesis through the RelA enzyme, further inhibiting macromolecular synthesis and driving the bacterial cell into a dormant state, which is resistant to β-lactam antibiotics (*97*). Quantitative phosphoproteomics revealed many additional substrates of HipA and HipA7 mutant, including GltX as the main target in both wild-type and mutant HipA (*98*). Initial studies have shown that deletion of both *hipA* and *hipB* in *E. coli* resulted in normal

growth and a similar frequency of persistence to the parental strain, highlighting no direct phenotype associated with the deletion of *hipA* (*86*). However, HipA has been linked to the long-term survival of bacteria as it was shown to be highly expressed throughout the stationary phase (*99*).

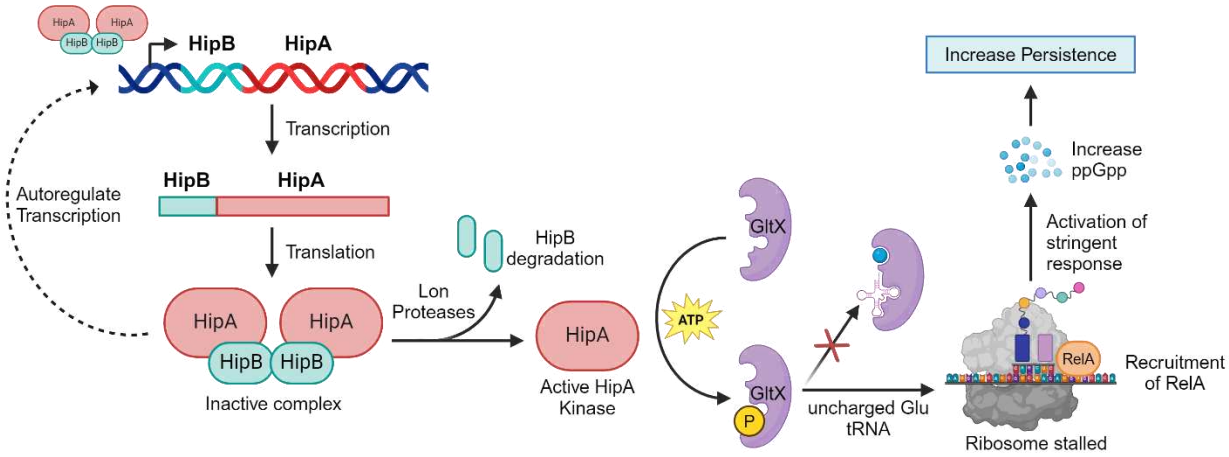

Figure 6. **Overview of HipBA-mediated persistence in *E. coli*.** The *hipBA* operon encodes for toxin-antitoxin HipA and HipB that form an inactive protein complex containing HipB-HipA-HipA-HipB. This complex can also bind to the promoter region and autoregulate the transcription (shown by the dashed line). Upon degradation of HipB by Lon proteases, HipA becomes active and phosphorylates GltX (Glutamate tRNA synthetase) to inhibit its aminoacylation activity. This results in the accumulation of uncharged Glu tRNA, which blocks the translation by stalling the ribosome. The stalled ribosome provides a platform for RelA binding and activation leading to (p)ppGpp synthesis and initiation of stringent response that ultimately increases persistence. This figure was adapted from Kaspy *et al.* 2013 (*95*) and Gerdes *et al*. 2021 (*100*) and created with BioRender.com.

Deletion of the *hipBA* locus resulted in a prolonged lifespan and higher levels of macromolecular synthesis than wild-type cells at the stationary phase. This implies that HipA induces a dormant state that helps *E. coli* cells survive under stress by slowing down macromolecular synthesis and metabolic activity, whereas, in its absence, cells remain more metabolically active and maintain their ability to produce macromolecules, resulting in prolonged survival during stationary phase (*99*). Deletion of *hipBA* also leads to a decrease in the formation of persister cells in both stationary phase and biofilm populations upon antibiotic exposure. This reduction in persister cell formation plays a critical role in ensuring the survival of bacterial populations under unfavorable conditions (*101*). Additionally, a *hipBA* mutant has been shown to decrease biofilm formation even in the absence of antibiotic stress, indicating that HipA plays an important role in regulating biofilm formation (*102*). The correlation between *hipBA* expression and

persister formation was also studied at the single-cell level. It showed that the fluorescently sorted cells with higher levels of chromosomal *hipBA* expression have better survival against antibiotic, ofloxacin compared to the cells with the deletion mutant of *hipBA* operon. This demonstrated that HipA contributes to persister formation in WT *E. coli (88)*. Together, these studies highlight that HipA not only plays a role in antibiotic persistence but also in the broader context of bacterial survival strategies, including biofilm formation.

In addition to its well-characterized role in persistence, HipA is part of a broader family of kinases that are conserved across many bacterial species and can contain mono- and tri-cistronic operons in different bacteria (**Figure 7**). This includes homologs of HipA, such as HipT in pathogenic *E. coli* as part of tricistronic operon *hipBST* or YjjJ (HipH) in *E. coli*, which is encoded by a monocistronic operon and may have an important role in bacterial physiology (*100*). YjjJ is a HipA-homologous kinase, which is also shown to inhibit cell growth upon overproduction (*103*). In this thesis, Manuscript II includes the molecular characterization of YjjJ in *E. coli* where overexpression of wildtype and kinase mutant are studied with a phosphoproteomics approach to identify the targets of this kinase and elucidate its role in bacterial cellular processes.

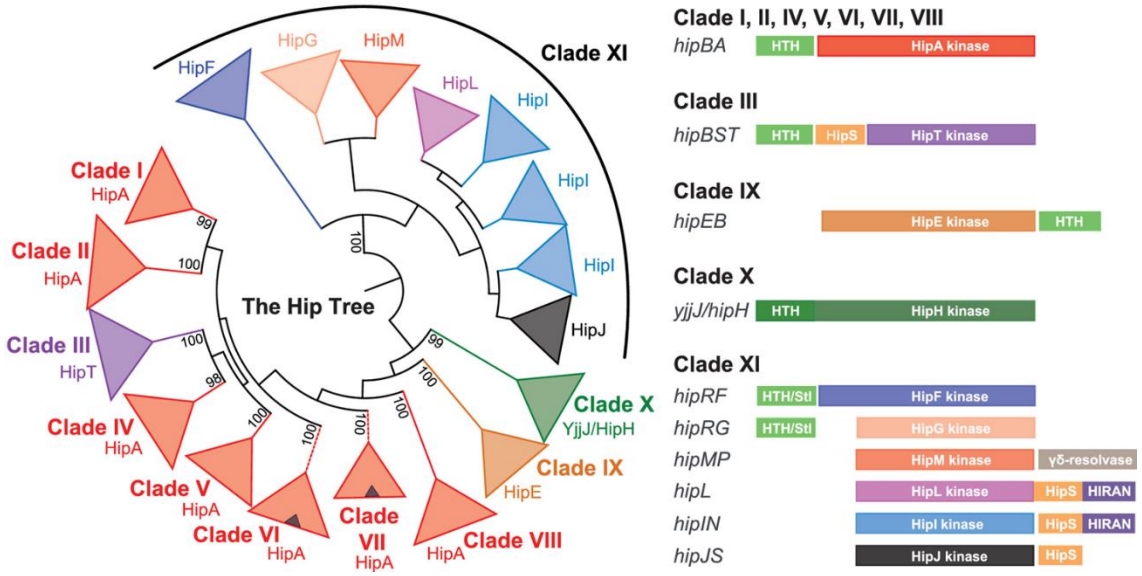

Figure 7. **Phylogenetic tree and gene organization for HipA-homologous kinases.** The Hip Tree consists of several clades that correspond to different kinase families as depicted by colors. The gene organization of TA modules differs between clades with variations in the position of their putative antitoxin-containing HTH domain (in light green). This figure was adapted from Gerdes *et al.* 2021 (*100*).

It is important to study HipA homologs to understand their roles in bacterial survival mechanisms such as persistence. Characterization of these kinases, especially in pathogenic bacteria like *K. pneumoniae*, may provide new drug targets to combat chronic and multidrug-resistant bacterial infections and enhance the efficacy of existing antibiotics. Section 3 of this thesis includes a manuscript on *hipA*-mediated antibiotic tolerance in *K. pneumoniae*. The evolution and functional diversity of these kinases provide valuable insights into the molecular basis of bacterial dormancy and survival under adverse conditions, thereby contributing to the broader field of bacterial pathogenesis and antibiotic resistance. The evolutionary conservation of *hipA*-like kinases across bacterial lineages highlights that persistence is an evolutionarily conserved strategy for survival, with potential implications for developing broad-spectrum antimicrobial therapies targeting these kinases. Overall, the HipBA system, particularly the kinase activity of HipA, represents a critical mechanism by which *E. coli* and potentially other bacteria survive antibiotic treatment. Therefore, understanding the role of *hipA*-like kinases and their modulation holds great potential for the development of novel therapeutic strategies to eradicate persister cells and combat multidrug-resistant and recurrent infections.

1.1.4 Potential applications of studying STK

STKs have been associated with almost every aspect of bacterial physiology and are shown to regulate processes such as metabolism, antibiotic persistence, cell division, morphogenesis, and host immune system manipulation (*29*). This section highlights key applications of studying STKs, including the development of novel antibiotics, vaccines, biofilm control, and improving therapeutic strategies for bacterial infections. It also shows how insights gained from STK studies can contribute to innovative therapeutic strategies and improve the management of bacterial infections.

1.1.4.1 Development of novel antibiotics

The rise of antibiotic resistance underscores the need for new antibacterial agents. STKs regulate critical bacterial functions like growth, signaling, and virulence, making them promising targets for new drug development. For instance, inhibitors of STKs such as PknB and PknG in *M. tuberculosis* have shown potential as antibacterial agents *(104,*

105). By targeting these kinases, bacterial pathogenicity can be reduced, and the effectiveness of existing antibiotics enhanced. Additionally, broad-spectrum antimicrobial agents that inhibit bacterial STKs without affecting human kinases could simultaneously target multiple bacterial kinases, reducing drug resistance. (*106*). However, challenges remain in translating *in vitro* success to *in vivo* efficacy due to issues with drug delivery and intracellular kinase function, necessitating further research to optimize drug design (*107*).

1.1.4.2 Development of new vaccines and biomarker discovery

Highly conserved STKs may serve as vaccine targets if they induce a strong, broad immune response. For example, the C-terminal PASTA domain of StkP in *S. pneumoniae* shows potential as a vaccine antigen, capable of inducing protective immune response in animals. StkP along with the protein PcsB has been shown to prevent infections caused by all serotypes of pneumococcus in old and young children (*108*). STKs involved in host immune modulation could also be leveraged to design vaccines that elicit robust immune responses. Also, specific STKs may serve as biomarkers for bacterial infections, aiding diagnostics by identifying pathogenic strains and distinguishing between virulent and non-virulent types, facilitating timely diagnosis and more targeted treatments.

1.1.4.3 Fighting against biofilms and improvement of phage therapy

Bacterial biofilms are extremely difficult to treat due to their inherent resistance to both antibiotics and the host immune system. Phage therapy, which involves using bacteriophages to selectively target and kill bacteria, has emerged as an alternative to traditional antibiotics, especially for the treatment of resistant bacteria and biofilms. The phages tend to effectively kill both antibiotic-sensitive and resistant bacteria and are also capable of disrupting bacterial biofilms (*109*). The effectiveness of phage therapy can be greatly improved by comprehending the function of STKs in the regulation of biofilm development, its maintenance, and bacterial defense mechanisms against phages. For example, the STK Stk2 in *S. epidermidis* has been involved in abortive infection mechanisms that prevent phage propagation (*79*). Therefore, combining phage therapy with inhibitors of STKs can potentially decrease the bacterial interactions to weaken the

biofilm architecture and increase the overall efficiency of phage treatments. These approaches will provide more robust treatment strategies against multidrug-resistant bacterial infections and biofilms.

1.1.4.4 Understanding pathogenesis and host-pathogen interactions

Studying STKs can also provide a deeper understanding of bacterial pathogenesis by elucidating the molecular mechanisms underlying virulence. Several STKs can control the expression of virulence factors, facilitate immune evasion, and promote intracellular survival. For instance, the role of PrkX in *S. enterica* and PknE in *M. tuberculosis* shows the significance of these kinases in mediating pathogenic processes (*58, 110*). The intricate interactions between bacteria and host immune systems can also be studied by understanding the role of STKs. The mechanisms by which bacterial STKs enter host cells, phosphorylate host proteins, and manipulate host cellular pathways to increase intracellular survival, can identify novel therapeutic strategies aimed at countering immune evasion strategies employed by pathogens. This understanding can guide the development of therapies that specifically target bacterial pathogenicity while simultaneously improving human immune responses.

1.1.4.5 Stress Response and Adaptation

Bacteria can adapt quickly to different environmental stresses, such as oxidative stress or nutrient deprivation for survival. This often requires a quick response to adapt to the changed environment using proteins like STKs. This allows pathogens to survive under unfavorable conditions. For example, the regulation of stress response pathways by kinases like Stk1/PknB in *S. aureus* highlights their importance in bacterial resilience (*74*). A comprehensive understanding of these adaptive mechanisms may improve the treatment strategies that exploit bacterial vulnerabilities, making them more susceptible to antibiotics and other treatments.

1.2 Antibiotic resistance in pathogenic bacteria

1.2.1 Antibiotic resistance, tolerance, and persistence

The failure of antibiotic treatments is a growing concern in modern medicine, primarily driven by the rise in antibiotic resistance. This phenomenon is marked by the ability of bacteria to withstand the effects of drugs that would normally inhibit their growth or kill them. However, antibiotic resistance is not the only factor that complicates the treatment strategies. In addition to antibiotic resistance, there are also other mechanisms, such as antibiotic tolerance and persistence, that play significant roles in reducing the susceptibility of antibiotic therapies (**Figure 8**). These mechanisms, while distinct, are often interrelated and can complicate the management of bacterial infections in clinical settings.

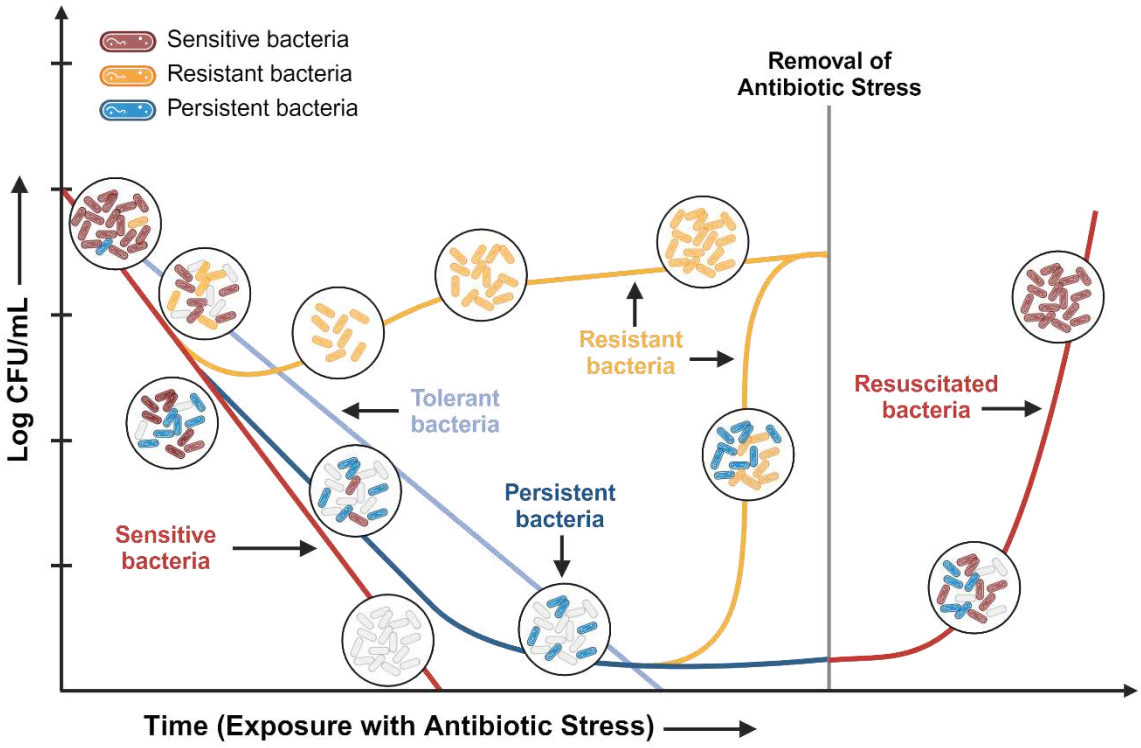

Figure 8. **Mechanisms of antibiotic resistance in bacteria**. Exposure to antibiotic stress rapidly eliminates the antibiotic-sensitive population, whereas tolerant cells take longer time than susceptible bacteria. In contrast, resistant bacteria can survive antibiotic exposure and continue to proliferate even during the antibiotic exposure. Persistent bacteria may remain dormant until the antibiotic stress is removed, at which point they either resume growth, restore the sensitive bacterial population, or potentially contribute to the emergence of resistant strains. This figure was adapted from Singla *et al.* 2022 (*111*) and re-created with BioRender.com.

Antibiotic resistance is the ability of bacteria to survive in the presence of antibiotics and replicate. These bacteria are genetically different from sensitive populations and give rise to a resistant population of bacteria. Resistant bacteria showed an increased minimum inhibitory concentration (MIC) of antibiotics that would otherwise inhibit the growth of bacteria or kill it (*112*). Genetic resistance can occur through mutations, which may result in decreased binding of drugs or alteration in the expression of genes for drug influx or efflux pumps. It can also be acquired by horizontal gene transfer of resistant genes, such as additional efflux pumps or antibiotic-inactivating/degrading genes (*113*).

Antibiotic tolerance, on the other hand, is the ability of bacteria to survive transient exposure to high concentrations of antibiotics without any change in their MIC. Unlike resistance, tolerance does not involve genetic changes that permanently alter the sensitivity of bacteria to antibiotics, but instead requires longer treatment durations, irrespective of the concentration of antibiotics used, to eradicate the bacterial population. Antibiotic tolerance is highly relevant in *K. pneumoniae*, where environmental conditions such as slow growth or increased lag phase can induce this phenotype and increase the tolerance of bacteria to certain classes of antibiotics, complicating treatment efforts (*114*). Both tolerance and resistance are features of the whole bacterial population.

A special subset of tolerance is antibiotic persistence. Persistence is the ability of a small subpopulation to survive exposure to high concentrations of antibiotics through growth arrest. These bacteria are phenotypic variants of normal sensitive populations and can give rise to a heterogenous population containing both sensitive and persistent bacteria (*115*). This phenomenon is distinct from antibiotic resistance in several key ways. Persistence is characterized by a biphasic killing curve, which shows that within a clonal population, not all bacteria are killed at the same rate when exposed to antibiotics (*116*). Unlike resistant bacteria, which can grow and replicate in the presence of antibiotics due to genetic adaptations, persister cells enter a non-replicating, dormant/slow-growing state that allows them to tolerate antibiotic exposure temporarily (*112*). In *K. pneumoniae*, biofilm formation further complicates the persistence by protecting these

persister bacteria from antibiotic exposure and immune response, which contributes to the reoccurrence of infections and makes it difficult to eradicate.

Antibiotic persistence can be either triggered or spontaneously occur in bacteria. Triggered persistence is where bacteria are triggered by unfavorable conditions such as starvation, acid stress, antibiotic stress, or immune factors to become a persister. They are also called Type I persisters and are typically found in stationary phase cultures or after encountering stressful conditions. After the removal of the stress or inoculation into a fresh medium, they can revert to normal, active cells but have an extended lag phase. An example of this type of persistence is *hipA7* persisters. On the other hand, spontaneous persisters are the persisters that are formed spontaneously during the exponential phase and remain constant throughout the exponential growth and are called Type II persisters. These persisters grow and divide at a very slow rate compared to non-persisters and are always present in a bacterial population at low levels. *hipQ* persisters are an example of this type of persistence (*82, 112*). This persister state is not permanent and once the antibiotic is removed, these cells can revert to normal growing cells. This transient tolerance mechanism and a slower rate of killing compared to the rest of the population makes them a significant challenge in the treatment of bacterial infections causing the failure of antibiotic treatments and contributing to the relapse of chronic infections (*117*).

1.2.2 Emergence of multidrug resistance and its challenges

The increase in multidrug-resistant (MDR) bacteria that are resistant to more than three antibiotic classes has coincided with a decline in the development of new antibiotics. This causes a serious risk to human health where the existing antibiotic treatment options are no longer effective against these multidrug-resistant bacteria. These antimicrobial-resistant pathogens have been classified as a potential threat to humans by World Health Organization (WHO) and Centers for Disease Control and Prevention (CDC). At least 1.27 million people have died across the globe due to antimicrobial resistance (AMR) in 2019, with nearly 5 million deaths associated with it (*118*). The main reasons behind the development of drug-resistant pathogens are the misuse and/or overuse of antibiotics to prevent, treat, or control infections in humans, animals, and

plants. It is also affected by poor hygiene and sanitation, inefficient infections and disease control, less access to good quality vaccines and antibiotics, poor diagnostics, and lack of awareness and surveillance of resistant development (*119, 120*).

The phenomenon of AMR has a huge economic burden on the healthcare systems and national economies overall in both developed and developing countries (*119*). However, the burden on developing countries is significantly higher due to poor healthcare systems, limited access to effective treatments, and higher rates of infection. The lack of comprehensive surveillance systems and regulatory mechanisms further intensifies the challenge, making it difficult to control the spread of AMR and increasing the economic strain on these nations (*121*).

Infections caused by MDR bacteria result in a greater number of hospital visits and diagnostic tests and longer duration of stay in hospitals, as standard treatments are ineffective against these infections and patients require prolonged care. This results in reduced productivity and a higher economic burden on families and communities. Since first-line antibiotics are not effective against these bacteria, this necessitates the requirement of more expensive last-resort antibiotics such as colistin, which are also associated with higher toxicity and limited availability. The use of last-resort drugs also has the risk of the emergence of resistance against these antibiotics in MDR bacteria. The emergence of resistance against last-resort antibiotics will further complicate treatment options. The financial burden is also increased by the need for more intensive care, especially for immunocompromised patients and those with severe infections (*122*). An estimated cost of 4.6 billion dollars was used in 2017 in the United States for the treatment of hospital-onset or community-acquired MDR infections, caused by six major antibiotic-resistant pathogens (*123*). This cost likely reaches hundreds of billions globally considering both direct and indirect impacts. This highlights the urgent need for the development of new strategies to restore the efficacy of existing antibiotics and prevent further resistance.

The WHO released a list of pathogens that pose a huge threat to hospitals, nursing homes, and patients, requiring the urgent need for the development of novel antimicrobial strategies including new antibiotics, due to their rising resistance to all

antibiotics available. This list included the ESKAPE group of pathogens as top and high priority (*124*). ESKAPE pathogens are a group of pathogenic bacteria that cause hospital-acquired (nosocomial) infections due to their ability to escape the lethal effects of antibiotics and showcase instances of bacterial pathogenesis, transmission, and resistance. It includes *Enterococcus faecium*, *Staphylococcus aureus*, *Klebsiella pneumoniae*, *Acinetobacter baumanni*, *Pseudomonas aeruginosa,* and *Enterobacter* species (*125*). These bacteria are highly prevalent in hospitals and are rapidly becoming resistant to a wide range of antimicrobial agents, posing a rising threat to public health. ESKAPE pathogens exhibit shared characteristics, including their ability to thrive in the modern healthcare environment and harboring inherent or acquired mechanisms of resistance that have positioned them as a major contributor to resistant infections over time (*126*). These bacteria can have several different mechanisms for antibiotic resistance, including, chemically modifying or breaking down the drug, preventing the influx of antibiotics, flushing the drug out of the cell via efflux pumps, or modifying the targets of antibiotics to prevent its action (*127*). For example, *K. pneumoniae* can produce inhibitor-resistant β-lactamases that break down β-lactam antibiotics (*128*), while *P. aeruginosa* employs efflux pumps to pump antibiotics out of the cell (*129*). These are some of the strategies that ESKAPE pathogens use to become drug-resistant and escape antibiotic treatment. Among the ESKAPE pathogens, *Klebsiella pneumoniae* is an important pathogenic bacterium due to its rapid acquisition of resistance mechanisms and its role in severe infections, making it a significant focus of concern in the fight against hospital-acquired infections.

1.2.3 *Klebsiella pneumoniae*- pathogenesis and virulence factors

K. pneumoniae is a gram-negative bacterium, which is generally encapsulated. It belongs to the Enterobacteriaceae family and, together with *Escherichia coli*, is a global threat, responsible for hospital- and community-acquired infections (*130*). This opportunistic pathogen mainly affects individuals with compromised immune systems or serious underlying conditions such as diabetes or chronic lung obstruction. Additionally, *K. pneumoniae* produces biofilms that are clinically significant due to their formation on the inside or the surface of medical devices like catheters and contribute to the colonization of bacteria in patients (*131*). The most frequently occurring nosocomial

infections include urinary tract infections, pneumonia, septicemia, and wound or surgical site infections (**Figure 9**). In intensive care units and neonatal settings, *K. pneumoniae* frequently causes infections, often leading to outbreaks that are challenging to treat because of increasing multiple-drug resistance in this bacteria (*132*). In addition to these hospital-acquired infections, hypervirulent strains have evolved, that can cause more serious and invasive diseases such as liver abscess, bacteremia, meningitis, endophthalmitis, and necrotizing fasciitis. These hypervirulent strains are particularly concerning because they can affect otherwise healthy individuals, cause multiple sites of infection, and are linked with high morbidity and mortality rates (*133*).

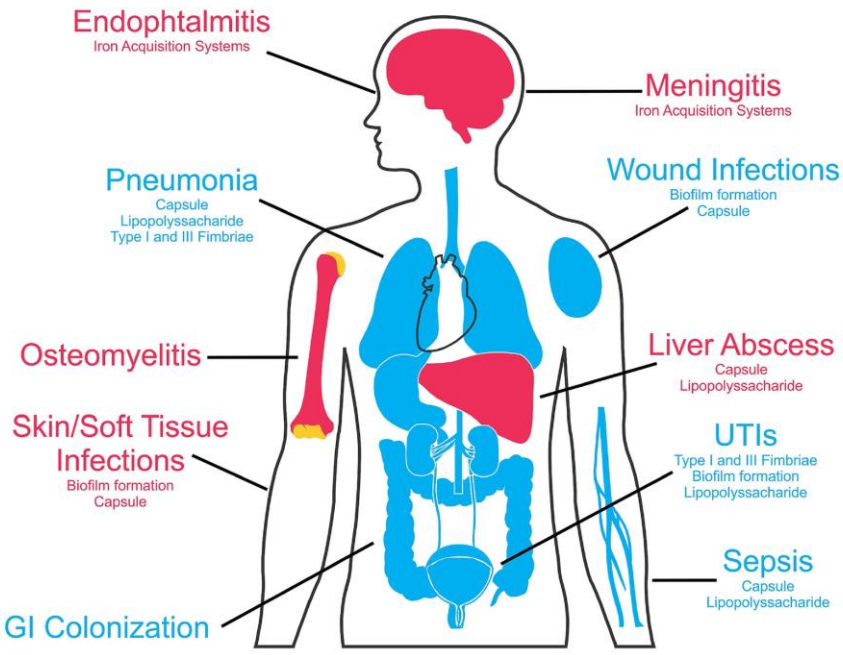

Figure 9. **Infections caused by *Klebsiella pneumoniae* in humans and their associated virulence factors**. Infections caused by classical *K. pneumoniae* strains (in blue) and those commonly associated with hypervirulent strains of *K. pneumoniae* (in red). This figure was taken from Assoni *et al.* 2024 (*134*).

Numerous species of *Klebsiella* are observed in the environment and are frequently found in soil, water, and a variety of surfaces. In humans, it is frequently found in colonizing mucosal surfaces, like the upper respiratory tract and the gut, with colonization rates varying widely among people due to their living conditions and exposures (*135*). The transmission of *K. pneumoniae* occurs primarily through direct or indirect contact with contaminated surfaces or materials. In healthcare settings, person-

to-person transmission is a common way, often mediated by workers or contaminated medical equipment such as catheters, ventilators, and endoscopes (*136*). These bacteria are capable of surviving for a long time on surfaces, which makes their spread within the healthcare environment easy. After acquiring the bacteria, it colonizes the mucosal surfaces in humans, particularly the GI tract or nasopharynx where it can persist as part of the normal flora or cause infection if the immune system of the host is compromised (*137*). Colonization of bacteria in the GI tract is concerning as it can serve as a major reservoir for subsequent infections and facilitate the spread of antibiotic-resistant strains (*138*).

The molecular pathogenicity of *K. pneumoniae* can be associated with a variety of virulence factors that allow these bacteria to avoid the host immune system and survive infections (**Figure 9**). These include capsule polysaccharide (CPS), lipopolysaccharide (LPS), fimbriae/pili, outer membrane proteins (OMP), and factors for iron acquisition and nitrogen source utilization (*132*). The polysaccharide capsule that surrounds the bacterial cell is among the most significant virulence factors. This thick capsule can prevent the bacteria from being adhered to and internalized, thereby protecting it from immune cell opsonization and phagocytosis. It also suppresses early inflammatory response by inhibiting cytokines and chemokines, inhibits the maturation of dendritic cells, and provides resistance to antimicrobial peptides by acting as a barrier that prevents the access of host-derived antimicrobial peptides (*138*). LPS, also called endotoxin, consists of lipid A, oligosaccharide, and O-antigens, which are the first molecules that the host immune system encounters. There are different variants of O-antigens in different strains that are responsible for protecting the pathogen from complement-mediated killing. They increase the bacterial virulence and lethality by promoting bacteremia (*139*). In addition to phagocytosis, the host also utilizes serum to kill the invading microorganisms. The bactericidal activity of human serum is primarily due to complement proteins, which are activated by OMP or LPS (*132*). These proteins either mark the bacteria for phagocytosis or directly kill the bacteria by pore formation. However, multidrug-resistant bacteria use several mechanisms such as capsule, LPS, and OMP to become resistant to serum (*140*). *K. pneumoniae* also produces several fimbriae/pili, for example, type 1, type 3, and Kpc. This facilitates the attachment of

bacteria to the host cells and surfaces. Type 1 pili are involved in the initial attachment of pathogens to epithelial cells in the urinary tract. Type 3 and Kpc pili, on the other hand, are associated with biofilm formation on surfaces such as catheters (*138*). Outer membrane proteins, like porins, which can allow the diffusion of antibiotics into the bacteria, can result in increased resistance to phagocytosis by not expressing these proteins (*141*). Efflux pumps, like AcrAB, can resist the innate immune system by exporting antibiotics and host antimicrobial peptides, ultimately contributing to multidrug resistance phenotype (*142*). *K. pneumoniae* can sequester iron, which is essential for its growth and metabolism and is also known to contribute to its virulence. The bacterium produces siderophores, which are small, high-affinity iron-chelating metabolites that chelate iron from the external environment and import it into the cells. This ability to sequester iron gives *K. pneumoniae* a competitive advantage in the iron-limited environment of the human body, particularly during infection (*143*). Hypermucoid (hypervirulent) strains of *K. pneumoniae* can acquire iron more efficiently and increase capsule production, which gives the hypermucoviscous phenotype to these bacteria (*144*).

The hypervirulent bacterial strains have developed two different resistance mechanisms: carbapenemases and extended-spectrum β-lactamases (ESBLs). ESBLs are enzymes that can hydrolyze many different β-lactam antibiotics, including penicillin, monobactams, and cephalosporins, making them ineffective. Carbapenems have been used to treat ESBL-producing infections but carbapenemases-producing strains can break down carbapenems (*145*). Since these strains are resistant to almost all available antibiotics, they cause treatment failures and higher mortality rates in patients. Novel approaches to tackle *K. pneumoniae* are desperately needed, due to increasing resistance in these bacteria. It is crucial to comprehend the resistance mechanisms in these bacteria to develop novel antibiotics or alternative therapeutic strategies.

1.2.4 Antibiotic persistence and its eradication in *K. pneumoniae*

The multidrug-tolerant persisters are present in both laboratory and clinical isolates of *K. pneumoniae* (*146-148*). The degree of persistence varies according to the concentration of the drug, its duration, and the type of antibiotics *(147)*. In clinical settings, this variability in persistence levels complicates treatment, as standard

antibiotic regimens may fail to completely eradicate the infection, leading to the relapse of infections. On exposure to high concentrations of antibiotics, high levels of tolerant persister cells are formed to help bacteria tolerate these treatments. Even lower doses of antibiotics and environmental stimuli during the stationary phase are capable of inducing the formation of persister cells in *K. pneumoniae* (*149*). In *K. pneumoniae*, extensive studies have shown that different intracellular stress responses, including (p)ppGpp, SOS response, and ROS response, which can be induced by subminimal concentrations of antibiotics, paraquat, and hydrogen peroxide stress, can promote persister cell formation in a subset of *K. pneumoniae* that can become tolerant to antibiotic treatments (*150*).

Several mechanisms and pathways have been associated with bacteria that enter a persister state and maintain it. For example, the stringent response acts as a global regulator of gene expression under starvation conditions and is known to drive persister formation. It involves the production of (p)ppGpp that downregulates the essential processes and makes the bacterial cells enter a dormant-like state that is less susceptible to antibiotics. Other mechanisms such as SOS response (DNA repair mechanism), ATP levels in the cell, and toxin-antitoxin systems have also contributed to the formation of persisters. These mechanisms shut down bacterial cellular processes such as protein synthesis or DNA replication and lead to antibiotic persistence by inducing a dormant-like state (*151*). HipBA was the first toxin-antitoxin module associated with persister formation, where the levels of *hipA* both a certain threshold induces the persister cell formation (*90*). However, many other TA systems have also been seen to play a role in enhancing the persistence such as RelBE, which is essential for persistence in *M. tuberculosis* and is up-regulated in *K. pneumoniae* and *S. aureus* upon high antibiotic exposure. Signaling molecules such as indole or quorum sensing are also shown to induce persister formation in many bacteria, highlighting the complexity of the persistence mechanism in *K. pneumoniae* (*152*). However, HipA-mediated tolerance has not yet been studied in *K. pneumoniae*.

Thus, understanding these mechanisms is important, particularly in *K. pneumoniae*, where these mechanisms contribute not only to treatment failures but also to the

potential emergence of resistance. In addition to the clinical burden of persister cells on the failure of antibiotic treatments, there is growing evidence that they also contribute to the development of resistance or virulence over time. The extended survival of persister cells under antibiotic treatment creates a reservoir for the acquisition of resistance-related genetic mutations (*153*). This is highly relevant in conditions of long and repeated antibiotic exposures, where persister cells get more chances to develop resistance. The increased stress response in persisters can also result in a higher mutation rate and accelerate the acquisition of resistant traits. This facilitates the genetic changes, including horizontal gene transfer associated with resistance, which can stimulate the spread of resistance genes in bacterial populations. Thus, while persisters themselves are not resistant, under antibiotic pressure, they can indirectly lead to the emergence of resistance phenotypes, which critically impairs the strategies for treatment and leads to the long-term failure of antibiotic therapies (*154*). This connection between resistance and persistence highlights the importance of targeting persisters to avoid the further spread of antibiotic resistance in the pathogenic bacterium *K. pneumoniae*.

The current research efforts for the eradication of persisters aim at developing novel strategies that specifically target these bacteria. This includes finding novel drugs or trying new antibiotic combinations or innovative cocktails with antibiotics and phages to fight against multidrug tolerance and resistance such as co-administration of different antibiotics increases the killing of a pan-drug resistant *K. pneumoniae* and suppresses the rate of persister formation (*155*). The antibiotics targeting inactive cells can be used for the treatment of these bacteria as persister cells escape antibiotic killing due to their metabolically inactive state. Other methods involve targeting the cell membrane with small molecules or antimicrobial peptides that can enter the cell and force the persister cells to resume their growth or increase their metabolism, which can make them more susceptible to antibiotics (*156*). For instance, the use of saccharides to increase the metabolism in *E. coli* and *S. aureus* persister cells showed increased uptake of aminoglycoside antibiotics (*157*). Current antibiotics can also be chemically modified to enhance entry into the bacterial cells or an antibody-antibiotic conjugate to target cells and promote phagocytosis. Phage therapy is also a potential way to kill bacteria in

combination with antibiotics can result in the lysis of cells and reduce virulence such as biofilm formation (*158*).

This highlights the importance of studying antibiotic-tolerant persister cells to develop better therapeutic approaches for the eradication of persistence-mediated bacterial infections. Especially, understanding the role of HipA-mediated antibiotic persistence in *K. pneumoniae* can provide new insights for targeting and overcoming these bacteria. It has been shown that inhibitors of HipA in *E. coli* have reduced bacterial persistence, independent of antibiotic treatment (*159*). In manuscript III of this thesis, HipA has been characterized in *K. pneumoniae* together with extensive phosphoproteome analysis to understand its role in antibiotic tolerance.

1.3 Mass spectrometry-based quantitative (phospho)proteomics

Mass spectrometry (MS) is a powerful analytical technique for chemical identification and quantification of unknown compounds, to elucidate their molecular structure (*160*). MS is mainly used for studying proteomics, metabolomics, and lipidomics. MS-based proteomics is an indispensable tool for studying the proteome of a cell or tissue. It can be applied for studying the complexity of signal transduction as it allows identification, quantification, and characterization of proteins and their PTMs. Proteomics has developed as a significant tool in the pharmaceutical industry, clinical settings, and molecular biology as it can provide precise identification and quantification of proteins and their modifications and interactions (*161*). Therefore, it has been utilized for the early detection of diseases, accurate diagnosis, and discovery of protein biomarkers to facilitate faster medical decisions to reduce mortality. Improvements in sensitivity, accuracy, and resolution have resulted in the identification of disease-specific proteoforms, including PTMs, which can be used for rapid identification of pathogens and quantification of therapeutic drugs (*161-163*). It is also widely used in the pharmaceutical industry for chemical proteomics, analysis of protein-protein interactions together with protein expression profiling, and targeted protein quantification (*164*). Understanding the bacterial signaling pathways is important for elucidating how bacteria sense, respond, and adapt to their environments, particularly in the context of

antibiotic resistance and persistence. MS-based proteomics in combination with quantitative methods can provide detailed insights into the dynamic changes in the protein expression, modification sites, and interaction networks in the cell.

1.3.1 Top-down and Bottom-up proteomics

Mass spectrometry-based on intact proteins is called top-down proteomics. This approach utilizes measurement of whole proteins without their digestion into peptides and provides more comprehensive information about individual proteins, including high sequence coverage, PTMs, and protein isoforms, but is limited to smaller proteins and has lower sensitivity due to difficulty in ionizing large intact proteins (*165*). In bottom-up proteomics, proteins are characterized after their digestion into peptides by specific proteases. Shotgun proteomics is the method that utilizes a bottom-up approach to a complex mixture of proteins rather than a single protein. This involves the digestion of proteins into peptides that are fractionated and measured by LC-MS/MS (Liquid chromatography-tandem mass spectrometry) analysis (*166*). It is the most widely used method that possesses certain advantages over the top-down method as peptides are easier to handle, more soluble, and generate better MS spectra compared to intact proteins, which can be difficult to solubilize and yield lower sensitivity. In addition, the mass spectrometers are more efficient in sequencing peptides that are around 20 amino acids long rather than whole proteins (*167*). The workflow of shotgun proteomics involves protein extraction from cells followed by its digestion (**Figure 10**). Many proteolytic enzymes can be used to digest proteins into peptides. Trypsin is one of the most commonly and extensively used proteases as it cleaves proteins very specifically on the C-terminus of basic amino acids, Arg and Lys to form peptides that are 7-20 amino acids long with molecular mass between 0.8 to 2 kDa. Other proteolytic enzymes such as chymotrypsin, Lys-C, Glu-C, or Asp-N can be utilized to get specific peptides that are usually not obtained from typical trypsin digestion (*167*). This can sometimes help in generating peptides that are not covered in trypsin digestion.

A new approach involves limited proteolysis to have longer peptides with molecular mass between 2.5 to 8 kDa and is called middle-down proteomics. This approach reduces the overall number of peptides compared to a bottom-up approach and

increases the chances of detecting unique peptides that are longer thereby increasing the overall sequence coverage (*168*).

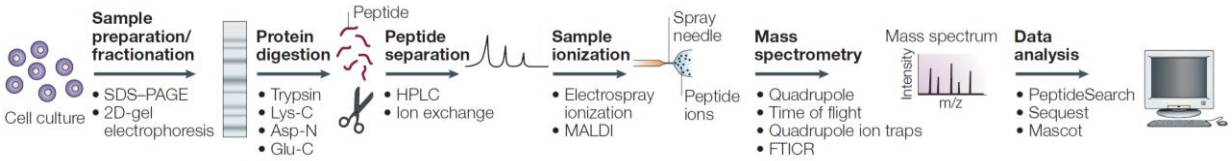

Figure 10. **General workflow of a shotgun proteomics experiment.** Sample preparation involves the fractionation or isolation of proteins from biological sources followed by their digestion into peptides. The generated peptide mixture is separated via liquid chromatography. Peptides eluted after separation are ionized and can be analyzed by many different mass analyzers. Finally, the obtained mass spectrum data is searched against protein databases to get information about peptides and proteins. This figure was taken from Steen & Mann 2004 (*167*).

1.3.2 LC-MS/MS instrumentation

To simplify the complex analytes entering the MS, peptides can be pre-fractionated based on their charge, polarity, size, or hydrophobicity. This can be achieved by separating peptides using high-pressure liquid chromatography (HPLC) coupled to MS or a pre-fractionation using high-pH reverse-phased fractionation or strong cation exchange (SCX) chromatography or hydrophilic interaction liquid chromatography (HILIC), and affinity- or gel-based separation of peptides. These techniques can simplify the complex peptide mixtures that can be further fractionated by liquid chromatography. HPLC includes loading of peptides onto a microcapillary chromatographic column containing C18 beads, which are later eluted to enter the MS. Acidified peptides get attached to the column and are eluted using a gradient of organic solvent such that very hydrophilic peptides are poorly attached to the column and are eluted first, followed by more hydrophobic peptides elution at high concentrations of organic solvent. The peptides come out of the column through the tip of the column, where the elution solution gets vaporized and the peptides get ionized and enter the MS (*167*).

A typical mass spectrometer consists of an ion source, a single or multiple mass analyzer, and a detector. It carries out measurements on ionized analytes in the gaseous phase and with high vacuum. The analytes can be volatilized and ionized for mass spectrometric analysis by two soft analyzation techniques, namely Matrix-assisted laser desorption/ionization (MALDI) and Electrospray Ionization (ESI) (*169*). The former

utilizes the desorption of ions from the solid phase, resulting in singly charged ions and it is used for relatively simple peptide mixtures or proteins (*170*). The latter involves the application of a high voltage (2kV) to a liquid sample to produce charged droplets that evaporate and release multiple charged ions for analysis. The analytes are dispersed as a fine spray of charged droplets, that are subjected to solvent evaporation and final ejection of ions, which enter MS for measurements (*171*). Therefore, it is coupled with liquid chromatography to measure complex mixtures of peptides.

Mass analyzers separate charged ions based on their mass-to-charge (m/z) values. They determine the resolution, mass accuracy, and sensitivity of mass spectrometric analysis. Different mass analyzers are used in proteomics, which vary in their resolution power, mass accuracy, and sensitivity based on their range of m/z measurements, amount of ions that will reach the detector, and their ability to separate two m/z that are similar or identical (*172*). Quadrupole mass analyzers use oscillating electric fields to selectively stabilize or destabilize the path of ions passing through it (*173*). It consists of four parallel electrical rods arranged in a square. With the help of variations in the radio frequency and direct current, only ions with specific m/z values are passed through the quadrupole to reach the detector while the other ions will collide with the rods and get ejected. On the other hand, time of flight (ToF) analyzers measure the time taken by ions to travel a certain distance as ions with different m/z will travel at different velocities and take different times to reach detectors. The main advantage of using a ToF analyzer is that all the ions will be reaching the detector (*174*). In ion trap mass analyzers, ions are trapped in a dynamic electric field and sequentially ejected based on their m/z values. It can be used to perform multi-dimensional tandem MS experiments that are not possible with a single quadrupole (*175*). Orbitrap and ion cyclotron resonance (ICR) mass analyzers incorporate Fourier transform (FT) mathematical operation for data processing to get high resolution and increased sensitivity and mass accuracy. FT-ICR mass spectrometry involves the trapping of ions in a strong magnetic field and a weak electric field. The Fourier transformation is used to detect, digitize, and convert coherently excited trapped ions into the frequency domain and later mass spectra (*176*). Orbitrap analyzers operate by trapping ions in an electrostatic field between a spindle-like central electrode and two outer cup-shaped electrodes. When a voltage is applied,

the ions oscillate harmonically along the axial directions, and their frequencies are measured to determine their mass-to-charge ratio (*177*). The Orbitrap is attached with a nitrogen-filled C-trap, where ions are trapped and pulsed into the mass analyzer by high voltages resulting in a very high mass accuracy and resolution.

Hybrid mass spectrometers are instruments that combine two or three mass analyzers to allow the analysis of both analytes and their fragments. Quadrupole and ion trap mass analyzers can also function as a mass filter for precursor ion selection and high-resolution mass analyzers such as orbitrap and ICR based on FT can be used for analysis of fragment or product ions. Tandem mass spectrometry (MS/MS or MS^2) facilitates the fragmentation of proteins and peptides to determine their amino acid sequence along with identification of PTMs on proteins and peptides and overall improve the performance of mass spectrometers (*178*). Tandem MS requires the selection or isolation of precursor ions followed by the fragmentation of those ions to produce fragments that are detected to plot the MS/MS spectrum.

MS/MS fragmentation of selected precursor ions is performed in a fragmentation chamber that is interposed of the two mass analyzers, which can result in a series of ion fragments. The most commonly used MS/MS fragmentation technique is collision-induced dissociation (CID), which involves the breakdown of precursor ions by the energy imparted by collisions with an inert gas such as nitrogen, argon, or helium. This leads to the breakage of the peptide at the C-N bond resulting in the formation of b- and y- ions. Another fragmentation method is higher-energy collisional dissociation (HCD), which uses higher energy than CID to have more extensive fragmentation. In addition to the formation of b- and y- ions, HCD also generates a- ions. HCD results in improved identification of peptides with modifications and isobaric labeling such as TMT or iTRAQ (*179*). Electron transfer dissociation (ETD) is another fragmentation method that breaks the peptide backbone at N-Cα bond resulting in c- and z- ions (*180*).

Current state-of-the-art MS methodology provides super high resolution, sensitivity, and MS/MS speed, which help in measuring low amounts of sample proteins with high accuracy and robustness. Q-Exactive and Orbitrap Exploris mass spectrometers from Thermo Fischer Scientific are hybrid systems with a quadrupole as the mass filter and

an orbitrap as the mass analyzer (**Figure 11A**). These instruments have high accuracy and resolving power up to 240,000 at m/z 200 for Q-Exactive and 480,000 at m/z 200 for Exploris. The newly available mass spectrometer Orbitrap Astral (Asymmetric Track Lossless analyzer) comprises of quadrupole-Orbitrap coupled to Astral analyzer (**Figure 11B**). Astral analyzer reduces the loss of low ions and improves single ion detection to produce 200 MS/MS spectra per second and the Orbitrap slowly produces high-resolution MS data with high dynamic range (*181*). Together, it provides faster throughput, deeper coverage, higher sensitivity, and accuracy.

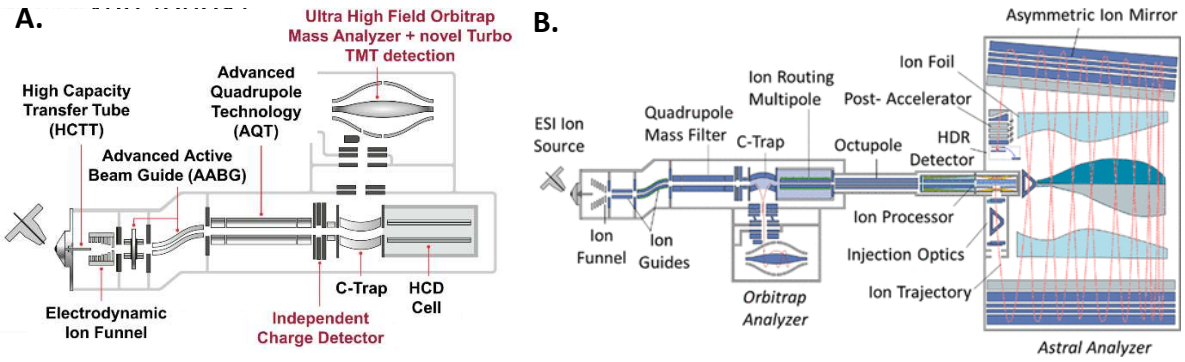

Figure 11. **Schematic representation of current state-of-the-art mass spectrometers**. The primary components of mass spectrometers are marked here. **A.** Orbitrap Exploris 480. It is a hybrid mass spectrometer with advanced quadrupole and ultra-high field orbitrap together with a C-trap and HCD for fragmentation of precursor ions. **B.** Orbitrap Astral. It combines quadrupole, Orbitrap, and Astral analyzers. This figure was adapted from Stewart *et al.* 2021 (*181*) and Denison *et al.* 2021 (*182*).

The mass spectrometry data from tandem mass spectrometry can be acquired in a non-targeted (global) proteomics strategy by two different approaches: data-dependent acquisition (DDA) and data-independent acquisition (DIA). In DDA mode, a full scan of MS1 is followed by MS2 analysis of only the most intense precursor ions selected from the full scan (**Figure 12A**) (*183*). The 'Top n' value specifies the number of the most intense precursor ions that will be selected from each full scan for further fragmentation. Since only the most intense peaks are chosen for fragmentation, this can result in a lack of analysis of low-abundance peptides. The dynamic exclusion strategy can be employed to prevent fragmentation of the same m/z ratio multiple times to increase the fragmentation of low-abundance precursor ions (*184*). DDA provides high specificity and high-quality MS/MS spectra that can be used to obtain detailed information about the sequence of the fragmented ions. It also allows for relative quantification based on

precursor ion intensities in the MS1 scan. As a downside, it provides less control over the selection of ions for fragmentation concerning order, retention time, and abundance of ions.

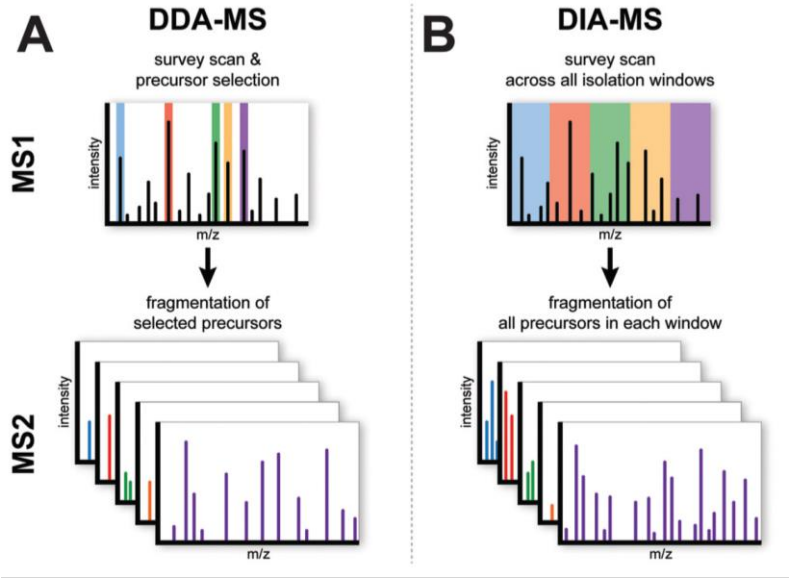

Figure 12. **Schematic depiction of data acquisition modes in mass spectrometry**. **A)** In DDA-MS, the 'Top n' number of most intense peaks as shown in colors are selected for further fragmentation in MS2. **B)** In DIA-MS, pre-defined isolation windows cover the complete range of m/z and fragment all the precursor ions in each window. This figure was taken from Krasny & Huang 2021 (*185*).

In DIA mode, the m/z range of precursors is divided into multiple overlapping or sequential windows, and all the ions within each window are fragmented at once in each MS/MS cycle (**Figure 12B**) (*186*). DIA enables comprehensive analysis of both high- and low-abundance precursor ions, making it useful in large-scale quantitative proteomics. It also provides a more complete dataset, improves reproducibility between the replicates, and reduces the missing value problem. However, it results in more complex data from the MS/MS spectrum, which are more difficult to analyze and require spectral libraries and advanced bioinformatics tools for data analysis (*187*). For quantification and identification in DIA, DIA spectra are compared with a library generated from a well-annotated MS2 spectrum from a DDA experiment or a spectral *in silico* library generated from the same DIA experiment (*188*). In DDA mode, the isolation window is typically narrow around 1-2 Th, allowing for precise selection of individual precursor ions for fragmentation whereas in DIA mode, isolation windows are wider around 10-25 Th to simultaneously fragment all precursor ions within the window.

However, advancements in faster mass spectrometers with high-speed acquisition can enable DIA to utilize isolation windows as narrow as DDA. This can allow DIA to achieve high sensitivity and precision as DDA, for more complex samples while still fragmenting all precursor ions in the sample, thereby providing comprehensive coverage with high-quality MS data (*188*).

1.3.3 Quantitative proteomics

Besides the identification of the proteins present in a biological sample, there is also a need to quantify their abundance to assess changes in protein expression under different conditions. For quantification of peptides, each peptide is compared individually between different experiments or conditions, which can result in variability due to sample handling and measurement between experiments. To minimize the technical variability, labeling techniques were developed to have more accurate and reliable quantification of proteins (*189*).

Protein quantification can be categorized as absolute and relative quantification. In absolute quantification (AQUA), an internal standard is used to determine the exact amounts of the target protein or peptide. This involves spiking a standard isotopically labeled peptide with a known concentration into the sample and comparing its intensity with the target protein (*190*). It is relatively more expensive and can only quantify a few proteins. On the other hand, relative abundance involves the addition of a chemically equivalent differential mass tag, which enables quantitative comparison of proteins between different samples with one another. The tags change the mass of protein without altering its analytical or biochemical properties (*191*). It is used to measure changes in protein or its abundance between samples or conditions, providing information on the up- or down-regulation of proteins. In this approach, the intensity of peptides is compared across different conditions. Techniques such as metabolic labeling, chemical labeling, enzymatic labeling, or label-free quantification (LFQ) are used to generate information about fold changes (**Figure 13**) (*192*).

LFQ can compare the results of two or more conditions by comparing the signal intensity of a peptide and the number of acquired spectra identifying that peptide/protein as an indication of their respective amounts in a sample (*193*). Another approach for LFQ is

spectral counting, which counts the number of MS/MS spectra assigned to a protein. It assumes that more abundant proteins will generate more tandem MS spectra and this number can be compared between experiments to get relative quantification. Intensity-based absolute quantification (iBAQ) can provide more accurate quantification than AQUA as it calculates the intensity of a protein by dividing the summed intensity of measured peptides by the theoretical number of peptides that could exist from the protein of interest (*194*). A significant advantage of the LFQ method lies in its capacity to compare an extensive number of samples and experimental conditions without the limitations imposed by labeling strategies. Unlike labeling techniques, which are restricted by the number of available labels, LFQ provides greater flexibility, making it particularly well-suited for large-scale proteomic studies that require comprehensive, unbiased comparison across diverse conditions. However, LFQ data measured by the DDA approach results in a large number of missing values, especially for low-abundance proteins (*195*). This can be solved by utilizing the DIA acquisition strategy.

In the label-based approaches, a label can be incorporated at the protein or peptide level using isotopes such as H^3, C^{13}, N^{15}, and O^{18}. In metabolic labeling, the stable isotopes are incorporated during protein synthesis in a metabolically active cell. A widely used method for metabolic labeling is SILAC (stable isotope labeling by amino acids in cell culture), where cells are cultured with different isotopes of amino acids to directly incorporate labeled amino acids into the newly synthesized proteins (*196, 197*). It allows for direct comparison of protein abundance between different conditions as the proteins are mixed before MS sample preparation and therefore minimizes the sample handling variability and missing values. The most commonly used amino acids are lysine and arginine. These proteins can be digested with trypsin to generate each peptide containing at least one labeled amino acid (*198*). Cells grown in SILAC light and heavy medium can be differentiated at the MS1 level based on specific mass differences introduced by the SILAC amino acid. It can be applied to study protein turnover with a dynamic SILAC or pulsed SILAC approach (*199*).

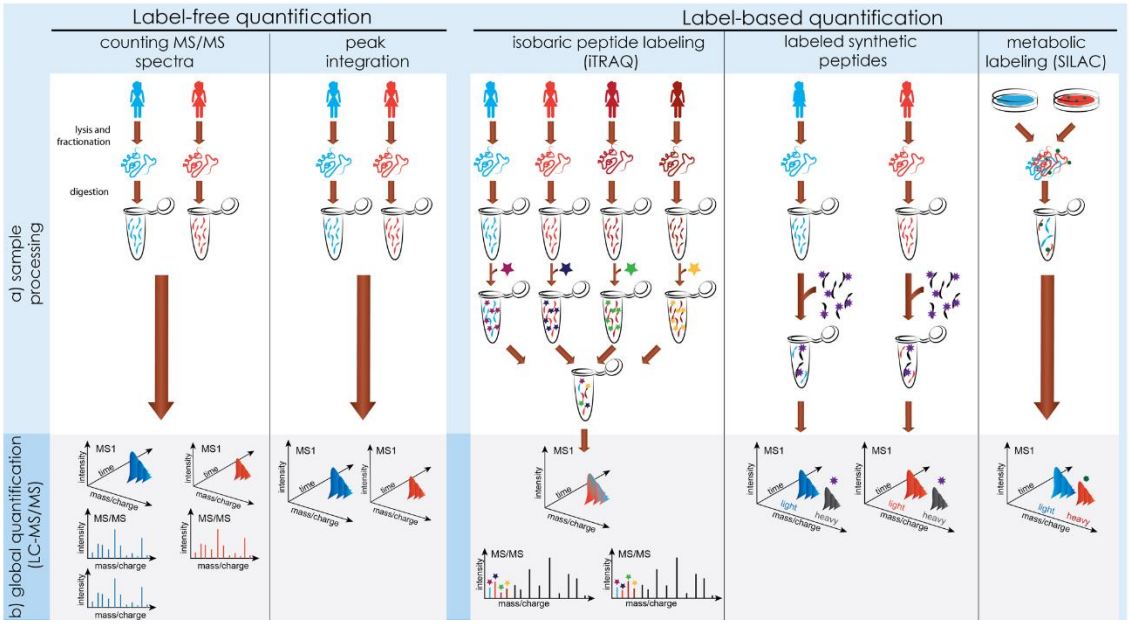

Figure 13. **Mass spectrometry-based quantitative proteomics**. The samples can be quantified using either a label-free approach or a label-based. In label-based quantification, the samples can be relatively quantified based on their labeling using metabolic or chemical methods and are mixed before MS measurements. Labeled synthetic peptides can also be used for absolute quantification in different samples. This figure was adapted from Käll & Vitek 2011 (*200*).

In chemical labeling, isotopic tags are covalently attached to peptides or proteins after protein extraction. The samples are mixed after the labeling. This involves the addition of small isotopic tags chemically such as dimethyl labeling (DML), ICAT (Isotope Coded Affinity Tag), TMT (Tandem Mass Tag), or iTRAQ (isobaric tags for relative and absolute quantification) (*191*). In DML, quantification occurs at MS1 levels whereas in TMT, the quantification of the peptides is at MS2 level (*201*). In DML, all primary amines such as the N-terminus and the side chain of Lys are converted into dimethylamines in a peptide mixture using isotopomers of formaldehyde and cyanoborohydride (*202*). On the other hand, in TMT each variant of the isobaric tag has an equal total mass, which results in a single peak at the MS1 level. This tag gets fragmented during MS2 fragmentation and is used for the relative quantification of peptides across samples (*187*). The recent advances in TMT reagents have led to the development of TMTpro reagents that can provide multiplexing of up to 35 different samples (*203*). These tags can also be used for single-cell proteomics (SCoPE) where two channels contain a carrier and a reference sample while other channels have single cells. These carrier and reference channels

contain a relatively larger number of cells. This can increase the overall amount of peptide from all channels in MS1 and enhance the peptide identification and quantification in MS2 (*204*).

1.3.4 Phosphoproteomics

Phosphoproteomics involves studying all the proteins that are phosphorylated in a cell at a particular time point. Phosphoproteins can be studied using various techniques like Sodium Dodecyl Sulfate- Polyacrylamide Gel Electrophoresis (SDS-PAGE), Two-Dimensional Gel Electrophoresis (2-DE), Western blotting, and mass spectrometry. These techniques can provide varying degrees of information about the presence, abundance, and specific position of phosphorylation on proteins.

Mass spectrometry-based phosphoproteomics provides precise identification and mapping of phosphorylation sites, making it a key method for studying the entire phosphoproteome under specific conditions. Due to the low abundance of phosphorylated peptides in the pool of all the peptides, phosphorylated peptides need to be enriched before mass spectrometry-based phosphoproteomics measurements. PTMs also need to remain stable during sample preparation and data acquisition for their accurate identification. Frequently used techniques for phosphopeptide enrichment include immunoaffinity chromatography, metal oxide affinity chromatography (MOAC) using titanium dioxide or zirconium dioxide beads (*205, 206*), and immobilized metal affinity chromatography (IMAC) using metal ions of iron, zirconium, gallium, aluminum or titanium (*207-211*). IMAC and MOAC techniques are based on the interaction between the negative charge on the phosphate group and the positive charge on metal ions or metal oxides bound to a stationary phase, which results in the enrichment of phosphopeptides. However, IMAC can also bind non-phosphorylated peptides due to the presence of negative charge on acidic amino acids such as aspartate and glutamate. This leads to the enrichment of non-phosphorylated peptides alongside phosphorylated peptides (*212*). Immunoaffinity chromatography utilizes antibodies such as phospho-tyrosine antibodies to immunoprecipitate tyrosine-phosphorylated peptides. Esterification of carboxyl groups or non-phosphopeptide excluders like organic acids can be utilized to selectively eliminate the binding of non-phosphorylated peptides.

MOAC is more stable, more selective, and resistant to interfering agents such as salts or detergents (*213*). TiO_2 enrichment has been shown to have a better selection for multiply phosphorylated peptides whereas ZiO_2 performs better for singly phosphorylated peptides (*214*). The workflow of phosphopeptide enrichment involves acidification of all digested peptides to ensure deprotonation of the phosphate group and protonation of acidic amino acids to prevent binding of non-phosphorylated peptides to the metal. This is followed by washing to remove any non-specific peptides. Finally, the phosphorylated peptides are eluted using alkaline buffers with pH 10-11 (*215*).

1.3.5 Applications of phosphoproteomics to pathogenic bacteria

To identify and study the substrates and functional roles of Ser/Thr kinases, various strategies can be employed that will provide unique insights into kinase activity, their substrate specificity, and the physiological role of the kinase. This includes genetic manipulation and affinity purification of kinases and substrates followed by mass spectrometry-based phosphoproteomics and computational analysis. Kinase knockout mutants and overexpression can be studied to help determine their physiological role in bacteria. These physiological changes can be associated with specific signaling pathways affected by the absence or overproduction of the kinase. This approach allows for identification of critical pathways and processes affected by the kinase such as overproduction of a kinase YjjJ led to longer cell type, indicating its potential role in regulating cell division pathways.

Screenings for genes that can suppress or mimic the kinase mutant phenotype help identify functionally interacting genes. However, this requires further testing using biochemical approaches to establish a direct association as they may be directly interacting with the kinase or participating in the same signaling pathway. Site-directed mutagenesis can be used to modify specific regions on the kinase or substrate to precisely identify the site of phosphorylation and the functional consequence of phosphorylation in regulating protein activity.

Global proteome and phosphoproteome profiling of kinase knockout and overexpression strains under specific conditions can help in understanding their overall impact on the proteome. Changes in protein levels or their phosphorylation state can indicate a direct

or indirect association with the overexpression or absence of kinase. This technique is highly useful in identifying potential substrates of a kinase and its impact on cellular processes. Many studies have been done in different bacteria where a kinase is overexpressed and then phosphoproteome has been measured to identify their substrates such as Ser/Thr kinases HipA and YeaG in *E. coli (98, 216)*. Affinity purification can be combined with mass spectrometry to identify proteins directly interacting with the kinase. This can provide insights into the protein-protein and protein-gene interactions to map out the interactome of a kinase and identify its substrates and regulatory proteins. High-throughput screening methods can be applied to identify the substrates of a kinase and its interaction partners. Computational analysis can also be used to predict kinase recognition motifs and substrate specificity, offering an initial screening for potential substrates. These predictions offer a faster screening of a large number of substrates to narrow down the list of candidates for further testing with wet lab experiments. Bioinformatics and machine learning approaches can be used to model and predict interactions between the kinase and substrate, providing a better understanding of signaling pathway.

2. Aims and Objectives

Ser/Thr kinases have been shown to play a crucial role in bacterial survival and adaptation, regulating key processes such as virulence, dormancy, spore formation, metabolism, and antibiotic persistence. With the growing problem of antibiotic resistance in pathogenic bacteria, novel therapeutic strategies are urgently needed to eradicate these resistant strains. Persister cells, which are associated with the relapse of chronic infections and the emergence of antibiotic resistance, are of particular concern. Therefore, understanding the genes involved in inducing bacterial persistence is essential. The Ser/Thr kinase HipA from *E. coli* has been extensively studied for its role in bacterial persistence. The aim of my thesis was to characterize HipA-like Ser/Thr kinases in *E. coli* and *K. pneumoniae* using quantitative phosphoproteomics to identify their substrates and examine their impact on the proteome and regulation of key bacterial cellular pathways. To achieve this, I studied the overexpression of these kinases and kinase mutants in bacterial cells to assess their effects on bacterial growth, both in the presence and absence of antibiotic exposure. Following this, I conducted quantitative mass spectrometry analysis to measure the bacterial phosphoproteome, followed by extensive data analysis to identify putative kinase substrates and their functional roles. Specific aims and objectives for each chapter were as follows:

1. ***E. coli* Toxin YjjJ (HipH) Is a Ser/Thr Protein Kinase That Impacts Cell Division, Carbon Metabolism, and Ribosome Assembly**

   The main objective was to validate the substrates of Ser/Thr kinase YjjJ in *E. coli* and identify its direct targets.

   a) Proteome and phosphoproteome analysis of Δ*hipBA E. coli* cells overexpressing YjjJ and kinase-dead YjjJ to identify its direct substrates.
   b) *In vitro* kinase assay with purified proteins followed by mass spectrometry to confirm direct phosphorylation of putative substrates by YjjJ.
   c) Analysis of the effect of phosphorylation by YjjJ on the substrate CsrA.
   d) Phenotypic characterization of Δ*yjjJ E. coli* mutant.

2. Deep phosphoproteomics of *Klebsiella pneumoniae* reveals HipA-mediated tolerance to ciprofloxacin

The main objective was to characterize the Ser/Thr kinase HipA in *K. pneumoniae* and identify its phosphorylation targets.

a) Comparison of sequence and structure of HipA and HipB in *E. coli* and *K. pneumoniae*.
b) Bioinformatic sequence analysis of the HipA gene in different bacteria.
c) Phenotypic characterization of overexpression of $hipA_{kp}$ in *E. coli* and *K. pneumoniae* to study its effect on bacterial growth.
d) Proteome and phosphoproteome analysis of overproduced $HipA_{kp}$ to identify its putative substrates in *E. coli* and *K. pneumoniae*
e) Evaluation of the effect of overproduced $HipA_{kp}$ on antibiotic tolerance to gentamicin and ciprofloxacin to study its effect on bacterial growth and phosphoproteome.
f) Comparison of different *K. pneumoniae* phosphoproteome datasets.

3. Results

3.1 Manuscript I

Recent progress in quantitative phosphoproteomics (Published)

Expert Review of Proteomics. 2023 Dec 2;20(12):469-82.

DOI: 10.1080/14789450.2023.2295872

EXPERT REVIEW OF PROTEOMICS
https://doi.org/10.1080/14789450.2023.2295872

Taylor & Francis
Taylor & Francis Group

REVIEW

Recent progress in quantitative phosphoproteomics

Katharina Zittlau, Payal Nashier, Claudia Cavarischia-Rega, Boris Macek, Philipp Spät and Nicolas Nalpas

Quantitative Proteomics, Interfaculty Institute of Cell Biology, University of Tuebingen, Tuebingen, Germany

ABSTRACT

Introduction: Protein phosphorylation is a critical post-translational modification involved in the regulation of numerous cellular processes from signal transduction to modulation of enzyme activities. Knowledge of dynamic changes of phosphorylation levels during biological processes, under various treatments or between healthy and disease models is fundamental for understanding the role of each phosphorylation event. Thereby, LC-MS/MS based technologies in combination with quantitative proteomics strategies evolved as a powerful strategy to investigate the function of individual protein phosphorylation events.

Areas covered: State-of-the-art labeling techniques including stable isotope and isobaric labeling provide precise and accurate quantification of phosphorylation events. Here, we review the strengths and limitations of recent quantification methods and provide examples based on current studies, how quantitative phosphoproteomics can be further optimized for enhanced analytic depth, dynamic range, site localization, and data integrity. Specifically, reducing the input material demands is key to a broader implementation of quantitative phosphoproteomics, not least for clinical samples.

Expert opinion: Despite quantitative phosphoproteomics is one of the most thriving fields in the proteomics world, many challenges still have to be overcome to facilitate even deeper and more comprehensive analyses as required in the current research, especially at single cell levels and in clinical diagnostics.

ARTICLE HISTORY
Received 11 August 2023
Accepted 12 December 2023

KEYWORDS
Isobaric labeling; protein phosphorylation; stable isotope labeling; LC-MS; quantitative phosphoproteomics; phosphopeptide enrichment; DIA; hotspot thermal profiling

1. Introduction

Phosphoproteomics, the global identification and quantification of post-translational protein phosphorylation, has developed from a niche discipline into an established field over the past decades [1,2]. Previously limited by high amounts and complexity of sample material, complex preparation procedure and data interpretation, quantitative phosphoproteomics nowadays allows for the routine quantification of tens of thousands of phosphosites (p-sites) across a wide dynamic range by streamlined and often automatized protocols [3–5].

In general, protein phosphorylation allows for the quick (within seconds) and reversible modulation of a proteins' physicochemical properties [6,7]. The addition or removal of a dianionic phosphoryl group by a protein kinase or phosphatase alters a proteins' three-dimensional structure and ability to form intra- and intermolecular interactions. Thereby, this post-translational modification (PTM) adds an additional layer in tuning protein activity, substrate binding, subcellular localization, or turnover far beyond the fundamental gene expression [8–10]. Consequently, protein phosphorylation represents a universal mechanism driving diverse processes from precise signal transmission to broad cellular reactions such as gene expression, cell growth, cell survival, differentiation, or proliferation [11–13]. Especially in biomedical science, phosphoproteomics is highly relevant, since phosphorylation events are associated with severe diseases such as cancer, Alzheimer's disease and diabetes or even bacterial pathogenesis during infection [14–17].

Regulatory (auto)phosphorylation on kinases are especially important, and their quantification can be used to indirectly infer activity [18]. In cancer, kinases or phosphatases are often found to be mutated, thus representing strong candidates for therapeutic therapies with over 72 kinase inhibitors already approved by the Food and Drug Administration in 2022 [19,20]. Apart from their significance as therapeutic targets, protein kinases and their protein substrates have been used as biomarkers e.g. in the early detection of Parkinson's disease in urine samples [18,21,22]. Thus, deep characterization of protein phosphorylation dynamics within different processes helps to classify their impact on many biological pathways and contributes to the development of new therapeutic agents.

The mere detection (or lack thereof) of phosphorylation on a specific protein is not always revealing, since not all copies of a protein are always modified and physiological effects frequently depend on fine changes in phosphorylation stoichiometry to trigger a reaction. Initially developed for global proteomics, quantitative strategies have soon been extended to the phosphoproteomic field to characterize phosphorylation kinetics over time or to compare transient phosphorylation events between multiple conditions such as during treatments or between phenotypes [12,23–25]. Application of stable isotope labeling,

CONTACT Nicolas Nalpas nicolas.nalpas@univ-rouen.fr INSA Rouen Normandie, CNRS, Polymers, Biopolymers, Surfaces Laboratory UMR6270, University of Rouen Normandie, Rouen F-76000, France; Philipp Spät philipp.spaet@uni-tuebingen.de Quantitative Proteomics, Interfaculty Institute of Cell Biology, Interfaculty Institute for Cell Biology, University of Tuebingen, Auf der Morgenstelle 15, Tuebingen 72076, Germany
Present affiliation of Nicolas Nalpas: INSA Rouen Normandie, CNRS, Polymers, Biopolymers, Surfaces Laboratory UMR6270, University of Rouen Normandie, Rouen F-76000, France

Article highlights

- LC-MS/MS based quantitativephosphoproteomics provides a powerful tool to analyze site-specific proteinphosphorylation.
- Recent developments in phosphopeptideenrichment and labeling techniques enhance the analytic depth, dynamic range,site localization, and data integrity in quantitative phosphoproteomics.
- Advanced workflows enable comprehensivephosphoproteome analyses with less and less input material, relevant forclinical samples and single-cell analyses.

including isobaric tags, enables sample multiplexing, which represented a breakthrough for the precise quantification of phosphorylation events across a multitude of different conditions. For example, multiplex isobaric labeling had been applied to evaluate the effect of different inhibitors of the mitogen-activated protein/extracellular signal-regulated kinase (MEK) on the mouse liver phosphoproteome or to study the time course of phosphorylation dynamics during sleep deprivation [26,27]. Respective metabolic or chemical labeling strategies proved to be robust and require less mass spectrometer (MS) instrument time compared to label-free based quantification [28,29].

2. Challenges of the quantitative phosphoproteomics workflow

Compared to standard quantitative bottom-up proteomic workflows, optimization at multiple stages from sample preparation to data analysis pipeline are required for quantitative phosphoproteomics (Figure 1) [30–32]. A typical quantitative phosphoproteomic workflow includes cell lysis in the presence of phosphatase inhibitors to prevent enzymatic dephosphorylation, followed by protein purification and enzymatic digestion into peptides. Subsequently, phosphorylated peptides, which are typically less abundant compared to their unmodified counterparts, can be enriched by diverse strategies [33]. Optional steps before or after phosphopeptide enrichment include stable isotope labeling for quantification and peptide fractionation to increase the analytical depth. Subsequently, peptide mixtures are delivered for liquid chromatography-tandem mass spectrometry (LC-MS/MS) analysis. Here, information on phosphorylated peptides are acquired by measuring the mass-to-charge ratio (*m/z*) and relative abundance of the precursor (MS), and subsequently of the corresponding peptide fragment ions (MS/MS) originating from precursor fragmentation. After the measurement, a processing of MS raw data is required, which comprises the identification of modified peptides and proteins via database search, the accurate determination of modified sites abundance and the gathering of functional knowledge about the modified sites as reviewed elsewhere [34,35]. Overall, these steps often require further adjustment and optimization since they are highly dependent on several factors, such as sample type or number of conditions to be compared.

Unsurprisingly, the field of quantitative phosphoproteomics has witnessed an explosion of advances in sample preparation and data analysis in the past years [1,30,36,37]. Major advances focus on a deeper coverage of the phosphoproteome, reduced sample input material, increased quantitation accuracy, a higher throughput of samples, more precise p-site localization, a wider dynamic range, a greater understanding of the function of modified sites and an increased knowledge of kinase-substrate relationships. However, the identification and quantification of phosphorylated peptides is dependent on the amount of protein input material and the selectivity of phosphopeptide enrichment strategies for modified peptides [38,39]. Additional challenges arise from the negatively charged phosphoryl group itself. It not only changes the chemical properties of the peptide such as hydrophobicity that can lead to sample losses during e.g. desalting steps but also affects the peptide ionization and peptide fragmentation during MS-based data acquisition [40–42]. In the following, we will point out challenges inherent to the quantitative phosphoproteomic workflow and provide state-of-the-art examples on how they have been overcome.

3. Improving the limit of detection of phosphorylated peptides

By compiling multiple phosphoproteome studies, it was estimated that only 40% to 60% of total p-sites had been so far covered by

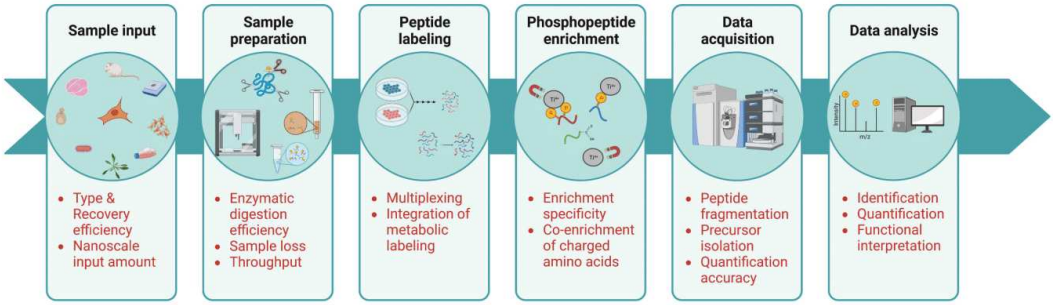

Figure 1. Basics and challenges of the quantitative phosphoproteomics workflow. A quantitative phosphoproteomics workflow requires the extraction of proteins from a given sample input, the efficient enzymatic digestion of these proteins into peptide as well as additional cleanup steps. If a chemical peptide labeling approach is chosen instead of e.g. a metabolic labeling technique, the peptide labeling step mostly precedes the enrichment for low abundant phosphorylated peptides. Ultimately, peptides are measured by LC-MS/MS and the resulting data are interpreted by dedicated software. Although this general protocol found application in a multitude of studies, challenges remain for each workflow step as indicated in red. State-of-the-art techniques aim to overcome these limitations and make the quantitative phosphoproteomics technique even more efficient in integrating ever more challenging and low abundant sample input materials, maximizing the number and quality of identifiable phosphorylation sites, and increasing the confidence in quantification of an ever greater multiplexing of samples.

single studies of different eukaryotic species, leaving room for improvements regarding the consistent identification of phosphorylated proteins [43]. The detection efficiency of phosphopeptides is usually limited by an excess of unmodified peptides during bottom-up proteomics sample preparation [44]. Therefore, dedicated phosphopeptide enrichment strategies have to be considered with species-specific sample input material requirements (between 1-10 mg) [45,46].

The sample input amount is a crucial limiting factor for in-depth phosphoproteomic studies. Although more than 75% of the human proteome is estimated to be phosphorylated, only 2–3% of all peptides are frequently found to be phosphorylated in a given sample and an increase in protein input material for phosphopeptide enrichment allows for deeper coverage of the phosphoproteome across a wider dynamic range [47,48]. While early phosphoproteomic studies required protein inputs of more than 20 mg for the identification of approx. 20,000 p-sites [49], more recent protocols could be optimized for the enrichment of almost 15,000 p-sites from just 12.5 µg starting material in combination with TMT-based quantification [50]. Multiple crucial factors contributed to this improvement such as more selective phosphopeptide enrichment strategies or advances in faster and more precise data acquisition during LC-MS/MS measurements. Phosphoproteomics studies often suffer from protein and peptide losses during sample preparation by e.g. nonspecific surface adsorption of labware. Such an issue can be overcome by reducing the number of pipetting steps as described for the 'all-in-one' one-pot sample preparation strategy [51,52].

As described for the first single cell proteomic approaches, boosting to amplify signal with isobaric labeling (BASIL) or the further improved boosting to amplify signal with isobaric labeling (iBASIL) strategy utilize a boosting/carrier sample (with several fold higher amounts) in a multiplexed analysis to increase the combined signal intensity of a given peptide for low input samples [53–55]. The boosting sample ideally mirrors the proteome composition from the samples of interest, otherwise peptides selected for fragmentation will not be representative. With this approach, more than 20,000 p-sites from human pancreatic islets (200,000 cells) had been quantified (Table 1) [53]. The idea of boosting the signal by the introduction of a carrier sample also found application in the analysis of low abundant tyrosine phosphorylation [56,57]. In comparison to standard bulk phosphoproteomics, nanoscale phosphoproteomics increases the sensitivity and resolution toward the single cell level as well as the throughput by multiplexing. By taking advantage of this new approach, it is now possible to even assess spatial phosphoproteomics with a resolution of 200 µm × 200 µm, as demonstrated for human spleen tissue voxels with 737 quantified p-sites allowing for the distinction between different tissue regions [52].

In addition to the limitations of the protein input material amount, the type of sample under investigation can limit the application of (quantitative) phosphoproteomic strategies. Archived formalin-fixed paraffin-embedded (FFPE) tissue is, for example, are a great resource for patient derived samples [58]. An optimized recovery of phosphorylated proteins by decrosslinking combined with a TMT-multiplexing approach allowed for the quantification of more than 14,000 p-sites, opening up the application of quantitative phosphoproteomics to so-far inaccessible input material [59]. A recent paper from Pujari et al. 2023 describes an adaptive focused acoustics (AFA)-assisted protein extraction that uses AFA-based ultrasonication combined with simultaneous trypsin digestion to enable automated sample processing of laser capture microdissection (LCM)-FFPE tissues in 96-well and 384-well plate formats [60]. Enhancing the extraction efficiency of Suspension-Trapping (S-Trap) method and optimizing it for phosphoproteomics studies, Wang et al. 2023 showed that Phosphoric Acid (PA) used together with methanol to prepare a protein suspension for trapping it on a filter might not be optimal for phosphoproteome studies due to similarities between PA and phosphate groups, and that PA can be replaced by TFA for phosphopeptide enrichment procedures. This method was applied on extracellular vesicles and can be further used for studying FFPE tissues and transmembrane proteins [61,62].

3.1. Optimizing the coverage of phosphorylated peptides

The application of the quantitative phosphoproteomic approach requires the enzymatic digestion of proteins into peptides prior to LC-MS/MS analysis. Classically, the endopeptidase trypsin has been used for the generation of suitable peptides, not only due to its high cleavage accuracy at the C-terminus of the basic amino acids arginine and lysine but also due to the length of generated peptides (~8–15 AA), which are easier to ionize and fragment in a mass spectrometer [63]. In phosphoproteins, the negative charge of the phosphate group can form salt bridges between the phosphorylated residue and positively charged amino acid residues such as arginine and lysine that mask the cleavage site [64]. A potential refinement of this has been introduced by the PhosphoShield strategy [65]. Here, a digallium complex mitigates the salt bridges, thereby enhancing the trypsin cleavage frequency by ~17%.

3.2. Increasing the recovery of phosphorylated peptides

The enrichment of low abundant phosphorylated peptides (or proteins) is one of the most challenging, though most important steps during sample preparation and can be based on different enrichment techniques, such as affinity chromatography or immunoprecipitation [38,66,67]. Without enrichment, low abundant phosphopeptides are typically 'masked' by the vast majority of unmodified peptides during MS-based data acquisition. As a result, the phosphopeptides are either not selected for fragmentation in a typical data-dependent acquisition-MS measurement, or reveal low-quality spectra. Many enrichment strategies have been established for the selective or combined enrichment of phosphorylated serine, threonine, tyrosine (S/T/Y), and less frequently, for histidine or arginine (H/R), as described elsewhere [68]. Independent of the strategy, three main steps are common between protocols. First, phosphorylated peptides are bound to a matrix, either by their chemical (charge) or structural (motif) appearance. Next, a washing step is required to purge non-phosphorylated peptides that are bound with low affinity to the matrix. Finally, phosphorylated peptides are eluted, for example, by increasing pH conditions to neutralize the negative charge state of the phosphoryl group relevant for matrix binding in affinity chromatography. Overall, the most

Table 1. Overview on features of improved LC-MS sample preparation methods and their advantages.

Method name	What is the method?	Advantage
(FFPE) optimized recovery of phosphorylated proteins (59)	Protein extraction with SDS-SP3 (Single pot solid-phase enhanced sample preparation) (120) followed by de-crosslinking combined with a TMT-multiplexing. Automated IMAC enrichment on AssayMap tips without desalting of the eluted phosphopeptides	It helps with inaccessible input material (FFPE) and reduces overall sample losses.
Suspension-Trapping (S-Trap) for phosphoproteomics (61 + 62)	TFA used along with methanol to create a suspension of protein for trapping it on a filter	It can be used for small sample amounts, like extracellular vesicles, FFPE tissues or transmembrane proteins.
Phosphopeptide enrichment for gram-positive bacteria (45)	Automated method with optimized buffers for TiO_2 (for lower sample amounts ≤100 µg) and Fe^{3+}NTA-IMAC (for higher sample amounts ≥250 µg) cartridge-based enrichment on the Agilent AssayMap platform	It is an optimized workflow for species-specific phosphopeptide enrichment for bacteria
Surfactant-assisted one-pot sample preparation (SOP-MS) (51)	n-Dodecyl β-D-maltoside (DDM) is used as surfactant. All steps are performed in the same tube with direct sample loading for LC-MS/MS analysis	It minimizes protein and peptide losses by reducing the number of pipetting steps and possible surface adsorption losses. It can be used for single-cell proteomics.
BASIL (Boosting to Amplify Signal with Isobaric Labeling) (53)	Boosting/carrier sample (with several fold higher amounts) in a multiplexed analysis to increase the combined signal intensity of a given low abundant peptide	It can be used for low input sample
iBASIL (54)	Combination of SOP and BASIL	It reduces both sample loss and processing time
Tandem C18-IMAC-C18 (nanoscale phosphoproteomics) (52)	Streamlined tandem tip-based sample preparation workflow: 1. SOP digestion 2. iBASIL 3. phospho enrichment in a tandem tip-based C18-IMAC-C18	It increases the sensitivity and resolution toward the single cell level, allow phosphopeptide enrichment at low nanogram level
TiO2/Bi/Fe/Zr nanocomposite (69)	Phosphopeptide enrichment using TiO2 co-doped with Bi^{3+}/Fe^{3+}/Zr^{4+} ions	Higher enrichment efficiency and selectivity of phosphopeptides from simple to complex biological samples
PhosphoShield strategy (65)	Addition of digallium complex during tryptic digestion	The digallium complex mitigates the salt bridges, thereby enhancing the trypsin cleavage frequency by ~ 17%
SuperSILAC (82 + 83)	Spiked heavy SILAC labeled which acts as an internal standard	It allows to increase the number of (phospho)proteome samples that can be compared to each other, facilitating the quantitative analysis of clinical samples
DeltaSILAC (85)	Metabolic labeling combined with PTM-specific enrichment to determine turnover rates of phosphoproteins compared to the unmodified forms	It discloses the regulatory role of specific p-sites in the regulation of protein half-lives and revealed an unexpected delaying effect on protein turnover and protein maturation
EasyPhos (6)	TFE-based digestion for low input material without peptide desalting. Rapid and parallel phosphopeptide enrichment in 96-well plate format	It improves coverage and reproducibility for studying the global phosphoproteome dynamics. Samples are measured in a single MS run without the need of fractionation
Improved EasyPhos (113)	Improved EasyPhos method, eliminated the protein precipitation steps and performed the entire protocol on a 96-well plate starting from cell lysis by SDC buffer	It minimizes sample loss and variability. It can be used for low sample input.
Rapid-robotic phosphoproteomics (R2-P2) (116)	SP3 method (120) in a 96-well format that uses a magnetic particle processing robot (KingFisherTM Flex)	It allows scalable and reproducible phosphoproteomics. It can be used for low sample input.

common chromatography strategies rely on the affinity between a Lewis base (phosphoric acid; $H_3PO_4^-$) and a Lewis acid (e.g. Fe^{3+}/Ti^{4+}/$Zr^{3/4+}$). Frequently applied methods are immobilized metal affinity chromatography (IMAC) or metal oxide affinity chromatography (MOAC). Usually, a low pH (2–3) is adjusted during sample loading, ensuring phosphate deprotonation (pKa = 2.12) and reducing the nonspecific binding of peptides containing acidic amino acids such as aspartate (pI = 2.9) and glutamate (pI = 3.0). To further decrease the contamination of non-phosphorylated peptides organic molecules such as lactic acid, glycolic acid, and 2,5-dihydroxybenzoic acid (DHB) can be added during sample loading as competitors with lower binding affinity than the phosphate groups [39]. Recently, TiO_2 co-doped with Bi^{3+}/Fe^{3+}/Zr^{4+} ions had been described, leading to the enrichment of 676 p-sites from 100 µg HeLa cell lysate [69]. Furthermore, the choice of the applied enrichment strategy depends on the amount of the available input material. To this end, it was shown that magnetic Fe^{3+}-NTA beads outperform agarose Fe^{3+}-NTA beads in terms of downscaling the input material, making magnetic beads more attractive for samples with micro- to nanoscale input material [48].

To decrease the sample complexity and thereby increase the identification of phosphorylated peptides, off-line peptide separation techniques have been used, such as high pH reverse phase (HpH-RP), strong-cation exchange (SCX) chromatography or hydrophilic interaction liquid chromatography (HILIC) [70–72]. Earlier studies already showed that with HpH-RP fractionation more phosphorylated peptides (>30,000) can be recovered, although with a bias toward singly phosphorylated peptides [72]. Indeed, multiple phosphorylated peptides interact less with the RP matrix, making these peptides vulnerable to be purged as they flow through during sample loading. The use of triethylammonium (TAE) as an additive mobile phase during HpH-RP elution revealed that more phosphorylated peptides can be recovered compared to the use of ammonia [39].

Interestingly, it had been shown that even without phosphopeptide enrichment more than 1,400 phosphopeptides can be quantified from a peptide mixture by a TMT multiplex

approach with a carrier channel consisting of enriched phosphopeptides [73].

Usually, a sample clean-up step by solid-phase extraction (SPE) is performed before samples are injected into LC-MS systems. So far, SPE based on RP C18 material or graphite are the most commonly applied strategies [74,75]. A recent study comparing 16 different SPE purification sorbents showed that vendor-dependent C18 material and graphite can minimize the loss of phosphorylated peptides by 3–33% [42]. In addition, the application of poly(styrene-divinylbenzene) copolymer during low-temperature solid-phase extraction (CoolTip) recovered 6.1-fold more phosphorylated peptides [76].

3.3. Selection of quantitative strategies for global phosphoproteomics

Quantitative strategies based on labeling with stable isotopes suffer from the increase in complexity during multiplexing. To reduce technical bias during the sample preparation, an early mixing of the differentially labeled samples, ideally on the level of metabolically labeled cells is beneficial. Chemical labeling strategies of proteins or peptides involve additional preparation steps that can lead to individual differences between samples, such as varying protein digestion efficiencies, affecting the pool of generated peptides and ultimately their quantification. The highest potential for sample preparation-related inaccuracies in quantification can be expected for label-free quantification, in which all preparation steps and MS measurements are separated for each sample. In the following, we will discuss different labeling strategies and their suitability in quantitative phosphoproteomics. Representative studies that combine these labeling strategies with phosphopeptide enrichment protocols for different input materials are represented in Figure 2.

3.3.1. Integration of metabolic labeling strategies

The quantification of global S/T/Y phosphorylation in discovery proteomics benefitted strongly from the establishment of an array of multiplexed labeling strategies such as metabolic stable isotope labeling by amino acids in cell culture (SILAC) [77]. Previous chemical labeling techniques suffered either from being restricted to phosphopeptides containing cysteine residues (isotope-coded affinity tags; ICAT) or were incompatible with tyrosine phosphorylation (phosphoprotein isotope-coded affinity tag; PhIAT) [78,79].

To date, a high number of phosphoproteome studies are based on SILAC, for example, the characterization of kinase-substrate relationships in human breast cancer cells, skeletal myotubes, or *E. coli* [25,80,81]. The initial strategy is still undergoing development, leading to broader fields of application. The superSILAC concept extended the number of (phospho) proteome samples that can be compared to each other by a spiked heavy SILAC labeled internal standard, facilitating the quantitative analysis of clinical samples [82]. Recently, the superSILAC approach has been used to study the impact of β-adrenergic receptor (β-AR) stimulation on the mouse heart phosphoproteome, quantifying more than 10,000 p-sites and

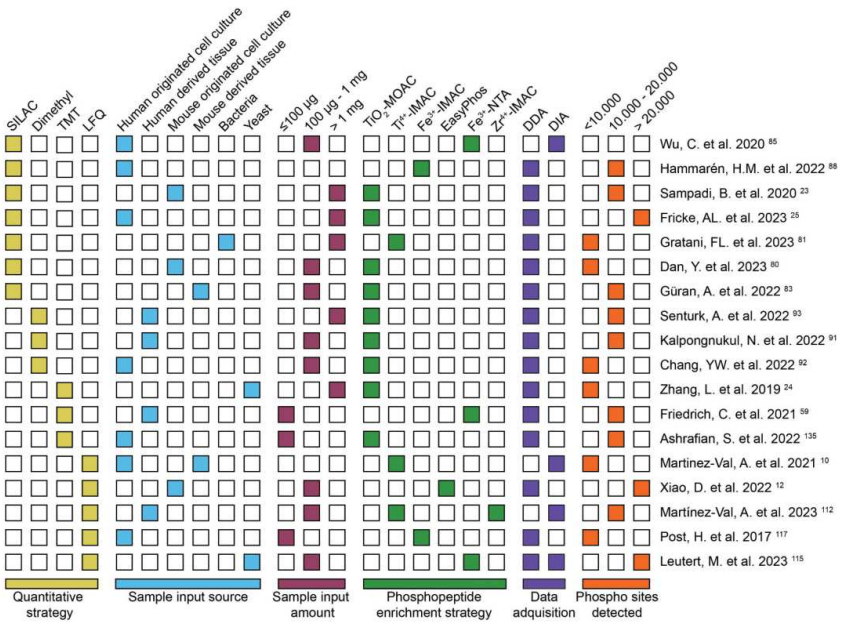

Figure 2. Heatmap of representative studies. Listed are recent references exemplifying the combinatorial possibilities for quantitative strategies with different phosphopeptide enrichment strategies for a diverse array of sample input materials and amounts, along with type of data acquisition method and the number of p-sites identified. Selected are key quantitative techniques that are most commonly found in recent studies. Indicated protein input amounts refer to single labeling channels. Empty fields mark unspecified information within the respective reference.

validating a rewiring of the intrinsic signaling network [83]. Moreover, the application of dynamic SILAC labeling became key for the global investigation of protein turnover by determining protein *de novo* synthesis and degradation rates, which are frequently regulated by phosphorylation [84]. Replacement rates of incorporated heavy SILAC amino acids provided after growth media exchange in cell culture are monitored during a time course. Consecutively, intracellular turnover rates can be calculated from measured isotope ratios for each (modified) peptide. This concept was recently optimized for the delta determination of turnover rates of phosphoproteins compared to the unmodified forms by SILAC (DeltaSILAC) [85]. Thereby, DeltaSILAC discloses the regulatory role of specific p-sites in the regulation of protein half-lives and revealed an unexpected delaying effect on protein turnover and protein maturation in human cancer cells. Further, important roles of protein phosphorylation on protein turnover and protein maturation had been previously identified in the phosphorylation of ubiquitin Ser65 and in bacterial arginine phosphorylation, both of which are molecular markers for protein degradation [86–88].

3.3.2. Chemical labeling and label-free strategies on the rise

Besides metabolic labeling, multiple other chemical labeling approaches have been developed after ICAT and successfully applied in quantitative phosphoproteomics. More recent developments, such as stable isotope-coded mass tags and isobaric mass tags, target peptide amine groups present on peptide N-termini and lysine side chains for stable isotope labeling. The former concept, to which dimethylation labeling is attributed, is a robust and cost-efficient labeling technique, which can be applied to literally any phosphoproteome sample [89–92]. This is especially favorable when labeling of large sample amounts (>1 mg) is required for the subsequent enrichment of low-abundant phosphopeptides, e.g. from prokaryotic samples. Clinical studies profit likewise from dimethylation labeling, such as for the investigation of aberrant phosphorylation signaling cascades in clear cell Renal Cell Carcinoma (ccRNC) [93].

In contrast, isobaric tags, such as tandem mass tags, isobaric tags for relative and absolute quantification (iTRAQ) or *N,N*-dimethyl leucine isobaric tags (DiLeu) provide a substantially higher level of multiplexing, with up to 18 channels in TMT experiments [94–97]. The high-throughput quantification is on the downside of high costs for labeling reagents, and therefore, usually restricted to phosphoproteome studies in eukaryotes with low input material such as clinical samples, or for labeling of purified phosphopeptides. For increased robustness and consistency in quantifying low-abundant phosphorylation events, sophisticated TMT-labeling protocols, such as streamlined TMT, have been further developed [3]. This approach combines single step spin column phosphopeptide enrichment with synchronous precursor selection on MS^3 levels in tribrid mass spectrometers. In an alternative nanoscale strategy, enriched phosphopeptides are solid-phase TMT labeled after on-column TiO_2 chromatography [98]. This procedure improves the recovery of singly phosphorylated peptides and simultaneously reduces the consumption of TMT reagent significantly, concomitantly leading to an improved sensitivity during MS measurements.

In contrast to the isotopic labeling strategies, label-free quantification (LFQ) does in general not require any predefined labeling conception and therefore allows a theoretically infinite number of samples that can be quantitatively compared. However, separate sample processing and measurements are prone to biased quantification, especially in phosphoproteomics. Respectively, more independent replicates (biological and technical) are required, which multiplies the expenditure of lab work and instrument time. The key to an accurate quantification in LFQ is the normalization of LC-MS run-to-run variations, for which dedicated software is required, such as MaxLFQ [99].

3.3.3. Analysis and quantification of phosphorylated peptides by mass spectrometry

Together with the optimal preparation workflow, accurate measurement of labeled phosphopeptides is important to generate high-quality data and support an unbiased downstream analysis. Several challenges have been identified so far that hamper high-quality data acquisition of phosphorylated peptides. For instance, the negative charge of the phosphoryl group hampers the ionization of overall positively charged tryptic peptides. In addition, the labile phosphoryl group can negatively influence the generation of peptide fragment ions [100].

In typical tandem MS approaches, m/z ratios of (phospho) peptide ions are determined in precursor scans, resulting in a MS spectrum. Depending on the data acquisition mode, precursor ions are either selected for MS/MS-based sequencing by their intensities during data-dependent acquisition (DDA) mode or isolated within a broader isolation window independent of peptide intensities during data-independent acquisition (DIA) mode. In DDA, a pre-defined number of high abundant peptides (top N) are selected after the precursor scan for subsequent peptide fragmentation and MS/MS analysis. Although being greatly used due to its straightforward down-stream data interpretation, this semi-statistic type of data acquisition is prone to missing out the fragmentation of low abundant peptides that will result in the so-called missing value problem. DIA overcomes this limitation, resulting in a deeper coverage of peptide species across a wider dynamic range, greatly increasing the data complexity as described below. Fragmentation of precursor ions generates different fragment ion types, e.g. b-/y-ions by collision induced dissociation (CID). The m/z ratios of fragment ions recorded in MS/MS spectra give sequence information for each precursor ion. A common observation for phosphopeptides is the neutral loss of the phosphoryl group that hampers peptide fragmentation, resulting in an incomplete fragment ion series of the phosphopeptide and putatively unassigned phosphorylation sites [100,101]. Back-to-back comparisons of different fragmentation methods such as electron transfer dissociation (ETD), Multi-Stage Activation (MSA) or UV light had been described and can be found elsewhere [100,102]. By using hybrid fragmentation methods, e.g. HCD in combination with ETD, better precursor fragmentation can be achieved resulting in improved sequence

coverage and ultimately more precise localization of the p-sites [103].

Characteristic for isobaric tags is the quantification of the labeled (phospho)peptides, which are indistinguishable on MS levels due to identical masses. Quantification of a selected (phospho)peptide is possible only after precursor isolation and fragmentation (mostly by HCD), when reporter ions are released from balance groups and corresponding reporter peak intensities can be quantified on MS/MS (or MS^3) level. Therefore, quantification strategies can be classified as either MS (see SILAC and dimethylation labeling) or MS/MS-based quantification (TMT). In the former method, intensities of differentially labeled peptides are compared relatively to each other. Thereby, the number of available labels is limited (usually to three), as this form of multiplexing leads to an increase in spectrum complexity. This is not the case in MS/MS-based quantification techniques, which rely on the comparison of reporter ion intensities in the low *m/z* range theoretically without increasing the spectrum complexity. However, a common drawback connected to MS/MS based quantification techniques results from co-isolated ions with similar m/z ratios, leading to a mixture of different co-fragmented precursors with undistinguishable reporter ions. Narrower isolation windows for peptide isolation and additional precursor isolation steps in MS^3 level-based quantification are beneficial for unbiased quantification. Similarly, ion-mobility dependent separation of precursor ions by high-field asymmetric waveform ion mobility spectrometry (FAIMS) had been proven to be especially beneficial in TMT-based quantification accuracy [104]. Muehlbauer et al. further validated an increase in the depth of p-site coverage of 25–20% by application of the FAIMS interface [105].

In contrast to bottom-up proteomics, which relies on the analysis of peptides after enzymatic protein digestion, intact proteins can be analyzed in top-down approaches. This technique has been proven to be beneficial especially for multi-PTM mapping of individual proteoforms [106], since information about the co-occurrence of PTMs on individual protein species is lost in the bottom-up proteomics approach. Recently, top-down proteomics has been applied to study altered protein phosphorylation during ischemic cardiomyopathy [107]. In addition, it has been expanded to the single cell level, where it has been recently applied to study multinucleated single muscle cells and showed high variability of the protein phosphorylation landscape between muscle fibers [108].

Based on findings by the above described methods applied in discovery phosphoproteomics, hypothesis-driven applications in targeted phosphoproteomics, notably selection (or multiple) reaction monitoring (SRM/MRM) and parallel reaction monitoring (PRM) overcome limitations in the reproducible and selective identification and quantification of phosphopeptide subpopulations as described in detail elsewhere [109,110]. In recent years, internal standard triggered-parallel reaction monitoring (IS-PRM) enriched the phosphoproteomics field by the usage of isotopically labeled synthetic phosphorylated peptides that aid in accurate data acquisition and quantification of phosphorylated peptides as shown for hundreds of tyrosine phosphorylations (SureQuant pTyr) [111]. This approach was only recently combined with the DIA strategy (hybrid-DIA) that combines global phosphoproteome and targeted analysis of defined phosphopeptides derived from low sample input material (<30 µg) [112].

3.4. Streamlining the (quantitative) phosphoproteomic workflow

To simplify and speed-up a workflow with many perturbations or large cohorts of samples, several automatized phosphoproteomic workflows have been developed. In 2015, Humphrey and coworkers developed a method called EasyPhos for studying the global phosphoproteome dynamics with improved coverage and reproducibility in a single MS run without the need of fractionation [6]. Peptide desalting was eliminated and phosphopeptide enrichment was performed using TiO_2 beads on a 96-well plate directly following protein digestion. In 2018, they improved this method further by eliminating the protein precipitation step among others to perform all the steps in a 96-well plate [113]. These optimizations further boosted the identification of 20,132 distinct phosphopeptides from 200 µg of proteins from glioblastoma cells.

Another method is the rapid-robotic phosphoproteomics (R2-P2), which is a novel method based on SP3 (single-pot solid-phase-enhanced sample preparation) proteomics workflow [114]. It is based on a magnetic particle processing robot, which performs protein and peptide clean-up via carboxylated magnetic beads followed by phosphopeptide enrichment via IMAC. With this end-to-end automatized sample preparation workflow, phosphopeptide enrichment with different magnetic beads (Fe^{3+}/Ti^{4+}-IMAC/Zr^{4+}-IMAC/TiO_2) can reach a depth of 13,417 phosphorylated peptides from 250 µg of yeast protein extract. A subsequent R2-P2 based high throughput analysis of 101 environmental and chemical perturbations resulted in a signaling network map of 25,000 regulated p-sites in yeast [115]. Muller and colleagues also used SP3 by implementing it in an automated 96-well format to process low-input clinical samples [116]. AutoSP3 has reduced the handling time, the variability and improved the reproducibility by performing protein purification, digestion, and directly delivering peptides for measurement.

Automatized workflows were moreover used to compare different enrichment strategies. For example, automatization has improved the overlap of enriched phosphopeptides between Ti^{4+}-IMAC, Fe^{3+}-IMAC, and TiO_2 by 76% [117]. In 2021, Birk and colleagues optimized the phosphopeptide enrichment for gram-positive bacteria and presented an automated method with optimized buffers for TiO_2 and Fe^{3+}-NTA-IMAC cartridge-based enrichment on the Agilent AssayMap platform [45]. While Fe^{3+}-NTA cartridges were shown to be more successful for the enrichment of phosphopeptides from high sample amounts (250 µg), TiO_2-based enrichment was shown to be more efficient for lower sample amounts (<100 µg).

3.5. Quantitative phosphoproteomics integration into systems biology

Systems biology seeks to integrate multi-level '–omics' data to explain functional similarities within higher-order networks [118]. With respect to its fundamental role within these networks, the dynamics of phosphorylation is an important component in the system-wide modeling of pathways to fully characterize cellular processes and disease development [119–121]. However, combining multiple –omics studies requires a compatible sample preparation procedure for each –omics level such as the extraction of RNA molecules, metabolites, lipids, and (phospho)proteins [122,123]. For example, the temporal mapping of mouse cardiac phosphoproteome, proteome, metabolome, and transcriptome required omic-dependent optimized sample preparation that excluded the analysis of the same mouse heart by (phospho)proteomics and metabolomics techniques [123]. Similar limitations of incompatible sample preparation procedures were encountered by Pang et al. in a multi-omics analysis combining transcriptomics, proteomics, phosphoproteomics, and metabolomics to elucidate the metabolic reprogramming upon ZIKV-infection in mouse brains [124]. Additional limitations in sample material amounts hampered the combined analysis of the proteome, phosphoproteome, and metabolome on the same sample, excluding transcriptomic analysis [124]. Despite these challenges, recent efforts allowed the combined analysis of the proteome, metabolome, and phosphoproteome from single cells [125,126].

Expanding the regulatory role of phosphorylation, multiple PTMs can contribute to a higher order of regulation by impacting each other's occurrence on the same or different proteins [127]. Multiple PTMs can compete for the same site (reciprocal crosstalk), enhance (positive crosstalk) or inhibit (negative crosstalk) each other's presence [128]. Similar to the phosphoproteomic workflow requires the analysis of other PTMs an enrichment step for modified peptides such as di-glycine remnants (KεGG)- or acetyl-lysine motif (Ac-K) immunoaffinity purification for ubiquitylated or acetylated peptides [129,130]. To compare the dynamics of these different PTMs, the enrichment strategies are streamlined and start with the same sample input, followed by a serial enrichment in which the flow-through of the previous enrichment protocol serves as input for the next. In addition, the integration of a multiplexing approach allows the comparison of multiple PTMs across various conditions. Previous studies applying SILAC quantification to simultaneously study the phosphoproteome, ubiquitylome, and acetylome with an extensive fractionation method quantified more than 20,000 phosphorylation, 15000 ubiquitylation, and 3,000 acetylation sites from 15 mg of starting material [131]. In 2022, Li and colleagues developed a novel strategy for enrichment of N-glycopeptides and phosphopeptides simultaneously by the application of a stationary phase chitosan-graphene oxide incorporated with ZIF8 (GO@CS@ZIF8) foam, enriching 40 phosphorylated and 423 N-glycosylated peptides from ~250 µg of human serum digest [132]. Furthermore, Fan and coworkers developed a strategy for the simultaneous enrichment and identification of OGlcNAc and phosphorylated peptides from RNA-binding proteins (RBP) with more than 450 OGlcNAc and 670 phosphorylated peptides identified [133]. In 2021, Abelin et al. developed a novel protocol via the use of a TMT multiplexing approach to interrogate low sample input material across multiple experimental conditions [134]. This method is called the multi-omic networked tissue enrichment (MONTE) protocol and allows the analysis of HLAI and HLAII immunopeptidome, proteome, ubiquitylome, phosphoproteome, and acetylome. With an input material of 0.5 mg, more than 28,000 phosphorylation, 14,000 ubiquitylation, and 6,000 acetylation sites had been quantified [134]. The re-usage of the flow through from one enrichment step as input for another found application also for the analysis of phosphorylation and acetylation dynamics to investigate the impact of safranal on triple negative breast cancer cells [135].

4. Data-independent acquisition for phosphoproteomics

As mentioned above, data-independent MS acquisition (DIA) has multiple benefits for the analysis of known targets compared to DDA. DIA provides greatly improved identification reproducibility, quantification accuracy and precision, and wider dynamic range [136,137]. In a DDA phosphoproteomic study, the number of missing values can be even more severe than in standard proteomic experiments. Thus, the reproducibility of identification takes a renewed importance and DIA can be an excellent strategy. However, DIA-generated data is much more complex due to the generation of mixed MS/MS spectra from co-eluting and -fragmented precursor ions [138] and thus requires dedicated software solutions.

Originally, DIA measurements were analyzed by matching MS/MS spectrum against organism-specific (or even sample-specific) spectral libraries using specialized software such as Spectronaut™, Skyline or OpenSWATH [137,139]. Such a spectral library contains considerably more information compared to the theoretical MS/MS spectra used in DDA strategy. Notably, the precursor and fragment ions mass-to-charge ratios and intensities, the chromatographic retention time, the precursor ionization charge and the ion species for each fragment. Traditionally, spectral libraries were generated from DDA measurement based on identical samples and chromatography, so that the library is fully compatible with the DIA measurements. This leads to an increase in cost and measurement time since each sample has to be measured by DDA before DIA can be applied, which is unfeasible for samples with low input material [138]. In recent years, this particular nuisance has been partially remedied, firstly with the availability of reference spectral libraries in public resources, such as PeptideAtlas or MassIVEKB [140,141], although these are not available for every organism or every analytical set-up. And secondly, several algorithms, such as DeepMass or Prosit, have been developed for *in silico* spectral library generation [142–144], which can in principle be applied to any organisms or PTMs, including phosphorylation [145]. This was exemplified in 2020 by Bekker-Jensen and colleagues who studied the

phosphorylation targets of 10 protein kinases in the epidermal growth factor signaling pathway [146]. Notably, library-free DIA resulted in the identification and quantification of over 10,000 p-sites across 186 samples, each measured on a 15 min LC gradient.

Another recent development, from Demichev and coworkers, consists in the application of deep neural networks to distinguish between target and decoy precursors in DIA data [147]. To do so, DIANN computes 73 different scores (e.g. mass accuracy, similarity of spectra) that describe the correspondence between each precursor (target or decoy) and the candidate elution peaks. The set of scores for each precursor are used as input to the neural networks, which return a single discriminant score per precursor indicating the likelihood that the candidate elution peaks originated from a precursor. Interestingly, the DIANN method displayed superior performance in comparison to other DIA analysis software when applied to proteomic datasets [148]. However, in the context of phosphoproteomics, Lou and colleagues suggest using DIANN in combination with other software to improve sensitivity, although its scoring model still proved excellent. The higher sensitivity of Spectronaut™ was also observed by Skowronek and coworkers via their DIAPASEF analytical setup [149].

5. Investigating the function of phosphorylated sites

While the large-scale quantitative measurement of p-sites is now becoming a routine [150], high amounts of data only increase the gap in our understanding of the function of modified sites [151]. To address this deficit, several wet-lab or bioinformatic methods have been reported. In 2018, Huang and colleagues described the Hotspot Thermal Profiling (HTP) to measure the thermal stability of modified proteoforms [152]. Through this approach, the authors showed that 719 proteins (out of 2,883) had a change in Tm as a result of 'hotspot' protein modification sites. The authors assert that HTP alone or together with protein–protein or protein–metabolite interaction datasets will provide functional information on individual sites. A follow-up study by Potel and colleagues optimized the HTP protocol, notably by labeling peptides with TMT prior to phosphopeptides enrichment to reduce variation during enrichment [153]. They showed that this resulted in higher biological replicates correlation and that the p-sites impacting thermal stability were not as numerous as reported by Huang et al. They did highlight some genuine examples, such as the phosphorylated tyrosine 397 within the non-receptor tyrosine protein kinase LYN, which directly affects the protein conformation.

One bioinformatic approach consists in the prioritization of p-sites in *H. sapiens* based on their functional score [151]. The integrated score, based on 59 metrics, was indicative of each p-site's relevance in context of protein structure, cell signaling, and even evolutionary conservation. However, as mentioned by the authors, the score did not perform equally for all functional characteristics, e.g. phosphorylated sites affecting protein cellular localizations were poorly prioritized. In another approach, Krug and colleagues compiled a database of p-sites-centric functional information based on the literature [154]. Notably, this database includes signatures of kinase-substrate, molecular signaling pathways and perturbation in humans, but also mouse and rat. The authors then adapted the algorithm for gene set enrichment analysis [155], so that it can test the enrichment of PTM signature (i.e. by including direction of change in abundance into specific signature). Yet another example is the ProteoSushi software, which facilitates, among other tasks, the retrieval of biological annotation from the UniProt online resource [156]. The generated output contains, for each modified residue, information at the site-, domain- or protein-centric, which can then be used for biological interpretation.

6. Expert opinion

In contrast to analyzing the mere presence or absence of protein phosphorylation in a specific sample, quantitative analysis of phosphorylation dynamics, e.g. between treated and untreated samples or over a time series, is fundamental to study the functional role of this versatile PTM. Since already fine changes in phosphorylation abundance (i.e. the site-specific occupancy) can trigger signal transduction, tune enzyme activity or regulate translation and transcription in a cell, high analytical sensitivity, precision, and accuracy are required, for all of which LC-MS/MS based quantification methods represent to date the method of choice for discovery studies.

Starting from the initial approach, there was always an attempt to push the existing boundaries of established quantitative phosphoproteome methods to make them even faster, deeper and more sensitive. In combination with the constantly improving performance of mass spectrometers, the field is now approaching a level where phosphoproteomes can be studied in samples with low protein yields, such as in tissue biopsies. At the same time, these technological advances on the LC-MS side have also extended the scope of phosphoproteome analyses beyond discovery studies, enabling routine analyses of dozens of samples per day based on data independent MS acquisition.

Despite cumulative research studies impressively highlight the advantages and great potential of quantitative phosphoproteomics, only a few applications have been established so far in routine medical diagnosis, predominantly for determining the phosphorylation levels of specific biomarkers in body fluids. Posing the question which crucial limitations still exist and have to be overcome for a broader application of quantitative phosphoproteomics in routine diagnostics, a combination of all factors rather than a single factor can be named. Besides the sensitivity, necessary optimizations also concern the robustness and reliability of analyses, which are influenced on many levels from sampling and sample preparation to the LC-MS/MS based measurement and data analysis.

Especially in the context of protein phosphorylation, which is per se susceptible to the broad and uncontrolled activity of cellular phosphatases during sampling and cell disruption, standardized protocols and common operating procedures are required to minimize the influence of artificial variations. While this can be largely prevented in cell cultures by the addition of phosphatase inhibitors and chaotropic substances in the laboratory environment, the sampling of clinical materials, such as patient derived

tissue dissections or postmortem specimen is more prone to variabilities, resulting in poor data quality. Streamlined procedures considering the lability of protein phosphorylation will be essential for the meaningful use of quantitative phosphoproteomics in clinical diagnostics.

More than 25 years after it entered the field of molecular biology, phosphoproteomics is still a thriving and dynamic discipline. Looking at the innovations of recent years highlighted in this review, it is conceivable that quantitative phosphoproteomics will become even more widely applicable within the next decade, overcoming many limitations that have existed to date. Eventually, we will be able to reach the single cell level.

From a technological perspective, the foundations are already there for this goal, represented by the newest generation of hybrid Orbitrap and time-of-flight mass spectrometers, both of which reach sensitivities required for single-cell analysis.

Funding

This research was funded by the Deutsche Forschungsgemeinschaft (DFG) through grant numbers GRK2364 "MOMbrane", EXC2124 "CMFI", FOR2816 "SCyCode", TRR 261- Project-ID 398967434, SPP2389 "Emergent Functions of Bacterial Multicellularity" and by the European Union's Horizon 2020 research and innovation program under the Marie Sklodowska-Curie grant agreement No. 955626.

Declaration of interest

The authors have no relevant affiliations or financial involvement with any organization or entity with a financial interest in or financial conflict with the subject matter or materials discussed in the manuscript. This includes employment, consultancies, honoraria, stock ownership or options, expert testimony, grants or patents received or pending, or royalties.

Reviewer disclosures

Peer reviewers on this manuscript have no relevant financial or other relationships to disclose.

ORCID

Philipp Spät http://orcid.org/0000-0001-6349-099X
Nicolas Nalpas http://orcid.org/0000-0002-7255-6214

References

Papers of special note have been highlighted as either of interest (•) or of considerable interest (••) to readers.

1. Nilsson CL. Advances in quantitative phosphoproteomics. Anal Chem. 2012;84:735–746. American Chemical Society. doi: 10.1021/ac202877y
2. Conrads TP, Issaq HJ, Veenstra TD. New tools for quantitative phosphoproteome analysis. Biochem Biophys Res Commun. 2002;290:885–890. Academic Press: doi: 10.1006/bbrc.2001.6275
3. Navarrete-Perea J, Yu Q, Gygi SP, et al. Streamlined tandem mass tag (SL-TMT) protocol: an efficient strategy for quantitative (phospho)proteome profiling using tandem mass tag-synchronous precursor selection-MS3. J Proteome Res. 2018 Jun 1;17(6):2226–2236. doi: 10.1021/acs.jproteome.8b00217
4. Amoresano A, Marino G, Cirulli C, et al. Mapping phosphorylation sites: a new strategy based on the use of isotopically-labelled dithiothreitol and mass spectrometry. Eur J Mass Spectrom. 2004;10(3):401–412. doi: 10.1255/ejms.599
5. Cao P, Stults JT. Phosphopeptide analysis by on-line immobilized metal-ion affinity chromatography–capillary electrophoresis–electrospray ionization mass spectrometry. J Chromatogr A. 1999;853:225–235. Elsevier. doi: 10.1016/S0021-9673(99)00481-1
6. Humphrey SJ, Azimifar SB, Mann M. High-throughput phosphoproteomics reveals in vivo insulin signaling dynamics. Nat Biotechnol. 2015 Sep 10;33(9):990–995. doi: 10.1038/nbt.3327
7. Blazek M, Santisteban TS, Zengerle R, et al. Analysis of fast protein phosphorylation kinetics in single cells on a microfluidic chip. Lab Chip. 2015 Feb 7;15(3):726–734. doi: 10.1039/C4LC00797B
8. Nishi H, Shaytan A, Panchenko AR, Physicochemical mechanisms of protein regulation by phosphorylation. Front Genet. 2014;5. Frontiers Research Foundation. doi: 10.3389/fgene.2014.00270
9. Humphrey SJ, James DE, Mann M. Protein phosphorylation: a Major switch mechanism for metabolic regulation. Trends Endocrinol Metab. 2015;26:676–687. Elsevier Inc. doi: 10.1016/j.tem.2015.09.013
10. Martinez-Val A, Bekker-Jensen DB, Steigerwald S, et al. Spatial-proteomics reveals phospho-signaling dynamics at subcellular resolution. Nat Commun. 2021 Dec 1;12(1). doi: 10.1038/s41467-021-27398-y
11. Olsen JV, Blagoev B, Gnad F, et al. Global, in Vivo, and site-specific phosphorylation dynamics in signaling networks. Cell. 2006 Nov 3;127(3):635–648. doi: 10.1016/j.cell.2006.09.026
12. Xiao D, Caldow M, Kim HJ, et al. Time-resolved phosphoproteome and proteome analysis reveals kinase signaling on master transcription factors during myogenesis. iScience. 2022 Jun 17;25(6):104489. doi: 10.1016/j.isci.2022.104489
13. Zhao P, Malik S. The phosphorylation to acetylation/methylation cascade in transcriptional regulation: how kinases regulate transcriptional activities of DNA/histone-modifying enzymes. Cell Biosci. 2022;12(1):1–23. BioMed Central Ltd. doi: 10.1186/s13578-022-00821-7
14. Singh V, Ram M, Kumar R, et al. Phosphorylation: implications in cancer. Protein J. 2017;36(1):1–6. Springer Science and Business Media, LLC. doi: 10.1007/s10930-017-9696-z
15. Wu D, Hu D, Chen H, et al. Glucose-regulated phosphorylation of TET2 by AMPK reveals a pathway linking diabetes to cancer. Nature. 2018 Jul 26;559(7715):637–641. doi: 10.1038/s41586-018-0350-5
16. Oliveira J, Costa M, De Almeida MSC, et al. Protein Phosphorylation is a Key Mechanism in Alzheimer's Disease. JJ Alzheimer's Dis. 2017;58:953–978. IOS Press. doi: 10.3233/JAD-170176
17. Bonne Køhler J, Jers C, Senissar M, et al. Importance of protein Ser/Thr/Tyr phosphorylation for bacterial pathogenesis. FEBS Lett. 2020;594:2339–2369. Wiley Blackwell. doi: 10.1002/1873-3468.13797
18. Korecka M, Shaw LM. Mass spectrometry-based methods for robust measurement of Alzheimer's disease biomarkers in biological fluids. J Neurochem. 2021;159:211–233. John Wiley and Sons Inc. doi: 10.1111/jnc.15465
19. Bhullar KS, Lagarón NO, McGowan EM, et al. Kinase-targeted cancer therapies: progress, challenges and future directions. Mol Cancer. 2018;17(1). BioMed Central Ltd. doi: 10.1186/s12943-018-0804-2
20. Roskoski R, Properties of FDA-approved small molecule protein kinase inhibitors: a 2023 update. Pharmacol Res. 2023;187: Academic Press. doi: 10.1016/j.phrs.2022.106552
21. Nirujogi RS, Tonelli F, Taylor M, et al. Development of a multiplexed targeted mass spectrometry assay for LRRK2-phosphorylated rabs and Ser910/Ser935 biomarker sites. Biochem J. 2021 Jan 1;478(2):299–326. doi: 10.1042/BCJ20200930
22. Hadisurya M, Li L, Kuwaranancharoen K, et al. Quantitative proteomics and phosphoproteomics of urinary extracellular vesicles define putative diagnostic biosignatures for Parkinson's disease. Commun Med. 2023 May 10 [cited 2023 Jun 7];3(1):64. doi: 10.1038/s43856-023-00294-w
23. Sampadi B, Pines A, Munk S, et al. Quantitative phosphoproteomics to unravel the cellular response to chemical stressors with different modes of action. Arch Toxicol. 2020 May 1;94(5):1655–1671. doi: 10.1007/s00204-020-02712-7

24. Zhang L, Winkler S, Schlottmann FP, et al. Multiple layers of phospho-regulation coordinate metabolism and the cell cycle in budding yeast. Front Cell Dev Biol. 2019 Dec 17 [cited 2023 Jun 3];7:338. Available from: https://www.frontiersin.org/article/10.3389/fcell.2019.00338/full
25. Fricke AL, Mühlhäuser WWD, Reimann L, et al. Phosphoproteomics profiling defines a target landscape of the Basophilic protein kinases AKT, S6K, and RSK in Skeletal Myotubes. J Proteome Res. 2023 Mar 3;22(3):768–789. doi: 10.1021/acs.jproteome.2c00505
26. Paulo JA, McAllister FE, Everley RA, et al. Effects of MEK inhibitors GSK1120212 and PD0325901 in vivo using 10-plex quantitative proteomics and phosphoproteomics. Proteomics. 2015 Jan 1 [cited 2023 Jun 6];15(2–3):462–473. doi: 10.1002/pmic.201400154
27. Wang Z, Ma J, Miyoshi C, et al. Quantitative phosphoproteomic analysis of the molecular substrates of sleep need. Nature. 2018 Jun 21;558(7710):435–439. doi: 10.1038/s41586-018-0218-8
28. Hogrebe A, Von Stechow L, Bekker-Jensen DB, et al. Benchmarking common quantification strategies for large-scale phosphoproteomics. Nat Commun. 2018 Dec 1;9(1):1–13. doi: 10.1038/s41467-018-03309-6
29. O'Connell JD, Paulo JA, O'Brien JJ, et al. Proteome-wide Evaluation of two common protein quantification methods. J Proteome Res. 2018 May 4;17(5):1934–1942. doi: 10.1021/acs.jproteome.8b00016
30. Urban J. A review on recent trends in the phosphoproteomics workflow. From sample preparation to data analysis. Anal Chim Acta. 2022;1199:338857. Elsevier B.V. doi: 10.1016/j.aca.2021.338857
31. Iliuk A. Identification of phosphorylated proteins on a global scale. Curr Protoc Chem Biol. 2018 Sep 1;10(3):e48. doi: 10.1002/cpch.48
32. Rogers LD, Fang Y, Foster LJ. An integrated global strategy for cell lysis, fractionation, enrichment and mass spectrometric analysis of phosphorylated peptides. Mol Biosyst. 2010 May 10;6(5):822–829. doi: 10.1039/b915986j
33. Qiu W, Evans CA, Landels A, et al. Phosphopeptide enrichment for phosphoproteomic analysis - a tutorial and review of novel materials. Anal Chim Acta. 2020;1129:158–180. Elsevier B.V. doi: 10.1016/j.aca.2020.04.053
34. Xiao D, Chen C, Yang P. Computational systems approach towards phosphoproteomics and their downstream regulation. Proteomics. 2023 Feb 1 [cited 2023 Nov 1];23(3–4):2200068. Available from: https://pubmed.ncbi.nlm.nih.gov/35580145/
35. Varshney N, Mishra AK. Deep learning in phosphoproteomics: methods and application in cancer Drug discovery. Proteomes. 2023;11(2):16. MDPI. doi: 10.3390/proteomes11020016
36. Paulo JA, Schweppe DK. Advances in quantitative high-throughput phosphoproteomics with sample multiplexing. Proteomics. 2021 May 30 [cited 2023 Jun 6];21(9):2000140. doi: 10.1002/pmic.202000140
37. Liu X, Fields R, Schweppe DK, et al. Strategies for mass spectrometry-based phosphoproteomics using isobaric tagging. Expert Rev Proteomics. 2021;18(9):795–807. doi: 10.1080/14789450.2021.1994390
38. Ino Y, Kinoshita E, Kinoshita-Kikuta E, et al. Evaluation of four phosphopeptide enrichment strategies for mass spectrometry-based proteomic analysis. Proteomics. 2022 Apr 28 [cited 2023 Jun 6];22(7):2100216. doi: 10.1002/pmic.202100216
39. Li J, Wang J, Yan Y, et al. Comprehensive Evaluation of different TiO2-based phosphopeptide enrichment and fractionation methods for phosphoproteomics. Cells. 2022 Jul 1;11(13):2047. doi: 10.3390/cells11132047
40. Hsu CC, Xue L, Arrington JV, et al. Estimating the efficiency of phosphopeptide identification by tandem mass spectrometry. J Am Soc Mass Spectrom. 2017 Jun 1;28(6):1127–1135. doi: 10.1007/s13361-017-1603-5
41. Winter D, Seidler J, Ziv Y, et al. Citrate boosts the performance of phosphopeptide analysis by UPLC-ESI-MS/MS. J Proteome Res. 2009 Jan;8(1):418–424.
42. Bugyi F, Tóth G, Kovács KB, et al. Comparison of solid-phase extraction methods for efficient purification of phosphopeptides with low sample amounts. J Chromatogr A. 2022 Dec 6;1685:463597. doi: 10.1016/j.chroma.2022.463597
43. Vlastaridis P, Kyriakidou P, Chaliotis A, et al. Estimating the total number of phosphoproteins and phosphorylation sites in eukaryotic proteomes. Gigascience. 2017 Feb 1;6(2). doi: 10.1093/gigascience/giw015
44. Macek B, Forchhammer K, Hardouin J, et al. Protein post-translational modifications in bacteria. Nat Rev Microbiol. 2019;17(11):651–664. Nature Publishing Group. doi: 10.1038/s41579-019-0243-0
45. Birk MS, Charpentier E, Frese CK. Automated phosphopeptide enrichment for gram-positive bacteria. J Proteome Res. 2021;20(10):4886–4892. doi: 10.1021/acs.jproteome.1c00364
46. Marzec KA, Rogers S, McCloy R, et al. SILAC kinase screen identifies potential MASTL substrates. Sci Rep. 2022 Dec 1;12(1):1–13. doi: 10.1038/s41598-022-14933-0
47. Sharma K, D'Souza RCJ, Tyanova S, et al. Ultradeep human phosphoproteome reveals a Distinct regulatory Nature of Tyr and Ser/Thr-based signaling. Cell Rep. 2014 Sep 11;8(5):1583–1594. doi: 10.1016/j.celrep.2014.07.036
48. Liu X, Rossio V, Thakurta SG, et al. Fe3±NTA magnetic beads as an alternative to spin column-based phosphopeptide enrichment. J Proteomics. 2022 May 30;260:104561. doi: 10.1016/j.jprot.2022.104561
49. Olsen JV, Vermeulen M, Santamaria A, et al. Quantitative phosphoproteomics reveals widespread full phosphorylation site occupancy during mitosis. Sci Signal. 2010 Jan 12 [cited 2023 Aug 3];3(104). Available from: https://pubmed.ncbi.nlm.nih.gov/20068231/
50. Koenig C, Martinez-Val A, Franciosa G, et al. Optimal analytical strategies for sensitive and quantitative phosphoproteomics using TMT-based multiplexing. Proteomics. 2022 Oct 1 [cited 2023 Jun 6];22(19–20):2100245. doi: 10.1002/pmic.202100245.
51. Tsai CF, Zhang P, Scholten D, et al. Surfactant-assisted one-pot sample preparation for label-free single-cell proteomics. Commun Biol. 2021 Dec 1;4(1):1–12. doi: 10.1038/s42003-021-01797-9
52. Tsai CF, Wang YT, Hsu CC, et al. A streamlined tandem tip-based workflow for sensitive nanoscale phosphoproteomics. Commun Biol. 2023 Dec 1;6(1). doi: 10.1038/s42003-022-04400-x
53. Yi L, Tsai CF, Dirice E, et al. Boosting to amplify signal with isobaric labeling (BASIL) strategy for Comprehensive quantitative phosphoproteomic characterization of small Populations of cells. Anal Chem. 2019 May 7;91(9):5794–801. doi: 10.1021/acs.analchem.9b00024

•• **This manuscript presents BASIL, a new approach for quantitative deep phosphoproteomics from low sample input by the use of a boosting channel within a TMT setup.**

54. Tsai CF, Zhao R, Williams SM, et al. An improved boosting to amplify signal with isobaric labeling (iBASIL) strategy for precise quantitative single-cell proteomics. Mol Cell Proteomics. 2020 May 1;19(5):828–838. doi: 10.1074/mcp.RA119.001857
55. Budnik B, Levy E, Harmange G, et al. SCoPE-MS: mass spectrometry of single mammalian cells quantifies proteome heterogeneity during cell differentiation. Genome Biol. 2018 Oct 22 [cited 2023 Jun 7];19(1):161. 10.1186/s13059-018-1547-5
56. Stopfer LE, Conage-Pough JE, White FM, Quantitative Consequences of protein Carriers in Immunopeptidomics and tyrosine phosphorylation MS2 analyses. Mol Cell Proteomics. 2021 Jan 1 [cited 2023 Aug 3];20:100104. Available from: https://pubmed.ncbi.nlm.nih.gov/34052394/
57. Chua XY, Mensah T, Aballo T, et al. Tandem mass tag approach utilizing pervanadate BOOST channels delivers deeper quantitative characterization of the tyrosine phosphoproteome. Mol Cell Proteomics. 2020 [cited 2023 Aug 3];19:730–743. Available from: https://pubmed.ncbi.nlm.nih.gov/32071147/
58. Piehowski PD, Petyuk VA, Sontag RL, et al. Residual tissue repositories as a resource for population-based cancer proteomic studies. Clin Proteomics. 2018 Aug 3 [cited 2023 Jun 8];15(1): 26. doi: 10.1186/s12014-018-9202-4
59. Friedrich C, Schallenberg S, Kirchner M, et al. Comprehensive micro-scaled proteome and phosphoproteome characterization of

archived retrospective cancer repositories. Nat Commun. 2021 Dec 1;12(1):1–15. doi: 10.1038/s41467-021-23855-w
60. Pujari GP, Mangalaparthi KK, Madden BJ, et al. A high-throughput workflow for FFPE tissue proteomics. J Am Soc Mass Spectrom. 2023 Jul 5;34(7):1225–1229. doi: 10.1021/jasms.3c00099
61. Wang F, Veth T, Kuipers M, et al. Optimized Suspension trapping method for phosphoproteomics sample preparation. Anal Chem. 2023 Jun 27;95(25):9471–9479. doi: 10.1021/acs.analchem.3c00324
62. Zougman A, Selby PJ, Banks RE. Suspension trapping (STrap) sample preparation method for bottom-up proteomics analysis. Proteomics. 2014 May 26 [cited 2023 Nov 1];14(9):1006–1000. doi: 10.1002/pmic.201300553
63. Swaney DL, Wenger CD, Coon JJ. Value of using multiple proteases for large-scale mass spectrometry-based proteomics. J Proteome Res. 2010 Mar 5;9(3):1323–1329. doi: 10.1021/pr900863u
64. Dickhut C, Feldmann I, Lambert J, et al. Impact of digestion conditions on phosphoproteomics. J Proteome Res. 2014 Jun 6;13(6):2761–2770. doi: 10.1021/pr401181y
65. Bubis JA, Gorshkov V, Gorshkov MV, et al. PhosphoShield: improving trypsin digestion of phosphoproteins by shielding the negatively charged phosphate moiety. J Am Soc Mass Spectrom. 2020 Oct 7;31(10):2053–2060. doi: 10.1021/jasms.0c00171
66. Abe Y, Nagano M, Tada A, et al. Deep phosphotyrosine proteomics by optimization of phosphotyrosine enrichment and MS/MS parameters. J Proteome Res. 2017 Feb 3;16(2):1077–1086. doi: 10.1021/acs.jproteome.6b00576
67. Kinoshita E, Kinoshita-Kikuta E, Koike T. History of phos-tag technology for phosphoproteomics. J Proteomics. 2022;252:104432. Elsevier B.V. doi: 10.1016/j.jprot.2021.104432
68. Carregari VC. Phosphopeptide enrichment techniques: a pivotal step for phosphoproteomic studies. Adv Exp Med Biol. 2022;1382:17–27.
69. Zhu B, Zhou Q, Zhen D, et al. Preparation of TiO2/Bi/Fe/Zr nanocomposite for the highly selective enrichment of phosphopeptides. Talanta. 2019 Mar 1;194:870–875. doi: 10.1016/j.talanta.2018.10.073
70. McNulty DE, Annan RS. Hydrophilic interaction chromatography reduces the complexity of the phosphoproteome and improves global phosphopeptide isolation and detection. Mol Cell Proteomics. 2008 May;7(5):971–980. doi: 10.1074/mcp.M700543-MCP200
71. Villén J, Gygi SP. The SCX/IMAC enrichment approach for global phosphorylation analysis by mass spectrometry. Nat Protoc. 2008 Oct 2;3(10):1638. doi: 10.1038/nprot.2008.150
72. Batth TS, Francavilla C, Olsen JV. Off-line high-pH reversed-phase fractionation for in-depth phosphoproteomics. J Proteome Res. 2014 Dec 5;13(12):6176–6186. doi: 10.1021/pr500893m
73. Kwon Y, Lee S, Park N, et al. Phosphoproteome profiling using an isobaric carrier without the need for phosphoenrichment. Anal Chem. 2022 Mar 15;94(10):4192–4200. doi: 10.1021/acs.analchem.1c04188
74. Callesen AK, Madsen JS, Vach W, et al. Serum protein profiling by solid phase extraction and mass spectrometry: a future diagnostics tool? Proteomics. 2009 Mar 1 [cited 2023 Jun 8];9(6):1428–1441. doi: 10.1002/pmic.200800382.
75. West C, Elfakir C, Lafosse M. Porous graphitic carbon: A versatile stationary phase for liquid chromatography. J Chromatogr A. 2010;1217(19):3201–3216. Elsevier. doi: 10.1016/j.chroma.2009.09.052
76. Ogata K, Ishihama Y. CoolTip: low-temperature solid-phase extraction microcolumn for capturing hydrophilic peptides and phosphopeptides. Mol Cell Proteomics. 2021 Nov 2;20:100170. doi: 10.1016/j.mcpro.2021.100170
77. Ong SE, Blagoev B, Kratchmarova I, et al. Stable isotope labeling by amino acids in cell culture, SILAC, as a simple and accurate approach to expression proteomics. Mol Cell Proteomics. 2002 May 1;1(5):376–386. doi: 10.1074/mcp.M200025-MCP200
78. Goshe MB, Conrads TP, Panisko EA, et al. Phosphoprotein isotope-coded affinity tag approach for isolating and quantitating phosphopeptides in proteome-wide analyses. Anal Chem. 2001 Jun 1;73(11):2578–2586. doi: 10.1021/ac010081x
79. Gygi SP, Rist B, Gerber SA, et al. Quantitative analysis of complex protein mixtures using isotope-coded affinity tags. Nat Biotechnol. 1999 Oct;17(10):994–999.
80. Dan Y, Radic N, Gay M, et al. Characterization of p38α signaling networks in cancer CellsUsing quantitative proteomics and phosphoproteomics. Mol Cell Proteomics. 2023 Apr 1;22(4):100527. doi: 10.1016/j.mcpro.2023.100527
81. Gratani FL, Englert T, Nashier P, et al. E. coli toxin YjjJ (HipH) is a Ser/Thr protein kinase that Impacts cell Division, Carbon Metabolism, and ribosome assembly. mSystems. 2023 Feb 23;8(1). doi: 10.1128/msystems.01043-22
82. Geiger T, Cox J, Ostasiewicz P, et al. Super-SILAC mix for quantitative proteomics of human tumor tissue. Nat Methods. 2010 May 4;7(5):383–385. doi: 10.1038/nmeth.1446
83. Güran A, Ji Y, Fang P, et al. Quantitative analysis of the cardiac phosphoproteome in response to acute β-adrenergic receptor stimulation in vivo. Int J Mol Sci. 2021 Nov 22 [cited 2023 Jun 12];22(22): 12584. doi: 10.3390/ijms222212584
84. Doherty MK, Hammond DE, Clague MJ, et al. Turnover of the human proteome: determination of protein intracellular stability by dynamic SILAC. J Proteome Res. 2009 Jan;8(1):104–112.
85. Wu C, Ba Q, Lu D, et al. Global and site-specific effect of phosphorylation on protein turnover. Dev Cell. 2021 Jan 11;56(1):111–124.e6. doi: 10.1016/j.devcel.2020.10.025
86. Trentini DB, Suskiewicz MJ, Heuck A, et al. Arginine phosphorylation marks proteins for degradation by a Clp protease. Nature. 2016 Oct 6;539(7627):48–53. doi: 10.1038/nature20122
87. Swaney DL, Rodríguez-Mias RA, Villén J. Phosphorylation of ubiquitin at Ser65 affects its polymerization, targets, and proteome-wide turnover. EMBO Rep. 2015 Sep 3 [cited 2023 Jun 10];16(9):1131–1144. Available from https://www.embopress.org/doi/10.15252/embr.201540298
88. Hammarén HM, Geissen EM, Potel CM, et al. Protein-peptide turnover profiling reveals the order of PTM addition and removal during protein maturation. Nat Commun. 2022 Dec 1;13(1):1–15. doi: 10.1038/s41467-022-35054-2
89. Boersema PJ, Raijmakers R, Lemeer S, et al. Multiplex peptide stable isotope dimethyl labeling for quantitative proteomics. Nat Protoc. 2009 Mar 19;4(4):484–494. doi: 10.1038/nprot.2009.21
90. Hsu JL, Huang SY, Chow NH, et al. Stable-isotope dimethyl labeling for quantitative proteomics. Anal Chem. 2003 Dec 15;75(24):6843–6852. doi: 10.1021/ac0348625
91. Kalpongnukul N, Bootsri R, Wongkongkathep P, et al. Phosphoproteomic analysis defines BABAM1 as mTORC2 downstream effector promoting DNA damage response in Glioblastoma cells. J Proteome Res. 2022 Dec 2;21(12):2893–2904. doi: 10.1021/acs.jproteome.2c00240
92. Chang YW, Wang CC, Yin CF, et al. Quantitative phosphoproteomics reveals ectopic ATP synthase on mesenchymal stem cells to promote tumor progression via ERK/c-fos pathway activation. Mol Cell Proteomics. 2022 Jun 1;21(6):100237. doi: 10.1016/j.mcpro.2022.100237
93. Senturk A, Sahin AT, Armutlu A, et al. Quantitative phosphoproteomics analysis uncovers PAK2- and CDK1-mediated malignant signaling pathways in clear cell renal cell carcinoma. Mol Cell Proteomics. 2022 Nov 1;21(11):100417. doi: 10.1016/j.mcpro.2022.100417
94. Frost DC, Greer T, Li L. High-resolution enabled 12-plex DiLeu isobaric tags for quantitative proteomics. Anal Chem. 2015 Feb 3;87(3):1646–1654. doi: 10.1021/ac503276z
95. Zhong X, Lietz CB, Shi X, et al. Highly multiplexed quantitative proteomic and phosphoproteomic analyses in vascular smooth muscle cell dedifferentiation. Anal Chim Acta. 2020 Aug 29;1127:163–173. doi: 10.1016/j.aca.2020.06.054
96. Li J, Cai Z, Bomgarden RD, et al. Tmtpro-18plex: the expanded and complete set of TMTpro reagents for sample multiplexing. J Proteome Res. 2021 May 7;20(5):2964–2972. doi: 10.1021/acs.jproteome.1c00168
97. Schweppe DK, Rusin SF, Gygi SP, et al. Optimized workflow for multiplexed phosphorylation analysis of TMT-Labeled peptides using high-field asymmetric waveform ion mobility spectrometry. J Proteome Res. 2020 Jan 3;19(1):554–560. doi: 10.1021/acs.jproteome.9b00759

98. Ogata K, Tsai CF, Ishihama Y. Nanoscale Solid-Phase Isobaric Labeling for Multiplexed Quantitative Phosphoproteomics. J Proteome Res. 2021 Aug 6;20(8):4193–4202. doi: 10.1021/acs.jproteome.1c00444
99. Cox J, Hein MY, Luber CA, et al. Accurate proteome-wide label-free quantification by delayed normalization and maximal peptide ratio extraction, termed MaxLFQ. Mol Cell Proteomics. 2014 Sep 1;13(9):2513–2526. doi: 10.1074/mcp.M113.031591
100. Potel CM, Lemeer S, Heck AJR. Phosphopeptide fragmentation and site localization by mass spectrometry: an update. Anal Chem. 2019;91(1):126–141. American Chemical Society. doi: 10.1021/acs.analchem.8b04746
101. Villén J, Beausoleil SA, Gygi SP. Evaluation of the utility of neutral-loss-dependent MS3 strategies in large-scale phosphorylation analysis. Proteomics. 2008 Nov 1 [cited 2023 Jun 10];8(21):4444–4452. 10.1002/pmic.200800283
102. Escobar EE, Venkat Ramani MK, Zhang Y, et al. Evaluating spatiotemporal dynamics of phosphorylation of RNA polymerase II carboxy-terminal domain by ultraviolet photodissociation mass spectrometry. J Am Chem Soc. 2021 Jun 9 [cited 2023 Aug 3];143(22):8488–8498. doi: 10.1021/jacs.1c03321
103. Brunner AM, Lössl P, Liu F, et al. Benchmarking multiple fragmentation methods on an orbitrap fusion for top-down phospho-proteoform characterization. Anal Chem. 2015 Apr 21;87(8):4152–4158. doi: 10.1021/acs.analchem.5b00162
104. Schweppe DK, Prasad S, Belford MW, et al. Characterization and optimization of multiplexed quantitative analyses using high-field asymmetric-waveform ion mobility mass spectrometry. Anal Chem. 2019 Mar 19;91(6):4010–4016. doi: 10.1021/acs.analchem.8b05399
105. Muehlbauer LK, Hebert AS, Westphall MS, et al. Global phosphoproteome analysis using high-field asymmetric waveform ion mobility spectrometry on a hybrid Orbitrap mass spectrometer. Anal Chem. 2020 Dec 15;92(24):15959–15967. doi: 10.1021/acs.analchem.0c03415
106. Toby TK, Fornelli L, Kelleher NL. Progress in top-down proteomics and the analysis of proteoforms. Annual Rev Anal Chem. 2016;9(1):499–519. Annual Reviews Inc. doi: 10.1146/annurev-anchem-071015-041550
107. Chapman EA, Aballo TJ, Melby JA, et al. Defining the sarcomeric proteoform landscape in ischemic cardiomyopathy by top-down proteomics. J Proteome Res. 2023 Mar 3;22(3):931–941. doi: 10.1021/acs.jproteome.2c00729
108. Melby JA, Brown KA, Gregorich ZR, et al. High sensitivity top-down proteomics captures single muscle cell heterogeneity in large proteoforms. Proc Natl Acad Sci U S A. 2023 May 9;120(19). doi: 10.1073/pnas.2222081120
109. Vidova V, Spacil Z. A review on mass spectrometry-based quantitative proteomics: targeted and data independent acquisition. Anal Chim Acta. 2017;964:7–23. Elsevier B.V. doi: 10.1016/j.aca.2017.01.059
110. Wu X, Liu YK, Iliuk AB, et al. Mass spectrometry-based phosphoproteomics in clinical applications. TrAC - Trends Analyt Chemy. 2023;163:117066. Elsevier B.V. doi: 10.1016/j.trac.2023.117066
111. Stopfer LE, Flower CT, Gajadhar AS, et al. High-density, targeted monitoring of tyrosine phosphorylation reveals activated signaling networks in human tumors. Cancer Res. 2021 May 1;81(9):2495–2509. doi: 10.1158/0008-5472.CAN-20-3804
112. Martínez-Val A, Fort K, Koenig C, et al. Hybrid-DIA: intelligent data acquisition integrates targeted and discovery proteomics to analyze phospho-signaling in single spheroids. Nat Commun. 2023 Dec 1;14(1):1–18. doi: 10.1038/s41467-023-39347-y
113. Humphrey SJ, Karayel O, James DE, et al. High-throughput and high-sensitivity phosphoproteomics with the EasyPhos platform. Nat Protoc. 2018 Sep 1;13(9):1897–1916. doi: 10.1038/s41596-018-0014-9
114. Leutert M, Rodríguez-Mias RA, Fukuda NK, et al. R2-P2 rapid-robotic phosphoproteomics enables multidimensional cell signaling studies. Mol Syst Biol. 2019 Dec;15(12). doi: 10.15252/msb.20199021
115. Leutert M, Barente AS, Fukuda NK, et al. The regulatory landscape of the yeast phosphoproteome. Nat Struct Mol Biol. 2023 Oct 16;1–3. Available from: https://www.nature.com/articles/s41594-023-01115-3
116. Müller T, Kalxdorf M, Longuespée R, et al. Automated sample preparation with SP 3 for low-input clinical proteomics. Mol Syst Biol. 2020 Jan 16 [cited 2023 Jun 8];16(1): e9111. [internet]. doi: 10.15252/msb.20199111
117. Post H, Penning R, Fitzpatrick MA, et al. Robust, sensitive, and automated phosphopeptide enrichment optimized for low sample amounts applied to primary hippocampal neurons. J Proteome Res. 2017 Feb 3;16(2):728–737. doi: 10.1021/acs.jproteome.6b00753
118. Tavassoly I, Goldfarb J, Iyengar R. Systems biology primer: the basic methods and approaches. Essays Biochem. 2018;62:487–500. Portland Press Ltd. doi: 10.1042/EBC20180003
119. Liu Y, Chance MR. Integrating phosphoproteomics in systems biology. Comput Struct Biotechnol J. 2014;10(17):90–97. Elsevier B.V. doi: 10.1016/j.csbj.2014.07.003
120. Kreitmaier P, Katsoula G, Zeggini E. Insights from multi-omics integration in complex disease primary tissues. Trends Genet. 2023;39:46–58. Elsevier Ltd. doi: 10.1016/j.tig.2022.08.005
121. Aggarwal S, Tolani P, Gupta S, et al. Posttranslational modifications in systems biology. Adv Protein Chem Struct Biol. 2021;127:93–126. Academic Press Inc.
122. Vandereyken K, Sifrim A, Thienpont B, et al. Methods and applications for single-cell and spatial multi-omics. Nat Rev Genet. 2023;24:494–515. doi: 10.1038/s41576-023-00580-2
123. Gu Y, Zhou Y, Ju S, et al. Multi-omics profiling visualizes dynamics of cardiac development and functions. Cell Rep. 2022 Dec 27;41(13):111891. doi: 10.1016/j.celrep.2022.111891
124. Pang H, Jiang Y, Li J, et al. Aberrant NAD+ metabolism underlies Zika virus–induced microcephaly. Nat Metab. 2021 Aug 1;3(8):1109–1124. doi: 10.1038/s42255-021-00437-0
125. Zhao P, Feng Y, Wu J, et al. Efficient sample preparation System for multi-omics analysis via single cell mass spectrometry. Anal Chem. 2022 May 9;95(18):7212–7219
126. Li Y, Li H, Xie Y, et al. An integrated strategy for mass spectrometry-based Multiomics analysis of single cells. Anal Chem. 2021 Oct 26;93(42):14059–14067. doi: 10.1021/acs.analchem.0c05209
127. Leutert M, Entwisle SW, Villén J. Decoding post-translational modification crosstalk with proteomics. Mol Cell Proteomics. 2021;20:100129. American Society for Biochemistry and Molecular Biology Inc. doi: 10.1016/j.mcpro.2021.100129
128. Adoni KR, Cunningham DL, Heath JK, et al. FAIMS enhances the detection of PTM crosstalk sites. J Proteome Res. 2022 Apr 1;21(4):930–939. doi: 10.1021/acs.jproteome.1c00721
129. Fulzele A, Bennett EJ. Ubiquitin diGLY Proteomics as an Approach to Identify and Quantify the Ubiquitin-Modified Proteome. In: Mayor T, Kleiger G, editors. The Ubiquitin Proteasome System. Methods in Molecular Biology. Vol. 1844. New York, NY: Humana Press; 2018. doi: 10.1007/978-1-4939-8706-1_23
130. Schilling B, Meyer JG, Wei L, et al. High-Resolution Mass Spectrometry to Identify and Quantify Acetylation Protein Targets. In: Brosh R Jr, editor. Protein Acetylation. Methods in Molecular Biology. Vol. 1983. New York, NY: Humana; 2019. doi: 10.1007/978-1-4939-9434-2_1
131. Mertins P, Qiao JW, Patel J, et al. Integrated proteomic analysis of post-translational modifications by serial enrichment. Nat Methods. 2013 Jul 9;10(7):634–637. doi: 10.1038/nmeth.2518
132. Liu R, Gao W, Yang J, et al. A novel graphene oxide/chitosan foam incorporated with metal–organic framework stationary phase for simultaneous enrichment of glycopeptide and phosphopeptide with high efficiency. Anal Bioanal Chem. 2022 Mar 1;414(6):2251–2263. doi: 10.1007/s00216-021-03861-z
133. Fan Z, Li J, Liu T, et al. A new tandem enrichment strategy for the simultaneous profiling of: O-GlcNAcylation and phosphorylation in RNA-binding proteome. Analyst. 2021 Feb 21;146(4):1188–1197. doi: 10.1039/D0AN02305A
134. Abelin JG, Bergstrom EJ, Rivera KD, et al. Workflow enabling deepscale immunopeptidome, proteome, ubiquitylome, phosphoproteome, and acetylome analyses of sample-limited tissues. Nat Commun. 2023 Dec 1;14(1):1851. doi: 10.1038/s41467-023-37547-0.

•• **This manuscript presents MONTE, a sensitive multi-omic workflow for immunopeptidome, ubiquitylome, proteome, phosphoproteome, and acetylome enrichment from native, sample limited tissues.**

135. Ashrafian S, Zarrineh M, Jensen P, et al. Quantitative phosphoproteomics and acetylomics of safranal anticancer effects in Triple-negative breast cancer cells. J Proteome Res. 2022 Nov 4;21(11):2566–2585. doi: 10.1021/acs.jproteome.2c00168
136. Pino LK, Just SC, MacCoss MJ, et al. Acquiring and analyzing data independent acquisition proteomics experiments without spectrum libraries. Mol & Cell Proteomics. 2020 Jul 1;19(7):1088–1103. doi: 10.1074/mcp.P119.001913
137. Röst HL, Rosenberger G, Navarro P, et al. OpenSWATH enables automated, targeted analysis of data-independent acquisition MS data. Nat Biotechnol. 2014;32(3):219–223. doi: 10.1038/nbt.2841. Nature Publishing Group
138. Krasny L, Huang PH. Data-independent acquisition mass spectrometry (DIA-MS) for proteomic applications in oncology. Mol Omics. 2021;17(1):29–42. Royal Society of Chemistry. doi: 10.1039/D0MO00072H
139. MacLean B, Tomazela DM, Shulman N, et al. Skyline: an open source document editor for creating and analyzing targeted proteomics experiments. Bioinformatics. 2010 Feb 9;26(7):966–968. doi: 10.1093/bioinformatics/btq054
140. Desiere F, Deutsch EW, King NL, et al. The PeptideAtlas project. Nucleic Acids Res. 2006;34(Database issue):D655–D658. doi: 10.1093/nar/gkj040
141. Wang M, Wang J, Carver J, et al. Assembling the community-scale discoverable human proteome. Cell Syst. 2018 Oct 24;7(4):412–421.e5. doi: 10.1016/j.cels.2018.08.004
142. Searle BC, Swearingen KE, Barnes CA, et al. Generating high quality libraries for DIA MS with empirically corrected peptide predictions. Nat Commun. 2020 Dec 1;11(1). doi: 10.1038/s41467-020-15346-1
143. Sinitcyn P, Hamzeiy H, Salinas Soto F, et al. MaxDIA enables library-based and library-free data-independent acquisition proteomics. Nat Biotechnol. 2021 Dec 1;39(12):1563–1573. doi: 10.1038/s41587-021-00968-7
144. Gessulat S, Schmidt T, Zolg DP, et al. Prosit: proteome-wide prediction of peptide tandem mass spectra by deep learning. Nat Methods. 2019 Jun 1;16(6):509–518. doi: 10.1038/s41592-019-0426-7
145. Lou R, Liu W, Li R, et al. DeepPhospho accelerates DIA phosphoproteome profiling through in silico library generation. Nat Commun. 2021 Dec 1;12(1). doi: 10.1038/s41467-021-26979-1
146. Bekker-Jensen DB, Bernhardt OM, Hogrebe A, et al. Rapid and site-specific deep phosphoproteome profiling by data-independent acquisition without the need for spectral libraries. Nat Commun. 2020 Dec 1;11(1). doi: 10.1038/s41467-020-14609-1
147. Demichev V, Messner CB, Vernardis SI, et al. DIA-NN: neural networks and interference correction enable deep proteome coverage in high throughput. Nat Methods. 2020 Jan 1;17(1):41–44. doi: 10.1038/s41592-019-0638-x

•• **This manuscript presents DIA-NN, a free and universal software for processing proteomics data from data-independent acquisition based on neural networks.**

148. Lou R, Cao Y, Li S, et al. Benchmarking commonly used software suites and analysis workflows for DIA proteomics and phosphoproteomics. Nat Commun. 2023 Dec 1;14(1). doi: 10.1038/s41467-022-35740-1
149. Skowronek P, Thielert M, Voytik E, et al. Rapid and in-depth coverage of the (phospho-) proteome with deep libraries and optimal Window Design for dia-PASEF. Mol Cell Proteomics. 2022 Sep 1;21(9):100279. doi: 10.1016/j.mcpro.2022.100279
150. Pasquier C, Robichon A. Evolutionary divergence of phosphorylation to regulate interactive protein networks in lower and higher species. Int J Mol Sci. 2022 Nov 1;23(22):14429. doi: 10.3390/ijms232214429
151. Ochoa D, Jarnuczak AF, Viéitez C, et al. The functional landscape of the human phosphoproteome. Nat Biotechnol. 2020 Mar 1;38(3):365–373. doi: 10.1038/s41587-019-0344-3
152. Huang JX, Lee G, Cavanaugh KE, et al. High throughput discovery of functional protein modifications by hotspot thermal profiling. Nat Methods. 2019 Sep 1;16(9):894–901. doi: 10.1038/s41592-019-0499-3

•• **This manuscript presents a high throughput method enabling efficient detection of functional protein phosphorylation sites by Hotspot Thermal Profiling.**

153. Potel CM, Kurzawa N, Becher I, et al. Impact of phosphorylation on thermal stability of proteins. Nat Methods. 2021;18:757–759. Nature Research. doi: 10.1038/s41592-021-01177-5
154. Krug K, Mertins P, Zhang B, et al. A curated resource for Phosphosite-specific signature analysis. Mol Cell Proteomics. 2019 Mar 1;18(3):576–593. doi: 10.1074/mcp.TIR118.000943
155. Subramanian A, Tamayo P, Mootha VK, et al. Gene set enrichment analysis: a knowledge-based approach for interpreting genome-wide expression profiles. Proc Natl Acad Sci U S A. 2005 Oct 25;102(43):15545–15550. doi: 10.1073/pnas.0506580102
156. Seymour RW, van der Post S, Mooradian AD, et al. ProteoSushi: a software tool to biologically annotate and quantify modification-specific, peptide-centric proteomics data Sets. J Proteome Res. 2021 Jul 2;20(7):3621–3628. doi: 10.1021/acs.jproteome.1c00203

3.2 Manuscript II

E. coli Toxin YjjJ (HipH) is a Ser/Thr protein kinase that impacts cell division, carbon metabolism, and ribosome assembly (Published)

mSystems. 2023 Feb 23;8(1):e01043-22.

DOI: 10.1128/msystems.00549-21

AMERICAN SOCIETY FOR MICROBIOLOGY | mSystems®

RESEARCH ARTICLE

E. coli Toxin YjjJ (HipH) Is a Ser/Thr Protein Kinase That Impacts Cell Division, Carbon Metabolism, and Ribosome Assembly

Fabio Lino Gratani,[a] Till Englert,[a] Payal Nashier,[a] Peter Sass,[b] Laura Czech,[c] Niels Neumann,[d] Sofia Doello,[d] Petra Mann,[e] Rudolf Blobelt,[a] Siegfried Alberti,[a] Karl Forchhammer,[d] Gert Bange,[c,e] Katharina Höfer,[e] Boris Macek[a]

[a]Quantitative Proteomics, Interfaculty Institute of Cell Biology, University of Tübingen, Tübingen, Germany
[b]Microbial Bioactive Compounds, Interfaculty Institute for Microbiology and Infection Medicine, University of Tübingen, Tübingen, Germany
[c]SYNMIKRO Research Center & Faculty of Chemistry, University of Marburg, Marburg, Germany
[d]Organismic Interactions, Interfaculty Institute for Microbiology and Infection Medicine, University of Tübingen, Tübingen, Germany
[e]Max Planck Institute for Terrestrial Microbiology, Marburg, Germany

ABSTRACT Protein Ser/Thr kinases are posttranslational regulators of key molecular processes in bacteria, such as cell division and antibiotic tolerance. Here, we characterize the *E. coli* toxin YjjJ (HipH), a putative protein kinase annotated as a member of the family of HipA-like Ser/Thr kinases, which are involved in antibiotic tolerance. Using SILAC-based phosphoproteomics we provide experimental evidence that YjjJ is a Ser/Thr protein kinase and its primary protein substrates are the ribosomal protein RpmE (L31) and the carbon storage regulator CsrA. YjjJ activity impacts ribosome assembly, cell division, and central carbon metabolism but it does not increase antibiotic tolerance as does its homologue HipA. Intriguingly, overproduction of YjjJ and its kinase-deficient variant can activate HipA and other kinases, pointing to a cross talk between Ser/Thr kinases in *E. coli*.

IMPORTANCE Adaptation to growth condition is the key for bacterial survival, and protein phosphorylation is one of the strategies adopted to transduce extracellular signal in physiological response. In a previous work, we identified YjjJ, a putative kinase, as target of the persistence-related HipA kinase. Here, we performed the characterization of this putative kinase, complementing phenotypical analysis with SILAC-based phosphoproteomics and proteomics. We provide the first experimental evidence that YjjJ is a Ser/Thr protein kinase, having as primary protein substrates the ribosomal protein RpmE (L31) and the carbon storage regulator CsrA. We show that overproduction of YjjJ has a major influence on bacterial physiology, impacting DNA segregation, cell division, glycogen production, and ribosome assembly.

KEYWORDS cell division, kinases, metabolism, phosphoproteomics, proteomics, serine/threonine kinases

Bacteria can quickly adapt to different growth conditions, which allows them to face continuous environmental changes and proliferate in numerous ecological niches. Sensing and responding to intra- and extracellular stimuli entails the regulation of many essential cellular mechanisms. The ability to rapidly and efficiently convert different signals into physiological response is the cornerstone of bacterial survival and adaptability (1). Dynamic protein phosphorylation is one of the key strategies used by the cell to transduce and convert the extracellular signals in the correspondent cellular response (2). The most known and studied examples in bacteria are the two-component systems (TCS), composed of a membrane bound receptor histidine kinase and a response regulator, generally a transcription regulator (3). Besides TCS, Ser/Thr/Tyr kinases represent another phosphorylation-based strategy for signal transduction and posttranslational regulation (4, 5). Contrary to TCS, members of this family of kinases

Editor Aleksandra Nita-Lazar, NIAID, NIH

Address correspondence to Boris Macek, boris.macek@uni-tuebingen.de.

The authors declare no conflict of interest.

Received 24 October 2022
Accepted 24 November 2022
Published 20 December 2022

typically phosphorylate multiple targets, affecting multiple aspects of cell physiology. Targets of Ser/Thr/Tyr kinases range from transcriptional and translational regulators (including TCS regulators), to metabolic enzymes as well as stress response proteins, underlying the crucial role of this regulatory mechanism in bacterial physiology (6). Recent studies demonstrate that Ser/Thr/Tyr phosphorylation is also involved in the regulation of antibiotic tolerance and persistence (7). The prominent example is the HipA kinase, a member of the *hipBA* Toxin-Antitoxin system (TA system), composed by the toxin HipA, which inhibits growth, and an antitoxin HipB, which counteracts the toxin activity (8). During normal growth conditions, the two genes are coexpressed and HipA is inactive; however, under specific conditions HipB is degraded, leading to HipA activation and growth inhibition. In this state of low metabolic activity, some bacterial cells can survive antibiotic treatments (antibiotic tolerance).

The kinase HipA inhibits growth by phosphorylating several proteins that are involved in different biological processes. A well-studied target of HipA is the glutamate-tRNA ligase GltX (7, 9). Phosphorylation by HipA inhibits the action of GltX and leads to an increase in the concentration of uncharged tRNA, mimicking amino-acid starvation and inducing growth inhibition. In a previous study we investigated the targets of HipA and its variant HipA7, which is responsible for high incidence of persister cells (10). Among the identified targets of HipA7 was the protein YjjJ, a toxin recently classified as a member of the family of HipA-like kinases and termed HipH (11, 12). This classification was supported by sequence similarity with HipA and conservation of amino acid residues involved in ATP and magnesium coordination, which are strictly required for kinase activity (12–15). However, unlike *hipA*, the *yjjJ* gene is not located in an operon with an antitoxin and its kinase activity was so far not experimentally verified.

Here, we show that YjjJ is a protein kinase that phosphorylates and negatively regulates the ribosomal protein RpmE (L31) and carbon storage regulator CsrA. Unlike HipA, overproduction of YjjJ does not directly lead to antibiotic tolerance but negatively impacts cell division and DNA segregation, ribosome assembly and regulation of central carbon metabolism. Overexpression of YjjJ influences the activity of HipA and other Ser/Thr kinases, and the resulting cell toxicity can be rescued by coexpression of the antitoxin HipB, pointing to a cross talk between these important regulatory proteins in bacterial cells.

RESULTS

YjjJ overproduction inhibits growth but has no direct impact on antibiotic tolerance. To investigate the function of *yjjJ*, we first assessed its impact on *E. coli* growth in LB medium. It was previously shown that strong overproduction of YjjJ leads to a drop in CFU (CFU) counts (11); therefore, we ectopically expressed *yjjJ* under the control of an inducible promoter and tested different concentrations of the inducer (arabinose) in order to identify the conditions that inhibited cell growth. Interestingly, we did not observe any significant difference between the tested conditions at the absorbance (OD_{600}) level; however, an increase in induction strength significantly reduced the number of CFU in a dose-dependent manner (Fig. 1A). Two hours after induction, at any arabinose concentration tested, bacteria lost the plasmid in a manner proportional to the induction intensity, indicating that *yjjJ* expression was toxic for the cell (Fig S1A). Importantly, overexpression of *hipB* antitoxin rescued the toxicity of YjjJ overproduction (Fig S1B), as previously shown (11).

The significant homology of YjjJ to HipA suggested a similar role in antibiotic tolerance (7, 10, 16). Thus, we probed the impact of YjjJ overproduction on cells grown in the presence of either ampicillin or ciprofloxacin. Cells expressing *yjjJ* died at similar rates to those expressing the empty vector under both antibiotic treatments, which was in stark contrast to cells expressing *hipA* (Fig. 1B, Fig S1C). Therefore, we conclude that overproduction of YjjJ is toxic for the cell and does not impact antibiotic tolerance under the tested conditions.

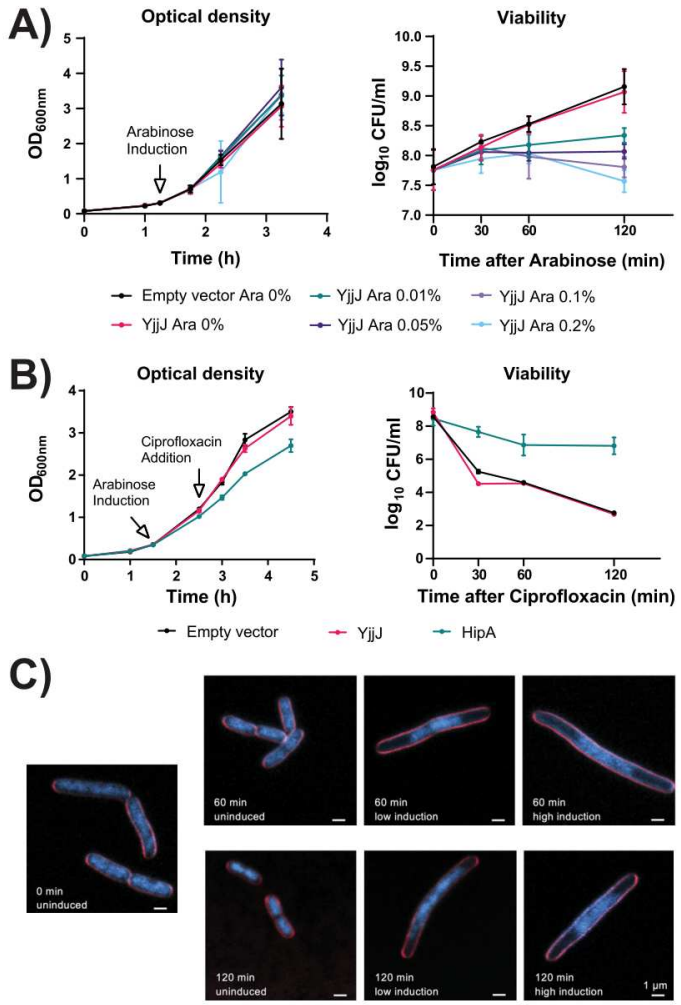

FIG 1 Ectopic expression of *yjjJ* leads to cell death, does not influence antibiotic tolerance, and impacts cell division and DNA segregation. (A) Growth curves of MG1655 strains transformed with either empty pBAD33 (Empty vector) or pBAD33::*yjjJ* (YjjJ) plasmid, in which *yjjJ* expression was under the control of arabinose-inducible promoter. Strains were grown in LB medium and expression was induced at OD_{600} of 0.3 using different arabinose concentrations. Growth was followed via optical density (OD_{600}) and CFU (CFU). (B) Antibiotic tolerance of MG1655 strains transformed with empty vector, pBAD33::*yjjJ* (YjjJ) or pBAD33::*hipA* (HipA), in which *yjjJ* and *hipA* expression was driven by the arabinose-inducible promoter. Strains were grown in LB medium and expression was induced at OD_{600} of 0.3 for 1 h followed by 1 μg/mL ciprofloxacin. Growth was followed via optical density and CFU. (C) Superresolution microscopy of cells transformed with pBAD33::*yjjJ* in exponentially growing culture supplemented with 0.01% (low induction) or 0.2% (high induction) arabinose, compared to uninduced (control) cells. Cells were stained with FM5-95 (membrane, red) and DAPI (DNA, blue) and examined by superresolution fluorescence microscopy. Overlaid fluorescence images show membranes (red) and DNA (blue). Images were taken at the indicated time points (60 and 120 min) after the addition of arabinose. YjjJ overproduction resulted in filamentous cells, indicating inhibition of cell division. DAPI staining revealed a deficient nucleoid segregation and DNA degradation. Scale bar: 1 μm. Images are representative of at least two biological replicate cultures.

YjjJ overproduction impacts DNA segregation and cell division. We next investigated whether YjjJ overproduction impacts subcellular structures, such as the cell membranes or the nucleoid. (Fig. 1C, Fig. S1D). In contrast to uninduced control cells, which showed regular chromosome segregation and cell division, induction of *yjjJ* resulted in a diffuse distribution of nucleoids accompanied by DNA degradation. As a

consequence, division septa failed to form while cell length increased, resulting in filamentous cells up to seven times longer than uninduced cells. This filamentation phenotype was in agreement with the drop in CFU counts upon *yjjJ* induction, and it explained the steady increase of optical density observed in Fig. 1A (17). We conclude that overproduction of YjjJ has a strong negative impact on cell division and DNA segregation even at low induction conditions.

Prolonged overproduction of YjjJ impacts carbon storage. To further analyze YjjJ impact on the proteome dynamics, we ectopically induced *yjjJ* expression at low inducer concentration (i.e., 0.01% arabinose) for 5 h in LB, which led to slow growth and high YjjJ abundance compared to cells carrying the empty vector (Fig. S2A and B). In a MS-based quantitative proteomics measurement, we quantified 1,270 proteins in at least two replicates (Data set S1, Sheet 1). Significantly regulated proteins were clustered in four groups based on their temporal profiles (Fig. 2A). The two main clusters presented opposite trends: one increased over time and showed an enrichment in proteins related to ATP biosynthesis, such as ATP-synthase components, whereas the other decreased over time and was enriched in proteins related to carbon metabolism, such as glycolysis and gluconeogenesis (Fig. 2B to D, Fig. S2C). Interestingly, several tRNA-ligases were decreased in abundance, with a notable exception of LysU that strongly increased 2 h after YjjJ overproduction (Fig. S2D). The levels of RecA were increased, suggesting DNA damage upon YjjJ overproduction. MinD and HtpG, both related to cell division/elongation, changed in abundance compared to empty vector strain, providing a possible link between YjjJ and the observed filamentation phenotype (Fig. S2D) (18, 19). Two smaller clusters contained the tRNA ligase AspS, which decreased strongly already 1 h after *yjjJ* induction, as well as the glycogen phosphorylase GlgP and bisphosphate nucleotidase CysQ, which increased after *yjjJ* induction. Since proteomic analysis indicated that YjjJ overproduction influences central carbon metabolism, we next analyzed glycogen production in cells expressing *yjjJ*-plasmid or the empty vector. Five hours after mild *yjjJ* induction (i.e., 0.01% arabinose) we measured a significantly higher abundance of glycogen in cells overproducing YjjJ, compared to empty vectors cells (Fig. 2E, Fig. S2E). We therefore conclude that YjjJ overproduction impacts central carbon metabolism and storage.

YjjJ is a protein kinase that phosphorylates CsrA, RpmE, and itself. YjjJ was proposed to be a protein kinase (11), but experimental evidence of its function was so far missing. To investigate *in vivo* YjjJ kinase activity and identify its putative targets, we used a SILAC-based phosphoproteomics approach, as described previously (10). Briefly, we induced overexpression of *yjjJ* in *E. coli* cultured in minimal medium supplemented with stable isotope-labeled derivatives of lysine (Lys0 and Lys8), and performed phosphoproteome analysis using liquid chromatography coupled to tandem mass spectrometry (LC-MS/MS). We compared two strains: one with the empty vector (Lys0 label) and one with the *yjjJ*-expressing plasmid (Lys8 label). After bacteria reached an OD_{600} of 0.4, we induced *yjjJ* expression for 2 h (Fig. S3A). At the protein level, we measured a strong increase in YjjJ abundance in triplicate measurements, confirming the efficiency of the expression strategy (Fig. 3A, Fig. S3B to D, Data set S1, Sheet 2). At the phosphoproteome level, we identified 201 phosphorylation sites on 126 proteins with good correlation among replicate measurements (Fig. S3B, Data set S1, Sheet 3). Upon YjjJ overproduction, we reproducibly detected an increase in the phosphorylation of the glutamate tRNA-ligase GltX (Ser239), carbon storage regulator CsrA (Ser56, Ser59) and L31 ribosomal protein RpmE (Ser69), making these proteins putative targets of YjjJ (Fig. 3B and C). In addition, we detected (auto)phosphorylation sites on YjjJ itself (Ser200, Ser201 and Ser217). Several additional phosphorylation sites were upregulated but could not be normalized for protein levels and will not be discussed further (Data set S1, Sheet 3).

Overproduction of kinase-dead YjjJ ($YjjJ^{DK}$) reveals an interplay between HipA and other kinases. Since overproduction of YjjJ may potentially activate other Ser/Thr kinases and bias the phosphoproteomics results, we repeated the SILAC phosphoproteome screen using a kinase-dead mutant of YjjJ ($YjjJ^{DK}$). Importantly, mutations in the

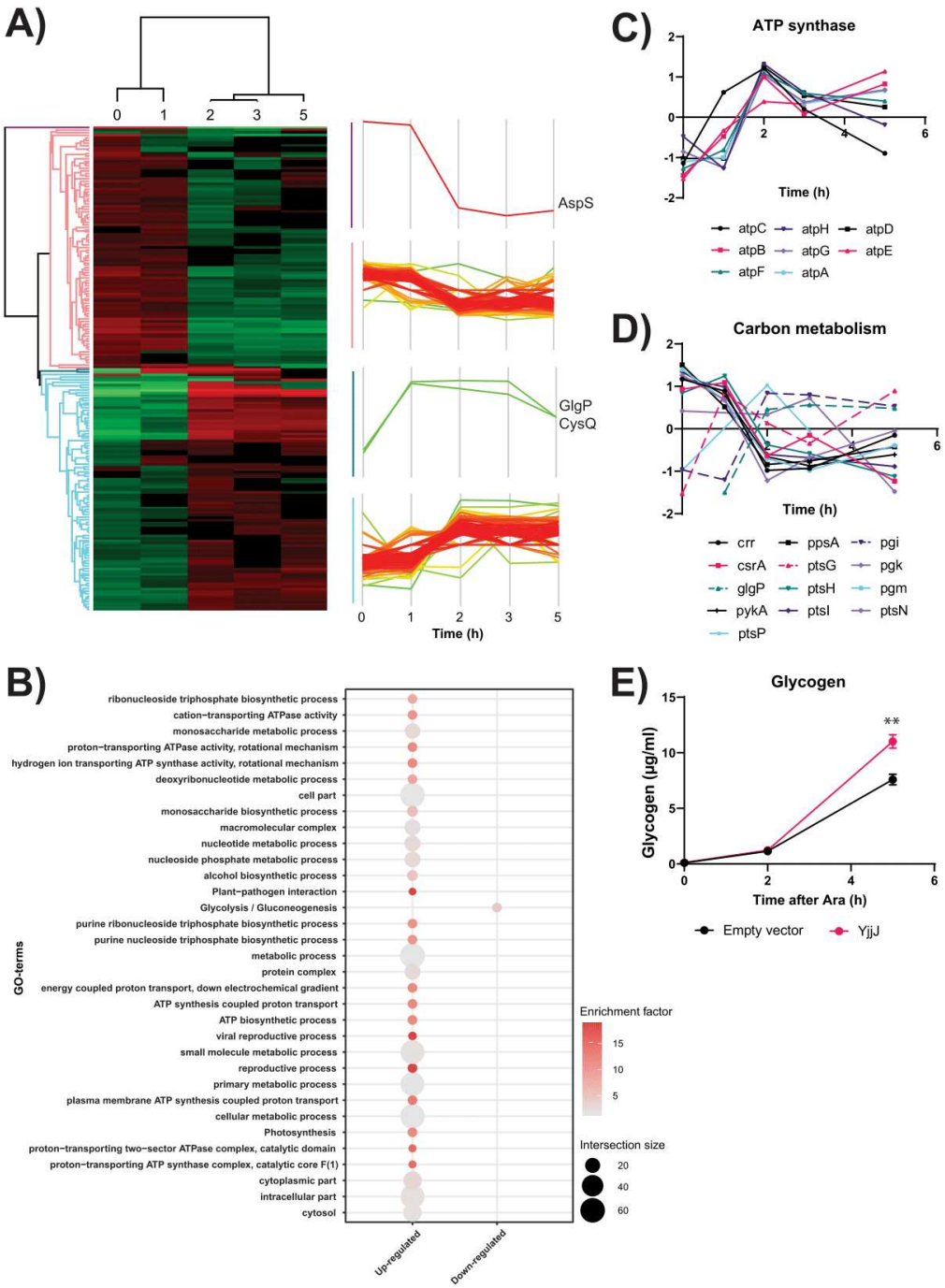

FIG 2 Prolonged overproduction of YjjJ impacts ATP synthesis and carbon storage. (A) Heat map of significantly regulated proteins after prolonged overproduction of YjjJ (Anova, FDR < 0.1; Post Hoc, FDR < 0.1). Color coding is based on YjjJ/Empty vector ratio. Temporal profiles were clustered on their dynamic over time. (B) Gene ontology (GO) enrichment of proteins grouped within the clusters. (C) Temporal profiles of selected proteins involved in ATP synthesis after induction of *yjjJ*. (D) Temporal profiles of selected proteins involved in carbon metabolism after induction of *yjjJ*. (E) Glycogen levels were measured in cells transformed with pBAD33 (Empty vector) or pBAD33::*yjjJ* (YjjJ), in which *yjjJ* expression is driven by the arabinose-inducible promoter. Cells were grown in LB medium until OD_{600} equal to 0.3 and supplemented with 0.01% arabinose. Bacteria were harvested before, two and 5 h after induction for absolute quantification of glycogen.

putative Mg^{2+}- and ATP-binding domains diminished the toxic effect on cell growth (Fig. S4A and D). On the phosphoproteome level, phosphorylation of most of the identified targets (CsrA, RpmE and YjjJ autophosphorylation) did not increase during $YjjJ^{DK}$ overproduction, confirming them as putative YjjJ targets. However, phosphorylation levels on GltX were similar in YjjJ- and $YjjJ^{DK}$-overproducing cells, indicating that GltX phosphorylation cannot be attributed to YjjJ activity alone (Fig. S4A to C, Data set S1, Sheet 4,5).

Since our previous study indicated potential cross talk between HipA and YjjJ activity (10), we reasoned that increased GltX phosphorylation may have resulted from HipA activation in the YjjJ-overproducing *E. coli* strain. To address this, we overproduced YjjJ or the $YjjJ^{DK}$ mutant in Δ*hipBA* background. Under these conditions we could not detect an increase in GltX phosphorylation (Fig. S4D to F; Data set S1, Sheet 6 and 7), revealing that the observed GltX phosphorylation after *yjjJ* induction should be attributed to the HipA kinase. Intriguingly, overproduction of $YjjJ^{DK}$ also led to a significant increase in the phosphorylation of the lysine tRNA-ligase LysS at Thr133 (Fig. S4C and F). This increase was not driven by a change in protein levels of LysS, and was also detected in the Δ*hipBA* background, revealing that LysS is phosphorylated neither by HipA nor by YjjJ. We therefore conclude that $YjjJ^{DK}$ overproduction indirectly regulates LysS phosphorylation, likely by regulation of a yet unknown kinase or a phosphatase. Of note, overexpression of *lysS* could not complement the toxic effect of *yjjJ* overexpression (Fig. S5A), and the exact physiological connection between the two genes remains to be determined.

To validate potential YjjJ substrates from the SILAC screen, we performed *in vitro* kinase assays with purified YjjJ and confirmed direct phosphorylation of RpmE and CsrA (Fig. 3D, Fig. S5B and C, Data set S1, Sheet 8 and 9). Interestingly, *in vitro* phosphorylation of CsrA was only observed when the small CsrB RNA was added to the assay, revealing that the RNA-bound pool of CsrA is predominantly targeted by YjjJ. Taken together, SILAC-based and *in vitro* phosphoproteomics experiments showed that YjjJ is a protein kinase that directly phosphorylates CsrA, RpmE and itself.

YjjJ kinase impacts activity of the carbon storage regulator CsrA. To further explore the influence of YjjJ on CsrA function, we overproduced either $CsrA_{WT}$ or its phospho-mimetic version $CsrA_{S56E}$ in wild type *E. coli* and followed the growth over time. Overexpression of $csrA_{wt}$ led to a drop in CFU by an order of magnitude, compared to uninduced cells. Importantly, unlike $CsrA_{WT}$, overexpression of $CsrA_{S56E}$ did not affect cell growth (Fig. 4A), indicating that YjjJ-mediated phosphorylation negatively regulates CsrA. Interestingly, the interaction of $CsrA_{S56E}$ with CsrC RNA did not change in electrophoretic mobility shift assays (Fig. S6A), indicating that YjjJ phosphorylation does not affect the interaction of CsrA with its RNA targets. This is in agreement with the *in vitro* kinase assay results showing that YjjJ preferentially phosphorylates RNA-bound CsrA. Taken together, these results demonstrate that YjjJ-mediated phosphorylation on Ser56 negatively affects the function of CsrA.

YjjJ overproduction affects RpmE (L31) function and ribosome assembly. The YjjJ substrate RpmE (L31) is a small ribosomal protein positioned at the interface between the 30S and the 50S ribosomal subunits (20). It was previously reported that deletion of eight amino acids at the C terminus of RpmE impairs the correct assembly of the 70S ribosome (20). Since the phosphorylated Ser69 is located in the C-terminal region of RpmE, we postulated that YjjJ-mediated phosphorylation may impact the ribosome assembly. To address this, we first analyzed ribosome profiles after moderate overproduction (i.e., 0.01% arabinose) of either native YjjJ or $YjjJ^{DK}$ and compared it to the strain expressing empty plasmid (Fig. 4B, Fig. S6B). Ribosomes purified from cells bearing empty plasmid showed the typical ribosomal profile with peaks representing 30S, 50S, 70S, and polysomes (Fig. 4B). Interestingly, overproduction of YjjJ led to disappearance of the 30S- and polysome signals and an increase in the 50S signal. Overproduction of $YjjJ^{DK}$ only mildly altered the native ribosome assembly and the elution profile, indicating that YjjJ impacts the ribosome assembly but not as the sole regulator. Interestingly, MS analysis showed the presence of YjjJ (both native and kinase-dead) in crude ribosome extracts, indicating the interaction between YjjJ and the ribosome (Fig. S6C, Data set S1, Sheet 10). To determine the potential phenotypic

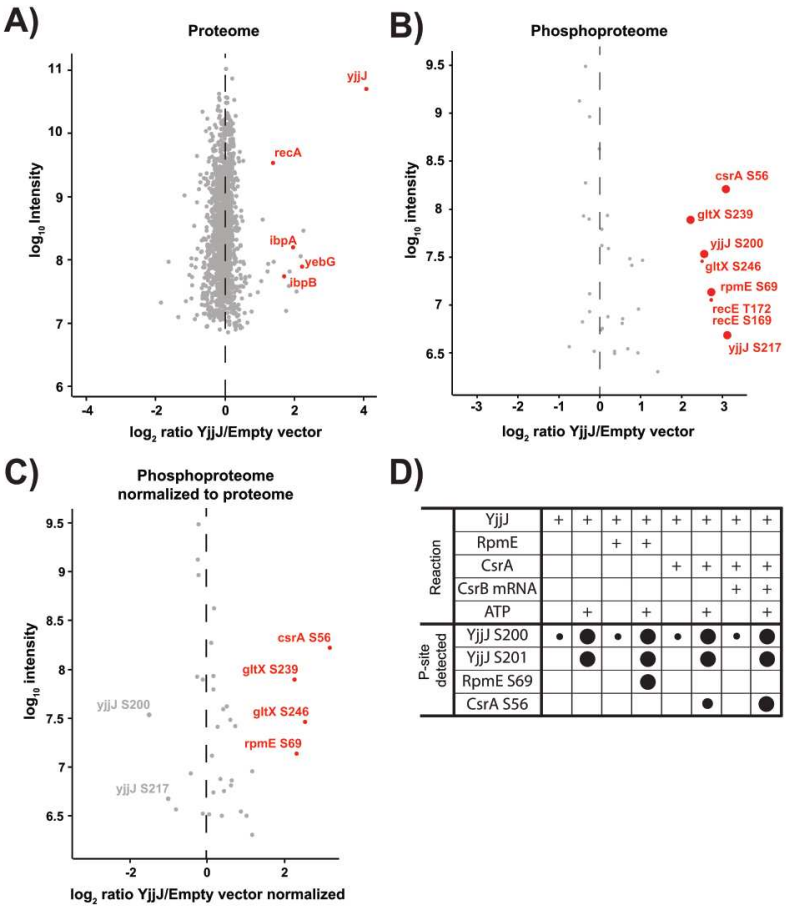

FIG 3 YjjJ is a protein kinase that phosphorylates CsrA, RpmE, and itself. (A) SILAC ratios of proteins measured 2 h after *yjjJ* induction. (B) Representation of phosphorylated sites following normalization to proteome abundance. The names of the phosphorylated proteins and the positions of the phosphorylation sites showing at least a 4-fold change in phosphorylation (red) are indicated. (C) Distribution of phosphorylation site ratios after normalization to the corresponding protein levels. The regulated sites (4-fold change in phosphorylation) are marked in red. (D) *In vitro* kinase assay of YjjJ with RpmE and CsrA as the substrates. After the phosphorylation reaction, the samples were analyzed by LC-MS/MS. Large circles: increased phosphorylation at the indicated sites was detected in at least two independent experiments. Small circles: two orders-of-magnitude lower intensity of phosphorylation site on YjjJ without ATP addition to the reaction mix; for CsrA the small circle represents an almost order of magnitude lower signal than without mRNA. Results represent an average of at least two replicates.

effect of RpmE (L31) phosphorylation, we performed a complementation experiment in the Δ*rpmE* strain, which is characterized by a delayed entrance in the exponential phase. Complementation of the *rpmE* null mutant with native *rpmE* rescued bacterial growth, while the phosphomimetic version $rpmE_{S69E}$ further delayed the entrance into exponential phase, demonstrating that YjjJ-mediated phosphorylation at Ser69 negatively regulates RpmE activity (Fig. 4C, Fig. S6D). In summary, these results demonstrate that YjjJ overproduction impacts ribosome assembly by phosphorylation and negatively affects the function of RpmE.

DISCUSSION

Bacterial Ser/Thr protein kinases HipA and YjjJ both belong to the HipA-kinase superfamily and contain the same conserved motifs (Mg- and ATP-binding sites) and

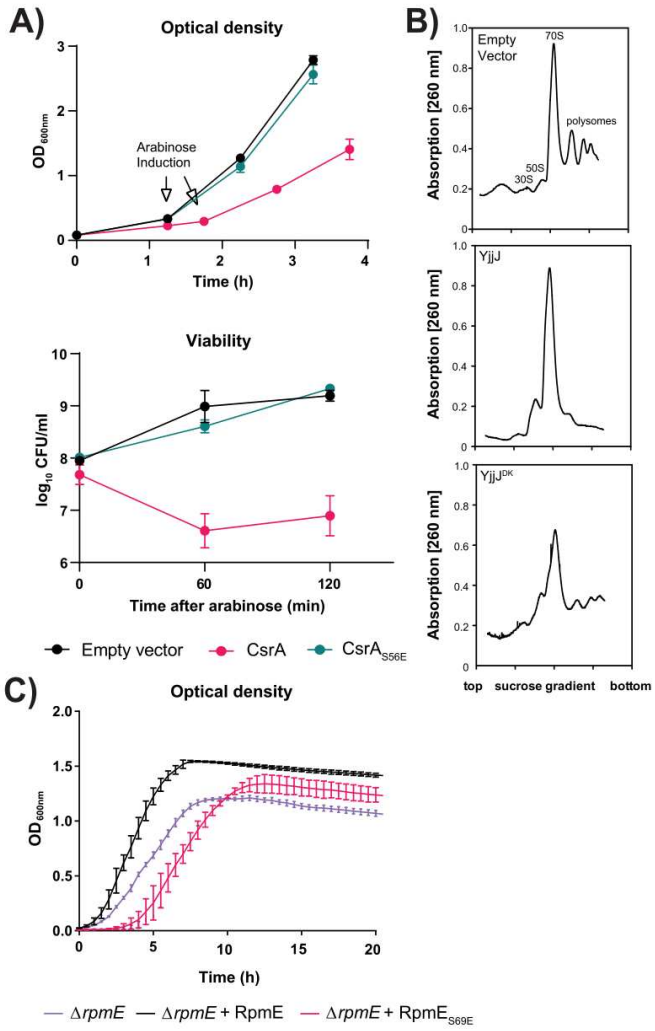

FIG 4 YjjJ kinase negatively regulates the function of carbon storage regulator CsrA and ribosomal protein RpmE (L31). (A) Impact of CsrA and phosphomimetic mutant $CsrA_{S56E}$ on *E. coli* viability. Growth curves of MG1655 strains carrying either empty pBAD33 (Empty vector), pBAD33::*csrA* (CsrA) or pBAD33::$csrA_{S56E}$ ($CsrA_{S56E}$), in which gene expression was under the control of an arabinose-inducible promoter. Cells were grown until OD_{600} of 0.3 and induced with 0.2% arabinose. Growth was followed at OD_{600} and CFU level. (B) Effect of YjjJ on ribosome assembly. Cells bearing pBAD33 (Empty vector), pBAD33::*yjjJ* or pBAD33::*yjjJ S342,364Q* ($YjjJ^{DK}$) were induced during exponential growth with 0.01% arabinose until OD_{600} of 0.7, followed by harvest. Ribosomes were extracted and separated on a sucrose gradient. (C) Complementation of RpmE and phosphomimetic mutant $RpmE_{S69E}$ on *E. coli* Δ*rpmE*. Cells carrying either pEG25::*rpmE* (RpmE) or pEG25::$rpmE_{S69E}$ ($RpmE_{S69E}$) were grown until an OD_{600} of 0.1 and induced with 1 mM IPTG. Growth was followed via OD_{600} measurements.

an autophosphorylation site (16). Homologs of YjjJ are spread among different bacterial families, indicating that this kinase is likely involved in conserved mechanism(s) of bacterial physiology (Fig. S7). Here, we confirm that strong ectopic overexpression of *yjjJ* leads to cell death, showing the need for a tight regulation of its endogenous levels. Overproduction of YjjJ at lower levels slows the growth in batch culture, which is a phenotype often connected to antibiotic tolerance (21). However, in contrast to HipA-overproducing cells, YjjJ-overproducing cells are almost equally sensitive to ampicillin and/or ciprofloxacin treatment as control cells. Therefore, under the investigated

conditions YjjJ is not directly involved in the establishment or maintenance of antibiotic tolerance. Nevertheless, several indirect lines of evidence connect the function of YjjJ and HipA: (i) the high persistence variant HipA7 was shown to phosphorylate YjjJ *in vivo* (10); (ii) the antitoxin HipB can rescue the toxic effect of both, HipA and YjjJ ([10] and this study); (iii) overproduction of YjjJ affects the activity of HipA (this study). The latter is demonstrated by increased levels of GltX phosphorylation in *yjjJ*-expressing cells, which cannot be attributed to YjjJ action. We speculate that the two kinases are likely connected at two levels: directly (via kinase activity) and indirectly (via competition for HipB). For example, HipA-mediated GltX phosphorylation in cells overproducing kinase-dead YjjJ (YjjJ^{DK}) may be explained by YjjJ^{DK}-mediated sequestering of HipB, which in turn increases the pool of active HipA copies. However, an exact understanding of the mechanistic and functional aspects of the cross talk between the two kinases will require a dedicated study.

YjjJ overproduction resulted in cell elongation and aberrant DNA segregation during cell division. This abnormal phenotype explained the increase of optical density of *yjjJ*-expressing cell cultures over time, despite the decrease in CFU. Upon induction of *yjjJ* we identified changing levels of HtpG and MinCDE, previously shown to influence cell shape and division (18, 19), which link YjjJ action to the observed phenotypes in cell division and DNA segregation. We also identified a strong increase of RecA over time, which indicates DNA stress and strengthen the potential damaging effect of YjjJ on DNA.

Careful tuning of the *yjjJ* expression levels allowed us to identify nontoxic inducing conditions and to analyze the physiological effect of YjjJ on the proteome level over a longer period of time. YjjJ overproduction caused an increase in the levels of ATP-related proteins and a decrease in the levels of proteins related to glycolysis and gluconeogenesis, indicating a rearrangement in energy production similar to that observed at the entrance of the stationary phase (22). This was further supported by overall downregulation of proteins involved in sugar transport and metabolism, as well as protein biosynthesis (e.g., tRNA-ligases). Despite the drop in CFU, pellet from *yjjJ*-expressing cells had a similar glycogen content as pellet from cells bearing the empty vector, which confirmed higher relative amounts of glycogen in *yjjJ*-expressing cells.

At the phosphoproteome level, overproduced YjjJ phosphorylates L31 (rpmE), CsrA, and itself. The phosphorylation site on RpmE is located in a region needed for correct ribosome assembly (20). Induction of *yjjJ* resulted in defects in ribosome assembly similar to deletion of *rpmE* (23), and overproduction of the kinase-dead mutant of YjjJ (YjjJ^{DK}) partially recovered the defective ribosome assembly. The phosphomimetic mutant *rpmE*$_{S69E}$ failed to complement the defective growth of the Δ*rpmE* strain, confirming that YjjJ-mediated phosphorylation negatively regulates RpmE. During stationary phase, in which a rearrangement of L31a (*rpmE*) and L31b (*ykgM*) takes place (24), the strong expression of native *rpmE* was toxic. We speculate that under these conditions L31a (*rpmE*) completely displaced L31b in the ribosome structure, impairing the correct ribosome rearrangement. This effect was not present in cells overexpressing the phosphomimetic *rpmE*$_{S69E}$, suggesting that YjjJ activity could be related to a rearrangement of ribosomal proteins in the stationary phase.

YjjJ-mediated phosphorylation of the carbon storage regulator CsrA is positioned on its regulatory domain (25–27). We showed that the strong toxic effect of CsrA overproduction in *E. coli* is absent in cells overexpressing the phosphomimetic mutant CsrA$_{S56E}$, demonstrating that YjjJ negatively regulates CsrA activity. The location of the phosphorylated Ser56 is distant from the mRNA-binding and dimerization domain of CsrA, but it is situated in a regulatory region (25–27). Interestingly, deletion of the *csrA* gene was previously shown to lead to higher glycogen content and longer cell shape (28, 29), phenotypes that we observed in YjjJ-overproducing cells.

Of note, deletion or CRISPRi-mediated silencing of the *yjjJ* gene did not have any significant effect on the cell growth (Fig. S8) or proteome dynamics (unpublished results) during exponential growth in batch culture, likely due to very low expression of the gene. However, most of the phenotypical consequences of YjjJ induction, such as arrest of cell division and DNA segregation, increased glycogen synthesis, and

altered ribosome assembly, are hallmarks of the stationary phase physiology. In this context it is interesting that previous studies showed an increase in *yjjJ* transcript levels during mid- and late-exponential phase (30) as well as an increase in the YjjJ protein level at the beginning of the stationary phase (31). This suggests that the kinase YjjJ is likely involved in regulatory mechanisms that govern bacterial physiology in the stationary phase and future research should address this aspect of YjjJ biology.

MATERIALS AND METHODS

Bacterial strains and plasmids. Strains, plasmids, primers, and cloning strategies used in this work are listed in the Text S1.

Bioinformatic analysis. PsiBLAST analysis was performed at the NCBI server (https://blast.ncbi.nlm.nih.gov/Blast.cgi). The sequence analysis of YjjJ focused on the motifs found in the protein, following the pipeline described in the Text S1.

Growth experiments. Culturing conditions and different growth strategies are described in the Text S1.

SILAC labeling. For quantitative phosphoproteomic experiments, *E. coli* cells were differentially labeled using stable isotope–labeled lysine derivatives as described previously (32). For more details, please refer to the Text S1.

Dimethyl-labeling. For the quantitative measurement of proteome dynamics, digested samples were on-stage tip dimethylation labeled as described previously (33), as explained in the Text S1.

Cell lysis and protein extraction. For proteomic analysis, proteins were extracted following the protocol explained in the Text S1.

Protein digestion in solution. Extracted proteins were digested for LC-MS/MS measurements. Different digestion strategies are detailed in the Text S1.

Phosphopeptide enrichment. For phosphoproteome experiment, previous LC-MS/MS measurement, phosphopeptides were enriched following the protocol described in the Text S1.

Incorporation and mixing check. The efficiency of SILAC labeling was determined by LC-MS/MS measurement of Lys4- and Lys8-labeled samples, as well as for dimethyl labeling. The different protocols are explained in the Text S1.

Peptide purification by StageTips. Before each LC-MS/MS measurement, all peptide samples were desalted and purified on C18 StageTips (34), as described in the Text S1.

LC-MS/MS measurement. Purified peptide samples were separated by an EASY-nLC 1000 or 1200 system (Thermo Fisher Scientific) coupled online to a Q Exactive HF mass spectrometer (Thermo Fisher Scientific) through a nanoelectrospray ion source (Thermo Fisher Scientific). Chromatographic separation was performed on a 20-cm-long, 75-μm–inner diameter analytical column packed in-house with reversed-phase ReproSilPur C18-AQ 1.9 μm particles (Maisch GmbH). The column temperature was maintained at 40°C using an integrated column oven. The different strategies adopted for the different experiment are detailed in the Text S1.

MS data processing and analysis. The different processing and data analysis pipelines for the different experiments are explained in details in the Text S1.

Protein purification. Plasmids for protein purification were transformed in *E. coli* One Shot BL21(DE3) and the different purification protocols are described in the Text S1.

***In vitro* transcription of CsrC.** DNA template for *csrC* transcripts was amplified by PCR. PCR products were analyzed by 1% agarose gel electrophoresis and purified using the QIAquick PCR purification kit (Qiagen). CsrC-RNA was synthesized by *in vitro* transcription (IVT) in the presence of 40 mM Tris, pH 8.1, 1 mM spermidine, 10 mM $MgCl_2$, 0.01% (Triton X-100), 5% DMSO, 10 mM DTT, 4 mM each NTP, 20 μg of T7 RNA polymerase (2 mg/mL) and 200 nM DNA template. For the preparation of 32-P-labeled csrC transcripts, IVT was performed in the presence of 0.4 μCi/μL ^{32}P-α-ATP (Hartmann Analytics). The IVT reaction mixtures were incubated at 37°C for 4 h and digested with DNase I (Roche). RNA was purified by denaturing PAGE and isopropanol-precipitation, resuspended in Millipore water, and RNA concentration determined by NanoDrop measurements.

Electromobility shift assay. EMSA was performed to study the interaction of CsrA or CsrA S56,59E to *csrC* transcripts. The binding assay was conducted in the presence of 0.6 nM radioactively labeled csrC RNA, 10 mM Tris–HCl, pH 7.5, 10 mM $MgCl_2$, 100 mM KCl, 7.5% glycerol, 20 mM DTT, 200 ng yeast tRNA and various concentrations (0 to 600 nM) of CsrA or CsrA S56,59E. Reaction mixtures were incubated at 30°C for 30 min and analyzed via 9% native polyacrylamide gels in precooled TBE buffer. Radiolabeled csrC transcripts were visualized using storage phosphor screens (GE Healthcare) and a Typhoon 9400 imager (GE Healthcare).

Phosphorylation assay of CsrA by YjjJ for autoradiography. Phosphorylation of CsrA and CsrA S56,59E was performed in the presence of 2 mM DTT, 10 mM $MgCl_2$, 8 mM $ZnCl_2$, 50 mM Tris pH 8.1, 0.5 mM ATP, 5 μCi ^{32}P-γ-ATP (Hartmann Analytics), 5 μM YjjJ, and 15 μM CsrA or CsrA S56,59E for 1h at 37°C. To characterize the influence of RNA, 6 pmol of CsrC was added to the reaction. Samples were taken before the addition of YjjJ (0 min), after 60 min of incubation and stopped by the addition of Tricine Loading Dye each. The reactions were analyzed by 15% Tricine-SDS-PAGE, autoradiography imaging and Coomassie staining.

***In vitro* kinase assay for MS analysis.** Kinase (1.2 μg) (His6-YjjJ) was incubated with 1.2 μg His-tagged substrate in a kinase buffer (50 mM Tris-HCl pH = 8,1 10 mM $MgCl_2$, 16 μM [ZnCl2]) with or without 10 mM ATP and with or without 6 pmol of CsrC for CsrA. Each reaction contained 2.4 μg of a total protein amount. Samples were incubated at 37°C for 2 h and stopped by the addition of nine volumes of denaturation buffer. Samples were split, followed by the protein digestion using chymotrypsin or

Lys-C endoproteinase, as previously described (see above). Digested peptides were purified using StageTips (see above), and 0.2 μg of each sample was measured by LC-MS/MS (see above).

Super-resolution fluorescence microscopy. *E. coli* were grown as described previously, at OD_{600} of 0.3 YjjJ expression was induced with 0.01% and 0.2% arabinose and cells were harvest at defined time points. Cells were stained using FM5-95 (10 μg/mL; Molecular Probes) and 4′,6-diamidino-1-phenylindole (DAPI; 1 μg/mL; Sigma-Aldrich) dyes for 7 min to visualize membranes and nucleoids, respectively. Then, samples were mounted on microscopy slides coated with 1% agarose in water to immobilize cells. Images were acquired using the Zeiss Axio Observer Z1 LSM800 equipped with Airyscan detector. Image analysis was performed via ZEN image analysis software (Zeiss).

Ribosome purification and density gradient. Ribosomes were purified and the assembly analyzed following the protocol in the Text S1.

Glycogen measurement. Glycogen was determined as described previously (35), with following modifications: 50 mL of culture were harvested and total absolute glycogen content was determined.

Transduction of *rpmE* and *yjjJ* deletion. Deletion strains of *rpmE* and *yjjJ*, in MG1655, were perpared by transduction with P1*vir* lysate, using the KEIO donor strain following the protocol explained in the Text S1.

CRISPRi *yjjJ* repression assay. Transformation of *YYdCas9*:BW25993 *intC::TetR-dcas9-aadA laqY::ypet-cat* (36) with the *yjjJ*-pgRNA plasmid (37) with the protocol described in the Text S1, followed by growth curve determination. RNA preparation for Real-time PCR to see the expression of *yjjJ* with details in the Text S1.

Data availability. The mass spectrometry proteomics data have been deposited to the ProteomeXchange Consortium via the PRIDE (38, 39) partner repository with the data set identifier PXD033071.

SUPPLEMENTAL MATERIAL

Supplemental material is available online only.

DATA SET S1, XLSX file, 4.2 MB.

TEXT S1, PDF file, 0.3 MB.

FIG S1, PDF file, 0.3 MB.

FIG S2, PDF file, 0.7 MB.

FIG S3, PDF file, 0.8 MB.

FIG S4, PDF file, 1 MB.

FIG S5, PDF file, 2.8 MB.

FIG S6, PDF file, 0.3 MB.

FIG S7, PDF file, 1.5 MB.

FIG S8, PDF file, 0.6 MB.

ACKNOWLEDGMENTS

We thank Libera Lo Presti for useful discussions and comments on the manuscript. B.M. was supported by grants from the Deutsche Forschungsgemeinschaft (German Research Foundation) Cluster of Excellence EXC 2124, SFB 766, FOR 2816, TRR 261-Project-ID 398967434, the European Union's Horizon 2020 research and innovation program under the Marie Sklodowska-Curie grant agreement No. 955626 and the German–Israeli Foundation grant I-1464–416.13/2018. G.B. acknowledges the Max Planck Society for generous support. Hannes Link kindly provided the YYdCas9 *E. coli* strain and sgRNA plasmid for CRISPRi experiments.

REFERENCES

1. Galperin MY. 2018. What bacteria want. Environ Microbiol 20:4221–4229. https://doi.org/10.1111/1462-2920.14398.
2. Janczarek M, Vinardell JM, Lipa P, Karaś M. 2018. Hanks-type serine/threonine protein kinases and phosphatases in bacteria: roles in signaling and adaptation to various environments. Int J Mol Sci 19:2872. https://doi.org/10.3390/ijms19102872.
3. Groisman EA. 2016. Feedback Control of Two-Component Regulatory Systems. Annu Rev Microbiol 70:103–124. https://doi.org/10.1146/annurev-micro-102215-095331.
4. Macek B, Gnad F, Soufi B, Kumar C, Olsen JV, Mijakovic I, Mann M. 2008. Phosphoproteome analysis of E. coli reveals evolutionary conservation of bacterial Ser/Thr/Tyr phosphorylation. Mol Cell Proteomics 7:299–307. https://doi.org/10.1074/mcp.M700311-MCP200.
5. Macek B, Forchhammer K, Hardouin J, Weber-Ban E, Grangeasse C, Mijakovic I. 2019. Protein post-translational modifications in bacteria. Nat Rev Microbiol 17:651–664. https://doi.org/10.1038/s41579-019-0243-0.
6. Mijakovic I, Macek B. 2012. Impact of phosphoproteomics on studies of bacterial physiology. FEMS Microbiol Rev 36:877–892. https://doi.org/10.1111/j.1574-6976.2011.00314.x.
7. Germain E, Castro-Roa D, Zenkin N, Gerdes K. 2013. Molecular mechanism of bacterial persistence by HipA. Mol Cell 52:248–254. https://doi.org/10.1016/j.molcel.2013.08.045.
8. Fraikin N, Goormaghtigh F. 2020. Type II Toxin-antitoxin systems: evolution and revolutions. J Bacteriol 202:e00763-19. https://doi.org/10.1128/JB.00763-19.
9. Kaspy I, Rotem E, Weiss N, Ronin I, Balaban NQ, Glaser G. 2013. HipA-mediated antibiotic persistence via phosphorylation of the glutamyl-tRNA-synthetase. Nat Commun 4:1–7. https://doi.org/10.1038/ncomms4001.
10. Semanjski M, Germain E, Bratl K, Kiessling A, Gerdes K, Macek B. 2018. The kinases HipA and HipA7 phosphorylate different substrate pools in Escherichia coli to promote multidrug tolerance. Sci Signal 11:5750. https://doi.org/10.1126/scisignal.aat5750.

11. Maeda Y, Lin CY, Ishida Y, Inouye M, Yamaguchi Y, Phadtare S. 2017. Characterization of YjjJ toxin of Escherichia coli. FEMS Microbiology Lett 364. https://doi.org/10.1093/femsle/fnx086.
12. Gerdes K, Bærentsen R, Brodersen DE. 2021. Phylogeny reveals novel hipa-homologous kinase families and toxin-antitoxin gene organizations. mBio 12. https://doi.org/10.1128/mBio.01058-21.
13. McClendon CL, Kornev AP, Gilson MK, Taylor SS. 2014. Dynamic architecture of a protein kinase. Proc Natl Acad Sci U S A 111:E4623–E4631. https://doi.org/10.1073/pnas.1418402111.
14. Fabbro D, Cowan-Jacob SW, Moebitz H. 2015. Ten things you should know about protein kinases: IUPHAR Review 14. Br J Pharmacol 172: 2675–2700. https://doi.org/10.1111/bph.13096.
15. Ardito F, Giuliani M, Perrone D, Troiano G, Muzio LL. 2017. The crucial role of protein phosphorylation in cell signalingand its use as targeted therapy (Review). Int J Mol Med 40:271–280. https://doi.org/10.3892/ijmm.2017.3036.
16. Correia FF, D'Onofrio A, Rejtar T, Li L, Karger BL, Makarova K, Koonin EV, Lewis K. 2006. Kinase activity of overexpressed HipA is required for growth arrest and multidrug tolerance in Escherichia coli. J Bacteriol 188: 8360–8367. https://doi.org/10.1128/JB.01237-06.
17. Sass P, Josten M, Famulla K, Schiffer G, Sahl H-G, Hamoen L, Brötz-Oesterhelt H. 2011. Antibiotic acyldepsipeptides activate ClpP peptidase to degrade the cell division protein FtsZ. Proc Natl Acad Sci U S A 108: 17474–17479. https://doi.org/10.1073/pnas.1110385108.
18. Balasubramanian A, Markovski M, Hoskins JR, Doyle SM, Wickner S. 2019. Hsp90 of E. Coli modulates assembly of FtsZ, the bacterial tubulin homolog. Proc Natl Acad Sci U S A 116:12285–12294. https://doi.org/10.1073/pnas.1904014116.
19. Shen B, Lutkenhaus J. 2009. The conserved C-terminal tail of FtsZ is required for the septal localization and division inhibitory activity of MinCC/MinD. Mol Microbiol 72:410–424. https://doi.org/10.1111/j.1365-2958.2009.06651.x.
20. Ueta M, Wada C, Bessho Y, Maeda M, Wada A. 2017. Ribosomal protein L31 in Escherichia coli contributes to ribosome subunit association and translation, whereas short L31 cleaved by protease 7 reduces both activities. Genes Cells 22:452–471. https://doi.org/10.1111/gtc.12488.
21. Kaldalu N, Tenson T. 2019. Slow growth causes bacterial persistence. Sci Signal 12:458–459. https://doi.org/10.1126/scisignal.aay1167.
22. Dietzler DN, Leckie MP, Lais CJ. 1973. Rates of glycogen stationary synthesis and the cellular and the levels of ATP and FDP during exponential growth and the nitrogen-limited stationary phase of Escherichia coli W4597 (K). Archives of Biochemestry 156:684–693. https://doi.org/10.1016/0003-9861(73)90321-4.
23. Lilleorg S, Reier K, Remme J, Liiv A. 2017. The intersubunit bridge B1b of the bacterial ribosome facilitates initiation of protein synthesis and maintenance of translational fidelity. J Mol Biol 429:1067–1080. https://doi.org/10.1016/j.jmb.2017.02.015.
24. Lilleorg S, Reier K, Pulk A, Liiv A, Tammsalu T, Peil L, Cate JHD, Remme J. 2019. Bacterial ribosome heterogeneity: changes in ribosomal protein composition during transition into stationary growth phase. Biochimie 156:169–180. https://doi.org/10.1016/j.biochi.2018.10.013.
25. Mukherjee S, Oshiro RT, Yakhnin H, Babitzke P, Kearns DB. 2016. FliW antagonizes CsrA RNA binding by a noncompetitive allosteric mechanism. Proc Natl Acad Sci U S A 113:9870–9875. https://doi.org/10.1073/pnas.1602455113.
26. Altegoer F, Rensing SA, Bange G. 2016. Structural basis for the CsrA-dependent modulation of translation initiation by an ancient regulatory protein. Proc Natl Acad Sci U S A 113:10168–10173. https://doi.org/10.1073/pnas.1602425113.
27. Oshiro RT, Dunn CM, Kearns DB. 2020. Contact with the CsrA core is required for allosteric inhibition by FliW in bacillus subtilis. J Bacteriol 203:e00574-20. https://doi.org/10.1128/JB.00574-20.
28. Romeo T, Gong M, Liu MY, Brun-Zinkernagel AM. 1993. Identification and molecular characterization of csrA, a pleiotropic gene from Escherichia coli that affects glycogen biosynthesis, gluconeogenesis, cell size, and surface properties. J Bacteriol 175:4744–4755. https://doi.org/10.1128/jb.175.15.4744-4755.1993.
29. Yang H, Liu MY, Romeo T. 1996. Coordinate genetic regulation of glycogen catabolism and biosynthesis in Escherichia coli via the CsrA gene product. J Bacteriol 178:1012–1017. https://doi.org/10.1128/jb.178.4.1012-1017.1996.
30. Kram KE, Henderson AL, Finkel SE. 2020. Escherichia coli has a unique transcriptional program in long-term stationary phase allowing identification of genes important for survival. mSystems 5:1–11. https://doi.org/10.1128/mSystems.00364-20.
31. Soares NC, Spät P, Krug K, Macek B. 2013. Global dynamics of the Escherichia coli proteome and phosphoproteome during growth in minimal medium. J Proteome Res 12:2611–2621. https://doi.org/10.1021/pr3011843.
32. Soufi B, Macek B. 2014. Stable isotope labeling by amino acids applied to bacterial cell culture. 1188:9–22. https://doi.org/10.1007/978-1-4939-1142-4_2.
33. Boersema PJ, Raijmakers R, Lemeer S, Mohammed S, Heck AJR. 2009. Multiplex peptide stable isotope dimethyl labeling for quantitative proteomics. Nat Protoc 4:484–494. https://doi.org/10.1038/nprot.2009.21.
34. Rappsilber J, Mann M, Ishihama Y. 2007. Protocol for micro-purification, enrichment, pre-fractionation and storage of peptides for proteomics using StageTips. Nat Protoc 2:1896–1906. https://doi.org/10.1038/nprot.2007.261.
35. Klotz A, Reinhold E, Doello S, Forchhammer K. 2015. Nitrogen starvation acclimation in Synechococcus elongatus: redox-control and the role of nitrate reduction as an electron sink. Life (Basel) 5:888–904. https://doi.org/10.3390/life5010888.
36. Lawson MJ, Camsund D, Larsson J, Baltekin O, Fange D, Elf J. 2017. In situ genotyping of a pooled strain library after characterizing complex phenotypes. Mol Syst Biol 13:1–9. https://doi.org/10.15252/msb.20177951.
37. Qi LS, Larson MH, Gilbert LA, Doudna JA, Weissman JS, Arkin AP, Lim WA. 2013. Repurposing CRISPR as an RNA-guided platform for sequence-specific control of gene expression. Cell 152:1173–1183. https://doi.org/10.1016/j.cell.2013.02.022.
38. Ternent T, Csordas A, Qi D, Gómez-Baena G, Beynon RJ, Jones AR, Hermjakob H, Vizcaíno JA. 2014. How to submit MS proteomics data to ProteomeXchange via the PRIDE database. Proteomics 14:2233–2241. https://doi.org/10.1002/pmic.201400120.
39. Perez-Riverol Y, Bai J, Bandla C, García-Seisdedos D, Hewapathirana S, Kamatchinathan S, Kundu DJ, Prakash A, Frericks-Zipper A, Eisenacher M, Walzer M, Wang S, Brazma A, Vizcaíno JA. 2022. The PRIDE database resources in 2022: a hub for mass spectrometry-based proteomics evidences. Nucleic Acids Res 50:D543–D552. https://doi.org/10.1093/nar/gkab1038.

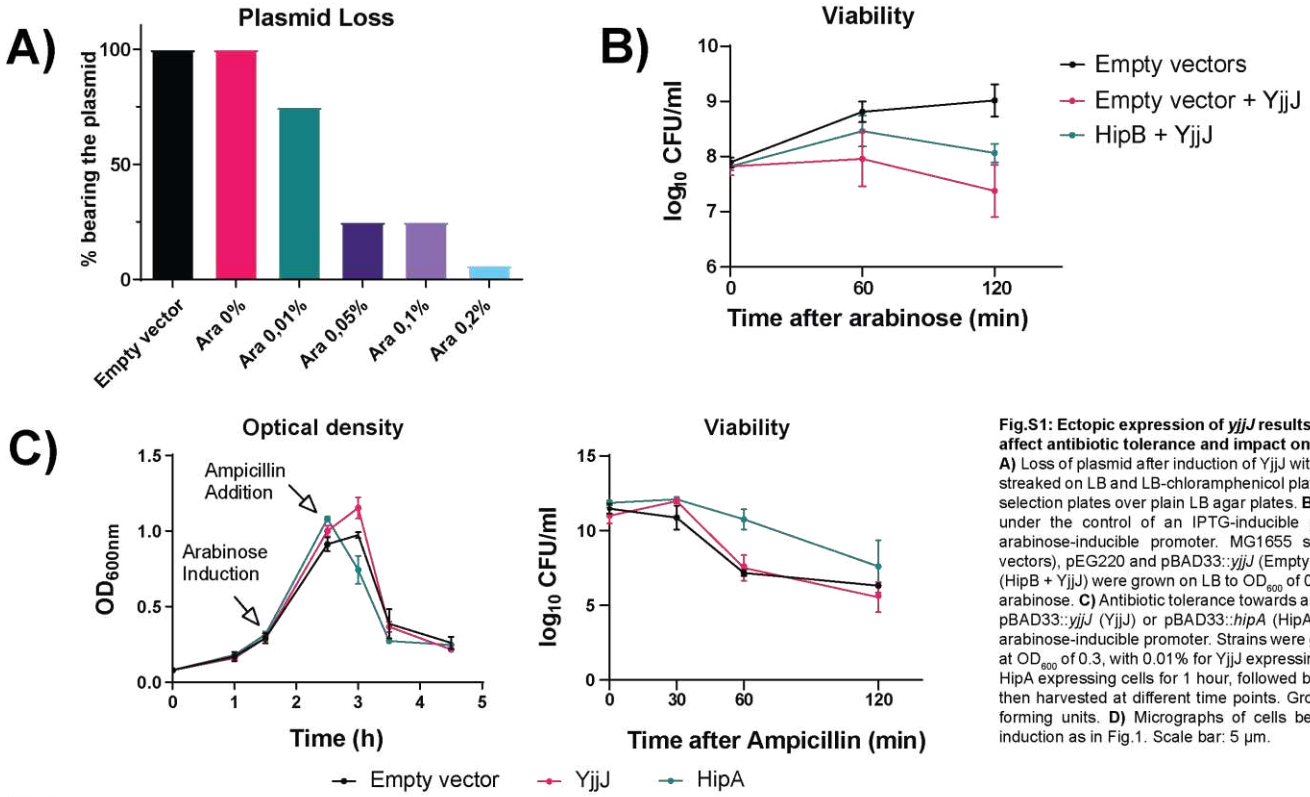

Fig.S1: Ectopic expression of *yjjJ* results toxic, can be complemented by HipB, doesn't affect antibiotic tolerance and impact on cell division and DNA segragation.
A) Loss of plasmid after induction of YjjJ with different concentration of arabinose. Cells were streaked on LB and LB-chloramphenicol plates and percentage was calculated as survivor on selection plates over plain LB agar plates. **B)** HipB complementation of YjjJ. *hipB* was cloned under the control of an IPTG-inducible promoter while *yjjJ* expression was under an arabinose-inducible promoter. MG1655 strains carrying pEG220 and pBAD33 (Empty vectors), pEG220 and pBAD33::*yjjJ* (Empty vector + YjjJ) or pEG220::*hipB* and pBAD33::*yjjJ* (HipB + YjjJ) were grown on LB to OD_{600} of 0.3 followed by addition of 0.1 mM IPTG and 0.1% arabinose. **C)** Antibiotic tolerance towards ampicillin of MG1655 strains bearing empty vector, pBAD33::*yjjJ* (YjjJ) or pBAD33::*hipA* (HipA). Genes *yjjJ* and hipA are under control of an arabinose-inducible promoter. Strains were grown in LB and plasmid expression was induced at OD_{600} of 0.3, with 0.01% for YjjJ expressing cells and 0.2% arabinose for empty vector and HipA expressing cells for 1 hour, followed by treatment with 100 µg/ml ampicillin. Cells were then harvested at different time points. Growth was followed via optical density and colony forming units. **D)** Micrographs of cells before, one hour and two hours after arabinose induction as in Fig.1. Scale bar: 5 µm.

Fig.S1

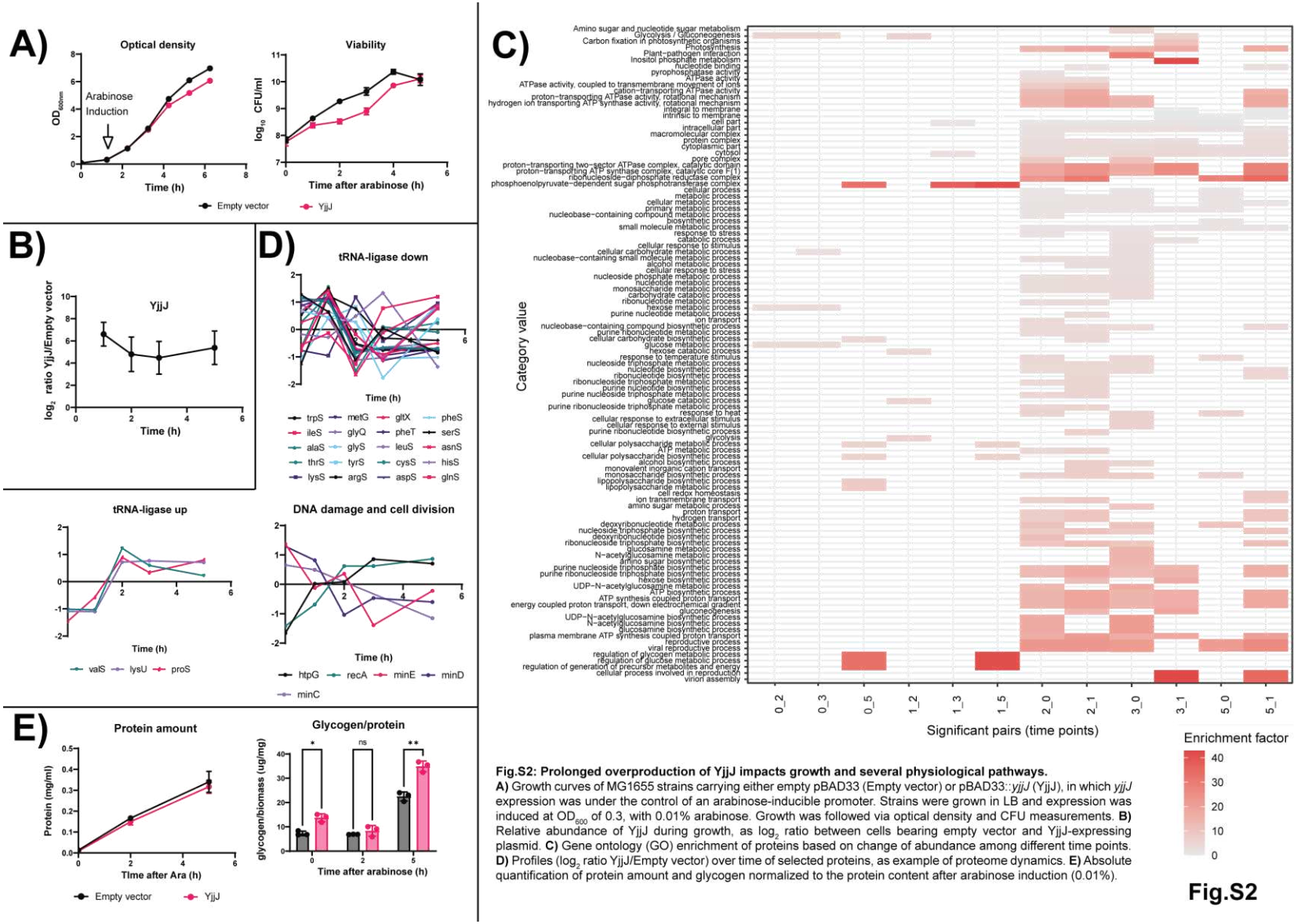

Fig.S2: Prolonged overproduction of YjjJ impacts growth and several physiological pathways.
A) Growth curves of MG1655 strains carrying either empty pBAD33 (Empty vector) or pBAD33::*yjjJ* (YjjJ), in which *yjjJ* expression was under the control of an arabinose-inducible promoter. Strains were grown in LB and expression was induced at OD_{600} of 0.3, with 0.01% arabinose. Growth was followed via optical density and CFU measurements. **B)** Relative abundance of YjjJ during growth, as $\log_2$ ratio between cells bearing empty vector and YjjJ-expressing plasmid. **C)** Gene ontology (GO) enrichment of proteins based on change of abundance among different time points. **D)** Profiles ($\log_2$ ratio YjjJ/Empty vector) over time of selected proteins, as example of proteome dynamics. **E)** Absolute quantification of protein amount and glycogen normalized to the protein content after arabinose induction (0.01%).

Fig.S2

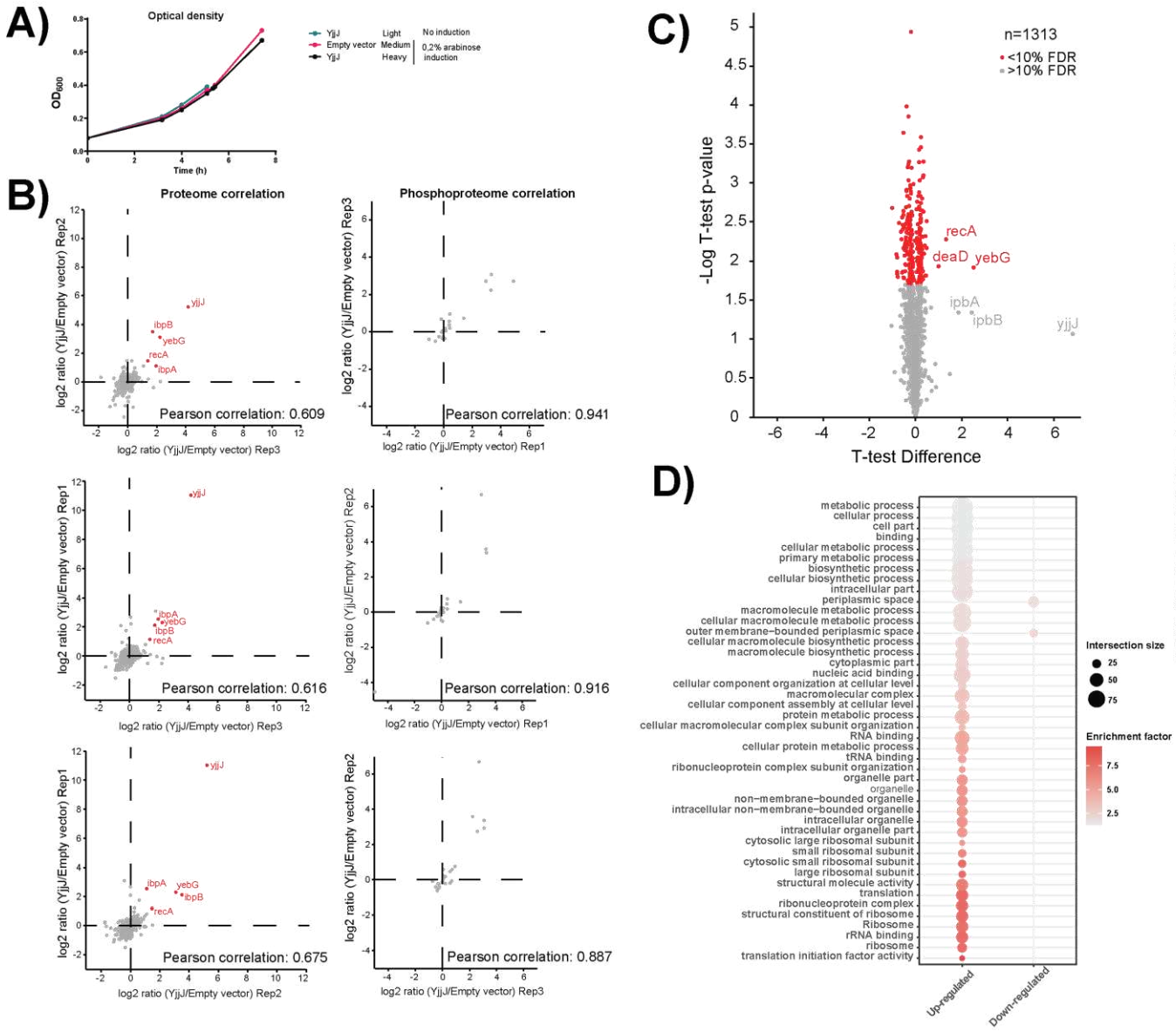

Fig.S3: YjjJ impacts proteome and phosphoproteome with good reproducibility.
A) Growth curves of *E. coli* K-12 MG1655 carrying the pBAD33::*yjjJ* plasmid (YjjJ), in which *yjjJ* expression is under the control of an arabinose-inducible promoter, or pBAD33 as empty vector control. Strains were grown in SILAC-labelled minimal medium containing stable isotope labelled lysine derivatives: "light" lysine (Lys0), "medium-heavy" lysine (Lys4), or "heavy" lysine (Lys8). **B)** Correlation of proteins and phosphorylation-site SILAC ratios from the *yjjJ* expressing strain relative to the strain bearing the empty vector for the three independent replicates. **C)** Volcano plot representing distributions of quantified proteins amongst the three replicates. Proteins with a significant increase (FDR<0.1) are marked in red. **D)** Gene ontology (GO) distribution of those proteins showing an increase in abundance 2 hours after *yjjJ* expression, enriched against the background of all identified proteins.

Fig.S3

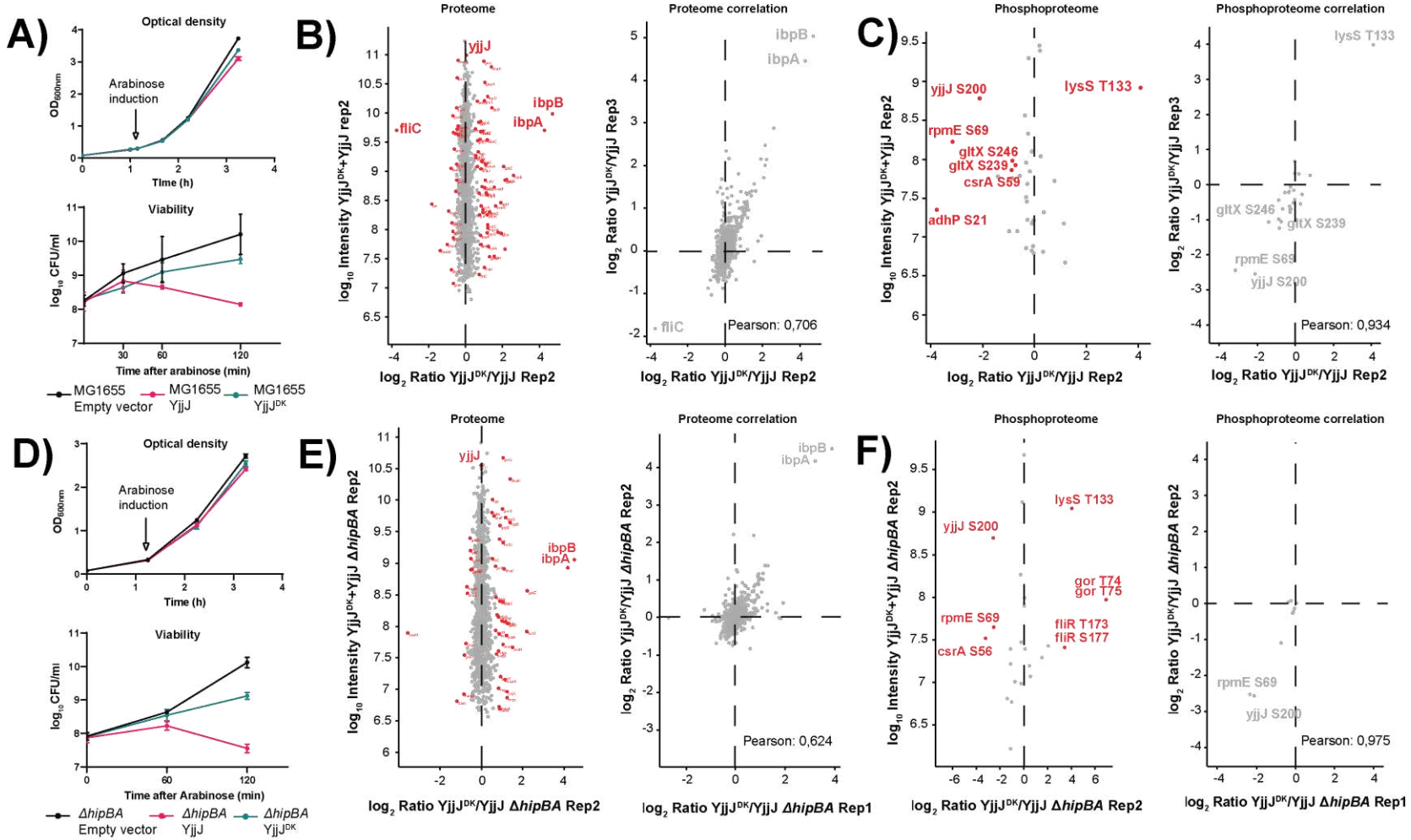

Fig. S4: YjjJ induction cross-talks with HipA pathways, leading to phosphorylation of GltX.

A) Growth curves of *E. coli* K-12 MG1655 wild type carrying the pBAD33::*yjjJ* or pBAD33::*yjjJ S342,364Q* ($YjjJ^{DK}$) plasmid, in which gene expression is under the control of an arabinose-inducible promoter, or pBAD33 as empty vector control. Strains were grown in LB medium. After reaching OD_{600} of 0.3, plasmid expression was induced with 0.2% arabinose. Growth was followed at OD_{600} and CFU level. **B)** Quantified proteins represented as log_2 ratio between YjjJ native and $YjjJ^{DK}$ expressing cells. Significantly changing proteins ($p<0.05$) are indicated (red) with good correlations between the two replicates. **C)** Distribution of phosphorylation sites upon YjjJ overproduction based on log2 ratio between native YjjJ and $YjjJ^{DK}$ expressing cells shows good correlation between the two replicates. **D)** Growth curve of *E. coli* Δ*hipBA* carrying either pBAD33::*yjjJ* or pBAD33::*yjjJ S342,364Q* ($YjjJ^{DK}$) plasmid. Growth was followed at OD_{600} and CFU level. **E)** Quantified proteins represented as log_2 ratio between native YjjJ and $YjjJ^{DK}$ expressing cells in Δ*hipBA* background. Significantly changing proteins ($p<0.05$) are indicated (red) with good correlations between the two replicates. **F)** Distribution of phosphorylated sites upon YjjJ overproduction in the Δ*hipBA* background, based on log_2 ratio between native YjjJ and $YjjJ^{DK}$ expressing cells shows good correlation between the two replicates.

Fig.S4

A)

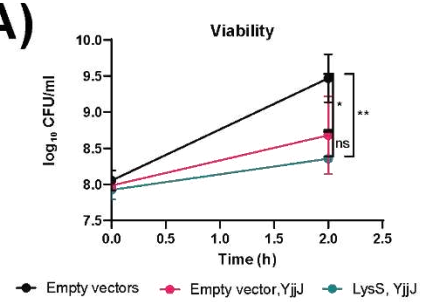

B)

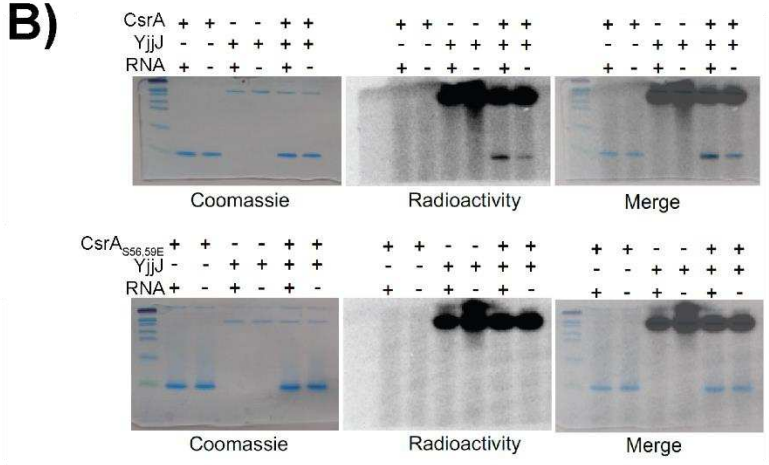

C)

Reaction	RpmE	+	+				
	CsrA			+	+	+	+
	CsrB mRNA					+	+
	ATP		+		+		+
P-site detected	RpmE S69						
	CsrA S56						

Fig.S5: CsrA phosphorylation is confirmed by *in vitro* kinase autoradiography, indicating mRNA as cofactor.
A) LysS complementation of YjjJ. *lysS* was cloned under the control of an IPTG-inducible promoter while *yjjJ* expression was driven by the arabinose-inducible promoter. MG1655 strains carrying pEG50 and pBAD33 (Empty vectors), pEG220 and pBAD33::*yjjJ* (Empty vector + YjjJ) or pEG25::*lysS* and pBAD33::*yjjJ* (LysS + YjjJ) were grown on LB to OD_{600} of 0.3, followed by addition of 1 mM IPTG and 0.1% arabinose. **B)** *in vitro* phosphorylation of CsrA. Purified YjjJ was incubated with [γ^{32P}] ATP, in the presence or absence of CsrC mRNA. The figure depicts the gel was Coomassie stained, radiograms of the gels and the merge. The negative control is represented by CsrA S56,59E mutant. **C)** Control reactions of *in vitro* kinase assay, measured by mass spectrometry, of Fig.2.

Fig.S5

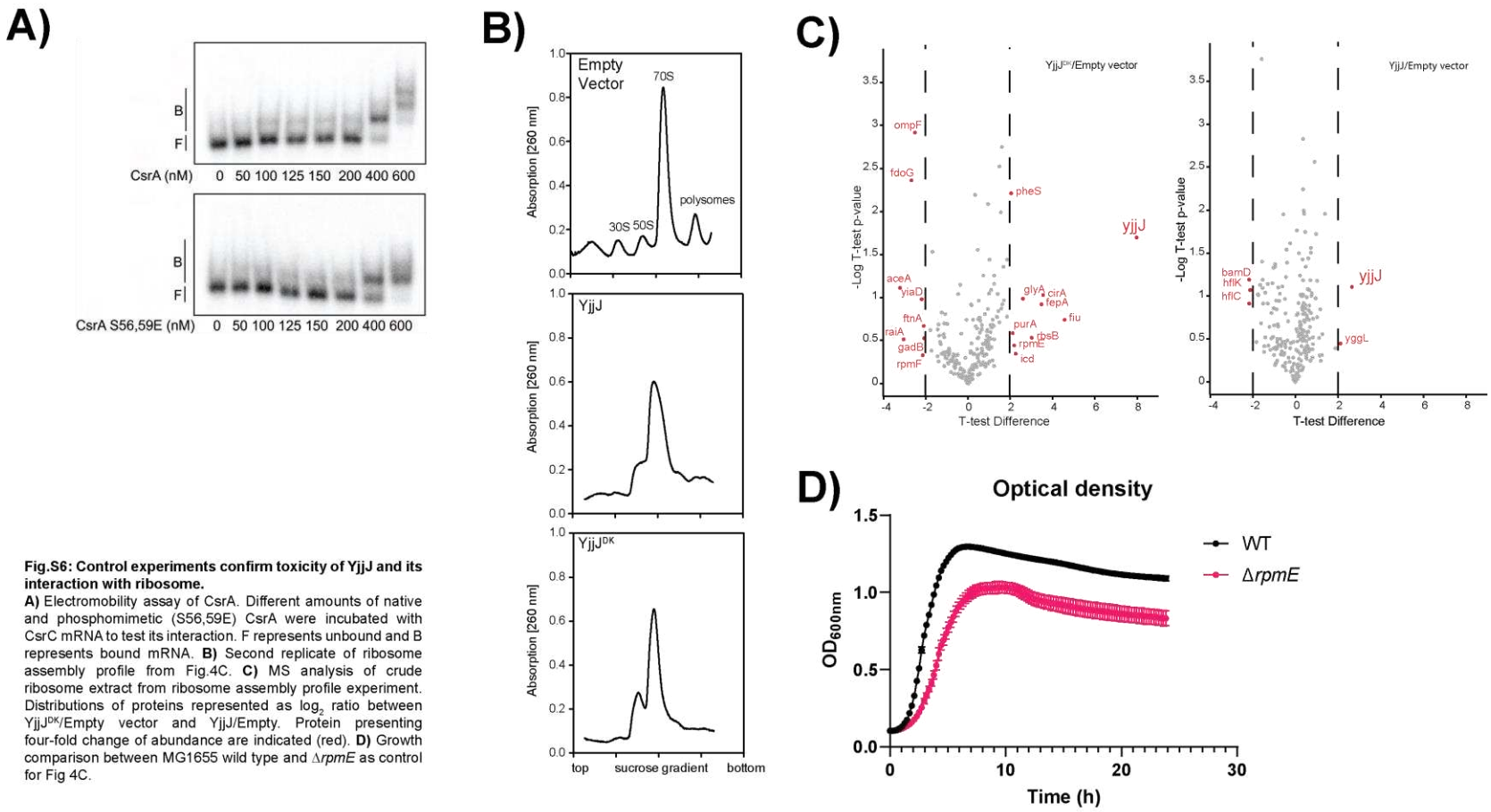

Fig.S6: Control experiments confirm toxicity of YjjJ and its interaction with ribosome.

A) Electromobility assay of CsrA. Different amounts of native and phosphomimetic (S56,59E) CsrA were incubated with CsrC mRNA to test its interaction. F represents unbound and B represents bound mRNA. **B)** Second replicate of ribosome assembly profile from Fig.4C. **C)** MS analysis of crude ribosome extract from ribosome assembly profile experiment. Distributions of proteins represented as $\log_2$ ratio between YjjJ^{DK}/Empty vector and YjjJ/Empty. Protein presenting four-fold change of abundance are indicated (red). **D)** Growth comparison between MG1655 wild type and Δ*rpmE* as control for Fig 4C.

Fig.S6

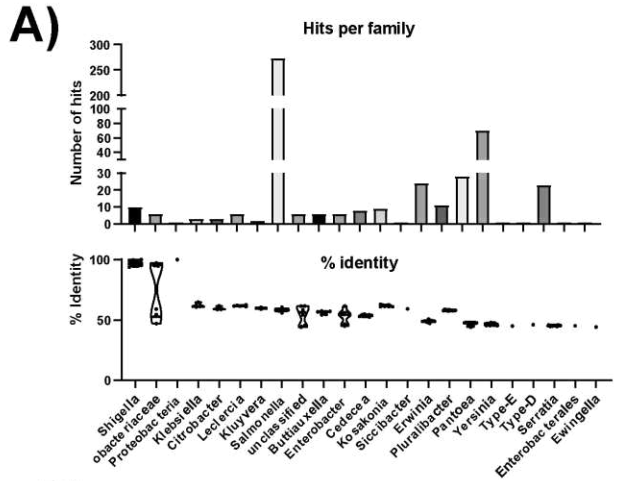

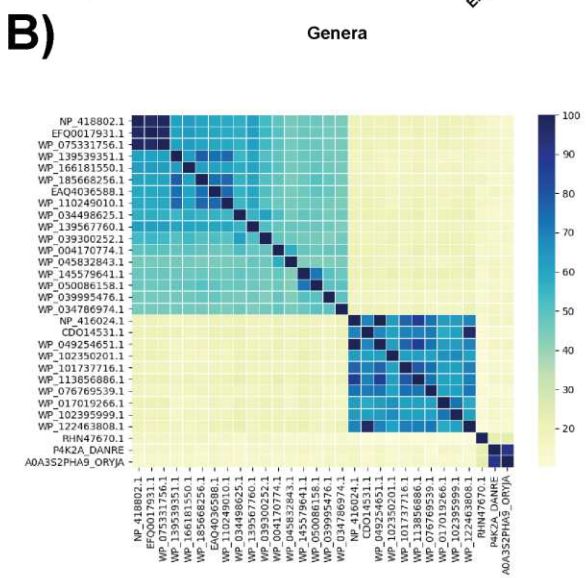

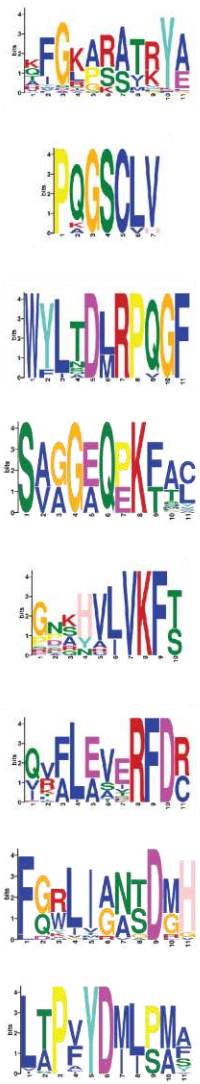

D)

```
YjjJ         1 MSELTDLLLQGPRSAPELRQRLAISQATFSRLVAREDRVIRFGKARATRY      50

HipA         1 ---------------------------------------------------       0

YjjJ        51 ALLRPYRGIERIPVW----RVDDTGK----AHKF-----------ADIR      80
                        :.:::..|    ||.:..|    ||.|           ..:.
HipA         1 --------MPKLVIWMNNQRVGELTKLANGAHTFKYAPEWLASRYARPLS      42

YjjJ        81 LCWPQGSCLVTGADGDEQMFDGLPWYLTD---LRPQGFLGRAWGRKLAAQ      127
               |..|.....:| :|....:||.|   |.|   :|.:  :.:.:..|....
HipA        43 LSLPLQRGNIT-SDAVFNFFDNL---LPDSPIVRDR--IVKRYHAKSRQP      86

YjjJ       128 LNLTDDIRLWQEEDVLYALTVFNGEYTGGWLVGEGNYQRWITAQHP----      173
               .:|..:|    ..|.:.|:|          |:.|..     |..||
HipA        87 FDLLSEI----GRDSVGAVT----------LIPEDE-----TVTHPIMAW      117

YjjJ       174 ---AEIPLDQKLTHYEQLASDALAGEIVG------SSAGGEQ--------      206
                  .|..|::.||.|:   :|...|.|..      |.||.::
HipA       118 EKLTEARLEEVLTAYK---ADIPLGMIREENDFRISVAGAQEKTALLRIG      164

YjjJ       207 -----PK----FTYYAQTPSGNKHVLVKFTVPQQT-----AVSQRWGDLL      242
                    ||    .|:..:.|.|      :...|..|     :|...:.||
HipA       165 NDWCIPKGITPTTHIIKLPIG------EIRQPNATLDLSQSVDNEYYCLL      208

YjjJ       243 IAESIA-----AQILRDGGIHAIESTVLVTSNRQVFLEAERFDCKGNDGR      287
               :|:.:.     |:|::.|.:.|              |..||||.:.|..|
HipA       209 LAKELGLNVPDAEIIKAGNVRA-------------LAVERFDRRWNAER      244

YjjJ       288 LPIVSL-----------EAVQSEFISSPGSWPQAMRRL------CEQQL      319
               ..::.|           .:|:.|....||     :.|:     ..:.|
HipA       245 TVLLRLPQEDMCQTFGLPSSVKYESDGGPG-----IARIMAFLMGSSEAL      289

YjjJ       320 VTHQSVAQTEVIWAFGRLIANSDMHAGNLSFYL-SEPPPALTPVYDMLPM      368
               .......:.:|   |..|.:|.|.|.|.:: :...:.||.||:::..
HipA       290 KDRYDFMKFQV---FQWLIGATDGHAKNFSVFIQAGGSYRLTPFYDIISA      336

YjjJ       369 VYAPNSAGMLRDAAIEVKFDLNVSKSAWLTAIPLAQQFWQTVARDPRISE      418
               .......| :..:.:::...||.||........:..:.:...|:..|..|
HipA       337 FPVLGGTG-IHISDLKLAMGLNASKGKKTAIDKIYPRHFLATAKVLRFPE      385

YjjJ       419 AFRH--------------------IAQEMPEK-IRQIEEKVARMGG----      443
               ...|                    :..:.||. :..:|..|.|:.|
HipA       386 VQMHEILSDFARMIPAALDNVKTSLPTDFPENVVTAVESNVLRLHGRLSR      435

YjjJ       444 -----    443

HipA       436 EYGSK    440
```

Fig.S7: A) Distribution of *yjjJ* among different genera (upper panel) and percentage of identity (lower panel). **B)** Multiple sequence alignment (Clustal Omega) of 16 different YjjJ, 13 HipA and three ¾ kinase protein sequences from various organisms. **C)** Visualization of motifs identified in multiple sequence alignment. **D)** Pairwise sequence alignment between YjjJ and HipA proteins.

Fig.S7

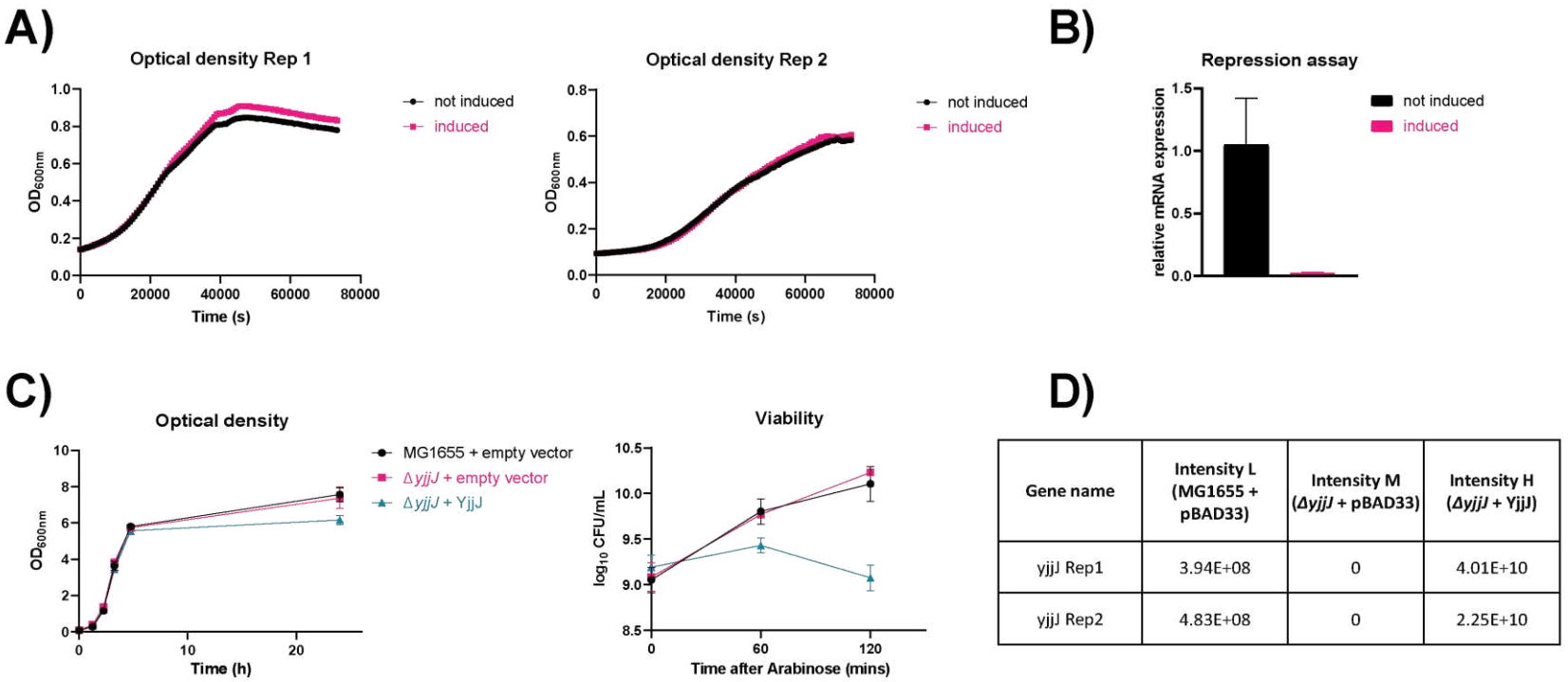

Gene name	Intensity L (MG1655 + pBAD33)	Intensity M (*ΔyjjJ* + pBAD33)	Intensity H (*ΔyjjJ* + YjjJ)
yjjJ Rep1	3.94E+08	0	4.01E+10
yjjJ Rep2	4.83E+08	0	2.25E+10

Fig.S8: Effect of CRISPRi-Silencing and Deletion of YjjJ on growth.
A) Growth curve of *E. coli* strain *YYdCas9:BW25993* cells with *yjjJ*-pgRNA. Expression of dCas9 induced by aTc 100ng/ml to repress *yjjJ* or not induced (as a control). Cells were grown in M9 minimal medium in 24-well microtiter plates. Growth was followed in two independent experiments. Samples harvested at the end of the growth curve for repression assay. **B)** Repression assay for relative mRNA levels of YjjJ induced vs not induced by doing real-time PCR with cDNA. Data is normalized to the expression of the endogenous control gene, *hcaT*. **C)** Growth curve of *E. coli K-12* MG1655 carrying the empty vector and *E. coli ΔyjjJ* carrying either the empty vector or pBAD33::*yjjJ* plasmid (YjjJ) in which *yjjJ* expression was under the control of an arabinose-inducible promoter. Strains were grown in LB medium and expression was induced at OD_{600} of 0.3, with 0.2% arabinose. Growth was followed via optical density and CFU measurements. **D)** Table for confirmation of knockout via MS measurements. Strains were grown in SILAC-labelled minimal medium containing stable isotope labelled lysine derivatives: "light" lysine (Lys0), "medium-heavy" lysine (Lys4), or "heavy" lysine (Lys8), harvested after 2 hrs of induction with 0.2% arabinose , followed by sample preparation and measurement via MS.

Fig.S8

3.3 Manuscript III

Deep phosphoproteomics of *Klebsiella pneumoniae* reveals HipA-mediated tolerance to ciprofloxacin (Under Revision)

Deep phosphoproteomics of *Klebsiella pneumoniae* reveals HipA-mediated tolerance to ciprofloxacin

Short Title: HipA-dependent antibiotic tolerance in *Klebsiella pneumoniae*

Payal Nashier[1], Isabell Samp[2], Marvin Adler[2], Carsten Jers[3], Ivan Mijakovic[3,4], Sandra Schwarz[2]*, Boris Macek[1]*

[1]Proteome Center Tübingen, Institute of Cell Biology, University of Tübingen, Tübingen, Germany
[2]Interfaculty Institute of Microbiology and Infection Medicine Tübingen, Institute of Medical Microbiology and Hygiene, University of Tübingen, Tübingen, Germany
[3]The Novo Nordisk Foundation, Center for Biosustainability, Technical University of Denmark, Kongens Lyngby, Denmark
[4]Systems and Synthetic Biology Division, Department of Life Sciences, Chalmers University of Technology, Gothenburg, Sweden

*Corresponding authors:

Dr. Boris Macek
Professor, Quantitative Proteomics
Director, Proteome Center Tübingen
Department of Biology
Institute for Cell Biology
University of Tübingen
Auf der Morgenstelle 15
72076 Tübingen
Germany
Tel.: (+49-7071) 29-70556
Fax: (+49-7071) 29-5779
E-mail: boris.macek@uni-tuebingen.de

Dr. Sandra Schwarz
Group leader
Institute of Medical Microbiology and Hygiene
Interfaculty Institute of Microbiology and Infection Medicine Tübingen
University of Tübingen
Elfriede Aulhorn Str. 6
72076 Tübingen
Germany
Tel.: (+49-7071) 29-81527
Fax: (+49-7071) 29-5440
E-mail: sandra.schwarz@med.uni-tuebingen.de

Abbreviations

ESBL: Extended-spectrum beta-lactamase

Hip: High persistence

LC-MS/MS: Liquid chromatography coupled to tandem mass spectrometry

PTM: Post translational modification

OD: Optical density

CFU: Colony forming units

MIC: Minimum inhibitory concentration

LB: Luria bertani

SDS: Sodium dodecyl sulfate

AcN: Acetonitrile

DTT: Dithiothreitol

IAA: Iodoacetamide

TFA: Trifluoroacetic acid

FA: Formic acid

HPLC: High performance liquid chromatography

RMSD: Root mean square deviation

Keywords

Phosphoproteome; *Klebsiella pneumoniae*; hipA; Antibiotic tolerance; Persistence; Mass Spectrometry

Abstract

Klebsiella pneumoniae belongs to the group of bacterial pathogens causing the majority of antibiotic-resistant nosocomial infections worldwide; however, the molecular mechanisms underlying post-translational regulation of its physiology are poorly understood. Here we perform a comprehensive analysis of *Klebsiella* phosphoproteome, focusing on HipA, a Ser/Thr kinase involved in antibiotic tolerance in *Escherichia coli*. We show that overproduced *K. pneumoniae* HipA ($HipA_{kp}$) is toxic to both *E. coli* and *K. pneumoniae* and its toxicity can be rescued by overproduction of the antitoxin $HipB_{kp}$. Importantly, $HipA_{kp}$ overproduction leads to increased tolerance against ciprofloxacin, a commonly used antibiotic in the treatment of *K. pneumoniae* infections. Proteome and phosphoproteome analyses in the absence and presence of ciprofloxacin confirm that $HipA_{kp}$ has Ser/Thr kinase activity, auto-phosphorylates at S150 and shares multiple substrates with $HipA_{ec}$, thereby providing a valuable resource to clarify the molecular basis of tolerance and the role of Ser/Thr phosphorylation in this human pathogen.

Author Summary

Klebsiella pneumoniae is a bacterial pathogen that causes hospital-acquired infections in immuno-compromised patients, often becoming resistant or tolerant to multiple antibiotics. These bacteria are becoming increasingly difficult to treat due to the relapse of infection by multidrug tolerant persister cells. These bacteria are a huge burden to healthcare systems and are becoming increasingly resistant to all available antibiotics. Our research focuses on characterizing HipA in *K. pneumoniae*, an *E. coli* kinase known to be involved in persistence. We studied HipA-dependent protein phosphorylation in *K. pneumoniae* to understand the mechanism of persistence. We also found HipA induces antibiotic tolerance, where HipA-induced *K. pneumoniae* persister cells survived ciprofloxacin treatment but not gentamicin. To the best of our knowledge, this is the first study that addresses post-translational regulation in *K. pneumoniae* and connects protein phosphorylation with drug tolerance in this important human pathogen. This study will be a valuable resource for both microbiologists and systems biologists in better understanding of persister infections.

Introduction

Klebsiella pneumoniae is a Gram-negative, extended-spectrum β-lactamase (ESBL)-producing, pathogenic bacterium that causes hospital-acquired infections in immunocompromised patients but also community-acquired infections in healthy individuals (1). *K. pneumoniae* poses a severe risk, causing potentially deadly infections like bloodstream infections and pneumonia, especially in healthcare environments with vulnerable patients and medical devices. The bacteria belong to the “ESKAPE” group of antimicrobial resistant and virulent pathogens (*Enterococcus faecium, Staphylococcus aureus, Klebsiella pneumoniae, Acinetobacter baumannii, Pseudomonas aeruginosa, Enterobacter spp.*), causing the majority of nosocomial infections worldwide (2). Furthermore, the WHO considers *K. pneumoniae* as a Priority I pathogen for the development of novel antibiotics due to the escalating resistance against antibiotics including last-resort antimicrobials (3, 4).

Antibiotic tolerance, defined as the ability of a whole bacterial population to survive a transient antibiotic exposure to concentrations much higher than the minimum inhibitory concentration (MIC) is an alternative mechanism enabling evasion of antibiotic therapy and causing relapse of infections. Extended exposure to an antibiotic, as opposed to a higher dosage of the drug, can cause the same amount of killing in tolerant and sensitive cells (5). Antibiotic tolerance plays a significant role in shaping the evolutionary dynamics of bacterial populations subjected to repeated antibiotic treatments. Notably, it was reported that antibiotic tolerance promotes the subsequent emergence of antibiotic resistance (6, 7). The molecular mechanisms of tolerance are also linked with the time-dependent antibiotic persistence, which emerges in a heterogenous population of clonal bacteria when only a subpopulation develops tolerance. These time-dependent persisters exhibit a biphasic killing curve characterized by slow growth and are insensitive to substantially high concentrations of antibiotics (5). Therefore, persister cells are phenotypic variants of the normal sensitive population of cells with the ability to survive high concentrations of antibiotic exposure (8, 9).

K. pneumoniae has the ability to produce persister cells, and their development was shown to be strongly stimulated by stationary-phase related environmental cues and

sublethal concentrations of antibiotics (10). Exposure to various bactericidal antibiotics commonly employed in the treatment of *K. pneumoniae* infections has revealed the presence of multidrug-tolerant persister cells in both laboratory and clinical strains, as determined through time-dependent killing curves (11). Additionally, persister cells have been identified in clinical isolates from individuals experiencing recurring bloodstream infections, demonstrating genomic alterations in relapsed isolates that evolved within the host (12). However, the mechanisms underlying the formation of these multidrug-tolerant persister cells in *K. pneumoniae* are understudied, although this knowledge could be important for managing chronic infections more efficiently and devising strategies to eliminate persisters.

HipA is a well-characterized protein in *Escherichia coli* ($HipA_{ec}$) that was previously shown to induce persistence and be involved in antibiotic tolerance (13, 14). Acting as its antitoxin, HipB, a DNA-binding transcriptional regulator, binds to HipA, forming a HipBA protein complex that represses its own operon under normal conditions (15). Degradation of HipB by Lon proteases, upregulated during stress conditions, results in the release and activation of HipA (16). $HipA_{ec}$ is a Ser/Thr kinase that phosphorylates glutamyl-tRNA synthetase (GltX) causing accumulation of uncharged Glu-tRNA. This in turn halts translation, leading to the activation of the stringent response and induction of persistence by RelA-mediated synthesis of the alarmone ppGpp (17, 18). Phosphoproteomic study based on over-expression of $hipA_{ec}$ has shown that $HipA_{ec}$ phosphorylates multiple proteins in addition to the well-described substrate GltX (19). A more recent bioinformatics study showed that HipA-like kinases are abundant across different bacterial species, and revealed the presence of a homolog in *K. pneumoniae* (20). Due to the association of *hipA*-related genes to antibiotic tolerance and persistence, we hypothesized that the HipA-homolog in *K. pneumoniae* may have a similar function to $HipA_{ec}$ and set out to investigate its activity and targets in this important human pathogen.

For the molecular characterization of the HipA-homolog in *K. pneumoniae*, we designed a series of experiments to analyze the effect of $hipA_{kp}$ overexpression in *E. coli* and *K. pneumoniae* cells. Using quantitative mass spectrometry-based phosphoproteomics

(21), we measured and analyzed the phosphoproteome of $HipA_{kp}$- overproducing cells to identify the potential substrates of $HipA_{kp}$ and also assessed its effect on antibiotic tolerance. Here we show that *hipA*$_{kp}$ overexpression is toxic to the cells and toxicity can be partially rescued by *hipB*$_{kp}$ overexpression. We confirmed that $HipA_{kp}$ is a Ser/Thr kinase that autophosphorylates at S150 and T158 and also phosphorylates GltX at S239 in both *E. coli* and *K. pneumoniae*. In addition to GltX, we discovered numerous additional putative substrates of the kinase, involved in translation, transcription, cell division and central metabolism. Finally, we found that overexpression of *hipA*$_{kp}$ leads to tolerance against the fluoroquinolone antibiotic ciprofloxacin, thereby connecting the function of this kinase with antibiotic tolerance in *Klebsiella*.

Results

1.1 *hipB*/*A* operon is conserved across *Klebsiella* and other bacteria

The *hipB/A* operon is established as one of the main drivers of antibiotic tolerance in *E. coli*; therefore, we first compared the amino acid sequence of HipB/A with its putative homolog in *K. pneumoniae*. Pairwise sequence alignment using pBLAST showed that $HipA_{kp}$ and $HipB_{kp}$ shared 69% and 56% of sequence identity with $HipA_{ec}$ and $HipB_{ec}$, respectively **(Fig. 1A, figs. S1A and S1B)**. The alignment of the $HipA_{kp}$ structure as predicted by AlphaFold (22, 23) with the experimentally determined $HipA_{ec}$ structure (24) showed a high degree of conservation (RMSD 0.444 Å), including within the ATP and Mg^{2+} ion binding pockets important for kinase activity **(Fig. 1B)**. Furthermore, several residues known to be essential for kinase activity were conserved between $HipA_{kp}$ and $HipA_{ec}$, such as the autophosphorylation site S150, the catalytic residue D309, the residue L181 involved in ATP-binding, and the residues N314 and D332 involved in Mg^{2+} binding (13) **(fig. S1A)**. Alignment of the AlphaFold-predicted structure of $HipB_{kp}$ with the experimentally determined structure of $HipB_{kp}$ (24) showed a similar degree of conservation (RMSD 0.405 Å) **(fig. S1C)**.

Protein BLAST analysis showed that the $HipA_{kp}$ is conserved and present in different species of *Klebsiella,* with the mean percent identity varying from 95% to 99% in different isolates of the same genus, species and subspecies **(Fig. 1C)**. For further visualization of the presence of $HipA_{kp}$ across all organisms, we plotted the percentage of sequence

identity of $HipA_{kp}$ homologs from the top 5,000 protein BLAST hits and determined that the sequence identity reaches up to 70% in many Gram-negative bacteria such as *E. coli* and bacteria belonging to the genus *Shigella, Serratia* and *Salmonella*. Some of the genera were under-represented due to the large number of hits originating from *Klebsiella* and *E. coli* **(fig. S1D)**. Combined, these results showed high structural similarity of HipB/A between *K. pneumoniae* and *E. coli*, as well as conservation of HipA among many Gram-negative bacteria.

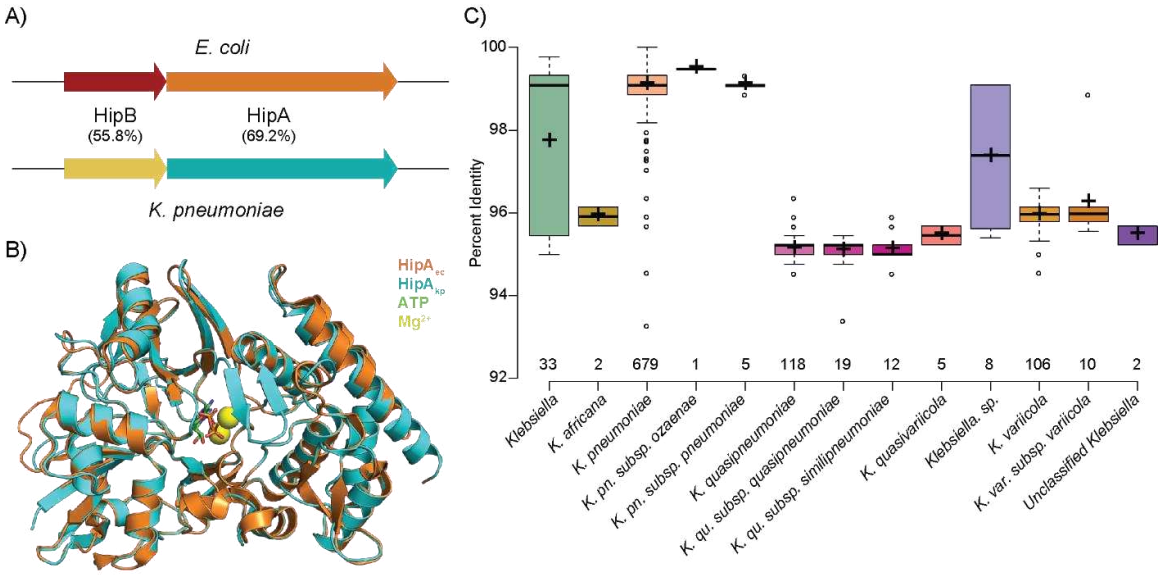

Fig. 1 Bioinformatic analysis of *$hipA_{kp}$* and *$hipB_{kp}$*. A) Schematic representation of the *hipB/A* operon in *K. pneumoniae* and *E. coli*. The numbers indicate the percent identity of HipA and HipB between the species. **B)** Alignment of AlphaFold predicted structure of $HipA_{kp}$, UniProt ID: A6T928 (cyan), with the experimentally determined structure of $HipA_{ec}$, PDB ID: 3DNT (orange), together with ATP (sticks), and Mg^{2+} molecules (yellow spheres), in the conserved pocket. **C)** Distribution of percentage of sequence identity of $HipA_{kp}$ homologs within the *Klebsiella* genus and the number of hits obtained upon analyzing the top 1,000 results from protein BLAST of $HipA_{kp}$ protein with all the default settings except limiting the organism search to "Klebsiella (taxid:570)" as "Organism" in Standard settings.

1.2 Overproduction of $HipA_{kp}$ in *E. coli* is toxic to the cells and can be counteracted by $HipB_{kp}$

To investigate the role of *$hipA_{kp}$*, we first analyzed its effect on growth and viability of *E. coli* cells in LB medium. As previously reported for *$hipA_{ec}$*, overexpression of *$hipA_{kp}$* was expected to be toxic to the cells. Therefore, we ectopically expressed *$hipA_{kp}$* in *E. coli* under the control of an arabinose-inducible promoter with optimized Shine-Dalgarno

sequence (25). We observed that overexpression of *hipA*$_{kp}$ was highly toxic to *E. coli* cells, resulting in reduction of their growth after 1 h post-induction by three-fold and survival by 2.5-fold, as measured by optical density (OD_{600nm}) and colony forming units (CFU), respectively **(Fig. 2A)**. To determine whether the overproduction of $HipB_{kp}$ counteracted the activity of *hipA*$_{kp}$ in *E. coli*, we simultaneously overexpressed *hipA*$_{kp}$ and *hipB*$_{kp}$ from different plasmids. Compared to the growth of *E. coli* overexpressing only *hipA*$_{kp}$, simultaneous overproduction of *hipB*$_{kp}$ restored the growth of *hipA*$_{kp}$-overexpressing *E. coli* + *hipA*$_{kp}$ + *hipB*$_{kp}$ and therefore reversed the *hipA*$_{kp}$-related toxic phenotype **(Fig. 2B).** We therefore concluded that overproduced $HipA_{kp}$ and $HipB_{kp}$ act as a canonical toxin/antitoxin pair in *E. coli.*

1.3 $HipA_{kp}$ has Ser/Thr kinase activity in *E. coli* and phosphorylates multiple substrates

Based on the sequence homology of $HipA_{ec}$ and conserved kinase and ATP-binding domains **(fig. S1A),** we postulated that $HipA_{kp}$ has kinase activity. In order to identify its putative substrates, we overexpressed *hipA*$_{kp}$ in *E. coli* and performed quantitative phosphoproteome analysis using liquid chromatography coupled to tandem mass spectrometry (LC-MS/MS). At the proteome level, we measured more than eight-fold increase in $HipA_{kp}$ in the cells upon *hipA*$_{kp}$ overexpression for 1 h in comparison with the empty pBAD33 vector control. These results confirmed the efficiency of the *hipA*$_{kp}$ overexpression strategy **(Fig. 2C, Dataset S1 Table T1)**.

At the phosphoproteome level, we identified 317 phosphorylation sites on 189 proteins in *E. coli* + *hipA*$_{kp}$ 1 h post-induction, with an excellent correlation between the replicates (**Fig. 2D, Dataset S1 Table T2**). Upon $HipA_{kp}$ overproduction, we reproducibly detected increased phosphorylation of multiple substrates; among them was phosphorylation of GltX at position S239, which showed more than 16-fold increase in all replicates **(figs. S2A and S2B, Dataset S1 Table T2)**. Importantly, the level of GltX protein did not significantly change upon $HipA_{kp}$ overproduction (**Dataset S1 Table T1**), which attributed the observed increase in phosphorylation to $HipA_{kp}$ kinase activity. In addition, we also detected autophosphorylation of $HipA_{kp}$ at S150 and T158 (the former with

significantly higher abundance). These measurements indicated that overproduced $HipA_{kp}$ has kinase activity and identified GltX as its major substrate in *E. coli*.

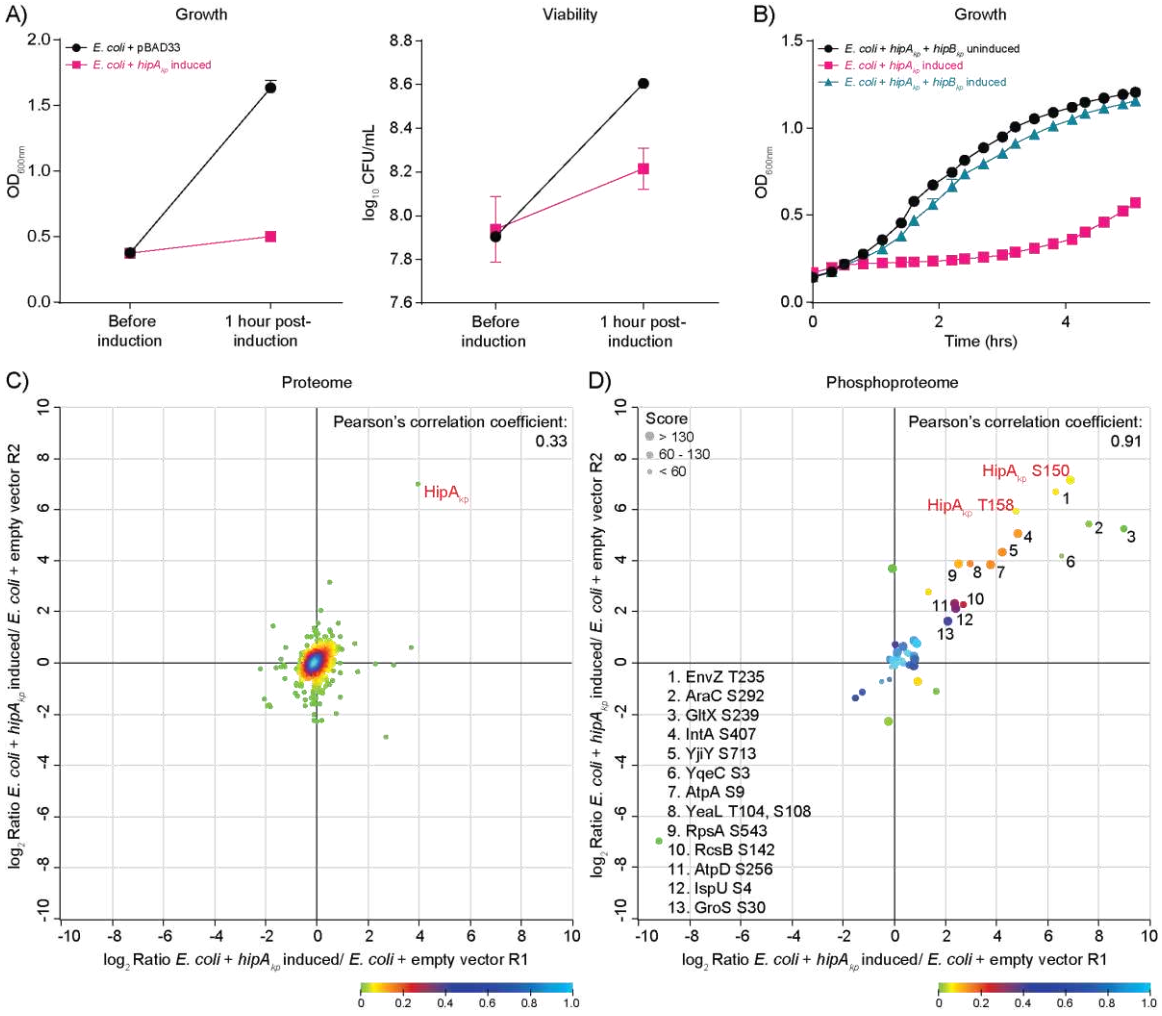

Fig. 2 Effect of overexpression of *hipA$_{kp}$* in WT *E. coli* cells. A) Growth curves of *E. coli* containing the empty pBAD33 vector and pBAD33::*hipA$_{kp}$*. The expression of *hipA$_{kp}$* is under the control of the arabinose-inducible promoter. After the cells reached an OD_{600nm} of 0.3, expression of *hipA$_{kp}$* was induced with 0.2% arabinose for 1 h. Growth was monitored by absorbance measurements at OD_{600nm} and viability was determined by CFU quantification. Data shown are mean values ± SD of three independent biological replicates. Bacteria were harvested at 1 h post-induction for proteome and phosphoproteome analysis. **B)** Growth curves of *E. coli* carrying pBAD33::*hipA$_{kp}$* alone or together with plasmid pGOOD::*hipB$_{kp}$* , in which *hipB$_{kp}$* is under the control of an IPTG-inducible promoter. Overnight cultures of the bacteria were used to inoculate the cultures for the assay at 0.08 OD_{600nm} in medium containing 0.2% arabinose and 1 mM IPTG. As a control, one set of samples was left uninduced and one strain carrying and expressing only *hipA$_{kp}$*. The growth was followed via OD_{600nm} measurements for 5 h in a plate reader (Tecan). The growth curve is based on mean values ± SD of three independent biological replicates. **C)** The same strains from growth experiment were labeled by dimethyl labeling for quantitative analysis as follows: WT *E. coli* with empty vector was labeled as “Light”, whereas WT *E. coli* with *hipA$_{kp}$*- expressing plasmid was labeled as “Medium”.

Quantified proteins represented as log_2 ratio between WT *E. coli* pBAD33::*hipA*$_{kp}$ and WT empty vector strain showing significant up-regulation of *hipA*$_{kp}$ as marked in red. **D)** Distribution of quantified phosphorylation sites upon *hipA*$_{kp}$ overexpression in WT *E. coli* background, based on log_2 ratio between WT pBAD33::*hipA*$_{kp}$ and WT empty vector, showed high correlation between the two replicates. The phosphorylation sites changing at least four-fold in phosphorylation upon *hipA*$_{kp}$ overexpression were numbered and listed in the graph. The name of the phosphorylated protein and the amino acid phosphorylated and the position of the amino acid within the protein sequence are indicated. The size of each phosphorylation site in the scatter plot corresponds to its respective peptide score and scale is provided on the top left corner of the plot. Color scale at the bottom of graph is indicative of density to two points in plane, with values closer to 1 not changing their ratio and closer to 0 changing the ratios in both replicates.

1.4 HipA$_{kp}$ activity is toxic to *K. pneumoniae* cells and partially counteracted by HipB$_{kp}$

We next overexpressed *hipA*$_{kp}$ in *K. pneumoniae.* To this end, we used the *K. pneumoniae* isolate ATCC13883 (wild type, WT), which harbors the *hipB/A* operon on the chromosome. First, we generated a deletion mutant of the *hipA*$_{kp}$ gene (Δ*hipA*) and assessed the impact of the deletion on growth and viability of *K. pneumoniae* by measuring the optical density (OD_{600nm}) and CFU levels. We observed that growth of the Δ*hipA* mutant was almost identical to that of the WT in LB over a 24 h incubation period. Likewise, the deletion of *hipA* did not affect survival of *K. pneumoniae* in exponential phase and resulted in a slight reduction of CFU/ml in stationary phase **(fig. S3A)**. We next overexpressed *hipA*$_{kp}$ from the pBAD33 vector in both WT and Δ*hipA K. pneumoniae.* The overproduction of HipA$_{kp}$ decreased growth and viability by a three-fold at 1 h post-induction (**Fig. 3A)**. We tested if the overexpression of *hipB*$_{kp}$ in *K. pneumoniae* WT + *hipA*$_{kp}$ and Δ*hipA* + *hipA*$_{kp}$ could counter the toxic effect of *hipA*$_{kp}$ expression. We observed that bacteria expressing both *hipA*$_{kp}$ and *hipB*$_{kp}$ grew better than Δ*hipA* + *hipA*$_{kp}$ indicating that HipB$_{kp}$ partially rescued the toxic effect of HipA$_{kp}$ **(Fig. 3B).** These results point to a similar role of the antitoxin HipB in *K. pneumoniae* and *E. coli* cells.

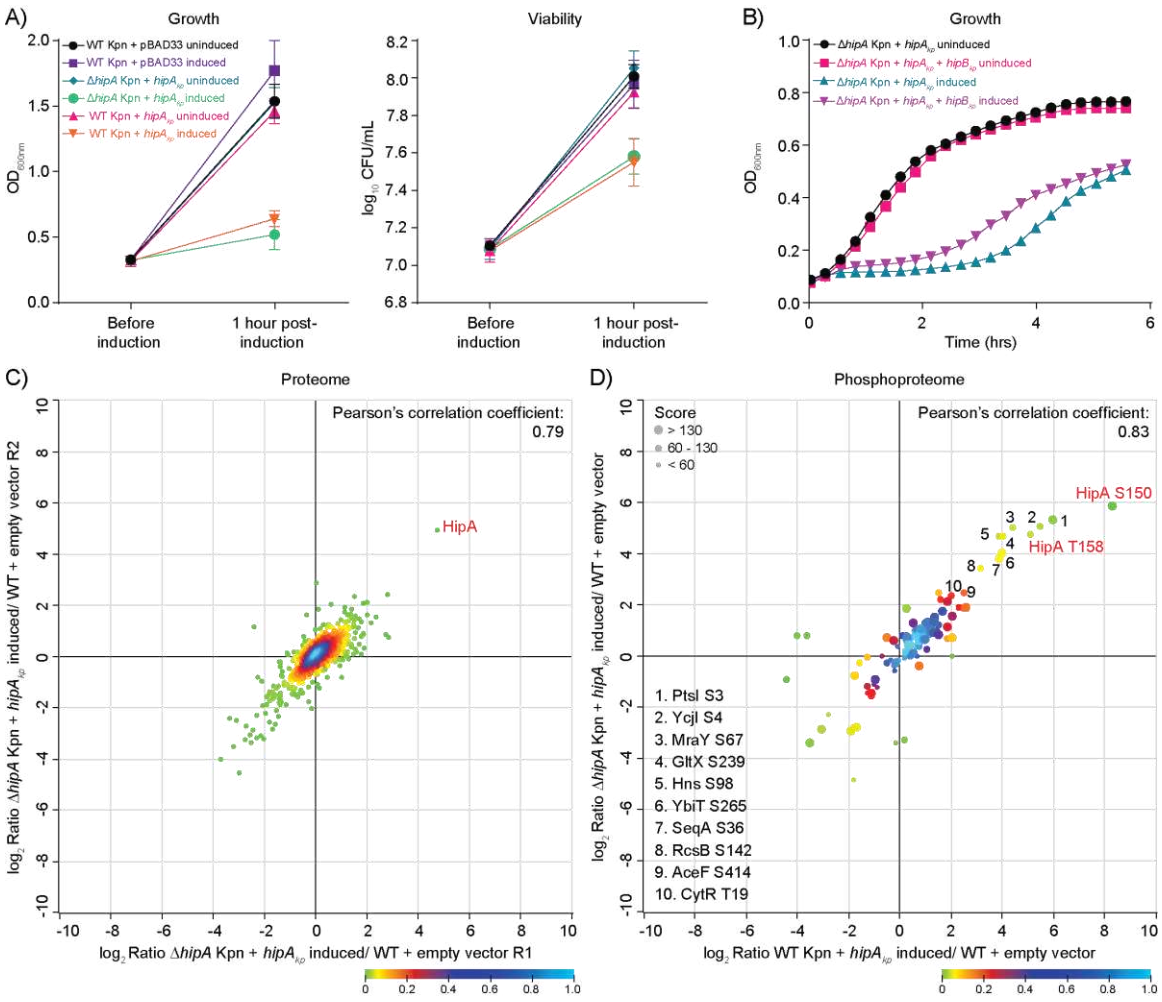

Fig. 3 Effect of overexpression of *hipA*$_{kp}$ in *K. pneumoniae*. A) Growth curves of WT *K. pneumoniae* harboring the empty pBAD33 plasmid and pBAD33::*hipA*$_{kp}$ and Δ*hipA* containing pBAD33::*hipA*$_{kp}$ with expression under the control of arabinose-inducible promoter. The strains were grown in LB Lennox and induced with 0.2% arabinose at OD_{600nm} 0.3 for 1 h and growth was followed by optical density at OD_{600nm} and CFU for viability on plate. The plots are representative of mean values ± SD of three independent biological replicates. Samples were harvested at 1 h post-induction for proteome and phosphoproteome analysis. **B)** Growth curves of Δ*hipA K. pneumoniae* carrying pBAD33::*hipA*$_{kp}$ and pGOOD::*hipB*$_{kp}$ in which expression of *hipA*$_{kp}$ and *hipB*$_{kp}$ is under the control of arabinose-inducible and IPTG-inducible promoters, respectively. Cultures were started at 0.05 OD_{600nm} and grown till OD_{600nm} of 0.3 and induced with 0.2% arabinose and 1 mM IPTG. Uninduced conditions served as controls. The growth was followed via optical density for approximately 5 h in a plate reader. Mean values ± SD of three independent experiments are shown. **C)** The following strains were compared quantitatively by chemical labeling: WT with empty vector (labeled "Light"), WT with *hipA*$_{kp}$- expressing plasmid (labeled "Medium") and Δ*hipA* with *hipA*$_{kp}$- expressing plasmid (labeled "Heavy"). Quantified proteins represented as log_2 ratio between Δ*hipA K. pneumoniae* pBAD33::*hipA*$_{kp}$ and WT empty vector with good correlation between two independent replicates, showing significant increase in $HipA_{kp}$ levels, marked in red. **D)** Distribution of quantified phosphorylation sites upon *hipA*$_{kp}$ overexpression in WT and Δ*hipA* background, based on log_2 ratio between WT *K. pneumoniae* pBAD33::*hipA*$_{kp}$ and WT empty vector vs Δ*hipA K. pneumoniae* pBAD33::*hipA*$_{kp}$ and WT empty

vector showed good correlation between these two backgrounds. The phosphorylation sites changing at least four-fold in phosphorylation upon *hipA*$_{kp}$ overexpression have been numbered and listed here.

1.5 HipA$_{kp}$ phosphorylates itself, GltX and additional substrates in *K. pneumoniae*

To investigate *in vivo* HipA$_{kp}$ activity and identify its potential targets in *K. pneumoniae*, we used a quantitative phosphoproteomics approach. We induced expression of *hipA*$_{kp}$ from pBAD33 in WT and Δ*hipA K. pneumoniae* in LB medium for 1 h and performed LC-MS/MS analysis. The results revealed a 16-fold increase in HipA$_{kp}$ levels in the Δ*hipA* **(Fig. 3C)** and WT background **(fig. S3B)** as compared to the empty vector **(Dataset S1 Table T3)**. Reproducibility between the proteome and phosphoproteome of three replicates in both WT and Δ*hipA* background with HipA$_{kp}$ overproduction was high **(fig. S3B)**. At the phosphoproteome level, we identified a total of 747 phosphorylation sites, belonging to 417 phosphoproteins **(Dataset S1 Table T4)**. Upon HipA$_{kp}$ overproduction, we reproducibly detected increased autophosphorylation of HipA on S150 and T158 by more than 16-fold, as well as phosphorylation of GltX on S239, also by 16-fold, in both WT and Δ*hipA K. pneumoniae* backgrounds **(Fig. 3D)**. Several additional phosphorylation sites in other proteins were up-regulated compared to bacteria harboring the empty pBAD33 vector, indicating that HipA$_{kp}$ acts on multiple substrates that may play a role in the toxic phenotype **(figs. S3C and S3D)**.

1.6 HipA$_{kp}$ overproduction in *K. pneumoniae* leads to increased tolerance to ciprofloxacin, but not to gentamicin

We next investigated the effect of HipA$_{kp}$ overproduction on growth and survival of *K. pneumoniae* in the presence of gentamicin or ciprofloxacin, antibiotics commonly used in treatments of *K. pneumoniae* infections. We first determined the susceptibility of the *K. pneumoniae* isolate ATCC13883 to gentamicin, an aminoglycoside that inhibits protein synthesis, and found that a concentration above 3 μg/mL led to complete growth inhibition after 24 h of exposure. We then exposed the cells with and without *hipA*$_{kp}$ overexpression to 4 μg/mL gentamicin and did not observe any influence of *hipA*$_{kp}$ on

survival of *K. pneumoniae* cells **(Fig. 4A, fig. S4A)**. These results were in agreement with a previously published antibiotic tolerance test where it was shown that $HipA_{ec}$ conferred protection against several different classes of antibiotics but not against the aminoglycoside tobramycin (13). We next focused on ciprofloxacin, a fluoroquinolone antibiotic that inhibits DNA replication in growing cells. Ciprofloxacin was shown to be effective in the treatment of *K. pneumoniae* infections (26) and was previously used for testing antibiotic tolerance in *E. coli* (27). We determined the susceptibility of the *K. pneumoniae* isolate ATCC13883 against ciprofloxacin and found that concentration above 0.5 µg/mL led to complete growth inhibition after 24 h of exposure **(fig. S4B)**. *K. pneumoniae* WT and Δ*hipA* expressing $hipA_{kp}$ from pBAD33 were exposed to 1 µg/mL ciprofloxacin for 2 h. Bacteria under uninduced conditions and bacteria harboring the empty pBAD33 vector were used as negative controls. The proteome measurement confirmed the overproduction of $HipA_{kp}$ in the induced strains after 2 h of ciprofloxacin treatment. Importantly, only cells expressing $hipA_{kp}$ showed survival after 2 h of ciprofloxacin treatment with mean $\log_{10}$ CFU/ml value of 8. In contrast, the viability of the negative controls was six orders of magnitude lower ($\log_{10}$ CFU/ml value of 2) **(Fig. 4B)**. We therefore conclude that $HipA_{kp}$ has a clear impact on antibiotic tolerance against ciprofloxacin in *K. pneumoniae* under the tested conditions, as also previously observed for $hipA_{ec}$ in *E. coli* (13).

1.7 Phosphoproteome analysis reveals potential $HipA_{kp}$ substrates in ciprofloxacin-treated *K. pneumoniae*

In order to detect the $hipA_{kp}$ targets potentially involved in the antibiotic survival, we overexpressed $hipA_{kp}$ in Δ*hipA K. pneumoniae* strain, treated the culture with ciprofloxacin for 2 h and compared the phosphoproteome results with uninduced and empty vector controls. At the proteome level, we identified a total of 1,889 proteins and confirmed $HipA_{kp}$ overproduction upon induction **(Fig. 4C, fig. S4C, Dataset S1 Table T5)**. It should be noted that we also observed a slight increase in $HipA_{kp}$ levels in the uninduced cells, indicating leaky expression of $hipA_{kp}$ from the pBAD33 plasmid without induction by arabinose and absence of glucose **(fig. S4D, Dataset S1 Table T5)**.

At the phosphoproteome level, we identified 547 phosphorylation sites that showed a high correlation between biological replicates **(Fig. 4D, Dataset S1 Table T6)**. After 2 h of ciprofloxacin treatment we observed a similar set of phosphorylation sites upregulated in *hipA*$_{kp}$ overexpressing cells, including the autophosphorylation and phosphorylation of GltX at S239, as compared to untreated *hipA*$_{kp}$ overexpressing cells **(Fig. 4D, figs. S4E and S4F, Dataset S1 Table T5)**. These results indicate that overproduction of HipA$_{kp}$ induced tolerance to ciprofloxacin by phosphorylating target proteins. All the putative phosphorylation sites of HipA$_{kp}$ have been listed in **Table T4** with the frequency of their occurrence to be more than four-fold increased or only identified upon *hipA*$_{kp}$ overexpression **(Datasheet S1 Tables T4, T6 and T8)**.

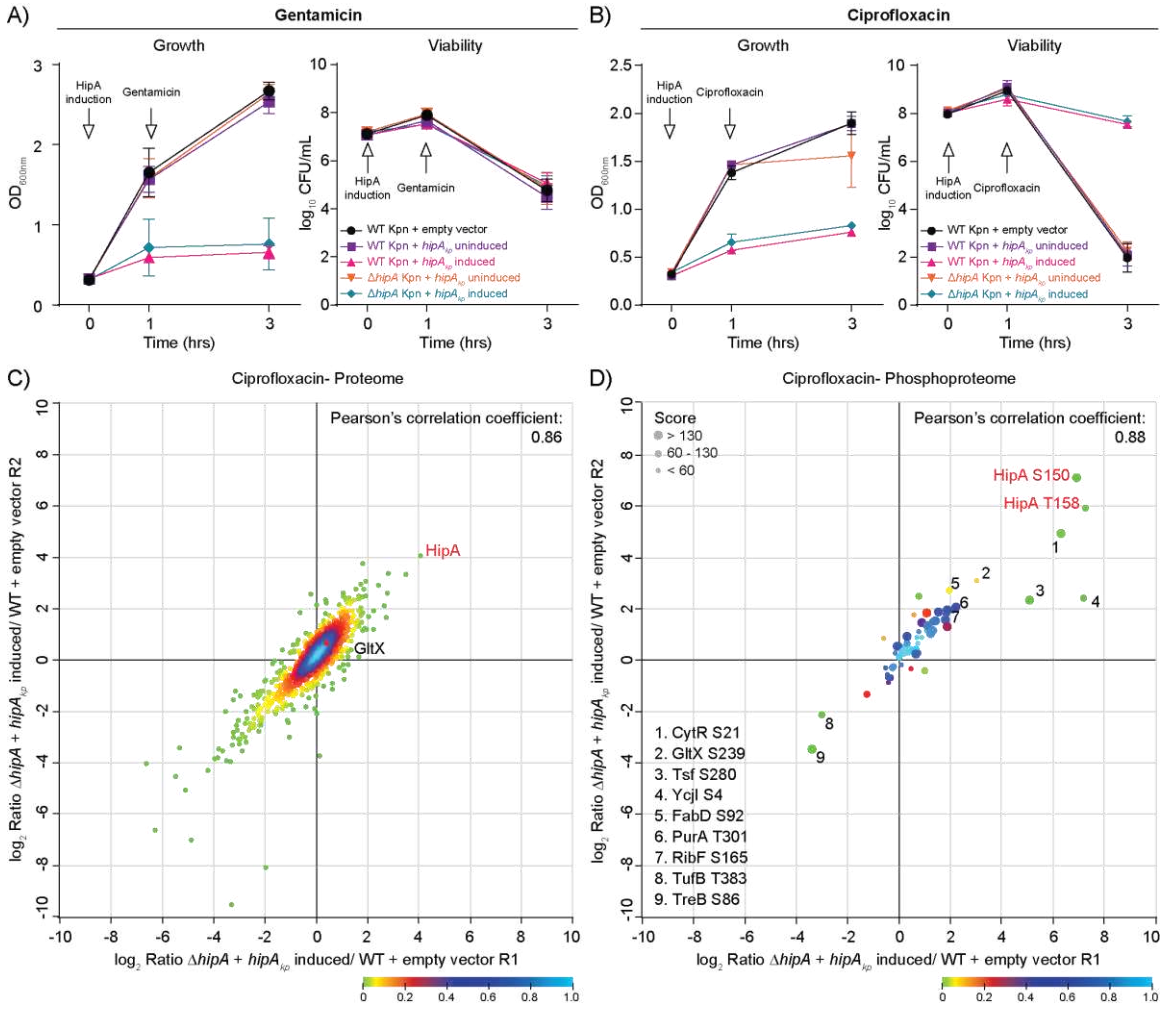

Fig. 4 Effect of over-expression of *hipA*$_{kp}$ on antibiotic tolerance in *K. pneumoniae*. A) Growth curve of WT and Δ*hipA K. pneumoniae* strains transformed with pBAD33 and pBAD33::*hipA*$_{kp}$, respectively in which *hipA*$_{kp}$ expression was driven by the arabinose-inducible

promoter. Strains were grown in LB Lennox medium and expression was induced at OD_{600nm} of 0.3 for 1 h followed by treatment with 4 µg/mL gentamicin for 2 h. Growth was followed via optical density and viability by measuring colony forming units. **B)** Growth curve of *K. pneumoniae* WT and Δ*hipA* strains transformed with pBAD33 and pBAD33::$hipA_{kp}$ with $hipA_{kp}$ expression driven by the arabinose-inducible promoter. Strains were grown in LB Lennox medium and expression was induced at OD_{600nm} of 0.3 for 1 h followed by treatment with 1 µg/mL ciprofloxacin for 2 h. Growth was followed via optical density and viability by measuring colony forming units. The plots are representative of mean values ± SD of three independent biological replicates. **C)** The three strains were labeled as: WT with empty vector ("Light"), Δ*hipA* with $hipA_{kp}$- expressing plasmid uninduced ("Medium") and Δ*hipA* with $hipA_{kp}$- expressing plasmid induced ("Heavy"). Quantified proteins after 2 h of ciprofloxacin treatment represented as log_2 ratio between Δ*hipA K. pneumoniae* pBAD33::$hipA_{kp}$ and WT empty vector strain with good correlation between two independent replicates, showing significant up-regulation of $HipA_{kp}$ as marked in red. **D)** Distribution of quantified phosphorylation sites after 2 h of ciprofloxacin treatment upon $hipA_{kp}$ overexpression, based on log_2 ratio between the two independent replicates of Δ*hipA K. pneumoniae* pBAD33::$hipA_{kp}$ and WT empty vector shows good correlation. The phosphorylation sites changing at least four-fold in phosphorylation upon $hipA_{kp}$ overexpression and ciprofloxacin treatment have been highlighted and listed here.

1.8 *K. pneumoniae* phosphoproteome reveals numerous pathways that are potentially regulated at the post-translational level

Our study provided the most comprehensive phosphoproteome dataset for K. pneumoniae so far (28-31), containing a total of 1439 phosphorylation sites from 741 proteins and a total of 2128 proteins from all experiments **(Table S3 and S4, Dataset S1 Tables T9 and T10)**. 37% phosphoproteins and 27% phosphopeptides occurred in multiple sets of independent experiments **(Fig. 5A and 5B)**. Further analysis revealed the distribution of phosphorylated serine, threonine and tyrosine was 46.2%, 39.7% and 14.0%, respectively **(Fig. 5C)** Functional enrichment analysis performed on all identified phosphoproteins revealed the cellular processes potentially regulated by phosphorylation **(Fig. 5D, Dataset S1 Table T11)**. Phosphoproteins were distributed across numerous cellular functions, with a significant proportion implicated in translation and RNA-binding. Additionally, many were associated with glycolysis, purine and pyrimidine biosynthesis and DNA repair. The comparison of all previously published *K. pneumoniae* phosphoproteomics datasets (28-30) with our combined dataset **(Dataset S1 Table T9)** revealed a large number of novel phosphoproteins and phosphopeptides that were previously unreported **(Fig. 5E and 5F)**. This dataset will serve as a valuable

resource for researchers interested in studying protein phosphorylation in *K. pneumoniae*.

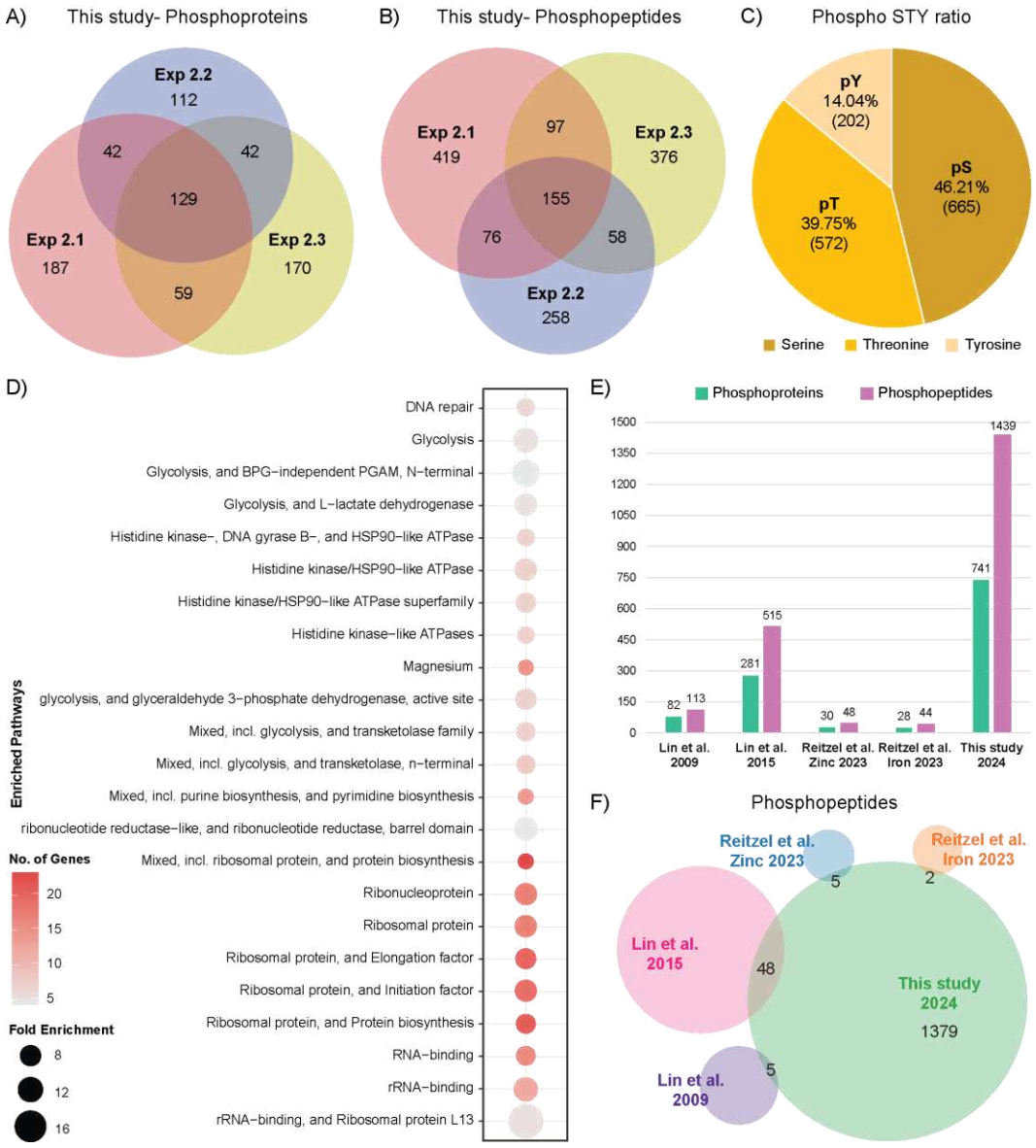

Fig. 5 Overview of the *K. pneumoniae* phosphoproteome datasets. A) and **B)** Venn diagram comparing the three phosphoproteome datasets of *K. pneumoniae* obtained in our study showing the overlap between phosphoproteins (A) and phosphopeptides (B) between them. **C)** Distribution of all phosphorylated serine (pS), threonine (pT) and tyrosine (pY) identified in the combined dataset from three experiments, showing the number of phosphorylation sites of each amino acid in bracket. **D)** Functional enrichment of phosphorylated proteins showing the fold enrichment and number of proteins phosphorylated in that pathway. **E)** Comparison of all previously published phosphoproteome datasets for *K. pneumoniae* with our dataset for the number of phosphoproteins and phosphopeptides identified. **F)** Analysis of the overlap between the number of phosphopeptides identified in *K. pneumoniae* in our study and those in published *K. pneumoniae* phosphoproteome (28-31).

Discussion

K. pneumoniae is a leading cause of nosocomial infections able to cause invasive infections and outbreaks in hospitals (32-34). A particular threat to human health is the emergence of carbapenem resistant strains that are associated with a high mortality rate and limited therapeutic options (35). Moreover, there are increasing reports of carbapenem resistant hypervirulent strains of *K. pneumoniae* (36-38). Protein post-translational modifications (PTMs) play a vital role in regulating the function of various cellular processes, which can either lead to the activation or inactivation of the protein activity (39). Protein phosphorylation is one of the major PTMs that provides a universal mechanism to regulate a large variety of process and several recent quantitative phosphoproteomics studies have focused on the molecular function of Ser/Thr kinases, such has HipA, HipA7 and YjjJ (HipH) in *E. coli* (19, 40). Due to the limited number of studies addressing antibiotic tolerance of *K. pneumoniae* at the molecular level, we investigated the phosphoproteome of *K. pneumoniae* cells after the overproduction of the kinase HipA. We hypothesized that the *hipB/A* operon from *K. pneumoniae* (*hipB/A*$_{kp}$) has similar functions to the well-characterized *hipB/A* operon from *E. coli* (*hipB/A*$_{ec}$), which is implicated in antibiotic tolerance and persistence. Although the primary sequence identity was lower than 70%, structural regions and residues essential for HipA kinase activity were conserved in both organisms. In addition, alignment of predicted and experimentally determined 3D-structures revealed a high level of conservation of the overall structure with a low RMSD value of 0.4 Å (41).

Using MS-based proteomics, we first showed that overexpression of *hipA*$_{kp}$ in *E. coli* led to the inhibition of growth, which could be restored upon simultaneous *hipB*$_{kp}$ induction. These experiments indicated the *in vivo* kinase activity of the HipA$_{kp}$ and its interplay with HipB$_{kp}$. Phosphoproteome analysis upon *hipA*$_{kp}$ induction in *E. coli* showed a variety of potential substrates of HipA$_{kp}$ including the well-known target of *hipA*$_{ec}$, GltX at S239. Since *K. pneumoniae* and *E. coli* have different genetic backgrounds, we expected different HipA substrate pools in the two organisms. Therefore, we next analyzed HipA$_{kp}$ activity in *K. pneumoniae*. Upon deletion of *hipA*$_{kp}$ in *K. pneumoniae* (Δ*hipA*) we observed no significant difference in growth and viability in comparison with the WT,

indicating that *hipA*$_{kp}$ is not an essential gene in the exponential phase, although we observed some reduction in viability in the late stationary phase which might suggest its role in stationary phase or non-growing cells. We performed further experiments in WT and Δ*hipA* background to rule out the possibility of any potential effect of native *hipA* gene on the phosphoproteome. As expected, overexpression of *hipA*$_{kp}$ in both WT and Δ*hipA Klebsiella* background was toxic to the cells and this could be partially rescued with *hipB*$_{kp}$ overexpression. In *E. coli* with *hipA*$_{kp}$ overexpression, we observed almost complete complementation with overproduction of HipB$_{kp}$ but in *Klebsiella*, the complementation was only partial. The reason for this is at present unclear, however we note that overexpression of *hipA*$_{kp}$ and *hipB*$_{kp}$ in *E. coli* point to a canonical toxin/antitoxin pair.

Phosphoproteomics analysis upon *hipA*$_{kp}$ induction in *K. pneumoniae* showed a total of 63 common phosphoproteins between *E. coli* and *K. pneumoniae* datasets. Among them was GltX, which appears to be a prominent target in both organisms. Several additional proteins were detected as potential targets of HipA$_{kp}$, most of them associated with essential biological processes. In our *K. pneumoniae* phosphoproteomics datasets, we observed 34 putative HipA$_{kp}$ substrates to be either exclusively phosphorylated upon *hipA*$_{kp}$ overexpression or more than four-fold increased in this condition, including *hipA*, *gltX*, *rcsB*, *tsf*, *ybiT* and *ycjI* **(Table S5)**. These sites should be prioritized as the most likely HipA$_{kp}$ targets for future biological follow-up experiments. A majority of these substrates are phosphorylated at either N- or C-termini in the regions that binds DNA or RNA or other proteins, hinting towards the function of these phosphorylation events in modulating processes dependent on protein/protein or protein/nucleic acid interactions **(fig. S5)**. For example, SeqA phosphorylation at S36 and S46 occurs in N-terminal region, essential for self-association (42), Tig phosphorylation at S4 is present in the N-terminal ribosome-binding region (43) and CueR phosphorylation at S4 is located in the N-terminal DNA-binding region of the protein (44). Conversely, proteins RbfA, BipA, FtsK, Hns, Rne, RpsA and Tsf are phosphorylated close to their C-termini. RbfA phosphorylation at S110 is in the region required for stable 30S ribosomal association *in vitro* and efficient 16S rRNA processing (45). BipA phosphorylation at S490 is in the region that binds to the A-site of tRNA in *E. coli* (46, 47), FtsK phosphorylation at S1373

is in the region essentially involved in chromosome segregation (48), whereas Hns at S98 in the DNA-binding region (49).

Interestingly, several of the observed phosphoproteins were previously reported to be phosphorylated or involved in phage infection. The ribonuclease E Rne, is a component of the RNA degradosome interacting with proteins such as RhlB helicase, enolase and PNPase via its C-terminal RNA-binding domain (50). Rne has been shown to be phosphorylated by the T7 phage kinase gp-0.7 (PK) to inhibit its activity upon phage infection (51). Similarly, small ribosomal subunit protein S1 RpsA, is also known to be phosphorylated by PK to enhance phage protein production (52). The elongation factor-Ts (Tsf), along with elongation factor-Tu (Tuf) and RpsA, form a complex and be part of the host-provided phage Qbeta RNA polymerase complex (53). The phosphorylation of a similar set of proteins by *hipA* and T7 phage kinase 0.7 suggests a potential link between these kinases, requiring further investigation.

The role of wild type and kinase-dead variants of $HipA_{ec}$ in tolerance has been studied against many antibiotics, resulting in no or limited tolerance in the absence of HipA activity against ofloxacin, mitomycin C and cefotaxime but not against tobramycin (13). Antibiotic tolerance observed in the *K. pneumoniae* strains overexpressing $hipA_{kp}$ seemed to be also specific to certain classes of antibiotics. We observed that *K. pneumoniae* cells overexpressing $hipA_{kp}$ showed increased survival after treatment with ciprofloxacin, but not against gentamicin. Although this is in agreement with earlier results from $hipA_{ec}$ (13), the reason for this is currently unclear. It is conceivable that cell growth inhibition due to overproduced $HipA_{kp}$ can provide the survival benefit during treatment with ciprofloxacin, which acts on dividing cells and inhibits their cell cycle. Gentamicin, on the other hand, inhibits protein synthesis by binding to 30S ribosomes. As already reported for $hipA_{ec}$, persistent cells have a basal level of protein synthesis which is potentially essential for their survival (27). Therefore, complete inhibition of the protein synthesis by gentamicin can lead to the killing of the cells expressing $hipA_{kp}$. However, further experiments are needed to address this. More than half of the phosphorylation sites obtained in ciprofloxacin-treated $hipA_{kp}$-overexpressing *K. pneumoniae* cells were identical with the phosphorylation sites in $hipA_{kp}$-overexpressing

K. pneumoniae cells in absence of antibiotic. This revealed that the tolerance mechanism is likely based on GltX-mediated activation of the stringent response, although many of the above-mentioned substrates also act on other levels of cellular processes to ensure survival.

Finally, our study provides a basis for the comparison of the molecular phenotype of the ciprofloxacin treatment in *E. coli* and *K. pneumoniae*. Among 821 phosphoproteins detected in a recent study of ciprofloxacin-treated *E. coli* cells (54), 100 phosphoproteins were also detected in our ciprofloxacin-treated $hipA_{kp}$-overexpressing *K. pneumoniae* cells. This indicates that numerous proteins are phosphorylated in both organisms in response to ciprofloxacin treatment. Autophosphorylation on $HipA_{ec}$ at S150 was up-regulated during ciprofloxacin treatment in *E. coli* cells even without any overproduction of $HipA_{ec}$ indicating that ciprofloxacin-treatment promotes the activity of this protein in *E. coli*. This also implies that this site may have a role in the regulation of kinase activity during antibiotic treatment (54). Combined, our results provide a rare insight into molecular mechanisms of post-translational regulation of antibiotic tolerance in *K. pneumoniae* and provide a resource for further studies on this important human pathogen.

Materials and Methods

1. Bacterial strains and plasmids

All strains, primers and plasmids used in this work are listed in the table below **(Table S1, S2)**. Due to the high homology of $hipA_{kp}$ with $hipA_{ec}$, the $hipA_{kp}$ gene was cloned with the same Shine-Dalgarno sequence containing the alternative starting codon GTG as used in previous work (19). $hipA_{kp}$ and $hipB_{kp}$ genes were amplified from the *Klebsiella pneumoniae* subsp. *pneumoniae* reference strain ATCC13883 with primers HipA.kpn.SD8.GTG.pBAD33-for and HipA.kpn.pBAD33-rev, and hipBkp.pGOOD-for and hipBkp.pGOOD-rev, respectively. The pBAD33 vector and pGOOD vector were digested with *Xba*I and *Bgl*II restriction enzymes, respectively and finally pBAD33 was ligated with $hipA_{kp}$ and pGOOD with $hipB_{kp}$ amplified PCR product using Gibson

assembly mix (55). The resulting plasmids were transformed into Top10 *E. coli* competent cells and confirmed by PCR for the presence of the gene of interest and sequenced before transforming them into final working strains in both *E. coli* and *K. pneumoniae*.

Generation of *K. pneumoniae* Δ*hipA* mutant

A markerless in-frame deletion of *hipA* was generated by amplifying approximately 600 bp up- and down-stream of *hipA*. PCR products were fused with SOE-PCR and cloned with In-Fusion cloning (TakaraBio) into the suicide vector pKNOCK-Km, a gift from Mikhail Alexeyev (Addgene #46262). The *sacB* gene including its promoter was amplified from the plasmid pEXG2 and cloned into pKNOCK-Km to introduce a counter selection marker. Plasmid inserts were verified by Sanger sequencing. The resulting plasmids were transferred into *E. coli* S17λ*pir* for the transformation of *K. pneumoniae* ATCC13883 by conjugation. *K. pneumoniae* merodiploids were selected on LB agar plates supplemented with 100 µg/ml kanamycin, streaked for single colony isolation and then incubated in LB without selection overnight. Counter selection was performed with 15% sucrose, and kanamycin sensitive colonies were tested for the deletion of *hipA* by PCR.

2. Bioinformatic analysis

The sequence of $HipA_{kp}$ from *Klebsiella pneumoniae subsp. pneumoniae* ATCC13883 was analyzed for its identity within *Klebsiella* genus and other organisms using protein BLAST at the NCBI server (https://blast.ncbi.nlm.nih.gov/Blast.cgi). For the initial pBLAST search, the search was limited to Klebsiella (taxid:570) as the organism and 1,000 maximum target sequences in the algorithm parameters. Percent identity and number of hits per species and subspecies were extracted from the pBLAST result. For the analysis of $HipA_{kp}$ identity across all organism without limiting the search to Klebsiella, we performed the pBLAST search for top 5,000 hits and plotted the results. Both the graphs were generated using the online tool, Shiny BoxPlotR (http://shiny.chemgrid.org/boxplotr/). The pairwise sequence alignment between $HipA_{kp}$ and HiA_{ec}, or $HipB_{kp}$ and $HipB_{ec}$ proteins was performed with EMBOSS Needle (56) using the default settings.

3. Growth Experiments

Growth of WT *E. coli* cells overexpressing *hipA$_{kp}$*

Overnight pre-cultures of WT *E. coli* MG1655, containing pBAD33 empty vector and pBAD33::*hipA$_{kp}$*, were prepared in liquid medium (Luria-Bertani medium from Roth) supplemented with 0.4% (w/v) glucose, 25 µg/mL chloramphenicol for the maintenance of pBAD33 plasmid. The next day cultures were started at an OD_{600nm} of 0.08 and induced with 0.2% arabinose for pBAD33 plasmid upon reaching an OD_{600} of 0.3 for 1 h and harvested afterwards for (phospho)proteome analysis. The OD_{600nm} and number of CFU were measured and calculated before and after 1 h of induction. The experiment was performed in 3 biological replicates and results were visualized using GraphPad Prism 8.0.1.

Growth of WT *E. coli* cells overexpressing *hipA$_{kp}$ and hipB$_{kp}$*

Overnight pre-cultures of WT *E. coli* MG1655, containing only pBAD33::*hipA$_{kp}$*, and both pBAD33::*hipA$_{kp}$* + pGOOD::*hipB$_{kp}$* were prepared in liquid medium (Luria-Bertani medium from Roth) supplemented with 0.4% (w/v) glucose along with 25 µg/mL chloramphenicol and 10 µg/ml tetracycline for the maintenance of pBAD33 and pGOOD plasmid, respectively. The following day, cultures were initiated at a starting OD_{600} of 0.08 with the control samples left uninduced and the others were induced with 0.2% arabinose for pBAD33 plasmid and 1 mM IPTG for pGOOD plasmid in a 24-well plate (Greiner) and incubated at 37°C and 300 rpm in a plate reader (Tecan). Three biological replicates were performed.

Growth and survival of *K. pneumoniae* Δ*hipA*

LB Lennox was inoculated to an OD_{600nm} of 0.05 with overnight cultures of *K. pneumoniae* wild type and Δ*hipA*. A 1 mL aliquot of the cultures was transferred to a 24-well plate (Greiner) and incubated at 37°C and 300 rpm in a plate reader (Tecan). The OD_{600nm} was measured every 30 mins for 24 h with four reads per well and the medium blank value was subtracted from the experimental values. Three independent experiments in triplicate were performed.

Growth and survival of *K. pneumoniae* overexpressing *hipA*

LB Lennox supplemented with 0.4% glucose and 50 µg/ml chloramphenicol was inoculated with *K. pneumoniae* wild type pBAD33, wild type pBAD33::$hipA_{kp}$ and Δ*hipA* pBAD33::$hipA_{kp}$ and incubated overnight. The next day, 250 ml LB Lennox was inoculated for each strain to an OD_{600nm} of 0.05 and incubated until an OD_{600nm} of approximately 0.3 was reached. Aliquots were taken to determine the number of CFU/mL by plating serial dilutions. Each culture was split into two. One fraction was induced with 0.2% arabinose and the other one was left uninduced. At 1 and 2 h post-induction, the OD_{600nm} and CFU/mL was determined. Three independent experiments were performed.

Growth of *K. pneumoniae* overexpressing *hipA* and *hipB*

K. pneumoniae Δ*hipA* harboring pBAD33::$hipA_{kp}$ alone or together with pGOOD::$hipB_{kp}$ were grown overnight in LB Lennox supplemented with 0.4% glucose and where necessary with 50 µg/ml chloramphenicol and 10 µg/ml tetracycline. The bacteria were used to start cultures at an OD_{600nm} of 0.05 in LB Lennox without supplements and grown to early exponential phase. The OD_{600nm} was adjusted to 0.3 and two fractions per strain were prepared, one for inducing conditions and the other one was left uninduced. Expression of $hipA_{kp}$ and $hipB_{kp}$ was induced with 0.2% arabinose and 1 mM IPTG, respectively. 1 ml of each culture was added to a 24-well plate (Greiner) and the OD_{600} was recorded every 15 mins for 5.5 h at 37°C and 300 rpm in a plate reader (Tecan). The average blank absorbance was subtracted from the sample values. Three independent experiments were performed in triplicate.

4. Antibiotic tolerance test of *K. pneumoniae* overexpressing $hipA_{kp}$

Gentamicin and Ciprofloxacin sensitivity of *K. pneumoniae* ATCC13883

Antibiotic resistance of the wild type *K. pneumoniae* ATCC13883 was tested by inoculating 2 mL LB Lennox supplemented with gentamicin (Sigma Aldrich) at concentrations ranging from 0 to 4 µg/ml and ciprofloxacin (Sigma Aldrich) at

concentrations ranging from 0 to 5 µg/ml to an OD_{600nm} of 0.05. The cultures were incubated at 200 rpm and 37°C for 24 h and the OD_{600nm} was measured.

Gentamicin and Ciprofloxacin tolerance test of *K. pneumoniae* with *hipA$_{kp}$* overexpression

K. pneumoniae wild type pBAD33, WT pBAD33::*hipA$_{kp}$* and Δ*hipA* pBAD33::*hipA$_{kp}$* were grown overnight in LB Lennox supplemented with 0.4% glucose and 50 µg/ml chloramphenicol. 200 mL LB Lennox was inoculated with the overnight cultures to an initial OD_{600nm} of 0.05 and incubated until an OD_{600nm} of approximately 0.3 was reached. Each culture was split into two subcultures, one was treated with 0.2% arabinose and the other one was left untreated. Following arabinose induction for 1 h, 4 µg/ml of gentamicin or 1 µg/ml ciprofloxacin was added. Immediately before induction, at 1 h post-induction and 2 h post-antibiotic treatment, the absorbance and colony forming units were determined. Three independent experiments were performed. Graphs were generated using GraphPad Prism 8.0.15.

5. Cell lysis and protein precipitation

Harvested cells were centrifuged at 4,000 g and the pellet was stored at -80°C. The pellet was then resuspended in an SDS lysis buffer containing 40 mg/ml SDS (sodium dodecyl sulfate), 100 mM Tris-HCl pH 8.6, 10 mM EDTA, 5 mM glycerol-2-phosphate, 5 mM sodium fluoride, 1 mM sodium orthovanadate and 1 tablet of complete protease inhibitors (Roche). The cell lysate was sonicated at 40% amplitude for 30 sec cycle at least five times or until a transparent, non-viscous lysate was obtained. The cell debris was pelleted by centrifugation at 13,000 g for 30 mins and the supernatant was collected for protein precipitation using methanol and chloroform method. The obtained protein pellet was air-dried and dissolved in denaturation buffer (6 M urea, 2 M thiourea and 10 mM Tris pH 8.0). The protein concentration was determined by using standard Bradford assay (Bio-Rad).

6. Protein in-solution digestion

For each phosphoproteomics experiment, 3-6 mg protein per sample (strain/condition) was used. Briefly, precipitated proteins were reduced by using 1 mM dithiothreitol (DTT)

for 1 h and then alkylated using 5.5 mM iodoacetamide (IAA) for an additional 1 h in the dark with constant shaking at 700 rpm. Half of the protein from each sample was diluted with four times volume of 62.5 mM Tris pH 8.0 and 12.5 mM $CaCl_2$ and digested with the enzyme chymotrypsin (1:100 w/w) overnight at room temperature (RT) in a shaker. The other half of the protein was pre-digested with the endoproteinase LysC (1:100 w/w) for 3 h and then diluted with four times volume of milli-Q water, adjusted to a pH higher than 8.0 and supplemented with the enzyme LysC (1:100 w/w) (for *E. coli* samples) and trypsin (1:100 w/w) (for *K. pneumoniae* samples) for overnight digestion at RT and shaking. The reaction was then stopped by acidification with trifluoroacetic acid (TFA) to pH 2.0 and centrifuged to get rid of precipitates.

7. Solid phase extraction and Dimethyl labeling

Acidified peptides were then purified by solid phase extraction on Sep-Pak C18 cartridges (Waters, Milford, MA) and labeled using triplex stable isotope dimethyl labeling as previously described (57). Briefly, C18 columns were activated with methanol and equilibrated with Solvent A* [2% (v/v) acetonitrile (AcN) and 1% (v/v) formic acid (FA)]. The digested and acidified peptide samples were loaded and later, the column was washed with HPLC Solvent A [0.1% (v/v) FA]. These samples were then labeled with 2.5 ml of the respective labeling solutions: CH_2O (Sigma-Aldrich) and $NaBH_3CN$ (Fluka) for Light label, and CD_2O (Sigma-Aldrich) and $NaBH_3CN$ for Medium label, and $C_{13}D_2O$ (Sigma-Aldrich) and $NaBD_3CN$ (96% D, Isotec) for Heavy label. The labeling solutions were flushed with approximately 10-15 mins contact time through with the column. Labeled peptides were washed again with HPLC Solvent A on the column and eluted with 600 µl HPLC Solvent B [80% (v/v) AcN in 0.5% (v/v) FA].

8. Labeling efficiency and mixing check

For the validation of labeling efficiency and accurate mixing of the labeled peptides, two sets of 5 µg of each eluted labeled sample was used for LC-MS/MS measurements, separately (for labeling efficiency) and mixed in 1:1:1 ratio for a pilot mixing check measurement. Adjustments were made based on the mixing ratios to achieve a target

ratio close to 1 to ensure optimal quantification. The labeling efficiency, for all labels, was >=95%.

9. Phosphopeptide enrichment

Phosphopeptides were enriched by titanium dioxide (TiO_2) beads with a ratio of 1:10 (beads: protein ratio) for five consecutive rounds of enrichment for 10 mins each. After mixing the labeled samples together and taking out an aliquot of 10 µg for proteome analysis, the peptides were acidified. TiO_2 beads were washed with 80% (v/v) AcN and 6% (v/v) TFA and incubated with the samples with constant mixing. The beads with bound phosphopeptides were washed again to remove any unbound or acidified peptides using 80% AcN and 6% TFA. These beads were then loaded onto C8 (Empore) StageTips and further washed with a wash buffer [80% AcN and 1% TFA] and Solvent B [80% AcN and 0.1% FA]. Phosphopeptides were eluted with 30 µl of elution solution I [1.25% (v/v) ammonium hydroxide of pH>10.5 into a tube containing 20 µl of 20% (v/v) TFA. This was followed by 70 µl elution solution II [5% (v/v) ammonium hydroxide in 60% (v/v) AcN (pH>10.5)] and finally with 20 µl of elution solution III [60% (v/v) AcN, 1% (v/v) TFA]. Each elution solution took at least 15 mins, at 1000-1500 rpm to elute. Acetonitrile was evaporated from eluates by vacuum centrifugation and samples were acidified to pH 2.0, and purified by StageTips.

10. Peptide purification by StageTips

Before LC-MS/MS measurements, sample for proteome analysis and eluted phosphopeptides were desalted and purified on C18 StageTips (58). Briefly, reverse-phase chromatography was applied using C18 discs (Empore). The discs were activated with methanol and equilibrated with Solvent A*. The acidified peptides were loaded onto the discs and washed with Solvent A. Peptides were eluted with 50 µl of Solvent B and vacuum centrifuged to evaporate AcN. Final sample volume was adjusted with Solvent A and final 10% (v/v) of Solvent A*.

11. LC-MS/MS measurement

Purified peptides were separated by an online coupled EASY-nLC 1200 system (Thermo Fischer Scientific) to an Orbitrap Exploris 480 spectrometer (Thermo Fischer Scientific) through a nano-electrospray ion source (Thermo Fischer Scientific). Chromatographic separation was performed on a 20 cm long and 75 µm inner diameter analytical column packed in-house with reversed-phase ReproSil-Pur C18-AQ 1.9 µm particles (Dr. Maisch GmbH). Peptides were loaded onto the column at 40°C, with 1 µl/min flow rate under maximum backpressure of 850 bar. Gradient was applied using HPLC Solvent A and 10 to 50% Solvent B at a 200nl/min constant flow rate. Labeling efficiency samples were eluted using 36 mins, mixing check using 60 mins, phosphopeptides using 60 mins and proteome samples using 130 mins or 230 mins gradients. Mass spectrometer was operated in positive ion and data-dependent acquisition mode. The acquisition of all full MS was in the scan range 300-1750 m/z at a resolution of 60k. For proteome measurements, 20 most intense peptides were picked for HCD fragmentation at 15k resolution and for phosphoproteome at 30k resolution. The normalized collision energy was set to 28% and dynamically excluded the mass of sequenced precursors for 30 secs from repeated fragmentation. The ions with single, unassigned or charge higher than six were also excluded from selection for fragmentation.

12. MS data processing with MaxQuant

The acquired raw files were processed using the MaxQuant software (version 2.2.0.0) (59). Raw files from each set of experiment were processed separately in a similar manner **(Table S3)**. In total, we used **130** files of which **110** were files from phosphopeptide enrichment fractions. The obtained peak list was searched using Andromeda search engine integrated in MaxQuant (60) against *E. coli* K-12 MG1655 proteome (Taxonomy ID 83333) (released 30.01.2024, 4416 entries), and *Klebsiella pneumoniae subsp. pneumoniae* MGH78578/ ATCC700721 (Taxonomy ID 272620) (released 10.11.2022, 5127 entries), and common potential contaminants list. All search parameters were kept to default except the ones mentioned here. Labeling was set to three multiplicity, with Light: DimethylLys0 and DimethylNter0, Medium: DimethylLys4 and DimethylNter4 and Heavy: DimethylLys8 and DimethylNter8. Phospho (STY) was

added as a variable modification for phosphopeptide enriched files. Proteome and phosphoproteome files were grouped in separately to only look for Phospho (STY) modification in phospho-files. For Lys-C digestion, Lys-C enzyme was selected with a maximum of two missed cleavages allowed, similarly for trypsin with two missed cleavages allowed and for chymotrypsin five missed cleavages allowed. To increase the number of quantified features, “match between runs” was enabled. Re-quantify was also enabled to allow quantification of dimethyl-labeled pairs. Different experiments were processed separately for individual analysis and also together for the final set of phosphoproteome data.

13. Data analysis with Perseus

For the statistical analysis of MaxQuant output data, we used Perseus software (version 1.6.5.0.) (61) and the figures were edited using Adobe Illustrator. All contaminants, reverse hits and diagnostic peaks were filtered out from the Phospho (STY) table. Phosphorylation site ratios were $\log_2$ transformed and plotted against $\log_{10}$ transformed sum of the intensities of phosphopeptide. Significantly regulated sites were determined by applying a threshold of 2 in $\log_2$ scale (four-fold). Correlation between the two replicates was plotted with the density estimation feature in Perseus and plotted $\log_2$ ratio of two replicates and calculated Pearson’s correlation value. Likewise, for the Protein groups files, contaminants, reverse hits and only identified by sites proteins were filtered. After $\log_2$ transformation of ratios, density estimation was performed. Scatter plots were prepared for the reproducibility between the replicates and Pearson’s correlation was calculated. Functional enrichment analysis of the final phosphoproteome dataset was performed using the online tool ShinyGO 0.77 (http://bioinformatics.sdstate.edu/go/) (62). All Protein IDs from the combined Phospho (STY) table (**Dataset S1 Table T9**) were added to the list and species was selected as “Klebsiella pneumoniae”. Using default values with FDR cut off of 0.05, we performed the enrichment analysis and obtained a table containing results of all enriched pathways, 149 pathways in total **(Dataset S1 Table T11)**. The data was further filtered using MS Excel for the number of genes per pathway ≥4, fold enrichment ≥4 and enrichment FDR

≤0.01. This resulted in 23 pathways that were used for plotting the highly enriched phosphorylated proteins in our dataset **(Fig. 5D)**.

Acknowledgments

We thank Fabio Lino Gratani and Claudia Cavarischia-Rega for the initial inputs for the project, and Libera Lo Presti for critical reading of the manuscript.

Author contributions:

Conceptualization, P.N., S.S. and B.M.; Methodology, P.N., B.M., S.S., I.S., M.A. and C.J.; Investigation, P.N., S.S. and B.M.; Visualization, P.N., S.S. and B.M.; Writing – original draft, P.N., S.S. and B.M.; Writing – review & editing, P.N., S.S., B.M., C.J. and I.M.; Project administration, B.M. and S.S.; Supervision, B.M. and I.M.; Funding acquisition, B.M., S.S. and I.M.

Data and materials availability: The mass spectrometry proteomics data have been deposited to the ProteomeXchange Consortium via the PRIDE (63) partner repository with the dataset identifier PXD051521. All data needed to evaluate the conclusions in this paper are available in the main text or the supplemental information.

Supplementary figures

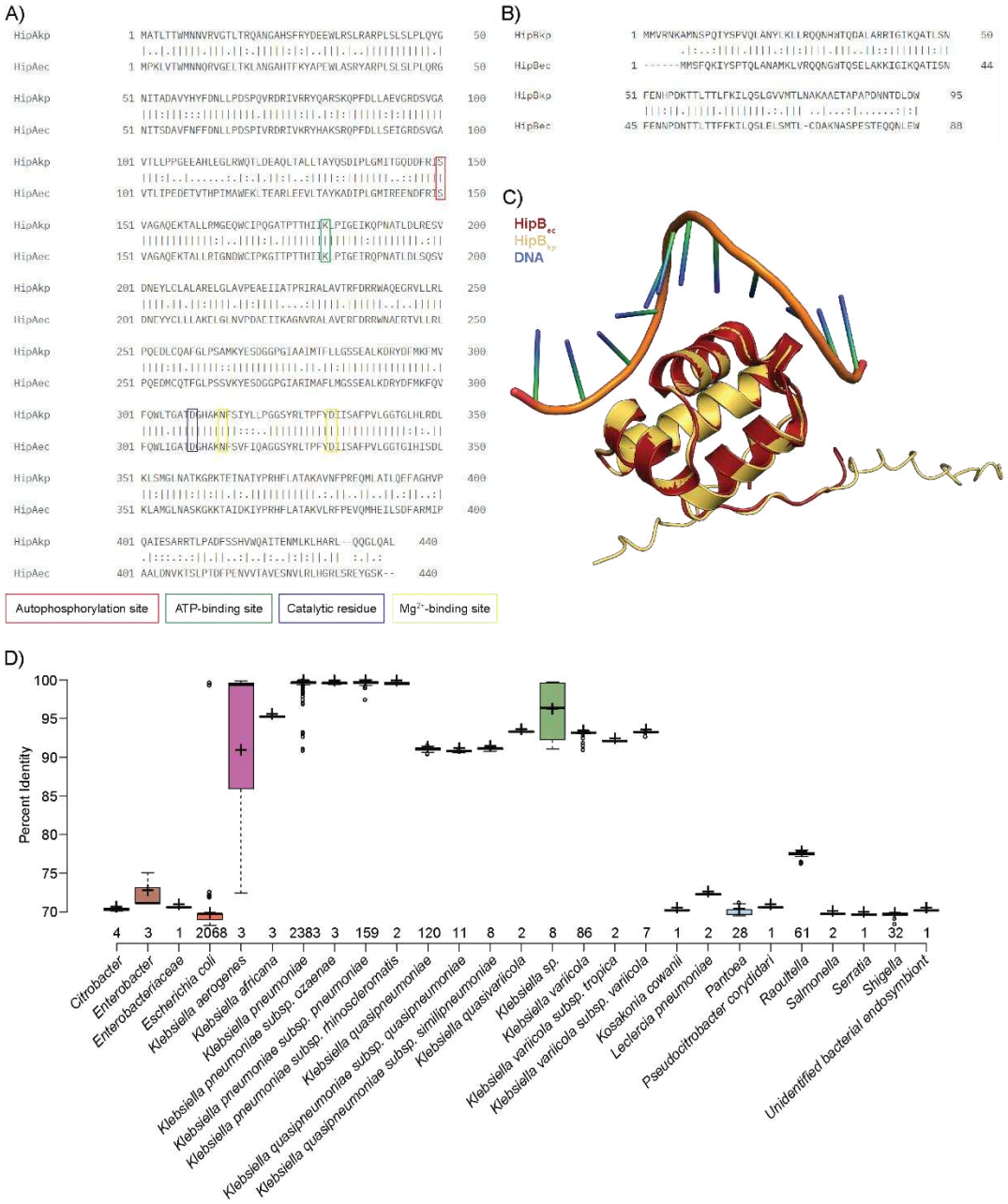

fig. S1 Additional bioinformatic analysis of *hipBA* from *K. pneumoniae*. A) Pairwise sequence alignment of $HipA_{kp}$ and $HipA_{ec}$ protein sequences. The boxes represent the conserved amino acid positions essential for kinase activity. **B)** Pairwise sequence alignment between $HipB_{kp}$ and $HipB_{ec}$ proteins. **C)** Alignment of the AlphaFold predicted structure of $HipB_{kp}$, UniProt ID: A6T947 (yellow), with the experimentally determined structure of $HipB_{ec}$, PDB ID: 3DNV (red), and their positioning with DNA molecule. **D)** Distribution of percentage of sequence identity of $HipA_{kp}$ homologs among different bacteria and the number of hits obtained upon analyzing the top 5,000 results from protein BLAST without limiting the search to any specific organism.

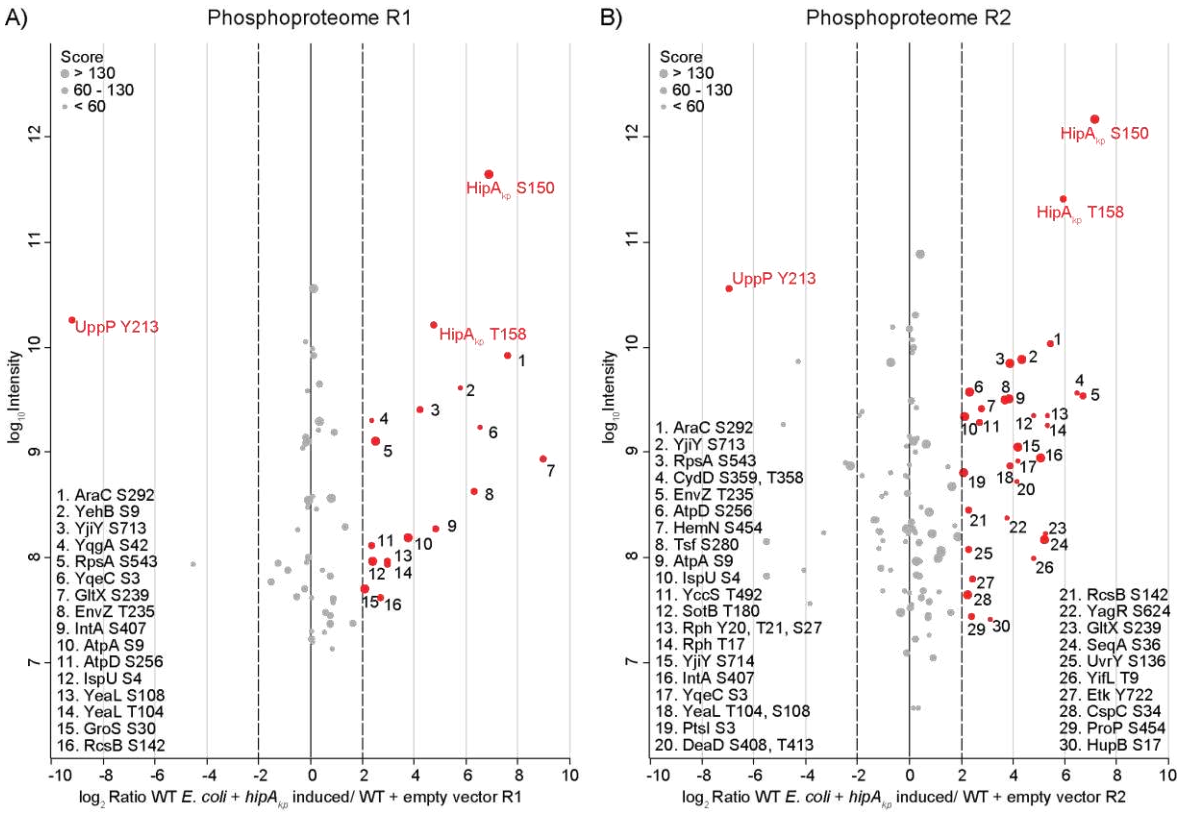

fig. S2 Additional analysis of phosphoproteome data from *hipA$_{kp}$* overexpression in *E. coli*. A) and **B)** Distribution of phosphorylation sites showing $\log_2$ ratio of *hipA$_{kp}$* overexpression in WT *E. coli* with empty vector control for two replicates and the sum of intensities. Phosphorylation sites with at least a four-fold increase in phosphorylation are highlighted in red and listed here.

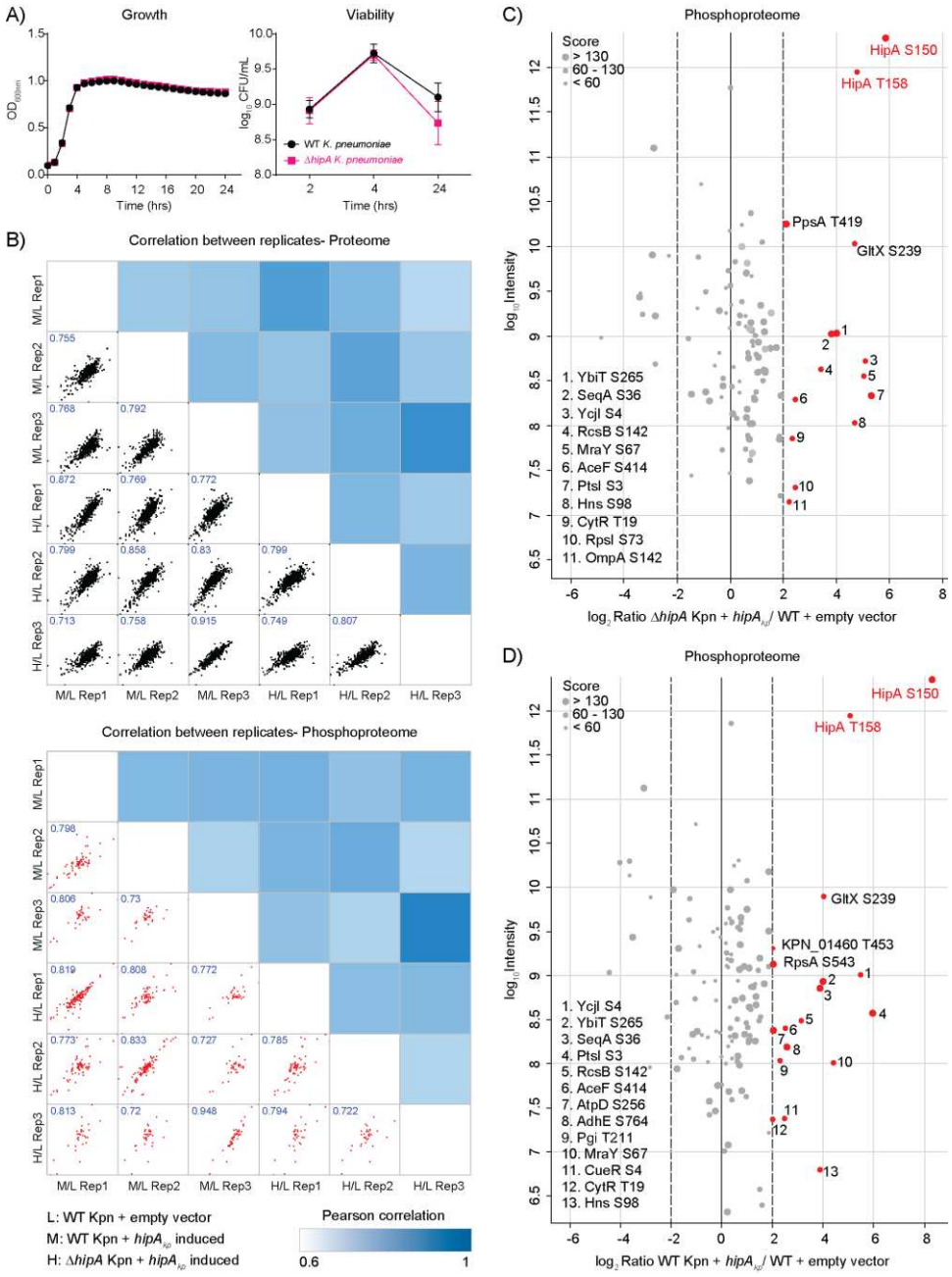

fig. S3 Additional analysis of proteomics and phosphoproteomics data from *hipA$_{kp}$* overexpression in *K. pneumoniae*. A) Growth curves of WT and Δ*hipA K. pneumoniae*. Overnight cultures were diluted to OD_{600nm} of 0.05 and growth was followed by optical density measurements in a plate reader for 24 h. Mean values ± SD of three independent experiments are shown here. **B)** Pearson correlation between the proteome and phosphoproteome, of three independent replicates, based on log_2 ratio values showing high correlation between the replicates and WT and Δ*hipA* backgrounds. L is WT Kpn with pBAD33, M is WT Kpn with pBAD33::*hipA$_{kp}$* induced and H is Δ*hipA* with pBAD33::*hipA$_{kp}$* induced. **C)** and **D)** Distribution of phosphorylation sites showing log_2 ratio of *hipA$_{kp}$* overexpression in Δ*hipA* **(C)** and WT **(D)** *K. pneumoniae* with empty vector control. Phosphorylation sites with at least a four-fold increase in phosphorylation are highlighted in red and listed here.

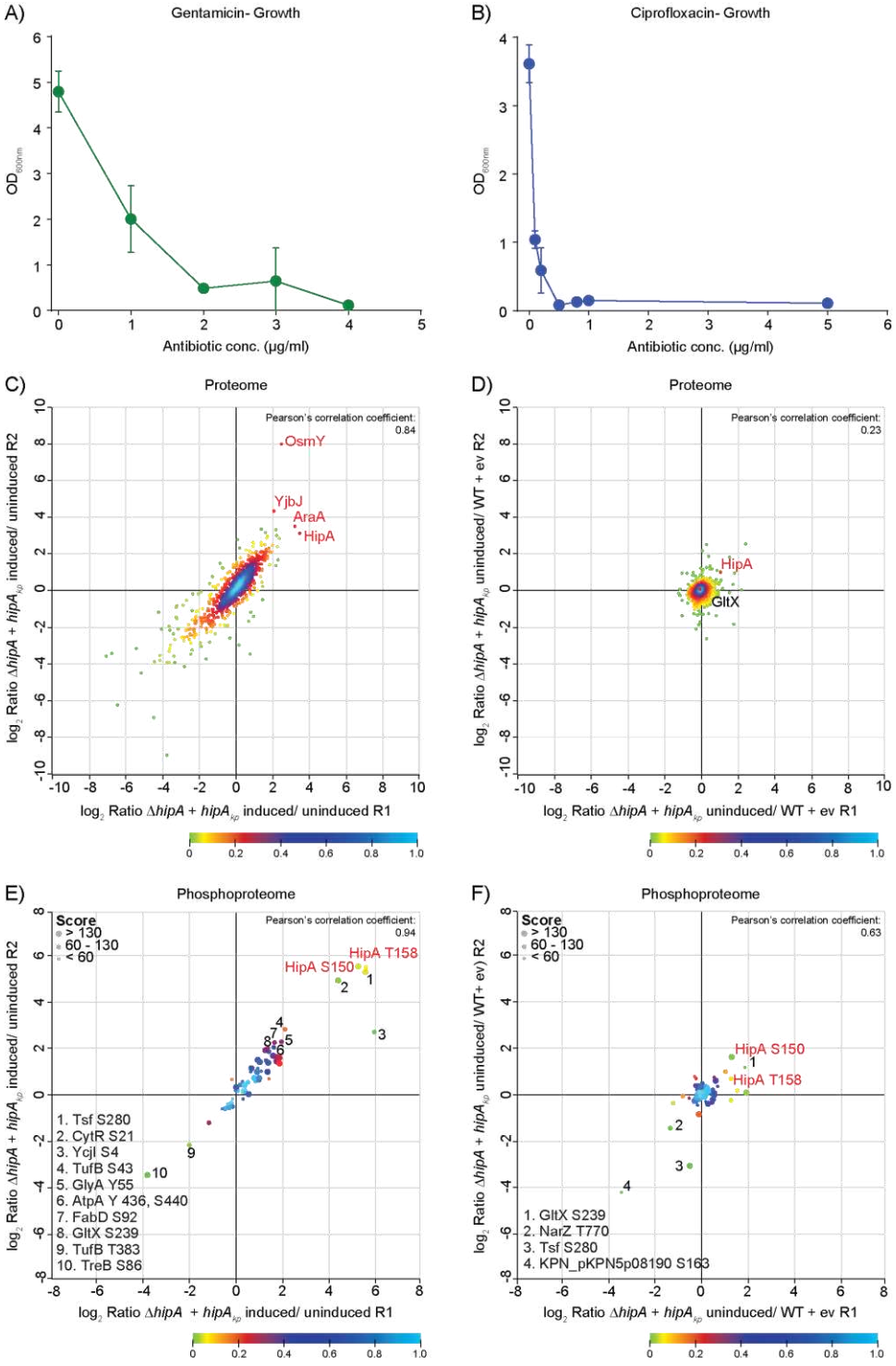

fig. S4 Additional analysis of proteomics and phosphoproteomics data from *hipA$_{kp}$* overexpression in *K. pneumoniae* after antibiotic treatment. A) and **B)** Susceptibility of *K. pneumoniae* ATCC13883 WT against gentamicin and ciprofloxacin. The strains were grown in LB Lennox medium diluted from an overnight culture to OD_{600nm} of 0.05 and grown for 24 h in

the presence of indicated antibiotics and concentrations. **C)** Quantified proteins after 2 h of ciprofloxacin treatment represented as $\log_2$ ratio between Δ*hipA K. pneumoniae* pBAD33::*hipA*$_{kp}$ induced and uninduced. **D)** Quantified proteins after 2 h of ciprofloxacin treatment represented as $\log_2$ ratio between Δ*hipA K. pneumoniae* pBAD33::*hipA*$_{kp}$ induced and WT empty vector strain which shows slight increase in *hipA*$_{kp}$ levels. **E)** Distribution of quantified phosphorylation sites after 2 h of ciprofloxacin treatment upon *hipA*$_{kp}$ overexpression, based on $\log_2$ ratio between the two replicates of Δ*hipA K. pneumoniae* pBAD33::*hipA*$_{kp}$ induced and uninduced showing significant correlation. **F)** Distribution of quantified phosphorylation sites after 2 h of ciprofloxacin treatment in control samples, based on $\log_2$ ratio between the two replicates of Δ*hipA K. pneumoniae* pBAD33::*hipA*$_{kp}$ uninduced and WT empty vector. All the phosphorylation sites changing significantly and at least four-fold in phosphorylation upon *hipA*$_{kp}$ overexpression, have been highlighted and listed here.

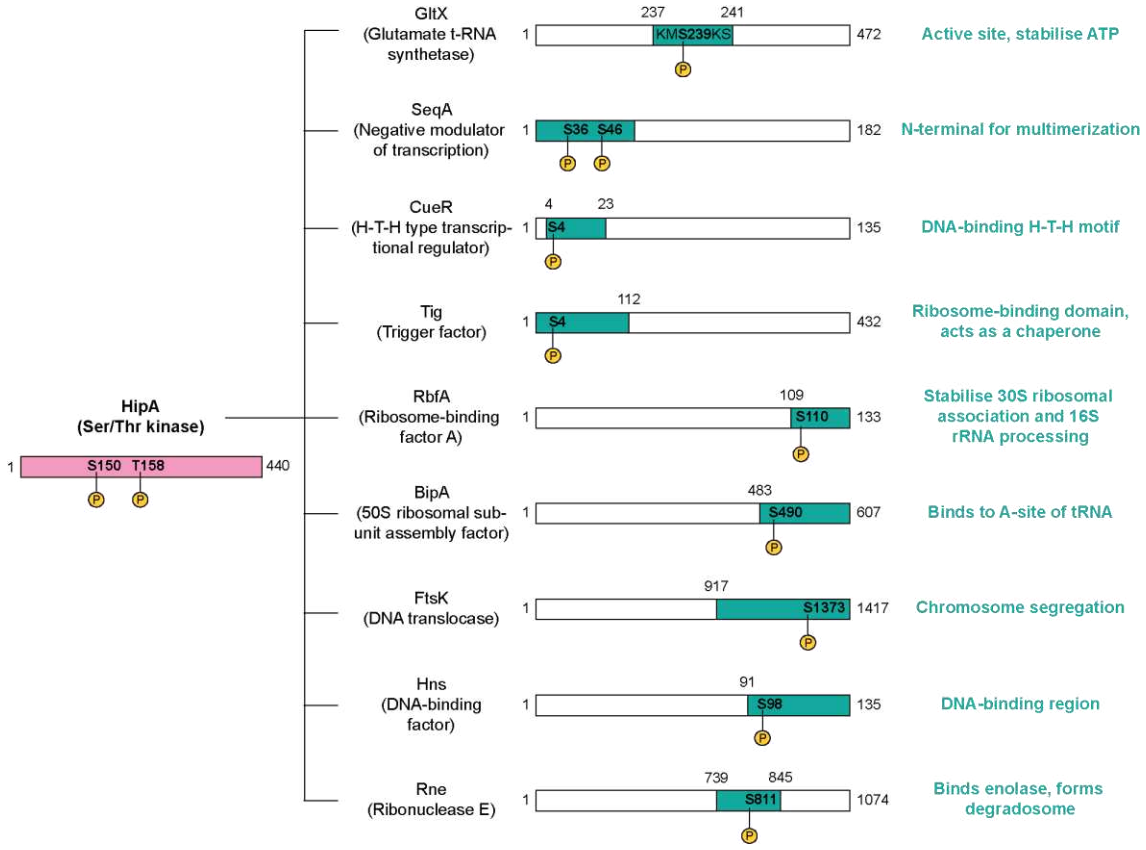

fig. S5 Localization and putative role of phosphorylation in potential substrates of HipA$_{kp}$. Schematic illustration of phosphorylated proteins by HipA$_{kp}$. The position of phosphorylation and corresponding amino acid are marked. The function of protein regions marked in green are explained on the right side.

Supporting information

Table S1. Bacterial strains and plasmids.

Table S2. DNA oligonucleotides.

Table S3. Overview of experiments for LC-MS/MS measurements.

Table S4. Analysis of proteome and phosphoproteome data from *Klebsiella pneumoniae*.

Table S5. List of putative substrates of $HipA_{kp}$.

Dataset S1. Protein groups and phosphorylation sites identified in this study.

References

1. Russo TA, Marr CM. Hypervirulent klebsiella pneumoniae. Clinical microbiology reviews. 2019;32(3):10.1128/cmr. 00001-19.

2. Rice LB. Federal funding for the study of antimicrobial resistance in nosocomial pathogens: no ESKAPE. 2008;197(8):1079-81.

3. World Health Organisation. WHO publishes list of bacteria for which new antibiotics are urgently needed. 2017:Online.

4. Grundmann H, Glasner C, Albiger B, Aanensen DM, Tomlinson CT, Andrasević AT, et al. Occurrence of carbapenemase-producing Klebsiella pneumoniae and Escherichia coli in the European survey of carbapenemase-producing Enterobacteriaceae (EuSCAPE): a prospective, multinational study. The Lancet infectious diseases. 2017;17(2):153-63.

5. Brauner A, Fridman O, Gefen O, Balaban NQ. Distinguishing between resistance, tolerance and persistence to antibiotic treatment. Nature Reviews Microbiology. 2016;14(5):320-30.

6. Cohen NR, Lobritz MA, Collins JJ. Microbial persistence and the road to drug resistance. Cell host & microbe. 2013;13(6):632-42.

7. Levin-Reisman I, Ronin I, Gefen O, Braniss I, Shoresh N, Balaban NQ. Antibiotic tolerance facilitates the evolution of resistance. Science. 2017;355(6327):826-30.

8. Balaban NQ, Merrin J, Chait R, Kowalik L, Leibler S. Bacterial persistence as a phenotypic switch. Science. 2004;305:1622-5.

9. Gefen O, Balaban NQ. The importance of being persistent: heterogeneity of bacterial populations under antibiotic stress. FEMS microbiology reviews. 2009;33(4):704-17.

10. Li Y, Zhang L, Zhou Y, Zhang Z, Zhang X. Survival of bactericidal antibiotic treatment by tolerant persister cells of Klebsiella pneumoniae. J Med Microbiol. 2018;67(3):273-81.

11. Ren H, He X, Zou X, Wang G, Li S, Wu Y. Gradual increase in antibiotic concentration affects persistence of Klebsiella pneumoniae. Journal of Antimicrobial Chemotherapy. 2015;70(12):3267-72.

12. Parsons JB, Sidders AE, Velez AZ, Hanson BM, Angeles-Solano M, Ruffin F, et al. In-patient evolution of a high-persister Escherichia coli strain with reduced in vivo antibiotic susceptibility. Proceedings of the National Academy of Sciences. 2024;121(3):e2314514121.

13. Correia FF, D'Onofrio A, Rejtar T, Li L, Karger BL, Makarova K, et al. Kinase activity of overexpressed HipA is required for growth arrest and multidrug tolerance in Escherichia coli. J Bacteriol. 2006;188(24):8360-7.

14. Schumacher MA, Balani P, Min J, Chinnam NB, Hansen S, Vulić M, et al. HipBA–promoter structures reveal the basis of heritable multidrug tolerance. Nature. 2015;524:59-64.

15. Black DS, Irwin B, Moyed HS. Autoregulation of hip, an operon that affects lethality due to inhibition of peptidoglycan or DNA synthesis. Journal of Bacteriology. 1994;176(13):4081-91.

16. Hansen S, Vulić M, Min J, Yen T-J, Schumacher MA, Brennan RG, et al. Regulation of the Escherichia coli HipBA toxin-antitoxin system by proteolysis. PloS one. 2012;7(6):e39185.

17. Germain E, Castro-Roa D, Zenkin N, Gerdes K. Molecular mechanism of bacterial persistence by HipA. Molecular cell. 2013;52(2):248-54.

18. Kaspy I, Rotem E, Weiss N, Ronin I, Balaban NQ, Glaser G. HipA-mediated antibiotic persistence via phosphorylation of the glutamyl-tRNA-synthetase. Nat Commun. 2013;4:3001.

19. Semanjski M, Germain E, Bratl K, Kiessling A, Gerdes K, Macek B. The kinases HipA and HipA7 phosphorylate different substrate pools in Escherichia coli to promote multidrug tolerance. Science Signaling. 2018;11:5750.

20. Gerdes K, Bærentsen R, Brodersen DE. Phylogeny reveals novel hipa-homologous kinase families and toxin-antitoxin gene organizations. mBio. 2021;12.

21. Zittlau K, Nashier P, Cavarischia-Rega C, Macek B, Spät P, Nalpas N. Recent progress in quantitative phosphoproteomics. Expert Review of Proteomics. 2023;20(12):469-82.

22. Jumper J, Evans R, Pritzel A, Green T, Figurnov M, Ronneberger O, et al. Highly accurate protein structure prediction with AlphaFold. Nature. 2021;596(7873):583-9.

23. Varadi M, Anyango S, Deshpande M, Nair S, Natassia C, Yordanova G, et al. AlphaFold Protein Structure Database: massively expanding the structural coverage of protein-sequence space with high-accuracy models. Nucleic Acids Res. 2022;50(D1):D439-D44.

24. Schumacher MA, Piro KM, Xu W, Hansen S, Lewis K, Brennan RG. Molecular mechanisms of HipA-mediated multidrug tolerance and its neutralization by HipB. Science. 2009;323(5912):396-401.

25. Moyed HS, Bertrand KP. hipA, a newly recognized gene of Escherichia coli K-12 that affects frequency of persistence after inhibition of murein synthesis. Journal of bacteriology. 1983;155(2):768-75.

26. Setiawan A, Widodo ADW, Endraswari PD. Comparison of ciprofloxacin, cotrimoxazole, and doxycycline onKlebsiella pneumoniae: Time-kill curve analysis. Annals of Medicine and Surgery. 2022;84.

27. Semanjski M, Gratani FL, Englert T, Nashier P, Beke V, Nalpas N, et al. Proteome Dynamics during Antibiotic Persistence and Resuscitation. mSystems. 2021;6.

28. Lin M-H, Hsu T-L, Lin S-Y, Pan Y-J, Jan J-T, Wang J-T, et al. Phosphoproteomics of Klebsiella pneumoniae NTUH-K2044 reveals a tight link between tyrosine phosphorylation and virulence. Molecular & Cellular Proteomics. 2009;8(12):2613-23.

29. Reitzel C, Sukumaran A, Muselius B, O'Connor S, Geddes-McAlister J. Profiling of the Klebsiella pneumoniae Phosphoproteome under Iron-Limited and Iron-Replete Conditions. Microbiology Resource Announcements. 2023:e00186-23.

30. Lin M-H, Sugiyama N, Ishihama Y. Systematic profiling of the bacterial phosphoproteome reveals bacterium-specific features of phosphorylation. Science signaling. 2015;8(394):rs10-rs.

31. Reitzel C, Sukumaran A, Zanetti C, Muselius B, Geddes-McAlister J. Phosphoproteome Profiling of Klebsiella pneumoniae under Zinc-Limited and Zinc-Replete Conditions. Microbiology Resource Announcements. 2023;12(7):e00258-23.

32. Asensio A, Oliver A, González-Diego P, Baquero F, Pérez-Díaz JC, Ros P, et al. Outbreak of a multiresistant Klebsiella pneumoniae strain in an intensive care unit: antibiotic use as risk factor for colonization and infection. Clinical Infectious Diseases. 2000;30(1):55-60.

33. Piazza A, Marchetti VM, Bielli A, Biffignandi GB, Piscopiello F, Giudici R, et al. A novel KPC-166 in ceftazidime/avibactam resistant ST307 Klebsiella pneumoniae causing an outbreak in Intensive Care Covid Unit, Italy. Journal of Microbiology, Immunology and Infection. 2024.

34. Snitkin ES, Zelazny AM, Thomas PJ, Stock F, Program NCS, Henderson DK, et al. Tracking a hospital outbreak of carbapenem-resistant Klebsiella pneumoniae with whole-genome sequencing. Science translational medicine. 2012;4(148):148ra16-ra16.

35. de Moraes LS, Magalhaes GLG, Soncini JGM, Pelisson M, Perugini MRE, Vespero EC. High mortality from carbapenem-resistant Klebsiella pneumoniae bloodstream infection. Microbial Pathogenesis. 2022;167:105519.

36. Gu D, Dong N, Zheng Z, Lin D, Huang M, Wang L, et al. A fatal outbreak of ST11 carbapenem-resistant hypervirulent Klebsiella pneumoniae in a Chinese hospital: a molecular epidemiological study. The Lancet infectious diseases. 2018;18(1):37-46.

37. Tian D, Liu X, Chen W, Zhou Y, Hu D, Wang W, et al. Prevalence of hypervirulent and carbapenem-resistant Klebsiella pneumoniae under divergent evolutionary patterns. Emerging microbes & infections. 2022;11(1):1936-49.

38. European Centre for Disease Prevention and Control. Emergence of hypervirulent Klebsiella pneumoniae ST23 carrying carbapenemase genes in EU/EEA countries, first update. 2024:ECDC: Stockholm.

39. Macek B, Forchhammer K, Hardouin J, Weber-Ban E, Grangeasse C, Mijakovic I. Protein post-translational modifications in bacteria. Nature reviews Microbiology. 2019.

40. Gratani FL, Englert T, Nashier P, Sass P, Czech L, Neumann N, et al. E. coli Toxin YjjJ (HipH) Is a Ser/Thr Protein Kinase That Impacts Cell Division, Carbon Metabolism, and Ribosome Assembly. mSystems. 2023;8(1):e0104322.

41. Carugo O, Pongor S. A normalized root-mean-spuare distance for comparing protein three-dimensional structures. Protein science. 2001;10(7):1470-3.

42. Fujikawa N, Kurumizaka H, Yamazoe M, Hiraga S, Yokoyama S. Identification of functional domains of the Escherichia coli SeqA protein. Biochemical and biophysical research communications. 2003;300(3):699-705.

43. Genevaux P, Keppel F, Schwager F, Langendijk-Genevaux PS, Hartl FU, Georgopoulos C. In vivo analysis of the overlapping functions of DnaK and trigger factor. EMBO reports. 2004;5(2):195-200.

44. Shi W, Zhang B, Jiang Y, Liu C, Zhou W, Chen M, et al. Structural basis of copper-efflux-regulator-dependent transcription activation. Iscience. 2021;24(5).

45. Xia B, Ke H, Shinde U, Inouye M. The role of RbfA in 16 S rRNA processing and cell growth at low temperature in Escherichia coli. Journal of molecular biology. 2003;332(3):575-84.

46. Kumar V, Chen Y, Ero R, Ahmed T, Tan J, Li Z, et al. Structure of BipA in GTP form bound to the ratcheted ribosome. Proceedings of the National Academy of Sciences. 2015;112(35):10944-9.

47. Fan H, Hahm J, Diggs S, Perry JJP, Blaha G. Structural and functional analysis of BipA, a regulator of virulence in enteropathogenic Escherichia coli. Journal of Biological Chemistry. 2015;290(34):20856-64.

48. Dubarry N, Possoz C, Barre FX. Multiple regions along the Escherichia coli FtsK protein are implicated in cell division. Molecular microbiology. 2010;78(5):1088-100.

49. Ueguchi C, Suzuki T, Yoshida T, Tanaka K-i, Mizuno T. Systematic Mutational Analysis Revealing the Functional Domain Organization of Escherichia coli Nucleoid Protein H-NS. Journal of molecular biology. 1996;263(2):149-62.

50. Liou G-G, Jane W-N, Cohen SN, Lin N-S, Lin-Chao S. RNA degradosomes exist in vivo in Escherichia coli as multicomponent complexes associated with the cytoplasmic membrane via the N-terminal region of ribonuclease E. Proceedings of the National Academy of Sciences. 2001;98(1):63-8.

51. Marchand I, Nicholson AW, Dreyfus M. Bacteriophage T7 protein kinase phosphorylates RNase E and stabilizes mRNAs synthesized by T7 RNA polymerase. Molecular microbiology. 2001;42(3):767-76.

52. Robertson ES, Nicholson AW. Phosphorylation of Escherichia coli translation initiation factors by the bacteriophage T7 protein kinase. Biochemistry. 1992;31(20):4822-7.

53. Carmichael G, Landers T, Weber K. Immunochemical analysis of the functions of the subunits of phage Qbeta ribonucleic acid replicase. Journal of Biological Chemistry. 1976;251(9):2744-8.

54. Lin M-H, Potel CM, Tehrani KH, Heck AJ, Martin NI, Lemeer S. A new tool to reveal bacterial signaling mechanisms in antibiotic treatment and resistance. Molecular & Cellular Proteomics. 2018;17(12):2496-507.

55. Gibson DG, Young L, Chuang RY, Venter JC, Hutchison CA, Smith HO. Enzymatic assembly of DNA molecules up to several hundred kilobases. Nature Methods. 2009;6:343-5.

56. Madeira F, Pearce M, Tivey AR, Basutkar P, Lee J, Edbali O, et al. Search and sequence analysis tools services from EMBL-EBI in 2022. Nucleic acids research. 2022;50(W1):W276-W9.

57. Boersema PJ, Raijmakers R, Lemeer S, Mohammed S, Heck AJR. Multiplex peptide stable isotope dimethyl labeling for quantitative proteomics. Nature Protocols. 2009;4:484-94.

58. Rappsilber J, Mann M, Ishihama Y. Protocol for micro-purification, enrichment, pre-fractionation and storage of peptides for proteomics using StageTips. Nature protocols. 2007;2(8):1896-906.

59. Cox J, Mann M. MaxQuant enables high peptide identification rates, individualized p.p.b.-range mass accuracies and proteome-wide protein quantification. Nature biotechnology. 2008;26:1367-72.

60. Cox J, Neuhauser N, Michalski A, Scheltema RA, Olsen JV, Mann M. Andromeda: A peptide search engine integrated into the MaxQuant environment. Journal of proteome research. 2011;10:1794-805.

61. Tyanova S, Temu T, Sinitcyn P, Carlson A, Hein MY, Geiger T, et al. The Perseus computational platform for comprehensive analysis of (prote)omics data. Nature Methods. 2016;13:731-40.

62. Ge SX, Jung D, Yao R. ShinyGO: a graphical gene-set enrichment tool for animals and plants. Bioinformatics. 2019;36(8):2628-9.

63. Perez-Riverol Y, Bai J, Bandla C, García-Seisdedos D, Hewapathirana S, Kamatchinathan S, et al. The PRIDE database resources in 2022: A hub for mass spectrometry-based proteomics evidences. Nucleic Acids Research. 2022;50:D543-D52.

4. Discussion

This chapter represents an extension of discussions from the manuscripts.

The HipA-like kinases are shown to be particularly responsible for modulating responses to environmental stress such as antibiotic exposure, which can result in bacteria entering a metabolically inactive, dormant-like state. While HipA has been extensively characterized in *E. coli*, HipA-homologous kinases such as HipH (YjjJ) in *E. coli* or HipA in *K. pneumoniae* are so far only poorly investigated. The work presented in this thesis aims to elucidate the role of HipA-like Ser/Thr kinases in these bacteria, with a specific focus on understanding their involvement in regulating key biological processes. They employed mass spectrometry-based quantitative phosphoproteomics to identify novel phosphorylation targets of these kinases and investigate their influence on phenotype, phosphoproteome, antibiotic tolerance, and protein function with over-expression of kinase from a plasmid. Given the low basal expression levels of HipA-like kinases and their likely induction only under specific stress conditions, we employed an overexpression system to study the impact of these kinases on bacterial physiology. This strategy has been successfully used in prior studies, such as HipA overexpression in *E. coli* (*92*), or PknI overexpression in *M. tuberculosis* (*217*). Here, the overproduction of HipH and $HipA_{kp}$ allowed for a detailed analysis of their effects on bacterial growth, antibiotic tolerance, cell division, and other cellular processes like metabolism, ribosome assembly, and DNA segregation.

4.1 Phenotypic effect of STKs in bacteria

Upon comparison of protein sequences, HipH showed very low sequence similarity to HipA in *E. coli*, although conserved kinase motifs, such as ATP-binding, Mg^{2+} binding, or autophosphorylation sites were present in HipH (*103*). Overproduction of HipH in *E. coli* resulted in cell toxicity where cell viability decreased despite an increase in optical density (OD) at high induction levels. Further analysis revealed that these cells adopted an elongated cell phenotype, characterized by improper chromosome segregation and failure of division septa formation, leading to defective cell division. This could have resulted in a drop in CFU while OD levels and overall biomass continued to increase. Additionally, HipH-overproducing cells exhibited increased glycogen levels, which could

be explained by the misregulation of CsrA, carbon storage regulator, which is one of the main phosphorylation targets of HipH. Proteome analysis revealed changes in levels of cell division proteins such as MinCDE and DNA repair protein RecA, which could also explain the effect of HipH on cell elongation and DNA segregation. This suggests that HipH negatively impacts cell division and DNA segregation in *E. coli*.

In contrast, $HipA_{kp}$ shared a relatively higher sequence similarity to $HipA_{ec}$, and its overproduction had a different phenotype on growth. Structural analysis of HipA and HipB from both *E. coli* and *K. pneumoniae* revealed a higher degree of conservation between their structures. Overproduction of $HipA_{kp}$ in both *E. coli* and *K. pneumoniae* resulted in a toxic phenotype, with decreased growth observed at both absorbance and viability levels. However, this inhibited growth was reversed by the simultaneous overproduction of $HipB_{kp}$, confirming that the *hipBA* operon in *K. pneumoniae* also functions as a toxin-antitoxin system. While the complementation in *E. coli* was complete, in *K. pneumoniae*, $HipB_{kp}$ overproduction could only partially complement the $HipA_{kp}$ toxicity. The reason behind this is currently unclear but one can suspect that it could be due to lower levels of HipB compared to HipA or higher proteolytic cleavage of HipB in *K. pneumoniae*, which could have resulted in only partial complementation.

4.2 Antibiotic tolerance in bacteria by STKs

Previous studies in bacteria, such as *S. aureus* have shown that the Ser/Thr kinase PknB along with its cognate phosphatase Stp can regulate antibiotic tolerance, where in the absence of Stp, the bacteria were able to tolerate higher concentrations of antibiotics due to the missing ability to dephosphorylate targets of PknB (*73*). Higher amounts of PknB have shown increased autophosphorylation and phosphorylation of its target protein, which are involved in cellular processes such as glycolysis, synthesis of cell walls, and protein biosynthesis (*218-220*). This leads to a decrease in ATP concentrations, changed cell wall synthesis, and reduced protein synthesis. Overproduction of $HipA_{ec}$ has been shown to confer antibiotic tolerance to certain antibiotics (*92*). Unlike $HipA_{ec}$, overproduction of the kinase HipH in *E. coli* did not confer tolerance to antibiotics like ciprofloxacin and ampicillin, suggesting that HipH may not regulate cellular processes linked to antibiotic tolerance, as $HipA_{ec}$ does. This indicates

that HipH and $HipA_{ec}$ likely have distinct physiological roles despite both belonging to the HipA-family of Ser/Thr kinases.

In contrast, when $HipA_{kp}$ was overproduced in *K. pneumoniae*, it provided tolerance against ciprofloxacin but not against gentamicin, indicating that $HipA_{kp}$ confers antibiotic tolerance selectively, depending on the antibiotic class. A similar observation has been made with $HipA_{ec}$, where tolerance was observed against fluoroquinolones and beta-lactams such as ofloxacin, and cefotaxime but not aminoglycosides like tobramycin (*92*). Aminoglycosides, such as gentamicin and tobramycin, exert their antibacterial effect by binding to the A-site of the 30S ribosomal subunit, causing mistranslation and the production of misfolded proteins, which can damage bacterial membranes and other cellular structures (*221*). While HipA overproduction induces a dormant-like state where key processes like metabolism, cell division, and replication are slowed down or halted, a recent study suggests that basal level of protein synthesis continues in these bacteria (*222*). If aminoglycosides target this residual protein synthesis, leading to the production of erroneous proteins even in the dormant cells, this could explain why HipA-overproducing bacteria are not tolerant to aminoglycosides.

On the other hand, fluoroquinolones like ciprofloxacin target rapidly dividing bacteria by inhibiting type II topoisomerases (e.g., DNA gyrase and topoisomerase IV), leading to disrupted DNA replication and repair (*223*). Since HipA-overproducing bacteria enter a dormant-like state with halted DNA replication, they become less susceptible to ciprofloxacin-induced killing, thereby exhibiting tolerance. This suggests that the dormant state induced by $HipA_{kp}$ protects the bacteria against certain classes of antibiotics, that kill actively growing cells, but not others, which aligns well with the observations from $HipA_{ec}$-mediated persistence.

4.3 Phosphoproteomics approach to study STKs in bacteria

The overexpression of a kinase results in increased phosphorylation on numerous proteins, enabling the identification of potential substrates. This can be used for determining the role of kinases in regulating proteins involved in specific cellular pathways. However, not all the up-regulated phosphorylation sites are direct targets of the overexpressed kinase, as overexpression can lead to unspecific phosphorylation or

activation of other kinases, which can influence the overall phosphoproteome. To distinguish direct substrates, additional biological assays such as mutant analysis or *in vitro* kinase assay are required.

4.3.1 Phosphorylation targets of HipH in *E. coli*

Phosphoproteomic analysis following the overexpression of *hipH* in *E. coli* revealed that HipH autophosphorylates at Ser200, Ser201, and Ser217. Additionally, increased phosphorylation levels were observed on proteins such as RpmE, CsrA, and GltX. Interestingly, GltX, a known substrate of kinase HipA in *E. coli* (*94, 95*), also exhibited upregulated phosphorylation.

To confirm whether GltX is a shared substrate of both HipH and HipA, phosphoproteomic analysis was performed in a Δ*hipBA E. coli* strain overproducing HipH. The absence of upregulated phosphorylation at GltX Ser239 in the mutant strain suggested that the phosphorylation of GltX by HipH was indirect, indicating cross-talk between HipH and HipA in *E. coli*. The other lines of connection between HipH and $HipA_{ec}$ include upregulation of HipH phosphorylation at Ser200 in cells overexpressing high persistence variant HipA7 (*98*) and rescue from HipH toxicity by HipB overproduction, as shown previously by Semanjski *et al.* 2018 (*98*) and this study.

Using *in vitro* kinase assays, RpmE and CsrA were confirmed as direct substrates of HipH. To investigate the functional consequences of their phosphorylation, overexpression of wild-type and phospho-mimetic mutants of CsrA and RpmE were studied. This revealed that HipH-mediated phosphorylation inhibits the activity of CsrA, a global regulator of carbon metabolism (*224*). This would also explain the increased glycogen levels observed in HipH-overproducing cells, as CsrA normally represses glycogen synthesis (*225, 226*). Overexpression of the phospho-mimetic mutant $CsrA_{S56E}$ did not have any effect on bacterial growth, while overexpression of the wild-type CsrA led to a reduced growth rate. This suggests that phosphorylation at Ser56 by HipH inhibited CsrA activity, potentially explaining the increased glycogen levels observed upon HipH overexpression.

Moreover, phosphorylation on RpmE (L31a) at S69, a small ribosomal protein that facilitates the association of 50S and 30S ribosomal subunits (*227*), disrupted the

ribosome assembly. Similar defects were also observed in the Δ*rpmE* strain suggesting that the phosphorylation of RpmE by HipH inhibits its activity and negatively affects ribosome function and assembly. Ribosomal protein RpmE (L31a) has a paralog YkgM (L31b), which replaces it during the transition from the exponential phase to the stationary phase (*228*) and HipH levels are also seen to increase in the stationary phase (*229*). This suggests that HipH might be involved in this post-translational regulation of proteins such as ribosomal proteins to transit bacteria into the stationary phase.

4.3.2 Phosphorylation targets of $HipA_{kp}$ in *K. pneumoniae*

Phosphoproteomic analysis of *K. pneumoniae* overproducing $HipA_{kp}$ with and without antibiotic treatment identified several phospho-sites to be up-regulated, some of which were consistently observed across multiple experiments. Several targets overlapped with those known to be phosphorylated by $HipA_{ec}$ in *E. coli*, such as the auto-phosphorylation site on HipA at Ser150 or GltX at Ser239. Phosphorylation at GltX Ser239 inhibits the charging of glutamate tRNA, leading to ribosome stalling and recruitment of RelA. Activated RelA increases the (p)ppGpp synthesis leading to the activation of stringent response, a key mechanism in persistence (*94, 95*). In general, inhibition of translation has been shown to increase persister cell formation in *E. coli* (*230, 231*).

Beyond the findings presented in the final manuscript, the broader consequences of $HipA_{kp}$-mediated phosphorylation in *K. pneumoniae* provide multiple avenues for a deeper understanding of bacterial regulatory mechanisms. For instance, 34 potential substrates of $HipA_{kp}$, which regulate different basic biological processes highlight the involvement of this kinase in many other cellular processes besides antibiotic tolerance. While the phosphoproteomic data highlighted specific phosphorylation events on different proteins, the biological impact of these modifications requires further elucidation. Notably, many of these identified phosphorylation sites on potential substrates are clustered at the terminal regions of the proteins that are often involved in protein-protein or protein-nucleic acid interactions, which suggests the role of $HipA_{kp}$ in regulating transcriptional and translational networks through post-translational

modifications. Further investigation using phospho-mimetic and -ablative mutants, could shed light on how phosphorylation influences the binding affinity of these proteins to their substrates, potentially altering their regulatory roles.

The phosphorylation on Rne, RpsA, and Tsf by $HipA_{kp}$ also increases the possibility of cross-talk between HipA and phage-induced phosphorylation pathways, as suggested by the overlap with phosphorylation substrates of the T7 phage kinase gp-0.7 (*232-234*). This similarity may indicate a common approach between bacterial persistence mechanisms and phage-driven regulatory pathways. For instance, phosphorylation of Rne by T7 kinase disrupts the RNA degradosome, thereby preventing the degradation of phage mRNA synthesized by T7 RNA polymerase (*235, 236*). Since phosphorylation by $HipA_{kp}$ is also located in the C-terminal region where the components of RNA degradosome bind, it may indicate that it is a bacterial strategy to shut off normal cellular functions to help bacteria survive under stress conditions. The identification of phosphorylation sites that coincide with previously known phage infection processes opens an exciting area of research into bacterial responses to phage infection. This may suggest a broader evolutionary approach where bacteria hijack phage mechanisms of infection to control their persistence. Elucidation of this connection is now enlightening into novel approaches that bacteria use to survive phage infection and perhaps to develop novel therapeutic approaches based on bacterial vulnerabilities in these pathways.

Although this work lays the groundwork for understanding $HipA_{kp}$-mediated phosphorylation in *K. pneumoniae*, there is still much to be understood regarding the biological significance of these kinases in bacteria. Indeed, the functional consequences of such $HipA_{kp}$ phosphorylation events on bacterial transcription, translation, and replication processes-especially regarding stress responses and persistence-require further studies. In this regard, direct interaction between the kinase and substrate and how $HipA_{kp}$ coordinates in such complex networks to promote bacterial survival will require substrate confirmation by *in vitro* kinase assays, structural modeling, and genetic manipulations of key substrates.

The findings in this thesis advance our understanding of Ser/Thr kinases in modulating important bacterial functions and open up avenues for future research on bacterial stress responses and persistence mechanisms, with potential applications in the development of new therapeutic strategies targeting bacterial persistence.

5. Conclusion and Future Perspectives

Mass spectrometry-based quantitative phosphoproteomics has been an excellent tool for studying Ser/Thr kinases in bacteria to gain insights into their physiological role and functional relevance. Due to increasing antibiotic resistance, it is of utmost importance to study these STKS in relation to antibiotic tolerance and persistence as these mechanisms can ultimately lead to antibiotic resistance and are frequently responsible for causing relapse of infections. In this work, two Ser/Thr kinases, namely HipH (YjjJ) in *E. coli* and HipA in *K. pneumoniae* are characterized for their effect on the growth, antibiotic exposure, proteome, and phosphoproteome of bacteria. Results obtained in this study have led to the following conclusions:

1. ***E. coli* toxin YjjJ (HipH) is a Ser/Thr protein kinase that impacts cell division, carbon metabolism, and ribosome assembly**
   a) Phosphoproteome analysis of Δ*hipBA E. coli* cells overexpressing *yjjJ* and kinase-dead *yjjJ* confirmed that RpmE and CsrA are direct substrates of YjjJ whereas GltX phosphorylation was not directly phosphorylated by YjjJ, instead was a result of cross-talk between HipA and YjjJ kinases.
   b) *In vitro* kinase assay confirmed that RpmE is phosphorylated at Ser69 and CsrA is phosphorylated at Ser56 by purified YjjJ kinase, CsrA even more profoundly in the presence of an mRNA CsrB. It also confirmed that YjjJ autophosphorylates at Ser200.
   c) Overexpression of wildtype and phospho-mimetic mutants of CsrA revealed that CsrA phosphorylation inhibits its activity and YjjJ negatively regulates its function.
   d) Δ*yjjJ E. coli* analysis revealed that YjjJ does not have any effect on the growth of exponential phase bacteria at absorbance or viability. The absence of YjjJ was confirmed by proteome analysis.
2. **Deep phosphoproteomics of *Klebsiella pneumoniae* reveals HipA-mediated tolerance to ciprofloxacin**
   a) Sequence analysis of HipA and HipB in *E. coli* and *K. pneumoniae* revealed that these proteins have around 55 to 70% identity between the

genes from two bacteria with conserved kinase domain in HipA. On the other hand, structure analysis showed that the overall structure is highly conserved.

b) Sequence comparison of HipA from *K. pneumoniae* revealed that it is present in other species of *Klebsiella* with relatively high sequence identity and in many other gram-negative bacteria with around 70% identity.
c) Overexpression of $hipA_{kp}$ leads to inhibited growth in both *E. coli* and *K. pneumoniae*. This growth was complemented by the overproduction of $HipB_{kp}$ in *E. coli* and partially in *K. pneumoniae*.
d) Phosphoproteome analysis showed up-regulation of GltX phosphorylation in addition to several other phospho-sites in $hipA_{kp}$-overexpressing bacteria in both *E. coli* and *K. pneumoniae*, which will need further validation.
e) Overproduced $HipA_{kp}$ conferred antibiotic tolerance to ciprofloxacin and not against gentamicin in *K. pneumoniae*. Phosphoproteome results showed a similar set of sites to be phosphorylated.
f) Comparison of my phosphoproteome dataset with the previously published datasets for *K. pneumoniae* revealed a large number of novel phosphorylations that were previously not reported in this bacterium.

This thesis has provided a comprehensive exploration of the biological processes regulated by serine/threonine kinases (STKs) in bacteria, particularly focusing on the HipA-family of kinases. The proteome and phosphoproteome datasets generated for *E. coli* and *K. pneumoniae* offer valuable insights into the post-translational regulation of a variety of proteins in response to STK overexpression. However, the overexpression system employed represents an artificial condition, which does not fully mimic the endogenous kinase levels present under physiological conditions. To gain a deeper understanding of the natural role of these kinases, it is essential to identify the environmental or stress conditions under which these kinases are naturally activated and expressed. Previous studies have indicated that STK levels, including those of HipH (YjjJ), HipA, and YeaG in *E. coli*, increase during the stationary phase. Therefore, a logical next step would be to investigate the activity of these kinases during the

stationary phase in comparison to the log phase, which was the focus of this study. This would provide insight into their role in bacterial survival strategies under nutrient-limiting or stressful conditions. Additionally, the presence of a helix-turn-helix (HTH) domain in the N-terminal region of HipH, similar to the DNA-binding motif in HipB of the *hipBA* operon, presents a compelling avenue for future research. Exploring the function of this domain could reveal whether HipH directly influences transcriptional regulation, potentially through promoter binding of specific genes via the HTH domain. Such a regulatory role could offer new perspectives on the connection between kinase activity and transcriptional control. Another aspect that might be important to explore is the possible cross-talk between different *E. coli* kinases. The likelihood of some substrates being common between these kinases or if these kinases can activate other kinases will probably further reveal regulatory complexities and give more insight into the kinase signaling networks in control of critical bacterial processes. Besides this, the similarity between the phosphorylation targets of HipA in *K. pneumoniae* and those observed upon T7 phage infection in *E. coli* suggests a possible evolutionary link between bacterial and phage kinase. Both appear to inhibit similar pathways, such as translation and RNA degradation. Phylogenetic and structural analyses could help identify a common link between them, shedding light on how they both have adapted similar pathways to modulate cells into a dormant-like state or takeover cell machinery for phage propagation. With all of these clarifications and analyses, a more complete understanding of the physiological role of STKs and their interplay in bacteria can be achieved.

6. References

1. D. F. Steiner, D. Cunningham, L. Spigelman, B. Aten, Insulin biosynthesis: evidence for a precursor. *Science* **157**, 697-700 (1967).
2. D. F. Steiner, P. E. Oyer, The biosynthesis of insulin and a probable precursor of insulin by a human islet cell adenoma. *Proceedings of the National Academy of Sciences* **57**, 473-480 (1967).
3. R. Chaudhary, S. Mishra, G. K. Maurya, Y. S. Rajpurohit, H. S. Misra, FtsZ phosphorylation brings about growth arrest upon DNA damage in Deinococcus radiodurans. *FASEB BioAdvances* **5**, 27 (2023).
4. T. Zou, Z. Lin, The involvement of ubiquitination machinery in cell cycle regulation and cancer progression. *International Journal of Molecular Sciences* **22**, 5754 (2021).
5. Y.-C. Wang, S. E. Peterson, J. F. Loring, Protein post-translational modifications and regulation of pluripotency in human stem cells. *Cell research* **24**, 143-160 (2014).
6. M. Merrick, Post-translational modification of P II signal transduction proteins. *Frontiers in Microbiology* **5**, 763 (2015).
7. V. Bidnenko *et al.*, B acillus subtilis serine/threonine protein kinase YabT is involved in spore development via phosphorylation of a bacterial recombinase. *Molecular Microbiology* **88**, 921-935 (2013).
8. B. Macek *et al.*, Protein post-translational modifications in bacteria. *Nature Reviews Microbiology* **17**, 651-664 (2019).
9. T. Hunter, Why nature chose phosphate to modify proteins. *Philosophical Transactions of the Royal Society B: Biological Sciences* **367**, 2513-2516 (2012).
10. T. Houles, S.-O. Yoon, P. P. Roux, The expanding landscape of canonical and non-canonical protein phosphorylation. *Trends in Biochemical Sciences*, (2024).
11. P. Cohen, The origins of protein phosphorylation. *Nature cell biology* **4**, E127-E130 (2002).
12. B. Huang, Z. Zhao, Y. Zhao, S. Huang, Protein arginine phosphorylation in organisms. *International journal of biological macromolecules* **171**, 414-422 (2021).
13. G. Hardman *et al.*, Strong anion exchange-mediated phosphoproteomics reveals extensive human non-canonical phosphorylation. *The EMBO journal* **38**, e100847 (2019).
14. J. Cieśla, T. Frączyk, W. Rode, Phosphorylation of basic amino acid residues in proteins: important but easily missed. *Acta Biochimica Polonica* **58**, 137-148 (2011).
15. S. Wang, Y. Z. Chen, S. Fu, Y. Zhao, In silico approaches uncovering the systematic function of N-phosphorylated proteins in human cells. *Computers in Biology and Medicine* **151**, 106280 (2022).
16. F. Falcioni *et al.*, Arginine kinase activates Arginine for phosphorylation by pyramidalization and polarization. *ACS catalysis* **14**, 6650-6658 (2024).
17. T. Hunter, A journey from phosphotyrosine to phosphohistidine and beyond. *Molecular cell* **82**, 2190-2200 (2022).

18. T. Y. Low *et al.*, Widening the bottleneck of phosphoproteomics: evolving strategies for phosphopeptide enrichment. *Mass spectrometry reviews* **40**, 309-333 (2021).
19. A. M. Stock, V. L. Robinson, P. N. Goudreau, Two-component signal transduction. *Annual review of biochemistry* **69**, 183-215 (2000).
20. R. Gao, S. Bouillet, A. M. Stock, Structural basis of response regulator function. *Annual review of microbiology* **73**, 175-197 (2019).
21. R. Gao, T. R. Mack, A. M. Stock, Bacterial response regulators: versatile regulatory strategies from common domains. *Trends in biochemical sciences* **32**, 225-234 (2007).
22. M. Y. Galperin, Diversity of structure and function of response regulator output domains. *Current opinion in microbiology* **13**, 150-159 (2010).
23. F. D. Russo, T. J. Silhavy, The essential tension: opposed reactions in bacterial two-component regulatory systems. *Trends in microbiology* **1**, 306-310 (1993).
24. K. K. Koretke, A. N. Lupas, P. V. Warren, M. Rosenberg, J. R. Brown, Evolution of two-component signal transduction. *Molecular biology and evolution* **17**, 1956-1970 (2000).
25. J. Kuo, P. Greengard, An adenosine 3′, 5′-monophosphate-dependent protein kinase from Escherichia coli. *Journal of Biological Chemistry* **244**, 3417-3419 (1969).
26. M. Garnak, H. C. Reeves, Phosphorylation of isocitrate dehydrogenase of Escherichia coli. *Science* **203**, 1111-1112 (1979).
27. D. C. LaPorte, T. Chung, A single gene codes for the kinase and phosphatase which regulate isocitrate dehydrogenase. *Journal of Biological Chemistry* **260**, 15291-15297 (1985).
28. J. Dworkin, Ser/Thr phosphorylation as a regulatory mechanism in bacteria. *Current opinion in microbiology* **24**, 47-52 (2015).
29. S. N. Nagarajan, C. Lenoir, C. Grangeasse, Recent advances in bacterial signaling by serine/threonine protein kinases. *Trends in Microbiology* **30**, 553-566 (2022).
30. S. K. Hanks, T. Hunter, The eukaryotic protein kinase superfamily: kinase (catalytic) domain structure and classification 1. *The FASEB journal* **9**, 576-596 (1995).
31. G. K. Kanev *et al.*, The landscape of atypical and eukaryotic protein kinases. *Trends in pharmacological sciences* **40**, 818-832 (2019).
32. J. Zheng, C. He, V. K. Singh, N. L. Martin, Z. Jia, Crystal structure of a novel prokaryotic Ser/Thr kinase and its implication in the Cpx stress response pathway. *Molecular microbiology* **63**, 1360-1371 (2007).
33. K. B. Nguyen *et al.*, Phosphorylation of spore coat proteins by a family of atypical protein kinases. *Proceedings of the National Academy of Sciences* **113**, E3482-E3491 (2016).
34. V. Olivares-Illana *et al.*, Structural basis for the regulation mechanism of the tyrosine kinase CapB from Staphylococcus aureus. *PLOS biology* **6**, e143 (2008).
35. I. Mijakovic, C. Grangeasse, K. Turgay, Exploring the diversity of protein modifications: special bacterial phosphorylation systems. *FEMS microbiology reviews* **40**, 398-417 (2016).

36. J. Fuhrmann *et al.*, McsB is a protein arginine kinase that phosphorylates and inhibits the heat-shock regulator CtsR. *Science* **324**, 1323-1327 (2009).
37. D. B. Trentini *et al.*, Arginine phosphorylation marks proteins for degradation by a Clp protease. *Nature* **539**, 48-53 (2016).
38. E. A. Libby, L. A. Goss, J. Dworkin, The eukaryotic-like Ser/Thr kinase PrkC regulates the essential WalRK two-component system in Bacillus subtilis. *PLoS genetics* **11**, e1005275 (2015).
39. G. E. Pinas *et al.*, Crosstalk between the serine/threonine kinase StkP and the response regulator ComE controls the stress response and intracellular survival of Streptococcus pneumoniae. *PLoS pathogens* **14**, e1007118 (2018).
40. A. Frando, V. Boradia, C. Grundner, Regulatory intersection of two-component system and Ser/Thr protein kinase signaling in Mycobacterium tuberculosis. *Journal of Molecular Biology* **436**, 168379 (2024).
41. H. Nariya, S. Inouye, Identification of a protein Ser/Thr kinase cascade that regulates essential transcriptional activators in Myxococcus xanthus development. *Molecular microbiology* **58**, 367-379 (2005).
42. A. Kalantari, A. Derouiche, L. Shi, I. Mijakovic, Serine/threonine/tyrosine phosphorylation regulates DNA binding of bacterial transcriptional regulators. *Microbiology* **161**, 1720-1729 (2015).
43. D. R. Buelow, T. L. Raivio, Cpx signal transduction is influenced by a conserved N-terminal domain in the novel inhibitor CpxP and the periplasmic protease DegP. *Journal of bacteriology* **187**, 6622-6630 (2005).
44. L. Shi *et al.*, Cross-phosphorylation of bacterial serine/threonine and tyrosine protein kinases on key regulatory residues. *Frontiers in Microbiology* **5**, 495 (2014).
45. U. Kusebauch *et al.*, Mycobacterium tuberculosis supports protein tyrosine phosphorylation. *Proceedings of the National Academy of Sciences* **111**, 9265-9270 (2014).
46. A. J. Cozzone, Protein phosphorylation in prokaryotes. *Annual Reviews in Microbiology* **42**, 97-125 (1988).
47. J. Muñoz-Dorado, S. Inouye, M. Inouye, A gene encoding a protein serine/threonine kinase is required for normal development of M. xanthus, a gram-negative bacterium. *Cell* **67**, 995-1006 (1991).
48. G. Han, C.-C. Zhang, On the origin of Ser/Thr kinases in a prokaryote. *FEMS microbiology letters* **200**, 79-84 (2001).
49. I. A. Stancik *et al.*, Serine/threonine protein kinases from bacteria, archaea and eukarya share a common evolutionary origin deeply rooted in the tree of life. *Journal of molecular biology* **430**, 27-32 (2018).
50. P. Spaet, B. Maček, K. Forchhammer, Phosphoproteome of the cyanobacterium Synechocystis sp. PCC 6803 and its dynamics during nitrogen starvation. *Frontiers in Microbiology* **6**, 248 (2015).
51. T. Barske *et al.*, The Role of Serine/Threonine-Specific Protein Kinases in Cyanobacteria-SpkB Is Involved in Acclimation to Fluctuating Conditions in Synechocystis sp. PCC 6803. *Molecular & Cellular Proteomics* **22**, (2023).
52. A. Kamei, S. Yoshihara, T. Yuasa, X. Geng, M. Ikeuchi, Biochemical and functional characterization of a eukaryotic-type protein kinase, SpkB, in the

cyanobacterium, Synechocystis sp. PCC 6803. *Current microbiology* **46**, 0296-0301 (2003).
53. A. Mata-Cabana, M. García-Domínguez, F. J. Florencio, M. Lindahl, Thiol-based redox modulation of a cyanobacterial eukaryotic-type serine/threonine kinase required for oxidative stress tolerance. *Antioxidants & Redox Signaling* **17**, 521-533 (2012).
54. M. E. Ohl, S. I. Miller, Salmonella: a model for bacterial pathogenesis. *Annual review of medicine* **52**, 259-274 (2001).
55. A. Haraga, M. B. Ohlson, S. I. Miller, Salmonellae interplay with host cells. *Nature Reviews Microbiology* **6**, 53-66 (2008).
56. E. A. Groisman, H. Ochman, Pathogenicity islands: bacterial evolution in quantum leaps. *Cell* **87**, 791-794 (1996).
57. S. P. Faucher, C. Viau, P.-P. Gros, F. Daigle, H. Le Moual, The prpZ gene cluster encoding eukaryotic-type Ser/Thr protein kinases and phosphatases is repressed by oxidative stress and involved in Salmonella enterica serovar Typhi survival in human macrophages. *FEMS microbiology letters* **281**, 160-166 (2008).
58. N. Theeya *et al.*, An inducible and secreted eukaryote-like serine/threonine kinase of Salmonella enterica serovar Typhi promotes intracellular survival and pathogenesis. *Infection and immunity* **83**, 522-533 (2015).
59. K. L. O'brien *et al.*, Burden of disease caused by Streptococcus pneumoniae in children younger than 5 years: global estimates. *The Lancet* **374**, 893-902 (2009).
60. E. Gordon, N. Mouz, E. Duee, O. Dideberg, The crystal structure of the penicillin-binding protein 2x from Streptococcus pneumoniae and its acyl-enzyme form: implication in drug resistance. *Journal of molecular biology* **299**, 477-485 (2000).
61. L. Nováková *et al.*, Identification of multiple substrates of the StkP Ser/Thr protein kinase in Streptococcus pneumoniae. *Journal of bacteriology* **192**, 3629-3638 (2010).
62. L. Novakova *et al.*, Characterization of a eukaryotic type serine/threonine protein kinase and protein phosphatase of Streptococcus pneumoniae and identification of kinase substrates. *The FEBS journal* **272**, 1243-1254 (2005).
63. Y.-Y. Huang *et al.*, Sublethal β-lactam antibiotics induce PhpP phosphatase expression and StkP kinase phosphorylation in PBP-independent β-lactam antibiotic resistance of Streptococcus pneumoniae. *Biochemical and biophysical research communications* **503**, 2000-2008 (2018).
64. C. Giefing, K. E. Jelencsics, D. Gelbmann, B. M. Senn, E. Nagy, The pneumococcal eukaryotic-type serine/threonine protein kinase StkP co-localizes with the cell division apparatus and interacts with FtsZ in vitro. *Microbiology* **156**, 1697-1707 (2010).
65. K. Beilharz *et al.*, Control of cell division in Streptococcus pneumoniae by the conserved Ser/Thr protein kinase StkP. *Proceedings of the National Academy of Sciences* **109**, E905-E913 (2012).
66. A. Ulrych *et al.*, Cell wall stress stimulates the activity of the protein kinase StkP of Streptococcus pneumoniae, leading to multiple phosphorylation. *Journal of Molecular Biology* **433**, 167319 (2021).

67. F. Pompeo, E. Foulquier, A. Galinier, Impact of serine/threonine protein kinases on the regulation of sporulation in Bacillus subtilis. *Frontiers in microbiology* **7**, 568 (2016).
68. S. F. Pereira, R. L. Gonzalez Jr, J. Dworkin, Protein synthesis during cellular quiescence is inhibited by phosphorylation of a translational elongation factor. *Proceedings of the National Academy of Sciences* **112**, E3274-E3281 (2015).
69. L. Shi *et al.*, Structural analysis of the hanks-type protein kinase YabT from Bacillus subtilis provides new insights in its DNA-dependent activation. *Frontiers in Microbiology* **9**, 3014 (2019).
70. A. Derouiche, D. Petranovic, B. Macek, I. Mijakovic, Bacillus subtilis single-stranded DNA-binding protein SsbA is phosphorylated at threonine 38 by the serine/threonine kinase YabT. *Periodicum biologorum* **118**, (2016).
71. T. García García *et al.*, Phosphorylation of the Bacillus subtilis replication controller YabA plays a role in regulation of sporulation and biofilm formation. *Frontiers in Microbiology* **9**, 486 (2018).
72. F. D. Lowy, Staphylococcus aureus infections. *New England journal of medicine* **339**, 520-532 (1998).
73. M. Huemer *et al.*, Serine-threonine phosphoregulation by PknB and Stp contributes to quiescence and antibiotic tolerance in Staphylococcus aureus. *Science Signaling* **16**, eabj8194 (2023).
74. M. Debarbouille *et al.*, Characterization of a serine/threonine kinase involved in virulence of Staphylococcus aureus. *Journal of bacteriology* **191**, 4070-4081 (2009).
75. W. Zheng, X. Cai, S. Li, Z. Li, Autophosphorylation mechanism of the Ser/Thr kinase Stk1 from Staphylococcus aureus. *Frontiers in Microbiology* **9**, 758 (2018).
76. S. Tamber, J. Schwartzman, A. L. Cheung, Role of PknB kinase in antibiotic resistance and virulence in community-acquired methicillin-resistant Staphylococcus aureus strain USA300. *Infection and immunity* **78**, 3637-3646 (2010).
77. A. O. Moskovets, L. V. Pletnova, T. G. Maiula, D. O. Tverdyy, G. P. Volynets, Protein kinase PknB as a promising target for the development of antibacterial drugs toward Staphylococcus aureus. *Ukrainica Bioorganica Acta* **18**, 3-9 (2023).
78. S. J. Labrie, J. E. Samson, S. Moineau, Bacteriophage resistance mechanisms. *Nature Reviews Microbiology* **8**, 317-327 (2010).
79. F. Depardieu *et al.*, A eukaryotic-like serine/threonine kinase protects staphylococci against phages. *Cell host & microbe* **20**, 471-481 (2016).
80. A. G. Moller, J. A. Lindsay, T. D. Read, Determinants of phage host range in Staphylococcus species. *Applied and environmental microbiology* **85**, e00209-00219 (2019).
81. L. G. Valente *et al.*, Isolation and characterization of bacteriophages from the human skin microbiome that infect Staphylococcus epidermidis. *FEMS microbes* **2**, xtab003 (2021).
82. N. Q. Balaban, J. Merrin, R. Chait, L. Kowalik, S. Leibler, Bacterial persistence as a phenotypic switch. *Science* **305**, 1622-1625 (2004).

83. H. S. Moyed, K. P. Bertrand, hipA, a newly recognized gene of Escherichia coli K-12 that affects frequency of persistence after inhibition of murein synthesis. *Journal of bacteriology* **155**, 768-775 (1983).
84. R. Page, W. Peti, Toxin-antitoxin systems in bacterial growth arrest and persistence. *Nature chemical biology* **12**, 208-214 (2016).
85. D. S. Black, A. J. Kelly, M. Mardis, H. Moyed, Structure and organization of hip, an operon that affects lethality due to inhibition of peptidoglycan or DNA synthesis. *Journal of bacteriology* **173**, 5732-5739 (1991).
86. D. S. Black, B. Irwin, H. S. Moyed, Autoregulation of hip, an operon that affects lethality due to inhibition of peptidoglycan or DNA synthesis. *Journal of Bacteriology* **176**, 4081-4091 (1994).
87. M. A. Schumacher *et al.*, Molecular mechanisms of HipA-mediated multidrug tolerance and its neutralization by HipB. *Science* **323**, 396-401 (2009).
88. M. A. Schumacher *et al.*, HipBA–promoter structures reveal the basis of heritable multidrug tolerance. *Nature* **524**, 59-64 (2015).
89. S. Hansen *et al.*, Regulation of the Escherichia coli HipBA toxin-antitoxin system by proteolysis. *PloS one* **7**, e39185 (2012).
90. E. Rotem *et al.*, Regulation of phenotypic variability by a threshold-based mechanism underlies bacterial persistence. *Proceedings of the National Academy of Sciences* **107**, 12541-12546 (2010).
91. S. B. Korch, T. M. Hill, Ectopic overexpression of wild-type and mutant hipA genes in Escherichia coli: effects on macromolecular synthesis and persister formation. *Journal of bacteriology* **188**, 3826-3836 (2006).
92. F. F. Correia *et al.*, Kinase activity of overexpressed HipA is required for growth arrest and multidrug tolerance in Escherichia coli. *Journal of Bacteriology* **188**, 8360-8367 (2006).
93. M. A. Schumacher *et al.*, Role of unusual P loop ejection and autophosphorylation in HipA-mediated persistence and multidrug tolerance. *Cell reports* **2**, 518-525 (2012).
94. E. Germain, D. Castro-Roa, N. Zenkin, K. Gerdes, Molecular Mechanism of Bacterial Persistence by HipA. *Molecular Cell* **52**, 248-254 (2013).
95. I. Kaspy *et al.*, HipA-mediated antibiotic persistence via phosphorylation of the glutamyl-tRNA-synthetase. *Nature Communications* **4**, 1-7 (2013).
96. K. S. Winther, M. Roghanian, K. Gerdes, Activation of the stringent response by loading of RelA-tRNA complexes at the ribosomal A-site. *Molecular cell* **70**, 95-105. e104 (2018).
97. G. Bokinsky *et al.*, HipA-triggered growth arrest and β-lactam tolerance in Escherichia coli are mediated by RelA-dependent ppGpp synthesis. *Journal of bacteriology* **195**, 3173-3182 (2013).
98. M. Semanjski *et al.*, The kinases HipA and HipA7 phosphorylate different substrate pools in Escherichia coli to promote multidrug tolerance. *Science Signaling* **11**, 5750 (2018).
99. H. Kawano, Y. Hirokawa, H. Mori, Long-term survival of Escherichia coli lacking the HipBA toxin-antitoxin system during prolonged cultivation. *Bioscience, biotechnology, and biochemistry* **73**, 117-123 (2009).

100. K. Gerdes, R. Bærentsen, D. E. Brodersen, Phylogeny reveals novel hipa-homologous kinase families and toxin-antitoxin gene organizations. *mBio* **12**, (2021).
101. I. Keren, D. Shah, A. Spoering, N. Kaldalu, K. Lewis, Specialized persister cells and the mechanism of multidrug tolerance in Escherichia coli. *Journal of bacteriology* **186**, 8172-8180 (2004).
102. J. Zhao *et al.*, Escherichia coli toxin gene hipA affects biofilm formation and DNA release. *Microbiology* **159**, 633-640 (2013).
103. Y. Maeda *et al.*, Characterization of YjjJ toxin of Escherichia coli. *FEMS Microbiology Letters*, (2017).
104. P. Fernandez *et al.*, The Ser/Thr protein kinase PknB is essential for sustaining mycobacterial growth. *Journal of bacteriology* **188**, 7778-7784 (2006).
105. A. Walburger *et al.*, Protein kinase G from pathogenic mycobacteria promotes survival within macrophages. *Science* **304**, 1800-1804 (2004).
106. M. Schreiber, A. Matter, Protein kinases as antibacterial targets. *Current opinion in cell biology* **21**, 325-330 (2009).
107. J. Bonne Køhler *et al.*, Importance of protein Ser/Thr/Tyr phosphorylation for bacterial pathogenesis. *FEBS letters* **594**, 2339-2369 (2020).
108. C. Giefing *et al.*, Discovery of a novel class of highly conserved vaccine antigens using genomic scale antigenic fingerprinting of pneumococcus with human antibodies. *The Journal of experimental medicine* **205**, 117-131 (2008).
109. C. Loc-Carrillo, S. T. Abedon, Pros and cons of phage therapy. *Bacteriophage* **1**, 111-114 (2011).
110. D. Kumar, S. Narayanan, pknE, a serine/threonine kinase of Mycobacterium tuberculosis modulates multiple apoptotic paradigms. *Infection, Genetics and Evolution* **12**, 737-747 (2012).
111. M. Singla, V. Chaudhary, A. Ghosh, Bacterial Multidrug Tolerance and Persisters: Understanding the Mechanisms, Clinical Implications, and Treatment Strategies. *Antimicrobial Resistance: Underlying Mechanisms and Therapeutic Approaches*, 29-69 (2022).
112. N. Q. Balaban *et al.*, Definitions and guidelines for research on antibiotic persistence. *Nature Reviews Microbiology* **17**, 441-448 (2019).
113. J. M. Munita, C. A. Arias, Mechanisms of antibiotic resistance. *Virulence mechanisms of bacterial pathogens*, 481-511 (2016).
114. A. Brauner, O. Fridman, O. Gefen, N. Q. Balaban, Distinguishing between resistance, tolerance and persistence to antibiotic treatment. *Nature Reviews Microbiology* **14**, 320-330 (2016).
115. L. Dewachter, M. Fauvart, J. Michiels, Bacterial heterogeneity and antibiotic survival: understanding and combatting persistence and heteroresistance. *Molecular cell* **76**, 255-267 (2019).
116. B. Van den Bergh, M. Fauvart, J. Michiels, Formation, physiology, ecology, evolution and clinical importance of bacterial persisters. *FEMS microbiology reviews* **41**, 219-251 (2017).
117. K. Lewis, Persister cells, dormancy and infectious disease. *Nature Reviews Microbiology* **5**, 48-56 (2007).

118. C. J. Murray *et al.*, Global burden of bacterial antimicrobial resistance in 2019: a systematic analysis. *The lancet* **399**, 629-655 (2022).
119. World Health Organisation. (2023), vol. 2024.
120. A. Chokshi, Z. Sifri, D. Cennimo, H. Horng, Global contributors to antibiotic resistance. *Journal of global infectious diseases* **11**, 36-42 (2019).
121. G. Sulis, S. Sayood, S. Gandra, Antimicrobial resistance in low-and middle-income countries: current status and future directions. *Expert review of anti-infective therapy* **20**, 147-160 (2022).
122. A. N. Poudel *et al.*, The economic burden of antibiotic resistance: A systematic review and meta-analysis. *Plos one* **18**, e0285170 (2023).
123. R. E. Nelson *et al.*, National estimates of healthcare costs associated with multidrug-resistant bacterial infections among hospitalized patients in the United States. *Clinical Infectious Diseases* **72**, S17-S26 (2021).
124. World Health Organisation, WHO publishes list of bacteria for which new antibiotics are urgently needed. Online (2017).
125. L. B. Rice, Federal funding for the study of antimicrobial resistance in nosocomial pathogens: no ESKAPE. **197**, 1079-1081 (2008).
126. W. R. Miller, C. A. Arias, ESKAPE pathogens: antimicrobial resistance, epidemiology, clinical impact and therapeutics. *Nature Reviews Microbiology*, 1-19 (2024).
127. R. Jadimurthy, S. B. Mayegowda, S. C. Nayak, C. D. Mohan, K. S. Rangappa, Escaping mechanisms of ESKAPE pathogens from antibiotics and their targeting by natural compounds. *Biotechnology Reports* **34**, e00728 (2022).
128. P. Nordmann, G. Cuzon, T. Naas, The real threat of Klebsiella pneumoniae carbapenemase-producing bacteria. *The Lancet infectious diseases* **9**, 228-236 (2009).
129. D. M. Fernando, A. Kumar, Resistance-nodulation-division multidrug efflux pumps in gram-negative bacteria: role in virulence. *Antibiotics* **2**, 163-181 (2013).
130. J. N. Pendleton, S. P. Gorman, B. F. Gilmore, Clinical relevance of the ESKAPE pathogens. *Expert review of anti-infective therapy* **11**, 297-308 (2013).
131. E.-T. Piperaki, G. A. Syrogiannopoulos, L. S. Tzouvelekis, G. L. Daikos, Klebsiella pneumoniae: virulence, biofilm and antimicrobial resistance. *The Pediatric infectious disease journal* **36**, 1002-1005 (2017).
132. R. Podschun, U. Ullmann, Klebsiella spp. as nosocomial pathogens: epidemiology, taxonomy, typing methods, and pathogenicity factors. *Clinical microbiology reviews* **11**, 589-603 (1998).
133. T. A. Russo, C. M. Marr, Hypervirulent klebsiella pneumoniae. *Clinical microbiology reviews* **32**, 10.1128/cmr. 00001-00019 (2019).
134. L. Assoni *et al.*, Animal models of Klebsiella pneumoniae mucosal infections. *Frontiers in Microbiology* **15**, 1367422 (2024).
135. D. Chang, L. Sharma, C. S. Dela Cruz, D. Zhang, Clinical epidemiology, risk factors, and control strategies of Klebsiella pneumoniae infection. *Frontiers in microbiology* **12**, 750662 (2021).
136. W. R. Jarvis, V. P. Munn, A. K. Highsmith, D. H. Culver, J. M. Hughes, The epidemiology of nosocomial infections caused by Klebsiella pneumoniae. *Infection Control & Hospital Epidemiology* **6**, 68-74 (1985).

137. R. M. Martin, M. A. Bachman, Colonization, infection, and the accessory genome of Klebsiella pneumoniae. *Frontiers in cellular and infection microbiology* **8**, 4 (2018).
138. B. Li, Y. Zhao, C. Liu, Z. Chen, D. Zhou, Molecular pathogenesis of Klebsiella pneumoniae. *Future microbiology* **9**, 1071-1081 (2014).
139. J. Zhu, T. Wang, L. Chen, H. Du, Virulence factors in hypervirulent Klebsiella pneumoniae. *Frontiers in microbiology* **12**, 642484 (2021).
140. D. J. Doorduijn, S. H. Rooijakkers, W. van Schaik, B. W. Bardoel, Complement resistance mechanisms of Klebsiella pneumoniae. *Immunobiology* **221**, 1102-1109 (2016).
141. C. March *et al.*, Role of bacterial surface structures on the interaction of Klebsiella pneumoniae with phagocytes. *PloS one* **8**, e56847 (2013).
142. E. Padilla *et al.*, Klebsiella pneumoniae AcrAB efflux pump contributes to antimicrobial resistance and virulence. *Antimicrobial agents and chemotherapy* **54**, 177-183 (2010).
143. R. Abbas *et al.*, General Overview of Klebsiella pneumonia: Epidemiology and the Role of Siderophores in Its Pathogenicity. *Biology* **13**, 78 (2024).
144. A. S. Shon, R. P. Bajwa, T. A. Russo, Hypervirulent (hypermucoviscous) Klebsiella pneumoniae: a new and dangerous breed. *Virulence* **4**, 107-118 (2013).
145. H. Kazemian *et al.*, Phenotypic and genotypic characterization of ESBL-, AmpC-, and carbapenemase-producing Klebsiella pneumoniae and Escherichia coli isolates. *Medical Principles and Practice* **28**, 547-551 (2019).
146. C. Vuotto, F. Longo, M. P. Balice, G. Donelli, P. E. Varaldo, Antibiotic resistance related to biofilm formation in Klebsiella pneumoniae. *Pathogens* **3**, 743-758 (2014).
147. H. Ren *et al.*, Gradual increase in antibiotic concentration affects persistence of Klebsiella pneumoniae. *Journal of Antimicrobial Chemotherapy* **70**, 3267-3272 (2015).
148. J. E. Michiels, B. Van den Bergh, N. Verstraeten, J. Michiels, Molecular mechanisms and clinical implications of bacterial persistence. *Drug Resistance Updates* **29**, 76-89 (2016).
149. Y. Li, L. Zhang, Y. Zhou, Z. Zhang, X. Zhang, Survival of bactericidal antibiotic treatment by tolerant persister cells of Klebsiella pneumoniae. *J Med Microbiol* **67**, 273-281 (2018).
150. R. Trastoy *et al.*, Mechanisms of bacterial tolerance and persistence in the gastrointestinal and respiratory environments. *Clinical microbiology reviews* **31**, 10.1128/cmr. 00023-00018 (2018).
151. B. Gollan, G. Grabe, C. Michaux, S. Helaine, Bacterial persisters and infection: past, present, and progressing. *Annual review of microbiology* **73**, 359-385 (2019).
152. X. Shi, A. Zarkan, Bacterial survivors: Evaluating the mechanisms of antibiotic persistence. *Microbiology* **168**, 001266 (2022).
153. E. M. Windels *et al.*, Bacterial persistence promotes the evolution of antibiotic resistance by increasing survival and mutation rates. *The ISME journal* **13**, 1239-1251 (2019).

154. I. Levin-Reisman, A. Brauner, I. Ronin, N. Q. Balaban, Epistasis between antibiotic tolerance, persistence, and resistance mutations. *Proceedings of the National Academy of Sciences of the United States of America* **116**, 14734-14739 (2019).
155. J. N. Kaur *et al.*, Next generation antibiotic combinations to combat pan-drug resistant Klebsiella pneumoniae. *Scientific Reports* **14**, 3148 (2024).
156. R. A. Fisher, B. Gollan, S. Helaine, Persistent bacterial infections and persister cells. *Nature Reviews Microbiology* **15**, 453-464 (2017).
157. K. R. Allison, M. P. Brynildsen, J. J. Collins, Metabolite-enabled eradication of bacterial persisters by aminoglycosides. *Nature* **473**, 216-220 (2011).
158. O. Gholizadeh, H. E. G. Ghaleh, M. Tat, R. Ranjbar, R. Dorostkar, The potential use of bacteriophages as antibacterial agents against Klebsiella pneumoniae. *Virology Journal* **21**, 191 (2024).
159. T. Li, N. Yin, H. Liu, J. Pei, L. Lai, Novel inhibitors of toxin HipA reduce multidrug tolerant persisters. *ACS medicinal chemistry letters* **7**, 449-453 (2016).
160. R. D. Mittal. (Springer, 2015), vol. 30, pp. 121-123.
161. A.-N. Neagu *et al.*, Applications of tandem mass spectrometry (MS/MS) in protein analysis for biomedical research. *Molecules* **27**, 2411 (2022).
162. W. Li *et al.*, Rapid identification and antimicrobial susceptibility testing for urinary tract pathogens by direct analysis of urine samples using a MALDI-TOF MS-based combined protocol. *Frontiers in Microbiology* **10**, 1182 (2019).
163. A. Macklin, S. Khan, T. Kislinger, Recent advances in mass spectrometry based clinical proteomics: applications to cancer research. *Clinical proteomics* **17**, 17 (2020).
164. H. Yokota, Applications of proteomics in pharmaceutical research and development. *Biochimica et Biophysica Acta (BBA)-Proteins and Proteomics* **1867**, 17-21 (2019).
165. A. D. Catherman, O. S. Skinner, N. L. Kelleher, Top down proteomics: facts and perspectives. *Biochemical and biophysical research communications* **445**, 683-693 (2014).
166. Y. Zhang, B. R. Fonslow, B. Shan, M.-C. Baek, J. R. Yates III, Protein analysis by shotgun/bottom-up proteomics. *Chemical reviews* **113**, 2343-2394 (2013).
167. H. Steen, M. Mann, The ABC's (and XYZ's) of peptide sequencing. *Nature reviews Molecular cell biology* **5**, 699-711 (2004).
168. A. Cristobal *et al.*, Toward an optimized workflow for middle-down proteomics. *Analytical chemistry* **89**, 3318-3325 (2017).
169. R. Aebersold, M. Mann, Mass spectrometry-based proteomics. *Nature* **422**, 198-207 (2003).
170. A. El-Aneed, A. Cohen, J. Banoub, Mass spectrometry, review of the basics: electrospray, MALDI, and commonly used mass analyzers. *Applied spectroscopy reviews* **44**, 210-230 (2009).
171. C. S. Ho *et al.*, Electrospray ionization mass spectrometry: principles and clinical applications. *The Clinical Biochemist Reviews* **24**, 3 (2003).
172. E. J. Finehout, K. H. Lee, An introduction to mass spectrometry applications in biological research. *Biochemistry and molecular biology Education* **32**, 93-100 (2004).

173. P. E. Miller, M. B. Denton, The quadrupole mass filter: basic operating concepts. *Journal of chemical education* **63**, 617 (1986).
174. H. Wollnik, Time-of-flight mass analyzers. *Mass spectrometry reviews* **12**, 89-114 (1993).
175. P. B. Pandeswari, V. Sabareesh, Middle-down approach: a choice to sequence and characterize proteins/proteomes by mass spectrometry. *RSC advances* **9**, 313-344 (2019).
176. A. G. Marshall, F. R. Verdun, *Fourier transforms in NMR, optical, and mass spectrometry: a user's handbook*. (Elsevier, 2016).
177. R. A. Zubarev, A. Makarov. (ACS Publications, 2013).
178. G. L. Glish, D. J. Burinsky, Hybrid mass spectrometers for tandem mass spectrometry. *Journal of the American Society for Mass Spectrometry* **19**, 161-172 (2008).
179. G. C. McAlister, D. H. Phanstiel, J. Brumbaugh, M. S. Westphall, J. J. Coon, Higher-energy collision-activated dissociation without a dedicated collision cell. *Molecular & Cellular Proteomics* **10**, (2011).
180. M. S. Kim, A. Pandey, Electron transfer dissociation mass spectrometry in proteomics. *Proteomics* **12**, 530-542 (2012).
181. H. I. Stewart *et al.*, Parallelized acquisition of orbitrap and astral analyzers enables high-throughput quantitative analysis. *Analytical chemistry* **95**, 15656-15664 (2023).
182. E. Denisov, E. Damoc, A. Makarov, Exploring frontiers of orbitrap performance for long transients. *International Journal of Mass Spectrometry* **466**, 116607 (2021).
183. J. Guo, T. Huan, Comparison of full-scan, data-dependent, and data-independent acquisition modes in liquid chromatography–mass spectrometry based untargeted metabolomics. *Analytical Chemistry* **92**, 8072-8080 (2020).
184. V. Davies *et al.*, Rapid development of improved data-dependent acquisition strategies. *Analytical chemistry* **93**, 5676-5683 (2021).
185. L. Krasny, P. H. Huang, Data-independent acquisition mass spectrometry (DIA-MS) for proteomic applications in oncology. *Molecular omics* **17**, 29-42 (2021).
186. J. D. Chapman, D. R. Goodlett, C. D. Masselon, Multiplexed and data-independent tandem mass spectrometry for global proteome profiling. *Mass spectrometry reviews* **33**, 452-470 (2014).
187. N. Pappireddi, L. Martin, M. Wühr, A review on quantitative multiplexed proteomics. *Chembiochem* **20**, 1210-1224 (2019).
188. A. Hu, W. S. Noble, A. Wolf-Yadlin, Technical advances in proteomics: new developments in data-independent acquisition. *F1000Research* **5**, (2016).
189. O. T. Schubert, H. L. Röst, B. C. Collins, G. Rosenberger, R. Aebersold, Quantitative proteomics: challenges and opportunities in basic and applied research. *Nature protocols* **12**, 1289-1294 (2017).
190. S. A. Gerber, J. Rush, O. Stemman, M. W. Kirschner, S. P. Gygi, Absolute quantification of proteins and phosphoproteins from cell lysates by tandem MS. *Proceedings of the National Academy of Sciences* **100**, 6940-6945 (2003).
191. A. Iliuk, J. Galan, W. A. Tao, Playing tag with quantitative proteomics. *Analytical and bioanalytical chemistry* **393**, 503-513 (2009).

192. M. H. Elliott, D. S. Smith, C. E. Parker, C. Borchers, Current trends in quantitative proteomics. *Journal of Mass Spectrometry* **44**, 1637-1660 (2009).
193. M. Bantscheff, M. Schirle, G. Sweetman, J. Rick, B. Kuster, Quantitative mass spectrometry in proteomics: a critical review. *Analytical and bioanalytical chemistry* **389**, 1017-1031 (2007).
194. B. Schwanhäusser *et al.*, Global quantification of mammalian gene expression control. *Nature* **473**, 337-342 (2011).
195. B.-J. M. Webb-Robertson *et al.*, Review, evaluation, and discussion of the challenges of missing value imputation for mass spectrometry-based label-free global proteomics. *Journal of proteome research* **14**, 1993-2001 (2015).
196. B. R. Franza Jr, Y. P. Rochon. (Google Patents, 2003).
197. S.-E. Ong *et al.*, Stable isotope labeling by amino acids in cell culture, SILAC, as a simple and accurate approach to expression proteomics. *Molecular & cellular proteomics* **1**, 376-386 (2002).
198. J. V. Olsen, S.-E. Ong, M. Mann, Trypsin cleaves exclusively C-terminal to arginine and lysine residues. *Molecular & cellular proteomics* **3**, 608-614 (2004).
199. M. Semanjski *et al.*, Proteome dynamics during antibiotic persistence and resuscitation. *Msystems* **6**, 10.1128/msystems. 00549-00521 (2021).
200. L. Käll, O. Vitek, Computational mass spectrometry–based proteomics. *PLoS computational biology* **7**, e1002277 (2011).
201. A. Thompson *et al.*, Tandem mass tags: a novel quantification strategy for comparative analysis of complex protein mixtures by MS/MS. *Analytical chemistry* **75**, 1895-1904 (2003).
202. P. J. Boersema, R. Raijmakers, S. Lemeer, S. Mohammed, A. J. Heck, Multiplex peptide stable isotope dimethyl labeling for quantitative proteomics. *Nature protocols* **4**, 484-494 (2009).
203. J. Li *et al.*, TMTpro reagents: a set of isobaric labeling mass tags enables simultaneous proteome-wide measurements across 16 samples. *Nature methods* **17**, 399-404 (2020).
204. A. A. Petelski *et al.*, Multiplexed single-cell proteomics using SCoPE2. *Nature protocols* **16**, 5398-5425 (2021).
205. H. K. Kweon, K. Håkansson, Selective zirconium dioxide-based enrichment of phosphorylated peptides for mass spectrometric analysis. *Analytical chemistry* **78**, 1743-1749 (2006).
206. M. W. Pinkse, P. M. Uitto, M. J. Hilhorst, B. Ooms, A. J. Heck, Selective isolation at the femtomole level of phosphopeptides from proteolytic digests using 2D-NanoLC-ESI-MS/MS and titanium oxide precolumns. *Analytical chemistry* **76**, 3935-3943 (2004).
207. C. Baldwin, J. Cumming, A. T. Timperman, Isolation of naturally occurring aluminium ligands using immobilized metal affinity chromatography for analysis by ESI-MS. *The Analyst* **130**, 318-324 (2005).
208. H. Zhou *et al.*, Enhancing the identification of phosphopeptides from putative basophilic kinase substrates using Ti (IV) based IMAC enrichment. *Molecular & Cellular Proteomics* **10**, (2011).

209. S. Feng *et al.*, Immobilized zirconium ion affinity chromatography for specific enrichment of phosphopeptides in phosphoproteome analysis. *Molecular & Cellular Proteomics* **6**, 1656-1665 (2007).
210. L. Andersson, J. Porath, Isolation of phosphoproteins by immobilized metal (Fe3+) affinity chromatography. *Analytical biochemistry* **154**, 250-254 (1986).
211. M. C. Posewitz, P. Tempst, Immobilized gallium (III) affinity chromatography of phosphopeptides. *Analytical chemistry* **71**, 2883-2892 (1999).
212. P. R. Gafken, P. D. Lampe, Methodologies for characterizing phosphoproteins by mass spectrometry. *Cell communication & adhesion* **13**, 249-262 (2006).
213. D. Virág *et al.*, Current trends in the analysis of post-translational modifications. *Chromatographia* **83**, 1-10 (2020).
214. L. Higgins, H. Gerdes, P. R. Cutillas, Principles of phosphoproteomics and applications in cancer research. *Biochemical Journal* **480**, 403-420 (2023).
215. T. E. Thingholm, M. R. Larsen, Phosphopeptide enrichment by immobilized metal affinity chromatography. *Phospho-proteomics: Methods and protocols*, 123-133 (2016).
216. A. Sultan *et al.*, Phosphoproteome Study of Escherichia coli Devoid of Ser/Thr Kinase YeaG During the Metabolic Shift From Glucose to Malate. *Frontiers in Microbiology* **12**, (2021).
217. R. Gopalaswamy, P. Narayanan, S. Narayanan, Cloning, overexpression, and characterization of a serine/threonine protein kinase pknI from Mycobacterium tuberculosis H37Rv. *Protein expression and purification* **36**, 82-89 (2004).
218. R. Lomas-Lopez, P. Paracuellos, M. Riberty, A. J. Cozzone, B. Duclos, Several enzymes of the central metabolism are phosphorylated in Staphylococcus aureus. *FEMS microbiology letters* **272**, 35-42 (2007).
219. A. M. Beltramini, C. D. Mukhopadhyay, V. Pancholi, Modulation of cell wall structure and antimicrobial susceptibility by a Staphylococcus aureus eukaryote-like serine/threonine kinase and phosphatase. *Infection and immunity* **77**, 1406-1416 (2009).
220. N. Prust, S. van der Laarse, H. W. van den Toorn, N. M. van Sorge, S. Lemeer, In-depth characterization of the Staphylococcus aureus phosphoproteome reveals new targets of Stk1. *Molecular & Cellular Proteomics* **20**, (2021).
221. K. M. Krause, A. W. Serio, T. R. Kane, L. E. Connolly, Aminoglycosides: an overview. *Cold Spring Harbor perspectives in medicine* **6**, a027029 (2016).
222. M. Semanjski *et al.*, Proteome Dynamics during Antibiotic Persistence and Resuscitation. *mSystems* **6**, (2021).
223. L. S. Redgrave, S. B. Sutton, M. A. Webber, L. J. Piddock, Fluoroquinolone resistance: mechanisms, impact on bacteria, and role in evolutionary success. *Trends in microbiology* **22**, 438-445 (2014).
224. J. Timmermans, L. Van Melderen, Conditional essentiality of the csrA gene in Escherichia coli. *Journal of bacteriology* **191**, 1722-1724 (2009).
225. T. Romeo, M. Gong, M. Y. Liu, A.-M. Brun-Zinkernagel, Identification and molecular characterization of csrA, a pleiotropic gene from Escherichia coli that affects glycogen biosynthesis, gluconeogenesis, cell size, and surface properties. *Journal of bacteriology* **175**, 4744-4755 (1993).

226. N. A. Sabnis, H. Yang, T. Romeo, Pleiotropic regulation of central carbohydrate metabolism in Escherichia coli via the gene csrA. *Journal of Biological Chemistry* **270**, 29096-29104 (1995).
227. M. Ueta, C. Wada, Y. Bessho, M. Maeda, A. Wada, Ribosomal protein L31 in Escherichia coli contributes to ribosome subunit association and translation, whereas short L31 cleaved by protease 7 reduces both activities. *Genes to Cells* **22**, 452-471 (2017).
228. S. Lilleorg *et al.*, Bacterial ribosome heterogeneity: Changes in ribosomal protein composition during transition into stationary growth phase. *Biochimie* **156**, 169-180 (2019).
229. N. C. Soares, P. Spat, K. Krug, B. Macek, Global dynamics of the Escherichia coli proteome and phosphoproteome during growth in minimal medium. *Journal of proteome research* **12**, 2611-2621 (2013).
230. B. W. Kwan, J. A. Valenta, M. J. Benedik, T. K. Wood, Arrested protein synthesis increases persister-like cell formation. *Antimicrobial agents and chemotherapy* **57**, 1468-1473 (2013).
231. S. Song, T. K. Wood, ppGpp ribosome dimerization model for bacterial persister formation and resuscitation. *Biochemical and biophysical research communications* **523**, 281-286 (2020).
232. T. Suryanarayana, A. R. Subramanian, Function of the repeating homologous sequences in nucleic acid binding domain of ribosomal protein S1. *Biochemistry* **23**, 1047-1051 (1984).
233. G. Carmichael, T. Landers, K. Weber, Immunochemical analysis of the functions of the subunits of phage Qbeta ribonucleic acid replicase. *Journal of Biological Chemistry* **251**, 2744-2748 (1976).
234. E. S. Robertson, A. W. Nicholson, Phosphorylation of Escherichia coli translation initiation factors by the bacteriophage T7 protein kinase. *Biochemistry* **31**, 4822-4827 (1992).
235. I. Marchand, A. W. Nicholson, M. Dreyfus, Bacteriophage T7 protein kinase phosphorylates RNase E and stabilizes mRNAs synthesized by T7 RNA polymerase. *Molecular microbiology* **42**, 767-776 (2001).
236. G.-G. Liou, W.-N. Jane, S. N. Cohen, N.-S. Lin, S. Lin-Chao, RNA degradosomes exist in vivo in Escherichia coli as multicomponent complexes associated with the cytoplasmic membrane via the N-terminal region of ribonuclease E. *Proceedings of the National Academy of Sciences* **98**, 63-68 (2001).

7. Appendix

The supplementary information files containing extended methods, supplementary tables, and datasets for MS data analysis are available online in the published research articles.

8. Acknowledgments

This thesis would not have been possible without the support, guidance, and encouragement of many individuals and institutions to whom I am deeply grateful.

First and foremost, I would like to express my sincere gratitude to my supervisor, Prof. Dr. Boris Macek, for his invaluable guidance and support throughout my PhD. I am especially thankful for the opportunity to be part of the Marie-Curie-funded PEST-BIN project and for the numerous collaboration opportunities you facilitated. Your insightful feedback and constant encouragement motivated me to push boundaries and strive for excellence.

I would also like to extend my heartfelt thanks to the members of my thesis advisory committee, Prof. Dr. Karl Forchhammer, Prof. Dr. Heike Brötz-Oesterhelt, and Prof. Dr. Ivan Mijakovic, for their thoughtful feedback and constructive criticism during our annual TAC meetings. Your advice has been instrumental in improving my work, and your input has significantly enriched the quality of this thesis.

A special note of thanks goes to my current and former colleagues at Proteome Center Tübingen: Claudia, Bianca, Niels, Sebastian, Katharina, Philipp, Nicolas, Ignacio, Samuel, Anna, Irina, Mirita, Anke, Johannes, Jürgen, Siegfried. I am particularly grateful to Silke, Marisa, and Fabio for their assistance with initial experiments when I first joined PCT. I also wish to acknowledge the administrative support I received from Uli and Lena. A heartfelt thank you to Niels, Claudia, Bianca, Fabio, and Sebastian for their invaluable insights during scientific discussions and their unwavering support both in the lab and beyond. I would also like to thank my collaborator Dr. Sandra Schwarz for letting me work at BSL2 in her lab and for all the samples, she provided for my main project.

I would like to express my sincere appreciation to IMPRS "From Molecules to Organisms" and the University of Tübingen for allowing me to pursue my PhD in Tübingen, Germany. I am immensely grateful to Prof. Dr. Boris Macek for accepting me as his student and for his mentorship throughout this journey. My thanks also go to Sibylle, Jeanette, and the team at Max Planck Institute for helping me with the transition from India to Germany.

I am also grateful to the European Union for funding the PEST-BIN project, and to Darko for his assistance with project-related administration. Special thanks are due to my colleagues from the PEST-BIN project for their collaboration and support. I would also like to acknowledge the support from Carsten, Sara Ribeiro, Margaux, and Sara during my secondments at their respective institutions and companies. I am thankful for the stimulating scientific discussions during the PEST-BIN summer schools over the last three years and to Darko for organizing them.

On a personal note, I owe a great debt of gratitude to my family. To my parents and grandmothers, thank you for your unwavering belief in me and for encouraging me to pursue a PhD in another country. I am forever grateful to my siblings, Muskan and Vishant, for their unconditional love, support, and constant encouragement throughout this journey. Your presence, even from afar, has been a source of strength and joy during challenging times. I also extend my thanks to my friends back in India, Ankita and Monika, and extended family, cousins, and relatives for their consistent well-wishes.

Lastly, I would like to express my heartfelt gratitude to the friends I made in Tübingen: Ankita, Shubham, Avani, Radhika, Divanshu, and Muhunden. You have been my family away from home, and your understanding, humor, and companionship have been invaluable. Thank you for the amazing trips we took around Europe and for making these years truly memorable. A special mention goes to Vipul for his constant encouragement and support throughout this journey. Your positivity and belief in me uplifted my spirits during the most intense moments of this process.

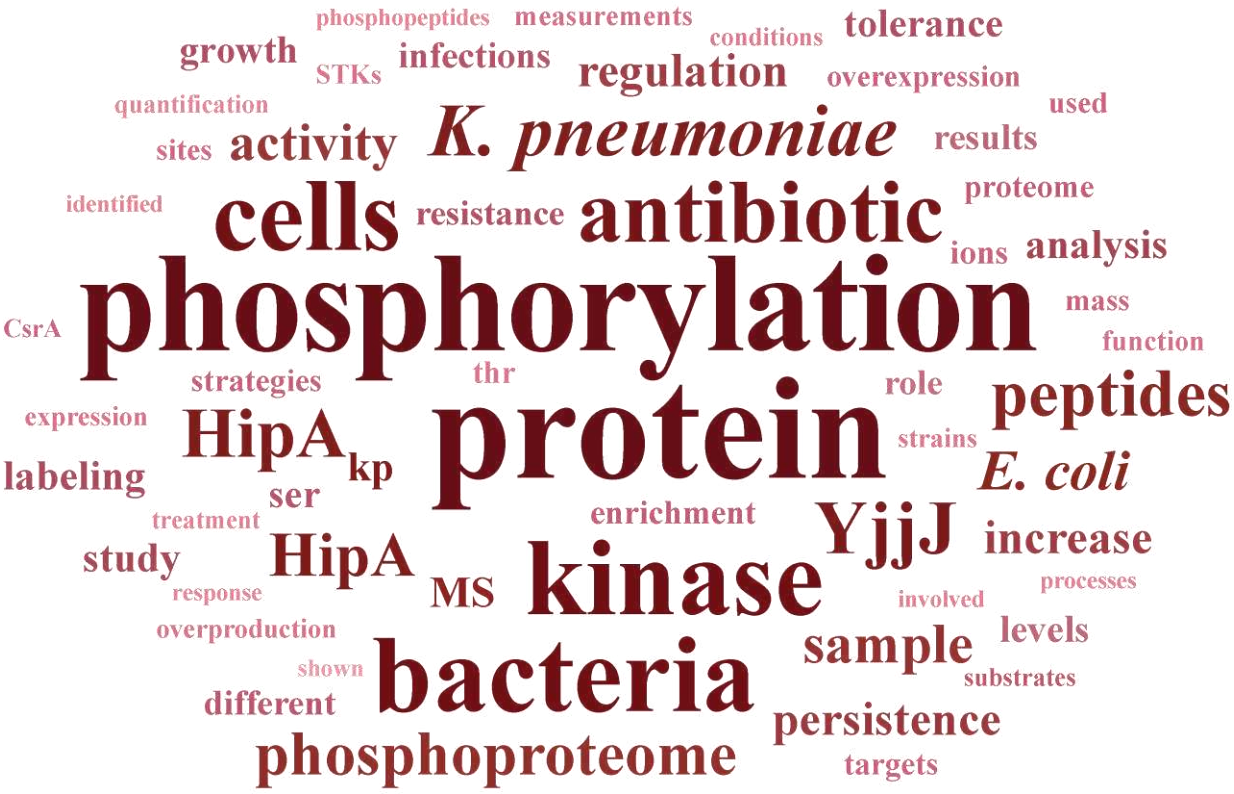

Final figure: **Word cloud of frequently used terms in this thesis**. This word cloud illustrates the most frequently occurring words in the thesis, with the size and color intensity of each word corresponding to its frequency. Larger and darker words appear more often throughout the text. The word cloud was created using TagCrowd.com to compile word frequencies, with an AI-assisted R-script used for generating the final plot, which was then refined using Adobe Illustrator.